AD-A131 575 HYDRAZINE APU STARTER DEVELOPMENT(U) ROCKET RESEARCH CORP REDMOND WASH D A PAHL JUN 83 RRC-83-R-905 AFWAL-TR-83-2039 F33615-78-C-2003 1/2

UNCLASSIFIED F/G 21/5 NL

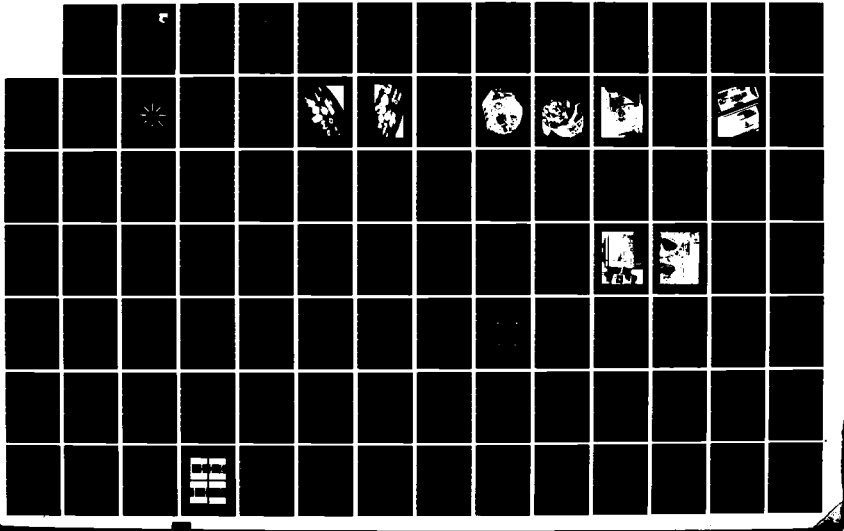

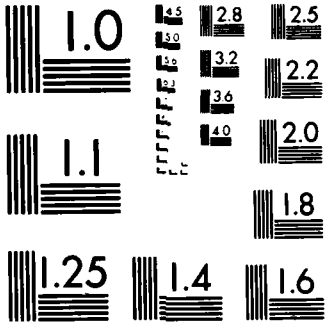

AFAPL-TR-83-2039

HYDRAZINE APU STARTER DEVELOPMENT

ROCKET RESEARCH COMPANY
YORK CENTER
REDMOND, WASHINGTON 98052

JUNE 1983

FINAL REPORT FOR PERIOD MARCH 1978 — MARCH 1983

Approved for public release; distribution unlimited.

AERO PROPULSION LABORATORY
AIR FORCE WRIGHT AERONAUTICAL LABORATORIES
AIR FORCE SYSTEMS COMMAND
WRIGHT-PATTERSON AIR FORCE BASE, OHIO 45433

NOTICE

When Government drawings, specifications, or other data are used for any purpose other than in connection with a definitely related Government procurement operation, the United States Government thereby incurs no responsibility nor any obligation whatsoever; and the fact that the government may have formulated, furnished, or in any way supplied the said drawings, specifications, or other data, is not to be regarded by implication or otherwise as in any manner licensing the holder or any other person or corporation, or conveying any rights or permission to manufacture use, or sell any patented invention that may in any way be related thereto.

This report has been reviewed by the Office of Public Affairs (ASD/PA) and is releasable to the National Technical Information Service (NTIS). At NTIS, it will be available to the general public, including foreign nations.

This technical report has been reviewed and is approved for publication.

B. L. MCFADDEN, Technical Area Mgr
Power Systems Branch
Aerospace Power Division
Aero Propulsion Laboratory

DAVID H. SCHORR, Major, USAF
Chief, Power Systems Branch
Aerospace Power Division
Aero Propulsion Laboratory

FOR THE COMMANDER

JAMES D. REAMS
Chief, Aerospace Power Division
Aero Propulsion Laboratory

"If your address has changed, if you wish to be removed from our mailing list, or if the addressee is no longer employed by your organization please notify AFWAL/POOS *, W-PAFB, OH 45433 to help us maintain a current mailing list".*

Copies of this report should not be returned unless return is required by security considerations, contractual obligations, or notice on a specific document.

DISCLAIMER NOTICE

THIS DOCUMENT IS BEST QUALITY PRACTICABLE. THE COPY FURNISHED TO DTIC CONTAINED A SIGNIFICANT NUMBER OF PAGES WHICH DO NOT REPRODUCE LEGIBLY.

Unclassified

SECURITY CLASSIFICATION OF THIS PAGE (When Data Entered)

REPORT DOCUMENTATION PAGE		READ INSTRUCTIONS BEFORE COMPLETING FORM
1 REPORT NUMBER AFWAL-TR-83-2039	2. GOVT ACCESSION NO.	3 RECIPIENT'S CATALOG NUMBER
4 TITLE (and Subtitle) HYDRAZINE APU STARTER DEVELOPMENT		5 TYPE OF REPORT & PERIOD COVERED Final Report for Period Mar 78 - Mar 83 6 PERFORMING ORG REPORT NUMBER 83-R-905
7 AUTHOR(s) D. A. Pahl		8 CONTRACT OR GRANT NUMBER(s) F 33615-78-C-2003
9 PERFORMING ORGANIZATION NAME AND ADDRESS Rocket Research Company York Center Redmond, Washington 98052		10 PROGRAM ELEMENT PROJECT TASK AREA & WORK UNIT NUMBERS 31450123 62W3P
11 CONTROLLING OFFICE NAME AND ADDRESS Aero Propulsion Laboratory (AFWAL/POOS) Air Force Wright Aeronautical Laboratories Wright-Patterson Air Force Base, Ohio 45433		12 REPORT DATE June 1983 13 NUMBER OF PAGES 174
14 MONITORING AGENCY NAME & ADDRESS(if different from Controlling Office)		15 SECURITY CLASS (of this report) Unclassified 15a DECLASSIFICATION DOWNGRADING SCHEDULE

16 DISTRIBUTION STATEMENT (of this Report)

Approved for public release: distribution unlimited.

17 DISTRIBUTION STATEMENT (of the abstract entered in Block 20, if different from Report)

18 SUPPLEMENTARY NOTES

19 KEY WORDS (Continue on reverse side if necessary and identify by block number)

APU starter
Hydrazine
Monopropellant
Vane motor
Hot gas motor

20 ABSTRACT (Continue on reverse side if necessary and identify by block number)

The purpose of this program was to develop a hot gas vane motor that would have application to advanced aircraft APU starting.

Over the course of the program, the motor design evolved to the point that -65°F starts, hot restarts above 1300°F, and multiple starts without refurbishment were possible. Analytical studies evaluated concepts for reducing motor internal friction.

DD FORM 1 JAN 73 1473 EDITION OF 1 NOV 65 IS OBSOLETE

Unclassified

SECURITY CLASSIFICATION OF THIS PAGE (When Data Entered)

FOREWORD

This report summarizes the fabrication, assembly and development test of a rotary vane type hot gas motor intended for use as the prime mover in an advanced hydrazine-fueled aircraft APU starter system. Details of the motor design and analysis have been previously reported in AFAPL-TR-77-76, "Hydrazine APU Starter Design," November 1977, for work conducted under Wright-Patterson AFB, Contract F33615-76-C-2148.

The work described herein was directed by Messrs. W. E. Jorgenson and D. A. Pahl of Rocket Research Company, Redmond, Washington. The project was sponsored by the Air Force Aero Propulsion Laboratory, Air Force Systems Command, Wright-Patterson AFB, Ohio, under Project, Task, and Work Unit No. 31450123 with Dr. B. L. McFadden, AFWAL/POOS, as project engineer in charge.

TABLE OF CONTENTS

LIST OF ILLUSTRATIONS

LIST OF ILLUSTRATIONS (Continued)

APPENDIX

LIST OF ILLUSTRATIONS -- APPENDIX (Concluded)

LIST OF TABLES

APPENDIX

SECTION I
INTRODUCTION

This section provides background information relating to prior work in the design of a hot gas high pressure rotary vane motor, presents the baseline motor design and discusses the program requirements and goals.

Successful accomplishment of the goals results in a compac . ılti-start capability system having full capability to an operational temperature of -65'

1. BACKGROUND

Design of the baseline motor was accomplished under t-Patterson AFB contract F33615-76-C-2148, and reported in AFAPL-TR-77-76, "Hydrazine APU Starter Design," dated November 1977. A cross-section taken from the assembly drawing of the motor (RRC drawing 26650) is shown in Figure 1.

REQUIREMENTS

The basic operating requirements for the starter motor are summarized as follows:

1. The starter motor must be as small and lightweight as possible consistent with aircraft-mounted components.

2. The starter motor must operate after extended exposure to ambient temperatures in the range of -65 to +130°F.

3. The starter motor must be capable of operating through a minimum of 1,000 full power, full duration starter operating cycles without maintenance.

4. The starter motor must be capable of operating in a successful manner when powered by the products of decomposition of the hydrazine-based propellant blend delivered by the hot gas supply system.

5. The starter motor must be capable of operating successfully during APU restart attempts in the event that the first start attempt is unsuccessful.

6. The starter motor shall develop torque versus speed characteristics at the output shaft of the gearbox consistent with the APU load characteristics, and providing a reasonable torque margin.

Typical APU torque/speed requirements at three ambient temperatures are shown in Figure 2. The .ritical requirement occurs at -65°F (where a high breakaway torque is required at zero speed), with a second torque peak slightly above 20,000 rpm. A 10:1

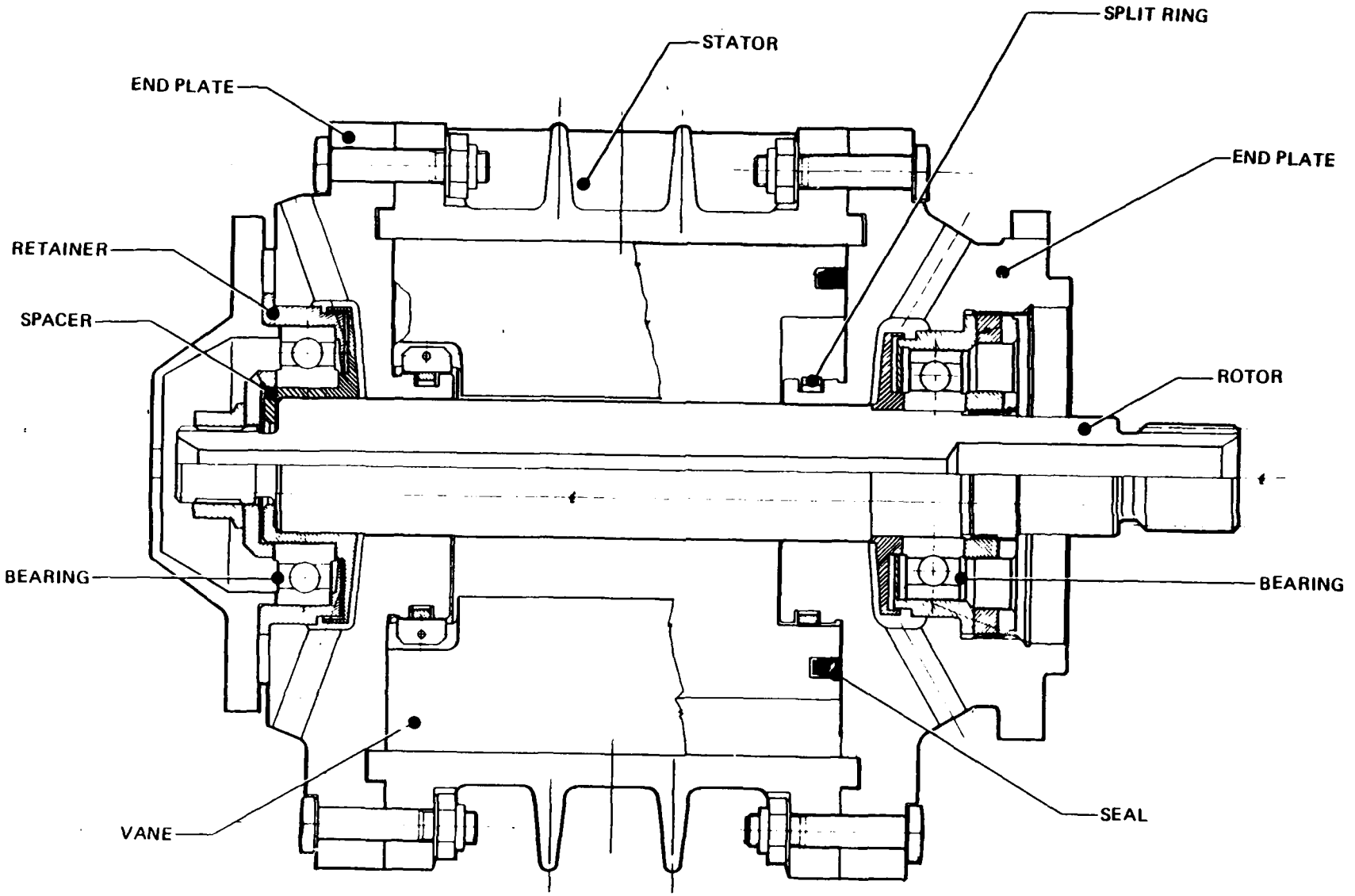

Figure 1. Cross Section of Rotary Vane Motor

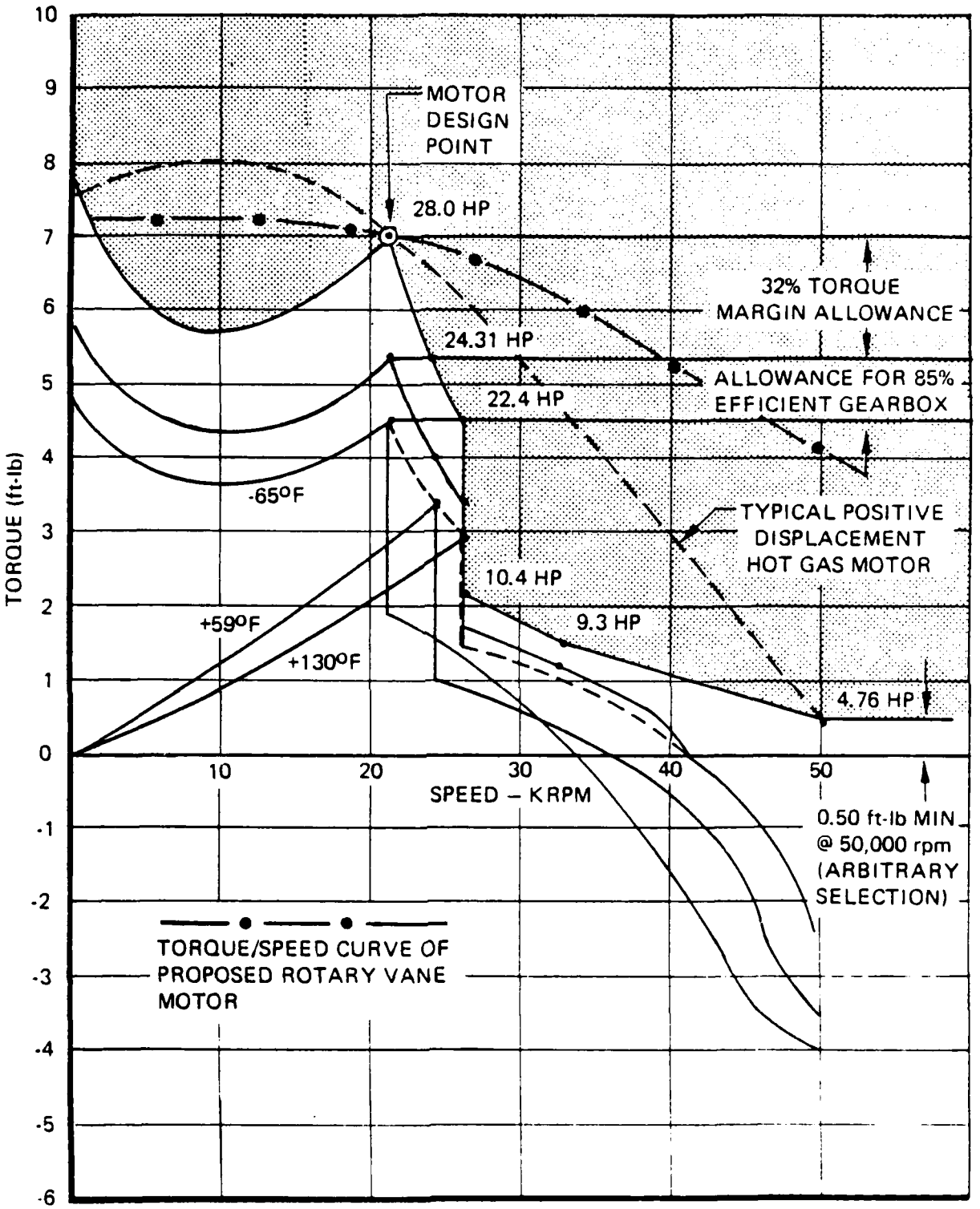

Figure 2. Starter System Operating Requirements

gearbox reduces the required motor speed to a reasonable operating range and increases the required motor torque by the same factor. Since the torque/speed curve for a rotary vane expander is relatively flat, the mid-speed range was selected as the design point for the motor, including allowances for gearbox efficiency (85%) and a 32% torque margin.

2. MOTOR DESIGN

The dimensions of the motor and porting arrangements are shown in Figure 3. For high expansion ratio and adiabatic efficiency, the arc of admission must be kept small, generally less than 0.3 radians. In this range, Reference (1)* shows performance improvement up to as many as 12 blades. Considerations of rotor and blade strength led to a compromise of 8 blades for the baseline motor design.

*Numbers in parentheses refer to references at end of report.

ROTOR DIAMETER 3.655 in. (92.84 mm)
ROTOR LENGTH 3.655 in. (92.84 mm)
STATOR INSIDE DIAMETER 4.125 in. (104.8 mm)

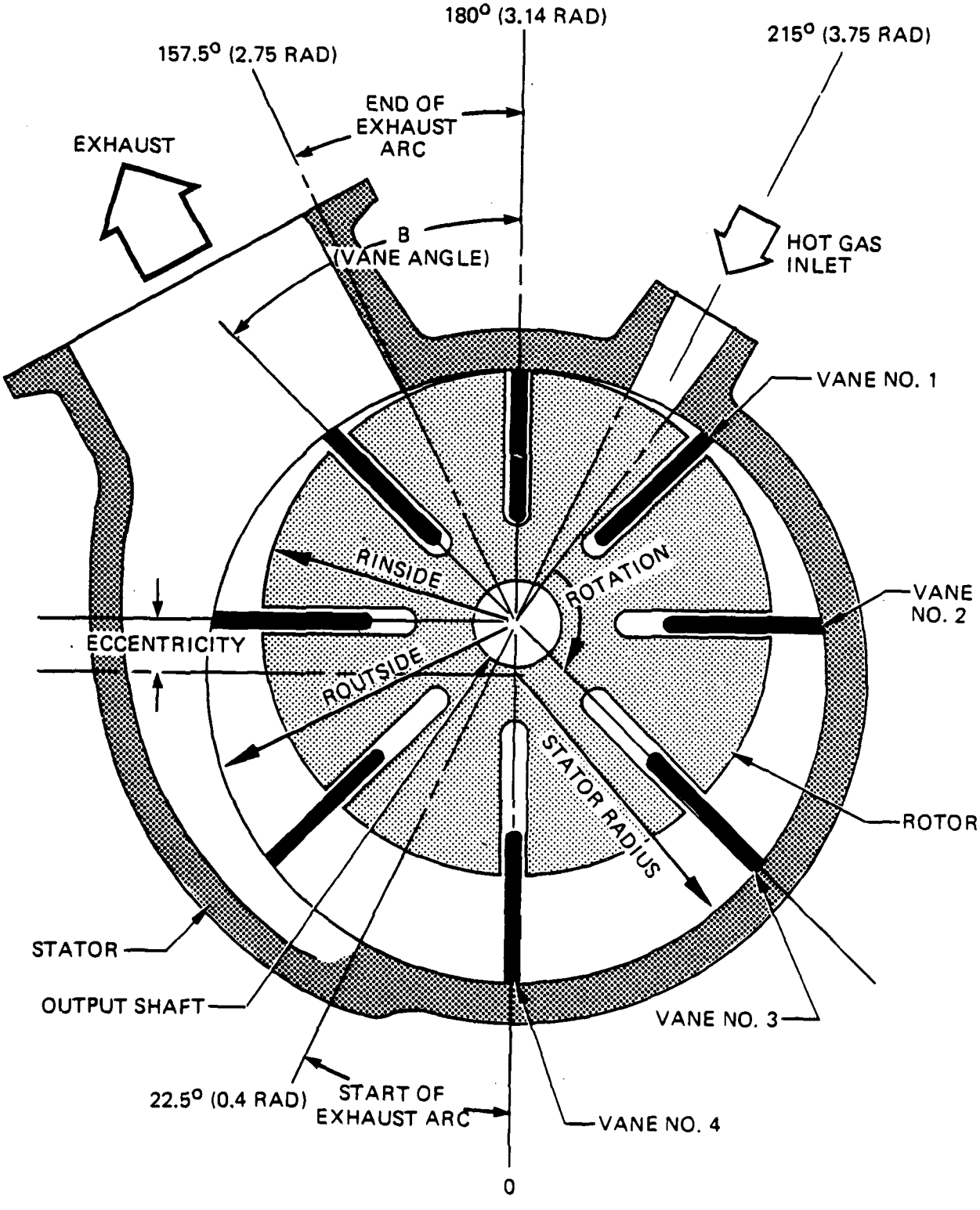

Figure 3. Rotary Vane Motor Geometry

SECTION II

PHASE I - HARDWARE FABRICATION AND TEST EQUIPMENT

This section describes the detail parts of the vane motor and test stand together with the appropriate test equipment and instrumentation.

1. VANE MOTOR DESCRIPTION

The major components of the motor include the ball bearing mounted rotor, 8 rotor vanes, the stator shell, end plates which support the rotor bearings and position the rotor eccentrically in the stator bore, and various seals and springs. Each end plate contains an eccentrically machined cam boss. These retain flexible split cam rings which bear on the base of each blade and provide a force to preload the blades against the stator. The mating contact points on the blades are provided with metal slippers, pinned to the blade. Segmented end seals located circumferentially between the blades on both ends of the rotor are spring loaded against the end plates to minimize leakage to the bearings. The bearings are further protected from hot gas by deflectors arranged in a labyrinth form, together with large overboard vents to preferentially duct leakage gas away from the bearings. Major materials of construction selected were:

Rotor	Waspaloy
Stator	Hastelloy C
End plates	Hastelloy C
Deflectors and bearing seats	Titanium 6Al-4V
Split cam rings	Inconel X-750
Vanes	P-658 RCH carbon

Two views of the motor piece parts (and partial assemblies) are shown in Figures 4 and 5. The piece parts are identified by horizontal rows, starting at the left end of the top row, as follows:

Top Row	Top Row (Continued)
End cap	Output end plate
End plate	Rotor installed in end plate
Stator	

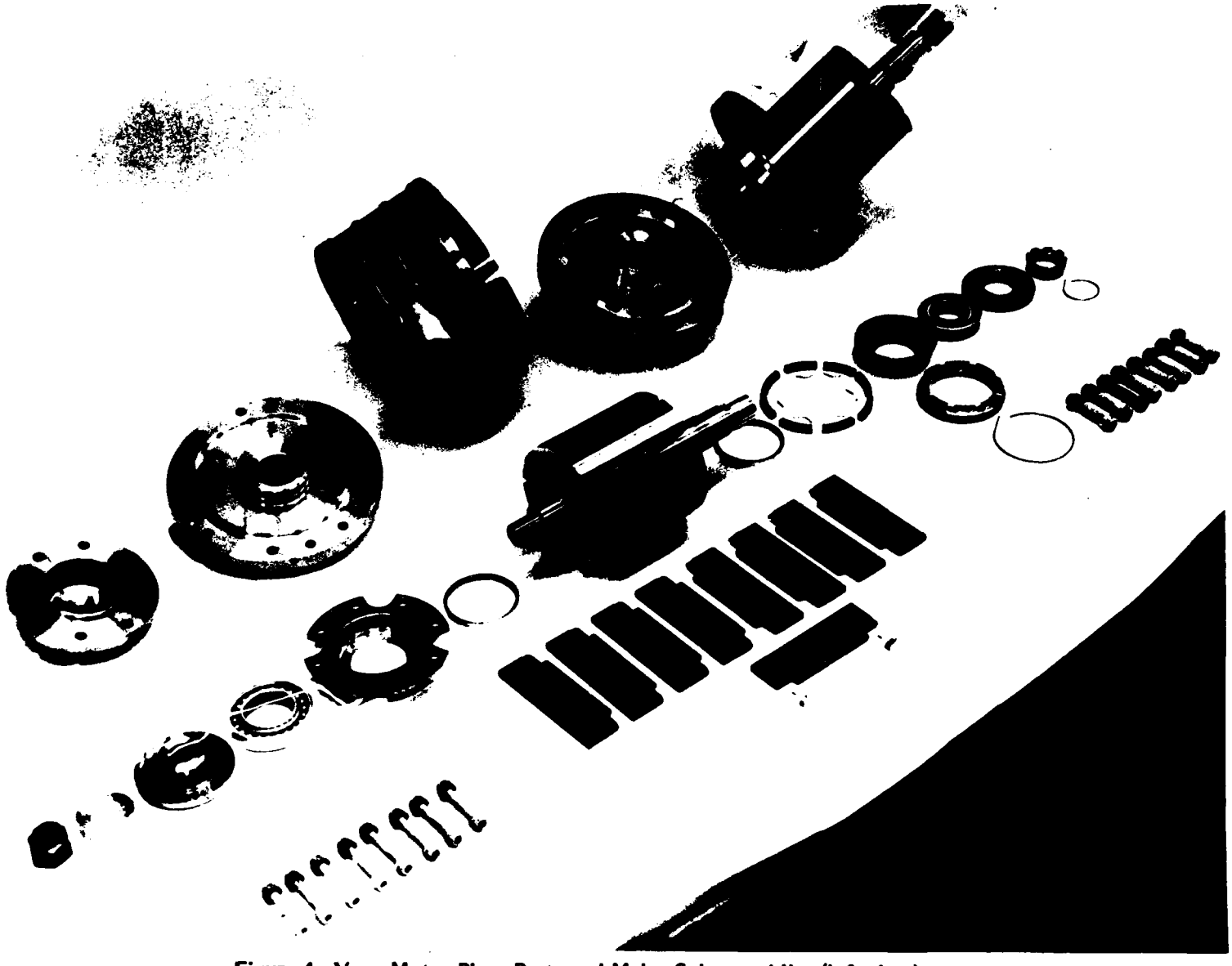

Figure 4. Vane Motor Piece Parts and Major Subassemblies (left view)

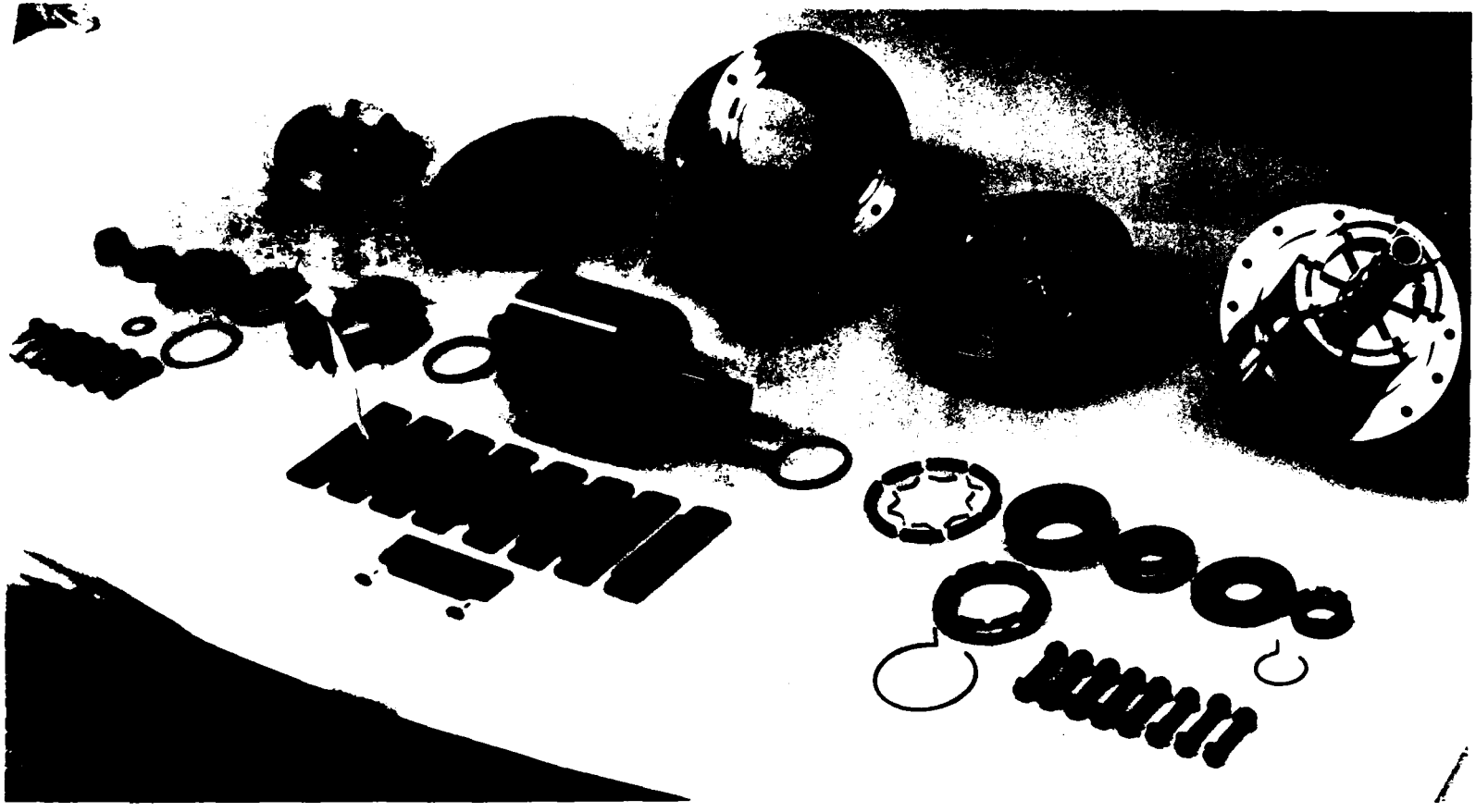

Figure 5. Vane Motor Piece Parts and Major Subassemblies (right view)

Middle Row

Nut
Washer
"G" shim (below washer)
Bearing
"H" shim (below bearing)
Spacer
Split ring
Rotor

Middle Row (Continued)

Split ring
One set of carbon seals and springs
Bearing seat
Ring nut (below bearing seat)
Bearing
Deflector
Nut
Lockwire (below nut)

Bottom Row

Stator to end plate fasteners
Carbon vane assemblies (8)
Carbon vane, 2 slippers and 2 pins (below vane assemblies)
Lockwire, large
Stator to end plate fasteners

The assemblied motor is shown in Figure 6 looking toward the inlet with a portion of the exhaust port visible at the right side of the motor. The opposite orientation showing the exhaust port can be seen in Figure 7.

2. TEST EQUIPMENT (COLD GAS TESTS)

This section describes the test stand, test equipment, and instrumentation employed for cold gas tests conducted with the motor throughout the program. Modifications to the test system for hot gas tests are discussed in Section IV.

3. VANE MOTOR TEST STAND

The vane motor test stand is shown in Figure 8, with the photograph taken from the flywheel end of the test stand. The flywheel is located behind the vertical plate in the front of the photograph. The disc brake caliper is shown near the bottom of the vertical plate, and the tachometer for monitoring the drive shaft speed is located near the middle of the vertical plate. Hydraulic brake fluid for the brake caliper is stored in the small cylinder located in the upper left-hand corner of the photograph. The brake fluid is pressurized with plant air when the remote electrical solenoid valve is energized. Flywheel speed is monitored independently of the drive shaft speed (rotor speed) via a photo cell mounted in the center of the top plate. The photocell detects the passage of a black stripe that is painted on the flywheel. Stall torque is monitored with a load cell that can be partially seen at the extreme right, just below the removable torque arm

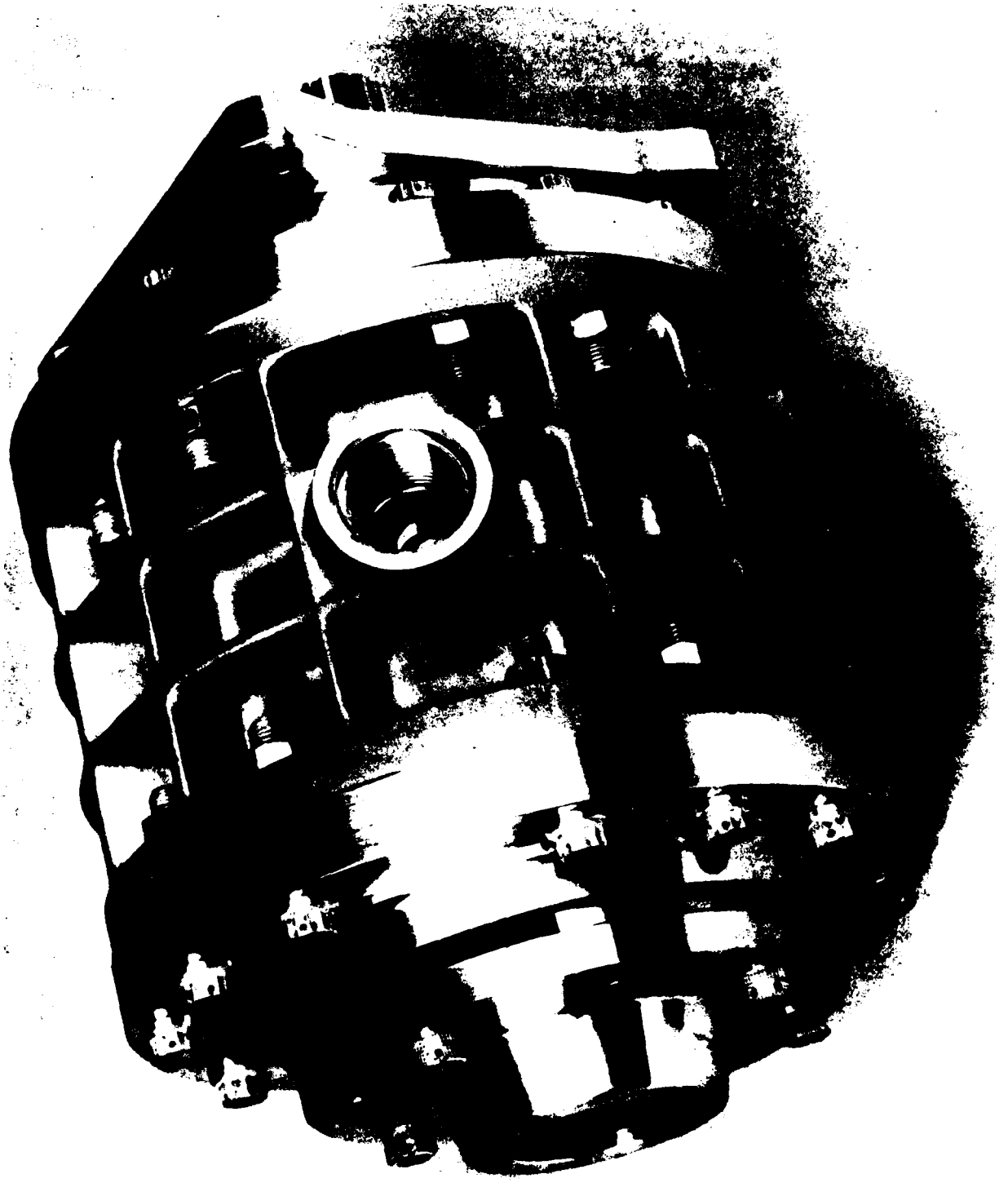

Figure 6. Vane Motor Assembly – Inlet Side

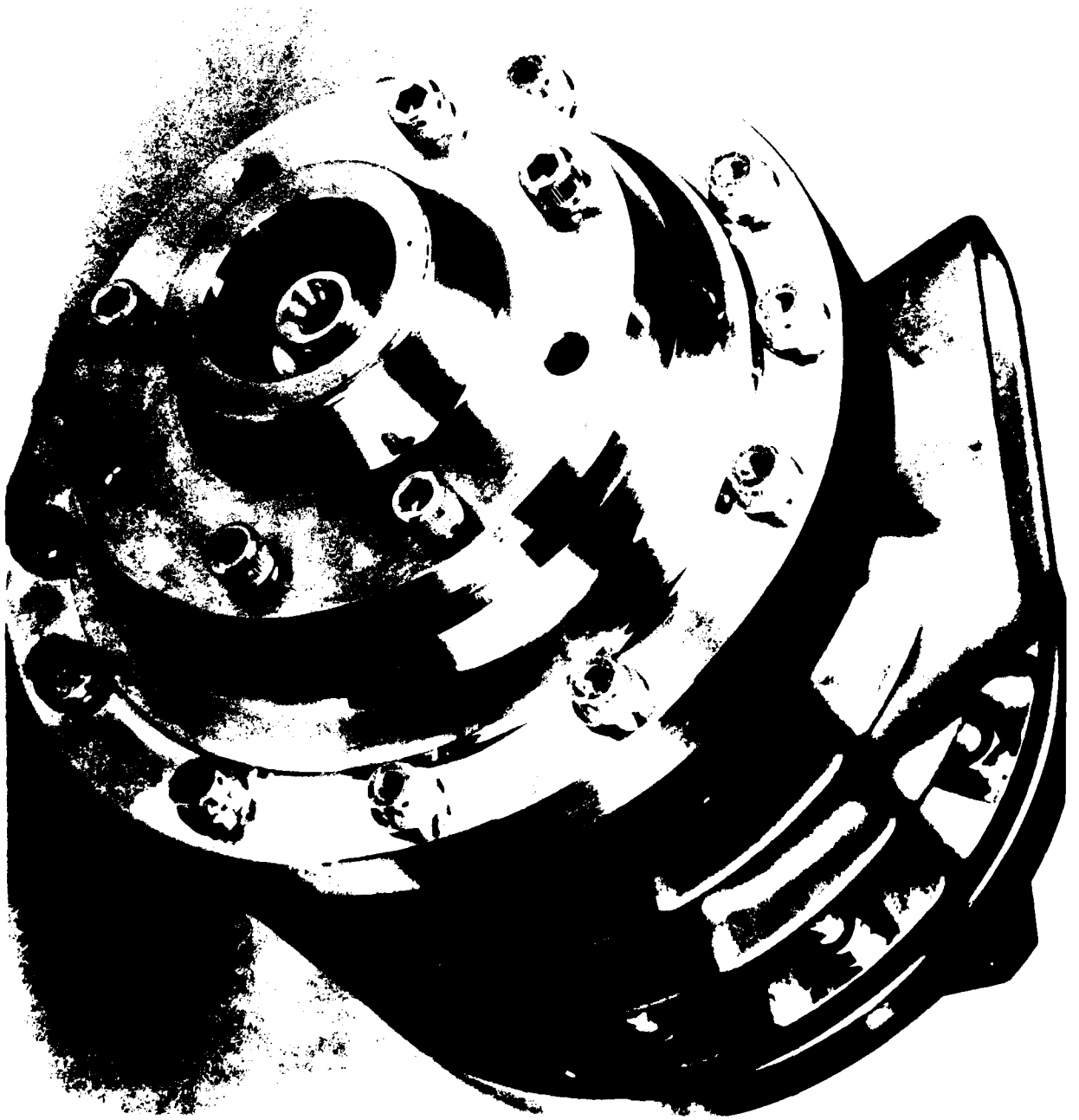

Figure 7. Vane Motor Assembly – Exhaust Side

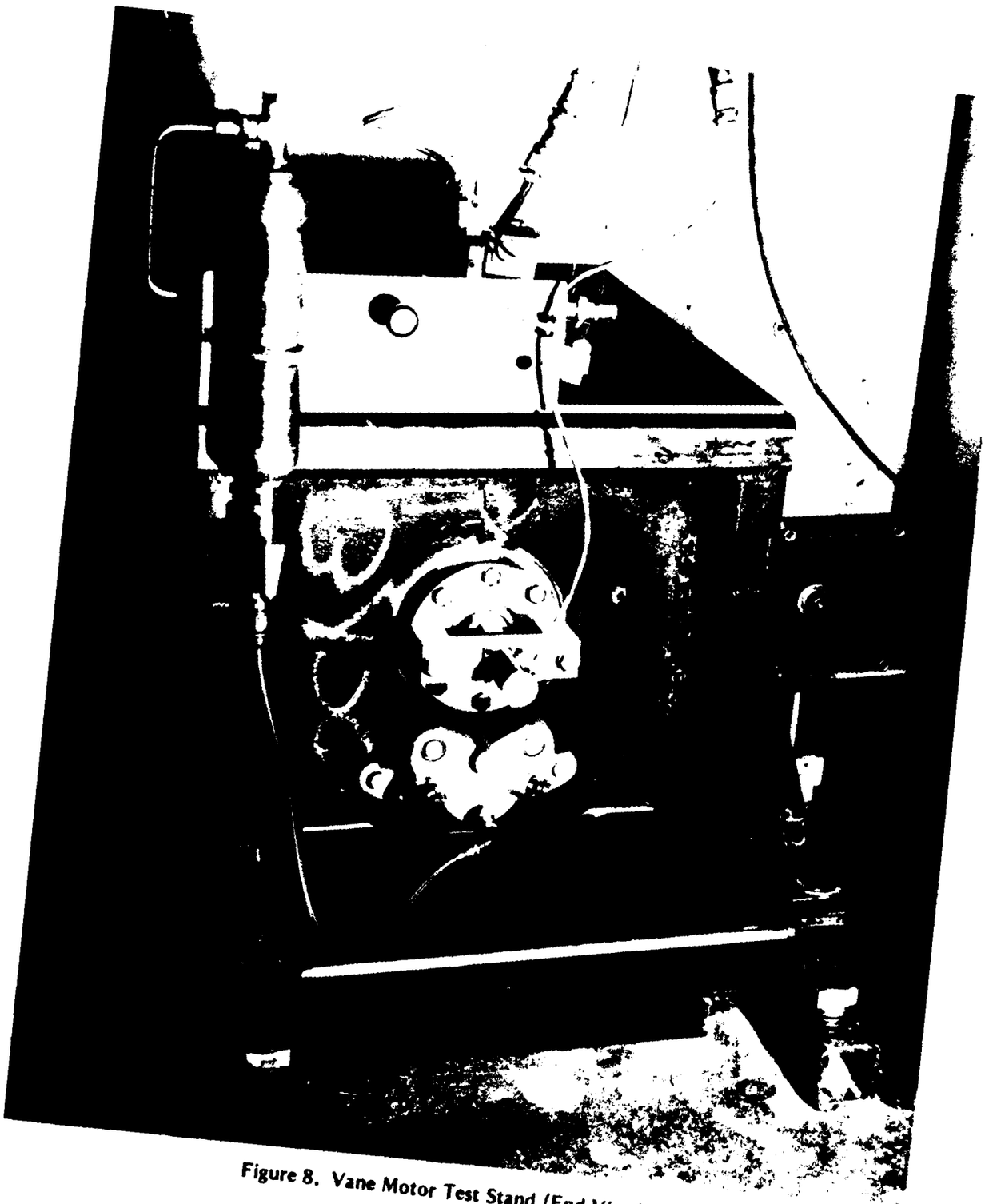

Figure 8. Vane Motor Test Stand (End View)

(projecting horizontally) which is attached to the flywheel when these tests are to be conducted.

A top view of the test stand, with the cover plate removed, is shown in Figure 9. The vane motor is seen at the top. The No. 1 flywheel is in the center, and the disc brake is at the bottom. The partial black stripe (for photocell flywheel speed monitoring) can be seen on the No. 1 flywheel. It should be noted that the No. 2 flywheel can be added for -65°F testing in the space that is available between the No. 1 wheel and the disc brake. The capped fitting in the upper left hand corner of the photograph is the gas inlet line to the vane motor. The vane motor exhaust port is located underneath the motor and is not visible.

4. COLD GAS SUPPLY SYSTEM

The test schematic for cold gas testing is shown in Figure 10. To provide for pressure control during motor spin-up (to control maximum torque) a pressure ramp generator, employing two pressure regulators, was installed. In use the solenoid pressurization valves are opened and initial low pressure is established in the accumulator tank connected to the dome of the high flow capacity main regulator. The valve immediately upstream of the accumulator is ther closed, and the upstream regulator is adjusted to the final desired high pressure. The motor is started at the low pressure previously established in the accumulator. When satisfactory rotation is observed, the intermediate solenoid valve is opened permitting high pressure to build up in the accumulator at a rate controlled by the inlet orifice. This varying pressure applied to the dome of the main regulator produces the desired ramp rate of pressure to the motor inlet. During tests, nitrogen flow rate is measured with a Daniel's type orifice meter located in the supply line.

5. TEST INSTRUMENTATION (COLD GAS TESTS)

Typical instrumentation used during cold gas testing is shown in Table 1.

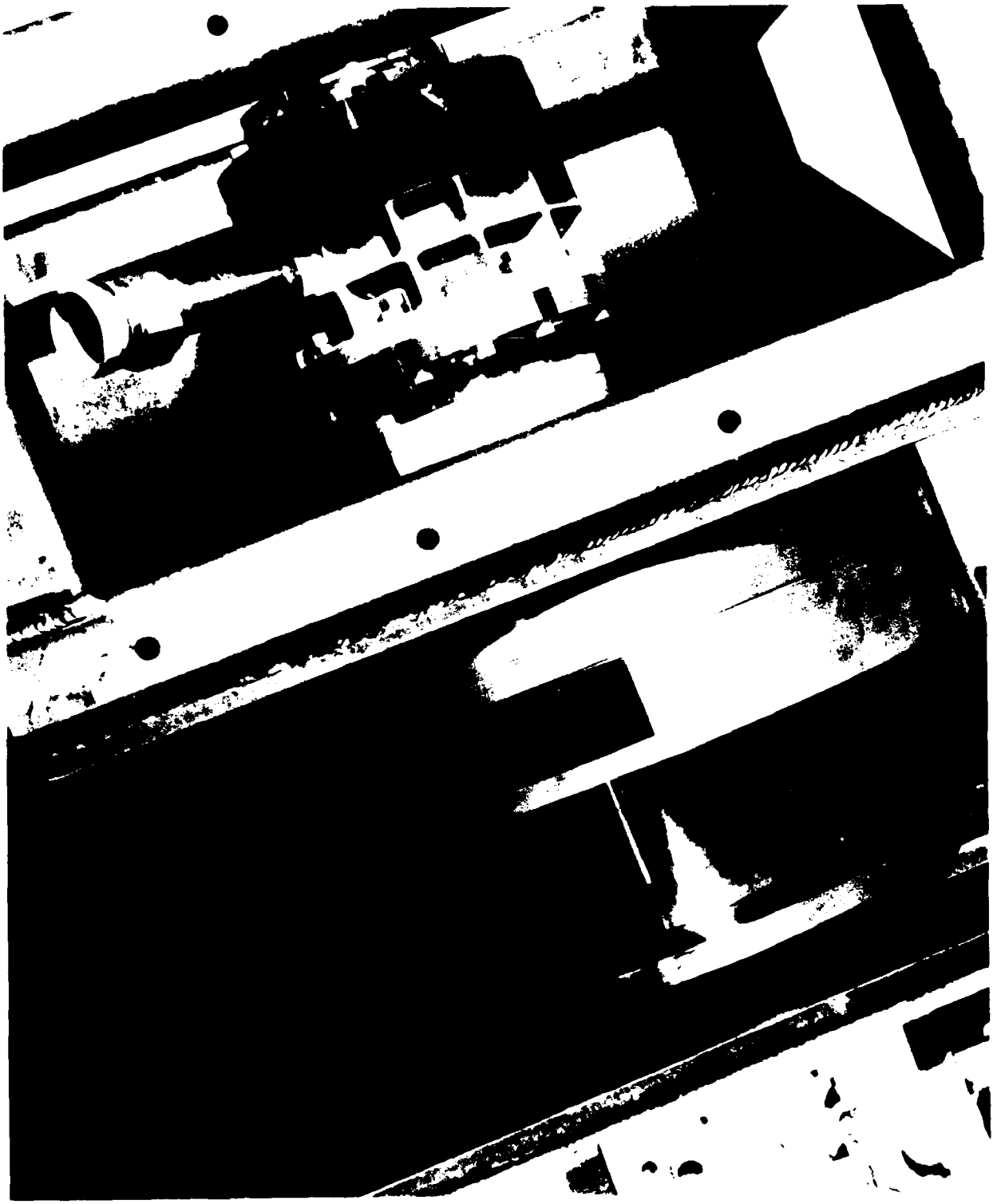

Figure 9. Vane Motor Test Stand (Top View)

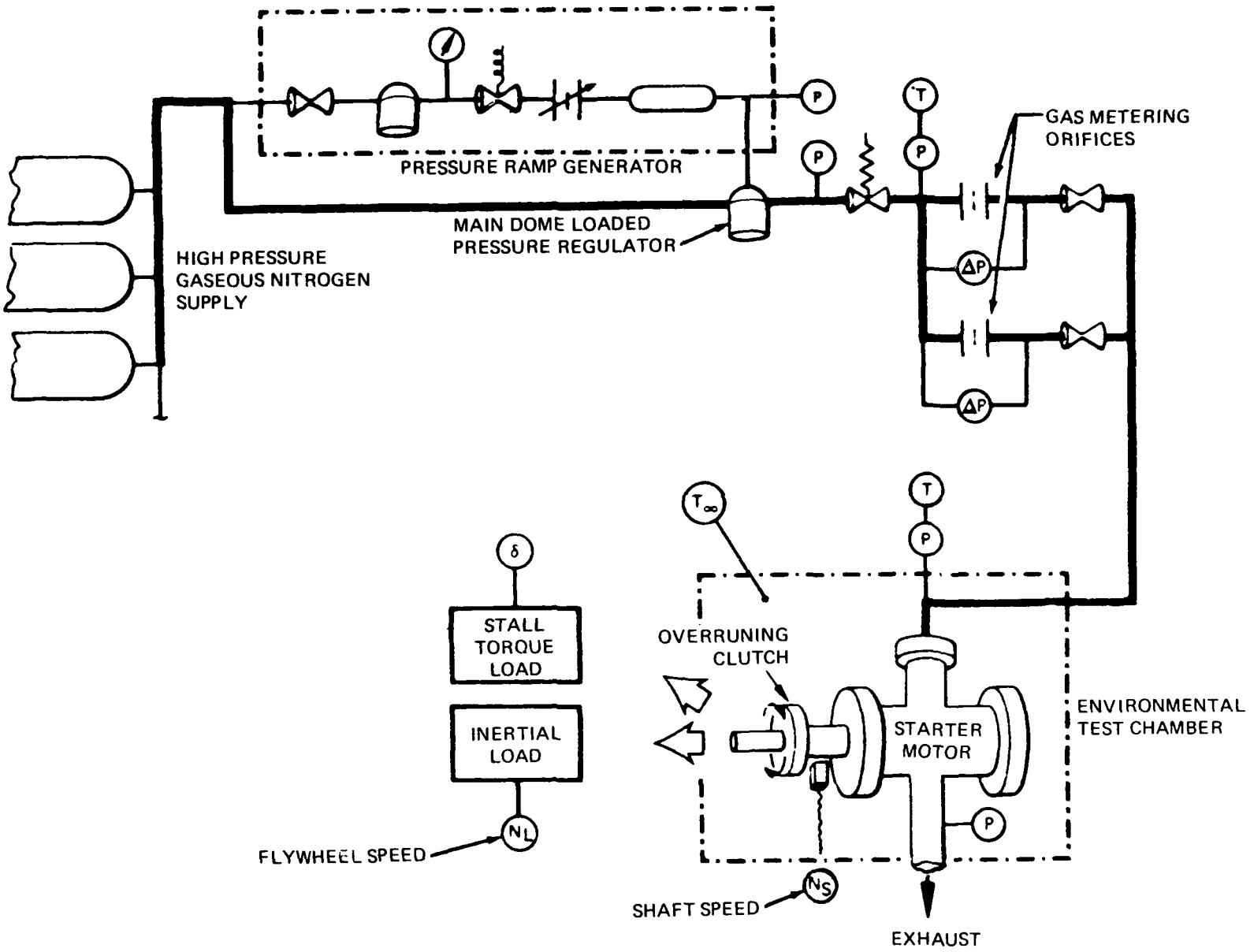

Figure 10. Test Setup – Cold Gas Testing

TABLE 1
INSTRUMENTATION REQUIREMENTS

Symbol	Nomenclature	Record On	
		Strip-Chart	Oscillograph
P_r	Pressurization ramp generator output	X	X
P_s	Nitrogen supply pressure	X	
P_u	Nitrogen flow meter pressure	X	
ΔP_u	Nitrogen flow meter ΔP	X	
P_o	Starter inlet pressure	X	X
P_∞	Ambient pressure	Barometer	Reading
P_{ex}	Starter exhaust pressure	X	X
τ	Stall torque	X	X
N_s	Starter shaft speed	X	
N_l	Flywheel speed	X	
$T_{(s)}$ (various)	Starter component temperature	X	
T_∞	Environmental test chamber temperature	X	
T_{N_2}	Nitrogen supply temperature	X	
T_{gs}	Starter inlet temperature		
T_{es}	Starter exhaust temperature		

SECTION III
COLD GAS TESTING

This section presents the results of cold gas development testing conducted on the vane motor prior to committing the design to hot gas tests.

1. STALL TORQUE TESTING

Run No. 1A -- Stall torque testing was initiated with the No. 1 vane motor with one of the 8 vanes located under the inlet port, per the WPAFB-approved test plan. The inlet pressure was increased incrementally in nominal steps of 100 psig while monitoring stall torque and leak rate. The object of this test was to determine the maximum allowable inlet pressure to avoid exceeding the 120 ft-lb stall torque limit. When the inlet pressure was raised to approximately 1,000 psig, the stall torque was indicating 80 ft-lb. As the inlet pressure was again raised, the stall torque suddenly dropped to zero and the test was terminated.

The starter was disassembled and it was noted that three vanes were broken. After analysis of the problem it was decided that the test procedure (or the test approach) was in error and the stall torque test, as conducted, was not realistic.

In an actual application for APU starting, the vane motor rotor would begin to spin as soon as enough stall torque was developed to overcome the APU breakaway torque. Once the rotor starts to turn, there would be at least three pressurized vane cavities contributing torque with pressure differentials existing between cavities. With the rotor locked in place, as was the case in the initial stall torque test, the primary contributor to stall torque is a single pressurized vane cavity under the inlet port with maximum pressure drop applied across a single blade. As a result of this analysis, the following preliminary conclusions were drawn:

1. The initial pressure applied to a stationary rotor must be limited to a pressure level that is less than 1,000 psi.

2. The most important aspect of the preliminary stall torque testing should be to carefully monitor stall torque as a function of initial rotor angular position to assure that there is no rotor position that will result in a stall torque below the minimum breakaway requirement of the APU which would then result in a start failure.

Run No. 1B -- After the No. 1 vane motor was repaired, the stall torque tests were repeated with the inlet pressure limited to 300 psig at each rotor position. The rotor was

repositioned in 5^{o} steps after each data point. The stall torque varied from 30 to 60 ft-lb (as would be expected), as the rotor was repositioned through a total arc of 100^{o}. The data is shown in Figure 11. From these tests, it was concluded that the stall torque characteristics are acceptable, and that the vane motor pressure ramp starts would not subject a stationary rotor to a pressure that approaches the 1,000-psig blade failure point.

2. INITIAL SPIN TESTS 2 THROUGH 5 (1,000 rpm Limit)

The test program then progressed to spin testing, which was intentionally limited to a maximum rotor speed of 1,000 rpm for the early tests. This test series was conducted with due caution while monitoring the entire test installation to be sure that the system performed satisfactorily and to allow the test crew to gain some experience.

Run No. 2 -- The starter was slowly spun to 60 rpm, the inlet pressure was cut off, and the disc brake operation was verified.

Run No. 3 -- On the next spin, the inlet pressure was limited to 60 psig, and the flywheel was accelerated to approximately 500 rpm. The inlet pressure was shut off, and the flywheel was braked to a stop.

Run No. 4 -- For this test, the inlet pressure was raised incrementally to 60 psi, and the flywheel speed was allowed to reach the 1,000 rpm limit.

Run No. 5 -- In this test, the inlet pressure was rapidly raised to 60 psi as the flywheel speed was being monitored. When the flywheel speed reached 730 rpm, the rotor speed suddenly went to zero. This indicated that the vane motor internal drag had suddenly increased to a value in excess of the 3 ft-lb of torque being developed at the 60 psig inlet pressure.

Teardown inspection revealed that the split ring-to-vane slipper joints had galled badly. It appeared that an improper heat treatment had been used, therefore, new split rings and vane slippers were machined, heat treated, and installed in the motor.

Run No. 6 -- This series consisted of a number of tests with the reassembled motor, as summarized below, incorporating increased inlet pressures.

Runs 6A and 6B -- The vane motor was allowed to spin the flywheel to the 1,000 rpm target speed at low inlet pressure in each of these tests, and the flywheel was allowed to coast to monitor its speed decay rate and determine the flywheel drag. The flywheel drag was found to be negligible in the 0 to 1,000 rpm speed range.

Run 6C -- The APU starter inlet pressure was ramped from 50 to 100 psig during the flywheel acceleration from 0 to 1,000 rpm. Although the time to reach maximum speed was long, the test was encouraging.

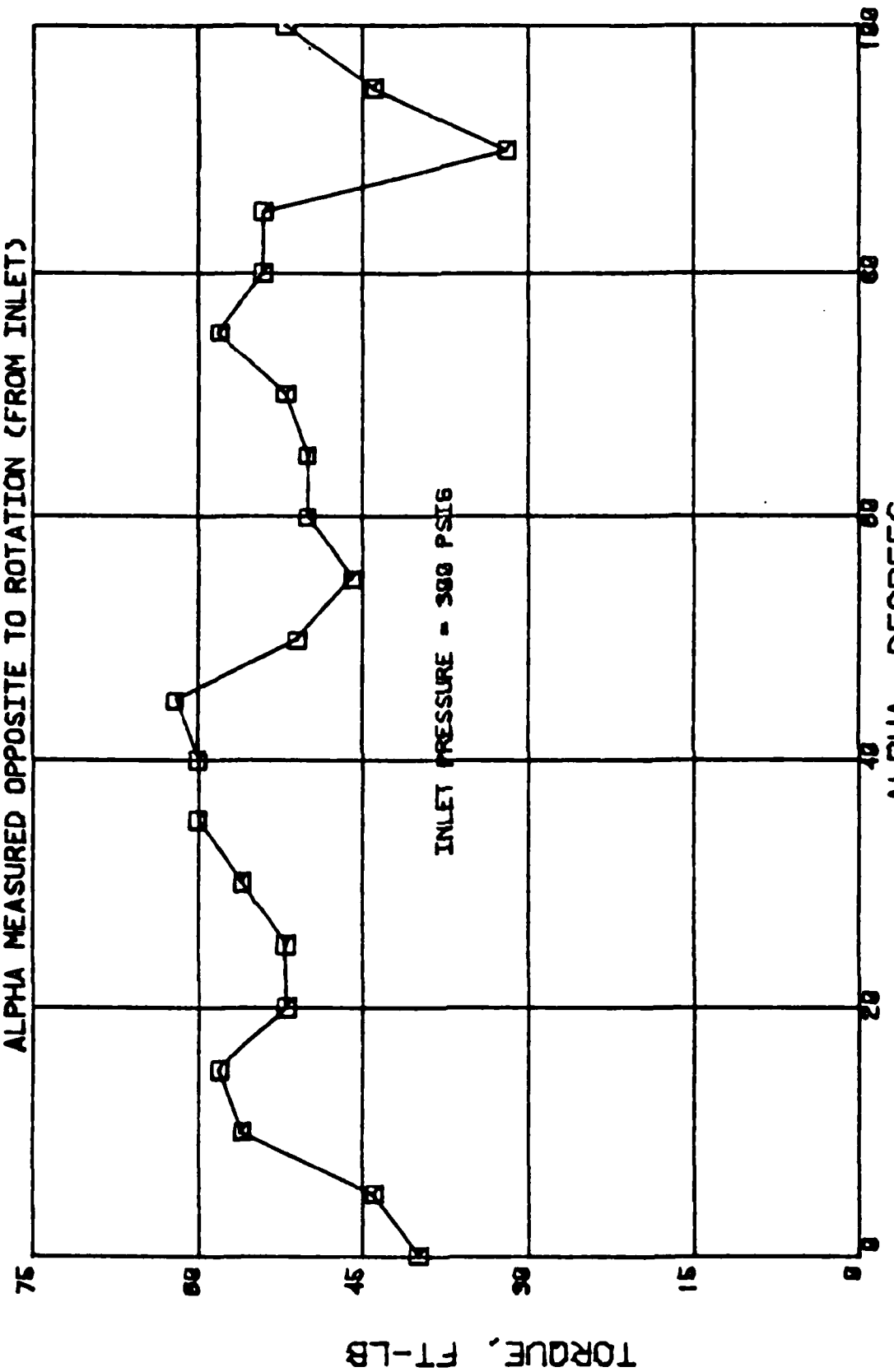

Figure 11. Static Torque Versus Rotation Angle

Run 6D — The APU starter inlet pressure was ramped from 100 to 300 psig during the flywheel acceleration from 0 to 1,000 rpm. The pressure ramp time was again excessive, but the run was successful.

Run 6E -- The APU starter inlet pressure was ramped rapidly from 100 to 300 psig. It was noted that the starter made three revolutions and stopped rotating.

Teardown inspection of the starter revealed one broken blade and galling of the cam surface where the slippers had made contact. This implied sufficient deflection of the split rings to permit the contact. The slippers and the split rings appeared gall free. It was assumed that the width of the "Z" slot in the split rings was excessive, and that the split ring deformed at the slot when at speed, catching the edge of the slipper and breaking the blade.

A new set of split rings were made and installed with the "Z" slot clearance minimized. The No. 1 starter was rebuilt and the spin testing resumed in test sequence 7, discussed in the following paragraphs.

Run 7A -- This run was a low-pressure run to 1,000 rpm to verify that the flywheel drag had not changed. Performance was consistent with the previous checkout run.

Run 7B -- This run utilized a rapid 100 to 300 psig pressure ramp. The flywheel was accelerated to 1,000 rpm in 3.3 seconds. Although the target time to a speed of 1,000 rpm in 0.6 seconds was not attained, this was the best run to date.

Run 7C -- The inlet pressure ramp was changed to 100 to 500 psig for this run, to decrease the time to speed. The flywheel was accelerated to 730 rpm in a time 0.4 seconds faster than Run 7B, but the vane motor stopped at this speed.

Teardown inspection revealed 5 broken blades, and it was assumed that the split ring had deformed again (at the "Z" slot) and caught a slipper.

At this point, the spin testing was terminated and the split ring-to-slipper joint was redesigned. The redesign efforts were concentrated on the split ring. The split ring was modified to a continuous slip ring (having no "Z" slot). The cam bosses on the end plates were redesigned such that the rotor end of each cam boss could be removed to allow the slip ring to be installed in the cam groove. The rotor end of the cam was replaced and retained by screws after installing the slip ring.

These modifications were incorporated into the test hardware which was reassembled for Run 8.

Run 8 -- This test utilized a rapid 100 to 500 psig pressure ramp. The vane motor accelerated to 1,000 rpm in 1.8 seconds (the best performance achieved up to that time), and the acceleration was allowed to continue. The vane motor reach 1,500 rpm in 2.8

seconds and stopped. Teardown inspection revealed that most of the blades had failed at the slipper attachment location.

The vane motor was then rebuilt with modified carbon blades. The slippers were removed from these blades, and the blades were modified at the slipper attachment joint to prevent any contact with the cam (or slip ring) surface.

Run 9A -- The inlet gas-line plumbing was changed to allow the starter gas inlet to be positioned vertically down. This would allow the blades to contact the stator walls near the inlet (by gravity). The main purpose of this modification was to see if the starter could be made to operate without the blade-positioning cam.

The starter was installed with the gas inlet down and the inlet pressure was slowly increased. When the inlet pressure reached 130 psig, the vane motor commenced rotation and accelerated the flywheel to 150 rpm. The test was terminated at this speed.

Run 9B -- A start was attempted with the inlet pressure starting at 130 psig instead of 0. No rotation occurred. The pressure was slowly increased to 200 psig. No rotation resulted. Teardown revealed 3 broken blades.

A review of the test results to this point indicated that the pure carbon blade design concept was not practical due to insufficient strength. A new set of blades was then fabricated from a fiberglass-reinforced phenolic material (typically used in air-operated vane motors) to permit the vane motor to be characterized at higher speeds with cold gas prior to designing new blades for the hot-gas testing in Phase III. The initial test results, from Run 10, with the phenolic composite blades and solid cam ring were as follows:

Run 10A -- The starter was accelerated to 1,000 rpm with low inlet pressure to verify that the flywheel drag was repeatable and that the test stand was functional. Previous results were verified.

Run 10B -- A 100 to 300 psig pressure ramp was applied and the motor was accelerated to 1,000 rpm prior to cutoff.

Run 10C -- The starter was accelerated to 1,000 rpm with a rapid 100 to 500 psig pressure ramp. The starter accelerated to 1,000 rpm in 2.2 seconds.

Run 10D -- The starter was accelerated with a rapid 100 to 500 psig pressure ramp. It was planned to allow the unit to accelerate to the 5,000 rpm terminal speed limit for the first time. The test was terminated at 4,000 rpm when it was noted that the acceleration rate was rapidly diminishing. A teardown inspection revealed a rather odd wear pattern on the reinforced phenolic blades where the blades contact the stator bore. It was assumed that the blade wear was causing high internal drag which, in turn, caused the acceleration rate to decay as the unit approached the 4,000 rpm operating speed.

Tests 11 through 19 involved a number of modifications to the motor in attempts to operate at higher inlet pressure to improve motor acceleration.

Run 11 -- Following a low pressure checkout spin test a test was conducted with a 100 to 1,000 psig pressure ramp. The motor stopped at 289 rpm. Teardown revealed no blade problems, however, the fixed end shaft bearing was in poor condition. The bearings were removed and replaced.

Run 12 -- A low pressure start was again accomplished for system checkout (Run 12A). Run 12B was conducted with a 100 to 1,000 psig pressure ramp. In this run the motor reached 400 rpm and again stopped. The jammed condition was released by manually rotating the flywheel and another start was attempted. Run 12C was conducted by manually increasing the regulated pressure. In this run a speed of 1,150 rpm was achieved at an inlet pressure of 945 psig prior to the motor stopping.

Teardown inspection following these runs revealed that the rotor shaft had galled on the bores through the end plates, most probably due to rotor deflection resulting from the high inlet pressure. The clearance in this bore was increased by 0.020 inches prior to re-assembly of the motor for the next series of tests.

Run 13 -- In this test series the motor was accelerated to 1,000 rpm with ramp pressure increased in 200 psi steps for each succeeding test. The results are summarized in the following paragraphs.

Run 13A -- This run was conducted at low pressure and was run at 1,000 rpm for 116 seconds.

Run 13B -- Pressure was ramped from 100 to 500 psig. The motor continued to accelerate at 1,000 rpm and was permitted to continue up to 5,000 rpm in a total time of 21 seconds.

Run 13C -- The pressure ramp was from 100 to 700 psig for this run. Normal speed increase occurred to 1,000 rpm and the test was terminated.

Run 13D -- Peak ramp pressure in this run was 900 psig. The motor accelerated normally to shutdown at 1,000 rpm.

Run 13E -- The next step was a peak ramp pressure of 1,100 psig. The motor would not initially spin at 100 psig and pressure had to be increased to 200 psig before rotation was noted. Acceleration started but the test was terminated due to decreasing supply pressure. The test was repeated the following day starting at 200 psig and achieved 1,000 rpm, however, motor acceleration rate was low.

Run 13F -- A final test was conducted with a peak ramp pressure of 1,300 psig. The motor did not start and was torn down for inspection. The vanes were found to be

deformed at the contact points with the slip rings. The vanes were reworked in this area and re-installed for further testing.

Run 14A -- This test was a low pressure spin which was successfully accomplished.

Run 14B -- Peak ramp pressure for this run was set at 1,300 psig. A speed of 1,000 rpm was reached in 1 second and the test was terminated.

Run 14C -- A test was attempted with a peak ramp pressure of 1,500 psig. The motor would not spin and was removed for inspection. Excessive wear was noted on the phenolic blades at the tip. The blades were reshaped prior to further testing.

Run 15A -- A low pressure spin test was conducted without difficulty.

Run 15B -- A peak ramp pressure of 1,500 psig was attempted. The motor ran to 1,500 rpm prior to shutdown.

Run 15C -- This test was planned to reach 5,000 rpm at a lower ramp pressure of 1,000 psig. Speed achieved was only 300 rpm when the motor stopped. The motor was disassembled and the original split rings were installed.

Run 15D -- A low pressure spin at 30 psig was accomplished without incident.

Run 15E -- Another attempt to achieve 5,000 rpm was made with 1,000 psig peak pressure. The motor reached a speed of 750 rpm and stopped.

Run 16A -- Prior to conducting this test the solid cam rings were re-installed. Since it appeared that some blade contact had occurred with the cam boss in prior tests, the blades were relieved on either side of the contact point with the cam ring. Thus, even under maximum deflection of the cam ring the blades could not contact the cam boss.

A low pressure spin was accomplished with this configuration.

Run 16B -- The vane motor was successfully accelerated to 5,000 rpm with an inlet pressure ramp of 100 to 1,000 psig. The acceleration time was 18.5 seconds.

Teardown inspection indicated excessive wear and chipping of the blades at the stator rubbing surface accounting for the rather excessive time to reach final speed.

A new set of phenolic blades was fabricated and installed in the motor prior to conducting additional tests.

Run 17A -- A low pressure spin test was conducted with the new blades. No anomalies were observed in the test.

Run 17B -- A pressure ramp of 100 to 1,000 psig was attempted. The run was terminated at 1,000 rpm due to a calibration error on the tachometer resulting in an incorrect speed readout.

Run 17C -- Run 17B was repeated. The motor reached a speed of 300 rpm and stopped. The blade tips were reworked prior to continuing tests.

Run 17D -- The run was repeated and the motor reached 714 rpm prior to stopping.

Run 17E -- For this run the motor was rotated to place the inlet down and a 100 to 1,000 psig pressure ramp was attemped. The motor would not rotate and was removed for inspection.

Run 18 -- For this series the phenolic blades were lubricated with Molycote Z applied as a spray prior to installation. A series of tests was conducted with constant inlet pressure. The plan was to hold the low pressure until a speed of 714 rpm was achieved and then to ramp the pressure to 1,000 psig. In each case the motor stopped before 714 rpm was achieved. The results of each of these tests are summarized below.

Run	Inlet Pressure psig	Maximum Speed rpm
18A	112.0	500
18B	187.5	678
18C	276.0	571
18D	345.0	428

Run 19A -- These runs were conducted with carbon blades made without the metal slippers used in the original design at the contact point between the blade and cam ring. A low pressure spin was conducted without problem.

Run 19B -- A 100 to 500 psig pressure ramp was tried initially with this configuration. A speed of 3,200 rpm was achieved at which point the motor stopped abruptly. Three of the blades were found to be broken on teardown inspection.

For the next series of runs phenolic blades were again used. It had been observed in previous inspections that sliding one of the segmented end seals in its circumferential end slot to the point where it contacted the blade could readily jam the blade in its slot. Very little side load was necessary to do this. Therefore, for this series, the end seals were removed.

Run Nos. 20A through 20E -- Five runs were conducted successfully to 5,000 rpm. Pertinent run data including orifice inlet and motor inlet pressures, orifice pressure differential, gas inlet temperature, time to reach 5,000 rpm from application of ramp pressure, and calculated flow rate are presented in Table 2 together with appropriate configuration data. Where more than one value is listed in the table, the numbers represent peak and end-of-run measurements. Similar data from Run 16B are included for comparison.

TABLE 2
COLD GAS COMPARATIVE PERFORMANCE DATA
(Runs 16A and 20 A—D)

Seq.	Configuration	Orifice Inlet Pressure (psig)	Motor Inlet Pressure (psig)	Orifice Pressure Drop (psid)	Gas Temp. (°R)	Ramp Time to 5,000 RPM (sec)	Gas Flow Rate (lbm/sec)	% Theoretical Flow
16B	● Cast stator ● Phenolic blades ● No vent slots ● Cam slip ring ● End seals in	1,023 P (800 F)	936 P (735 F)	97.6 P (77 F)	515	18.5	1.82 P (1.43 F)	(144.2 F)
20A	● Same as 16B except no end seals	988.5 P (406.5 F)	900 P (369 F)	86 P 33 F	517	34.5	1.68 P (0.67 F)	(132.7 F)
20B	● Same as 20A	1,500 P (1,343 F)	1,377 P (1,208 F)	—	510	9.3	—	—
20C	● Same as 20A	1,467 P (1,260 F)	1,320 P (1,133 F)	—	511	10.5	—	—
20D	● Same as 20A	1,500 P (900 F)	1,395 P (818 F)	— (83 F)	513	12.5	(1.58 F)	(142.9 F)
20E	● Same as 20A	1,490 P (750 F)	1,376 P (698 F)	— (82 F)	509	18.5	(1.393 F)	(146.0 F)

NOTES:

P – PEAK DURING RUN
F – FINAL AT END OF RUN

For all of these runs inlet pressure did not remain constant over the run. To correlate the ramp time to 5,000 rpm with inlet pressure, average pressures were used with the results shown in Figure 12. A curve fit of the Run 20A-D data was performed (also including 16B) with the results plotted on the figure.

Data from Run 20E was not included in the curve fit since blade wear was excessive after this run with an effect that is obvious in the plot. Run 16B is consistent with the results of the Run 20 series. This indicates that the end seals may produce forces on the blades leading to breakage or poor motor performance but do not contribute major friction drag to retard motor acceleration.

Run 21 -- The results without the end seals indicated that they might have been a contributor to previous breakage of the carbon blades. A test was therefore conducted with a set of carbon blades without slippers and with the end seals removed to evaluate this possibility. The notched cutouts in the carbon blades (where the slippers were normally installed) were also eliminated thus increasing the material thickness to that of the full blade to provide more strength in the area of contact with the cam ring.

The motor started to accelerate but as the pressure ramp to 1,000 psig was applied the blades again broke near the cam interface while at a speed of approximately 500 rpm.

Run 22A -- For this test series a set of two component blades was fabricated and installed in the vane motor. A base section of 440 C material was designed to transfer the cam load more uniformly into a pure carbon insert. A checkout run was conducted successfully at low pressure.

Run 22B -- This test with the two component blades resulted in failure of two blades at the stator interface at the end of the starter opposite the output shaft. The test was encouraging from the standpoint that the starter acceleration was of the order of 62.8 rad/sec^2 with an inlet pressure ramp of only 100 to 500 psig, a higher acceleration rate than previously accomplished. The vane motor achieved a speed of 2,600 rpm prior to failure. Teardown inspection revealed the omission of a bevel on the corner of the metallic base section. The square corner could ride on the corner radius between the cam boss and end plate, increasing the effective blade stroke to the point that the blade would jam on the stator.

Run 23A and B -- The metal carrier sections were modified, and a second test series was conducted. After a successful low pressure spin the vane motor accelerated to a speed of 4,500 rpm and stopped abruptly. All 8 blades were found to be broken at the stator interface on the output end of the rotor.

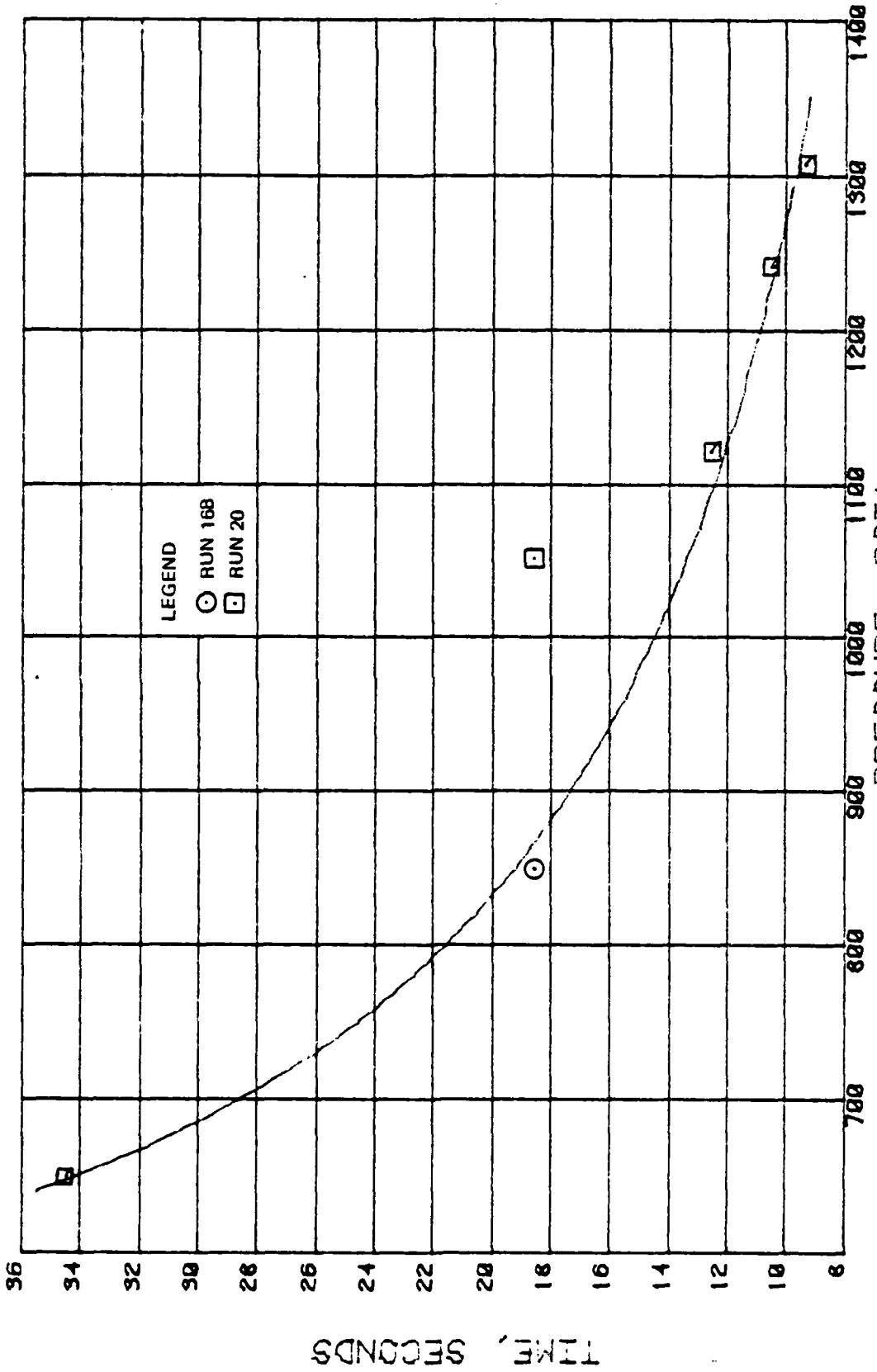

Figure 12. Time to Reach 5,000 rpm Vs. Inlet Pressure (Run 16B and 20A–D)

Runs 24A and B -- A new set of carbon blades was fabricated with a different type contour in an attempt to eliminate the breakage occurring at the blade-to-stator interface. The sharp corners of the rotor slots were radiused slightly to distribute the local stress into the blade at the rotor edge. A low pressure checkout spin was successful. In the second attempt, this configuration accelerated well with a pressure ramp of 100 to 500 psig to a speed of 3,600 rpm and stopped abruptly. Inspection revealed 3 broken blades, again at the stator interface.

Run No. 25 -- Problems in these tests led to a series of tests without cam rings. In their place, springs were installed under each blade to position the blade against the stator. No end seals were installed.

The first test was conducted with phenolic blades and leaf springs fabricated of 1095 carbon steel strips 0.020-inch thick by 0.188-inch wide, The spring installation is shown in Figure 13. The springs were made as long as possible and crescent shaped to attempt to produce the 0.462-inch travel required.

The spring travel turned out to be approximately 0.4 inch, which was adequate for blade positioning during the low-speed starting sequence. It was assumed that centrifugal force would assist in positioning the blades against the stator as the rotational speed increased. On assembly, these springs appeared to be too stiff, and the vane motor was very difficult to rotate by hand. The starter broke one blade at the spring slot when the rotor speed reached 1,700 rpm. It was also apparent that the blades had contacted the cam bosses.

Run No. 26 -- New phenolic blades were fabricated and the spring width was reduced 50 percent to weaken the springs. The new blades and springs were installed and it was noted that the starter was still very difficult to rotate by hand. With a 100 to 500 psig pressure ramp, motor speed increased to 500 rpm and stopped. Teardown revealed that a spring had come out of its slot and jammed a blade. No blades were broken.

Run No. 27A and B -- To eliminate the potential for loss of the spring from its slot, an additional modification was made. A small cutout was added at the closed end of the spring slot in the blade. The spring was brazed to a small pin which would retain the spring in the blade slot.

A slow speed run was conducted successfully. In Run 27B, application of a 100 to 500 psig pressure ramp resulted in a speed of 1,475 rpm at which point the motor stopped. In this case, six of the eight blades were broken.

Analysis of the spring-loaded blade failures indicated that the blades were failing due to being driven into the base of the rotor slots by the large pressure differential

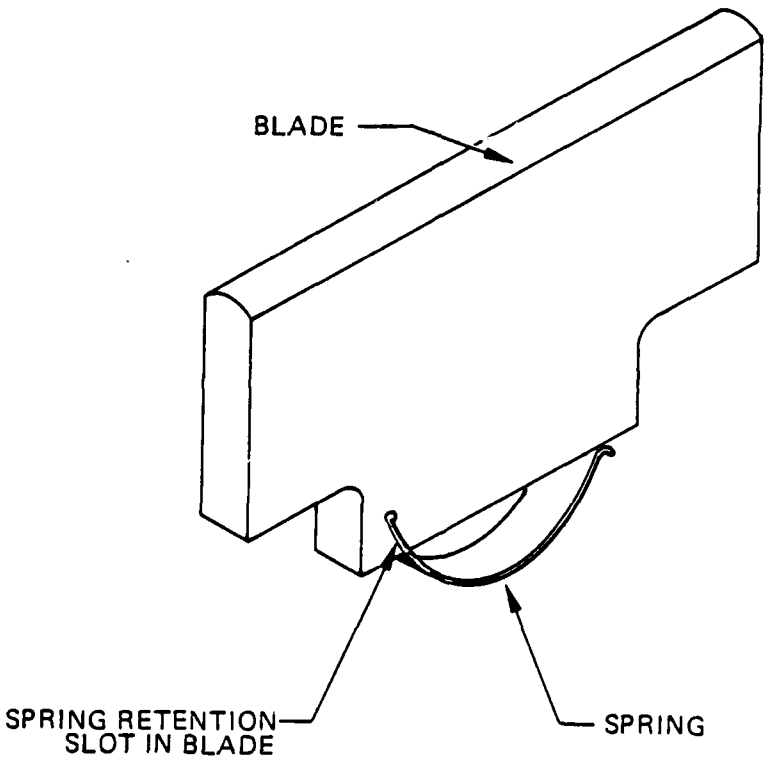

Figure 13. Spring-Loaded Blade Assembly

applied between the tip end of the blades and the pressure on the base of the blade at the bottom of the rotor slot.

Run No. 28A -- This test sequence was conducted with blades that were vented to provide a path to conduct pressure from the tip to the base of the blade to reduce the pressure differential. New phenolic blades were fabricated as shown in Figure 14 and installed with a new set of the lightest version springs. The blades were positioned with the slots on the back side relative to the direction of rotation. No cam rings or end seals were installed.

A pressure ramp of 90 to 420 psig was applied and the motor accelerated to 1,785 rpm at which point the test was terminated.

Run No. 28B -- The blades were reversed in the slots to put the vents on the forward side and the test was repeated. A pressure ramp from 90 to 420 psig produced slow acceleration and the test was terminated at 360 rpm.

Run No. 28C -- The blades were installed in the original orientation of Run 28A for a re-test. An attempt to reach 5,000 rpm was made with the 90 to 420 psig pressure ramp. The motor got to 3,300 rpm at which point the acceleration rate was decaying and the run was terminated. Two blades were broken at the spring slot as well as numerous springs.

Runs 29A through C -- It was assumed that the blade venting was favorable, since the rotational speed at failure had nearly doubled.

A new set of phenolic blades was then fabricated. These blades were vented and shaped to allow cam actuation to be used for blade positioning in lieu of the springs.

Again, preliminary tests verified that the starter accelerated best with the vent slots positioned on the back of the blades, as noted in tests up to a rotor speed of 2,500 rpm.

A test was conducted to attempt the full 5,000 rpm, with the cam-positioned vented blades. The acceleration rate was low at higher speed and the test was terminated at 4,200 rpm. The blades were removed and the tips were reconditioned. A final test was conducted with the vented blades and a 100 to 1,000 psig pressure ramp achieving a ramp time to 5,000 rpm on the order of 14 seconds.

Teardown revealed two blades chipped on the high pressure side of the tips. Minor damage to the cam was also noted.

Runs 30 through 30B -- For these tests the blades from the previous run were employed. Additional 0.5-inch diameter vent holes were drilled through the blades. The intent was to provide pressure balance on opposite sides of the blade within the slot.

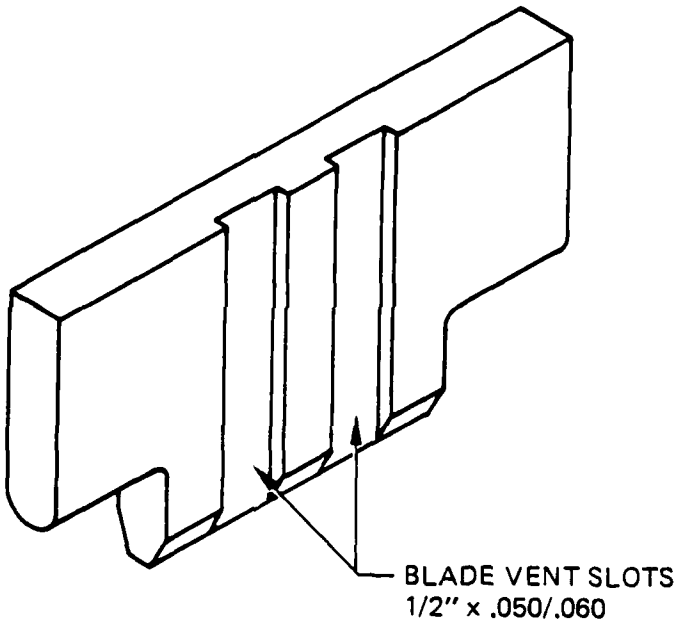

Figure 14. Phenolic Blades with Vent Slots

These holes were located within the vent slots (as shown in Figure 14) with their centers 0.5 inch from the base of the blade.

Tests were conducted to a speed of 2,500 rpm with pressure ramps of 100 to 500 and 100 to 1,000 psig. For the final test a pressure ramp of 10 to 1,000 psig was applied and the motor was allowed to continue to accelerate. At 4,500 rpm some roughness was noted in the speed trace and the test was terminated at a speed of 4,640 rpm.

Comparison of these runs with those of test series 29 revealed a lower acceleration rate, thus the vent holes did not result in an improvement in performance.

Test sequences 31 through 39 were conducted with a set of pyrolytic carbon blades fabricated by Hitco. Using the results of the previous tests, the blades were vented on the back side and set up to operate with the cam-positioning system. Again, no end seals were installed. Eight successful tests were conducted as summarized in Table 3, and described in the following paragraphs.

The latter two tests in the series were conducted after pre-conditioning the motor to the minimum and maximum operating temperatures (-65 and +130°F). Performance data for these runs as well as Runs 38 and 39 are presented in Table 4. Time to achieve 5,000 rpm versus average inlet pressure for Runs 31 through 37 is plotted in Figure 15.

The vane motor was disassembled after Runs 31, 32, 35, 36, and 37. These inspections revealed no damage at the blade-to-cam interface, after 8 runs.

Teardown inspection, after run 31, indicated that two of the blades showed a minor delamination of the reinforced pyrolytic material at one end of each blade on the high pressure side of the blade near the stator interface. The delamination on one blade chipped off during the second run.

TABLE 3

SPEED VERSUS TIME SUMMARY, RUNS 31 THROUGH 37

Run No.	Pre Test Starter Temp. (°F)	Pressure Ramp (psig)	Terminal Speed (rpm)	Time to Speed (sec)
31	50	100/500	5,000	14
32	50	100/1000**	5,000	7.6
33	50	100/1250**	5,000	6.6
33A	50	100/1250**	5,000	5.9
34	50	100/1250	5,000	5.8
35	50	100/1200	5,000	6.3
36	-65	100/1200	5,000	6.6
37	+130	100/1200	5,000	6.4

**Not constant, decayed during run.

TABLE 4
PERFORMANCE SUMMARY, RUNS 31—39B

Seq.	Configuration	Orifice Inlet Pressure (psig)	Motor Inlet Pressure (psig)	Orifice Pressure Drop (psid)	End Cavity Pressure (psig)	Gas Temp. (°R)	Ramp Time to 5,000 RPM (sec)	Gas Flow Rate (lbm/sec)	% Theoretical Flow
31	• Cam ring • Carbon composite blades vented on back side • Cast stator • No end seals	528	486	47.5	170 (S) 92 (E)	500	14.0	0.897	98.9
32	Same as 31	981 (S) 848 (E)	908 (S) 785 (E)	93.5 (S) 80.0 (E)	305 (S) 152 (E)	500	7.6	1.70 (S) 1.47 (E)	101.5 (E)
33A	Same as 31	1,217 (S) 930 (E)	1,127 (S) 855 (E)	114 (S) 94 (E)	372 (S) 170 (E)	495	6.6	2.11 (S) 1.67 (E)	105.0 (E)
33B	Same as 31	1,247 (S) 1,200 (E)	1,145 (S) 1,095 (E)	116 (S) 111 (E)	362 (S) 218 (E)	492	5.9	2.24 (S) 2.15 (E)	105.3 (E)
34	Same as 31	1,256	1,152	116	368 (S) 230 (E)	495	5.8	2.24	104.9 (E)
35	Same as 31	1,167	1,065	108	320 (S) 210 (E)	492	6.3	2.09	105.2 (E)
36	Same as 31	1,229	1,128	114	180 (S) 112.5 (E)	526	6.4	2.13	108.3 (E)
37	Same as 31	1,193	1,095	111	180 (S) 109.5 (E)	535	6.4	2.06	109.7 (E)
38	Same as 31	DATA NOT REDUCED							
39A	Same as 31 except end seals installed	1,190 (S) 1,043 (E)	1,113 (S) 825 (E)	113 (S) 91 (E)	—	517	3,860 RPM in 3.1 sec	2.11 (S) 1.773 (E)	120.5 (E)
39B	Same as 39A	1,229 (S) 975 (E)	1,125 (S) 885 (E)	114 (S) 97 (E)	—	499	4,930 RPM in 5.9 sec	2.19 (S) 1.803 (E)	110.4 (E)

NOTES: (S) START OF RAMP; (E) END OF RAMP.

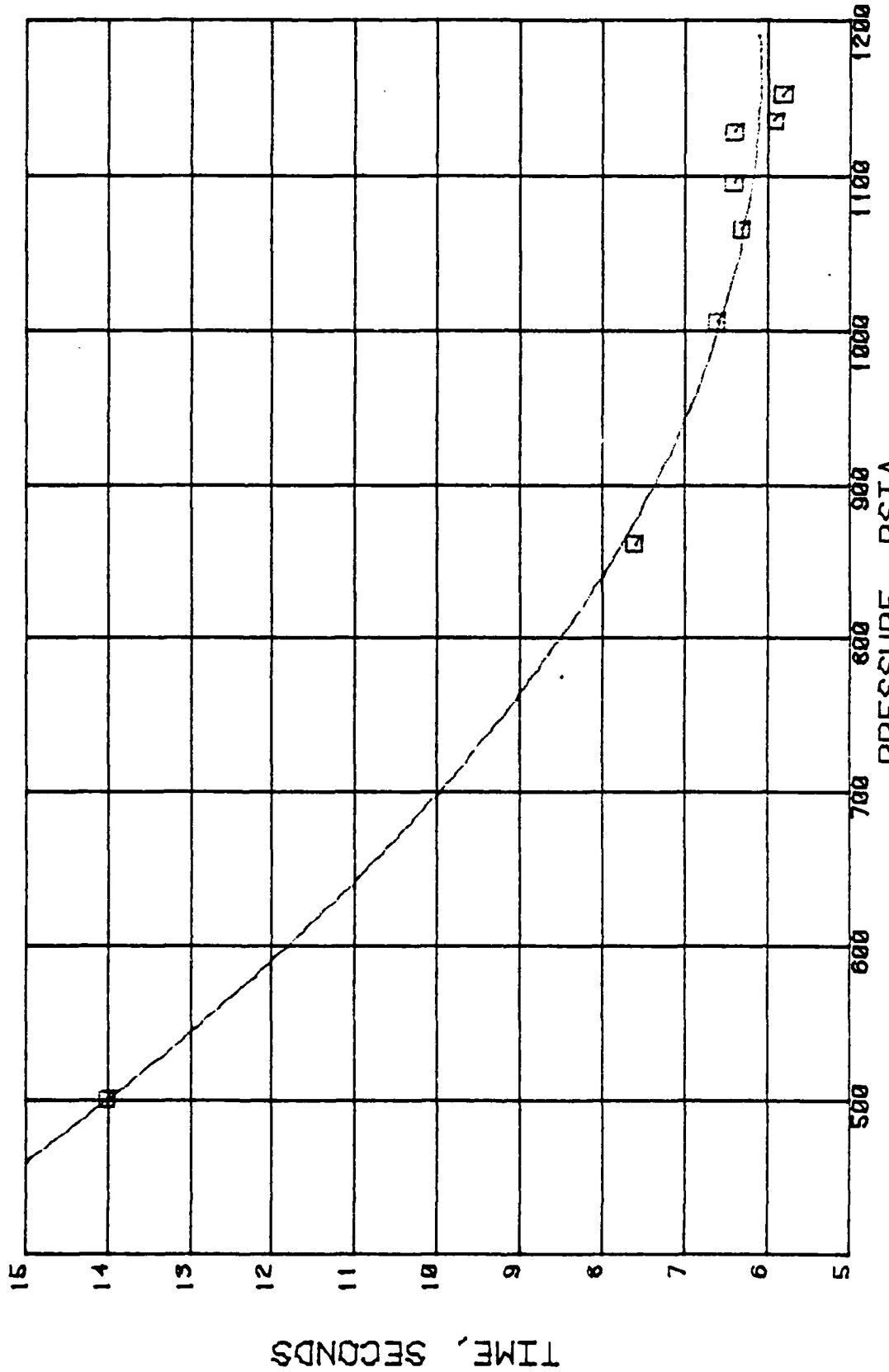

Figure 15. Time to Reach 5,000 rpm Vs. Inlet Pressure (Runs 31 through 37)

Teardown inspection after Run 36 indicated that 6 blades had chipped near the center of the blades (in the area between the vent slots) at the stator interface where the blades pass over the exhaust port in the stator. The blade chipping noted was minor, and no change in the operation of the vane motor was noted.

Run No. 38 -- This was a single run to 5,000 rpm for the specific purpose of recording the sound of the motor in operation.

Runs 39A and B -- A final test series was conducted with the same blades but with the end seals installed. The first test with a 100 to 1,200 psig ramp reached 3,860 rpm in approximately 6 seconds but the inlet pressure decayed rapidly and the test was shut down. A second attempt reached 4,928 rpm in 12.5 seconds but again the inlet pressure decayed badly.

The successful results of these tests concluded Phase II of the program and preparation for Phase III, Hot Gas Testing, was begun.

SECTION IV
HOT GAS TESTING

This section presents the results of initial hot gas testing, cold gas tests conducted to evaluate problems, motor redesign, blade material evaluations and analytical studies leading to successful demonstration of performance requirements with hot gas.

1. TEST FACILITY MODIFICATIONS

The test setup of Figure 10, employed for cold gas testing, was to be utilized for hot gas testing with minimum modifications. The resulting setup is shown in Figure 16. A fuel supply tank, on-off control valves, flow measurement equipment, and a gas generator together with appropriate instrumentation were added to the basic test system. The pressure ramp feature was retained, however its function was now to provide a controlled pressure input to the fuel tank.

A 3-liter fuel system was installed in the left side of the environmental chamber, as shown in Figure 17. Temperature-conditioned fuel is supplied to the gas generator/vane motor through the flex hose shown.

The assembled gas generator was to be attached to the flex hose and installed in the chamber (on the right-hand side of Figure 17), along with the vane motor. After temperature conditioning the vane motor would be removed from the chamber and installed in the test stand. Starter removal and installation can be done rapidly, preventing major shifts in the conditioned temperature.

Figure 18 shows the gas generator after the first system check-out firing without the vane motor. The gas generator had been mounted, temporarily, on the test stand structure for this test. The fuel-control valve is located just upstream of the gas generator, behind the mounting bracket. Hot gas leaves the gas generator, turns 90°, and exits through a small nozzle attached to the hot gas discharge tube. (The nozzle was used to simulate the back pressure of the vane motor for checkout testing.) Hot gas temperature and pressure was measured just upstream of the nozzle with the thermocouple and pressure transducer noted.

2. INITIAL HOT GAS TESTING

Using the results of Phase II testing, initial hot gas tests were conducted with cam-operated reinforced pyrolytic blades incorporating vent slots on the high-pressure side of the blade. The results of these tests are summarized in the following paragraphs.

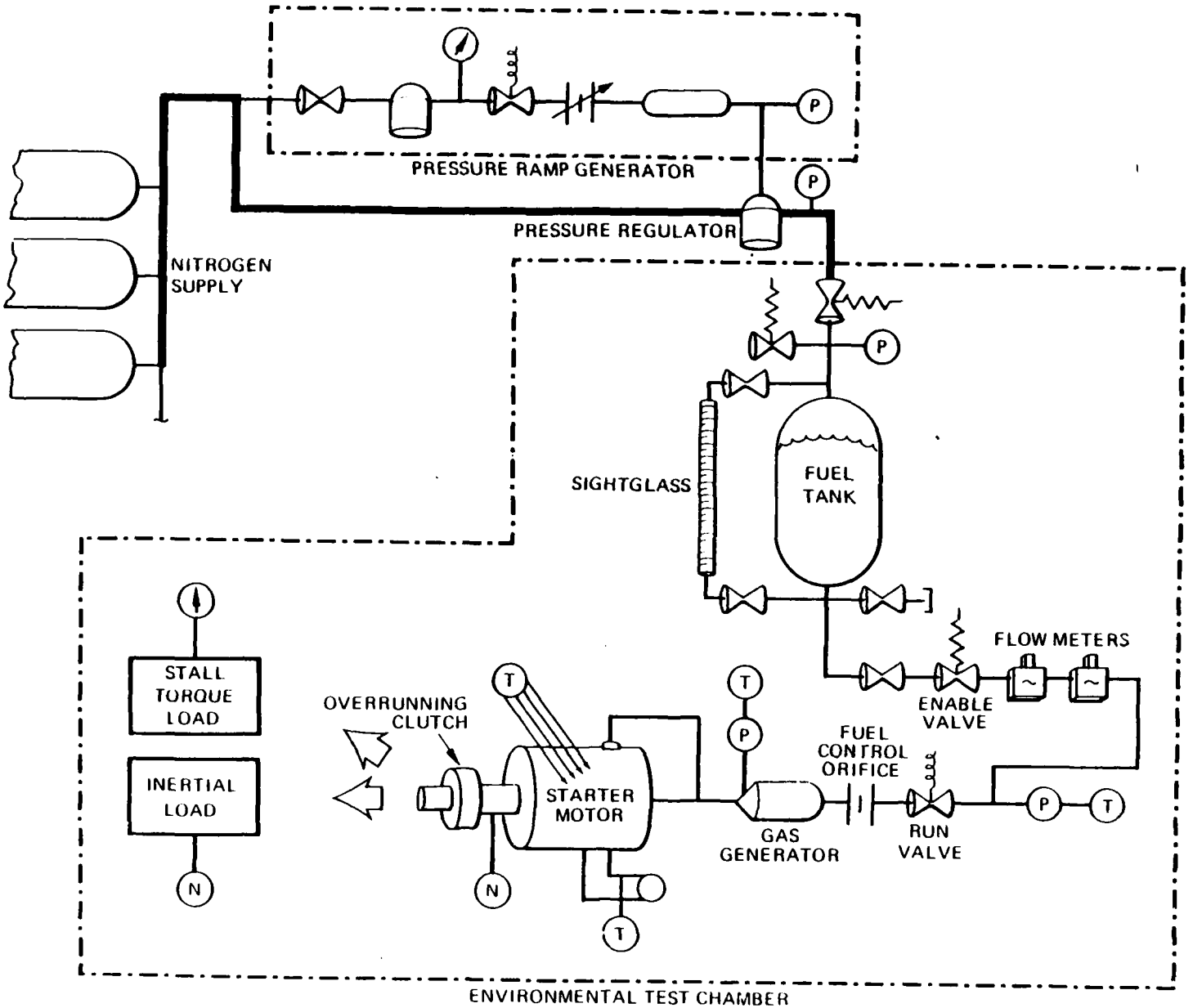

Figure 16. Test Setup – Hot Gas Testing

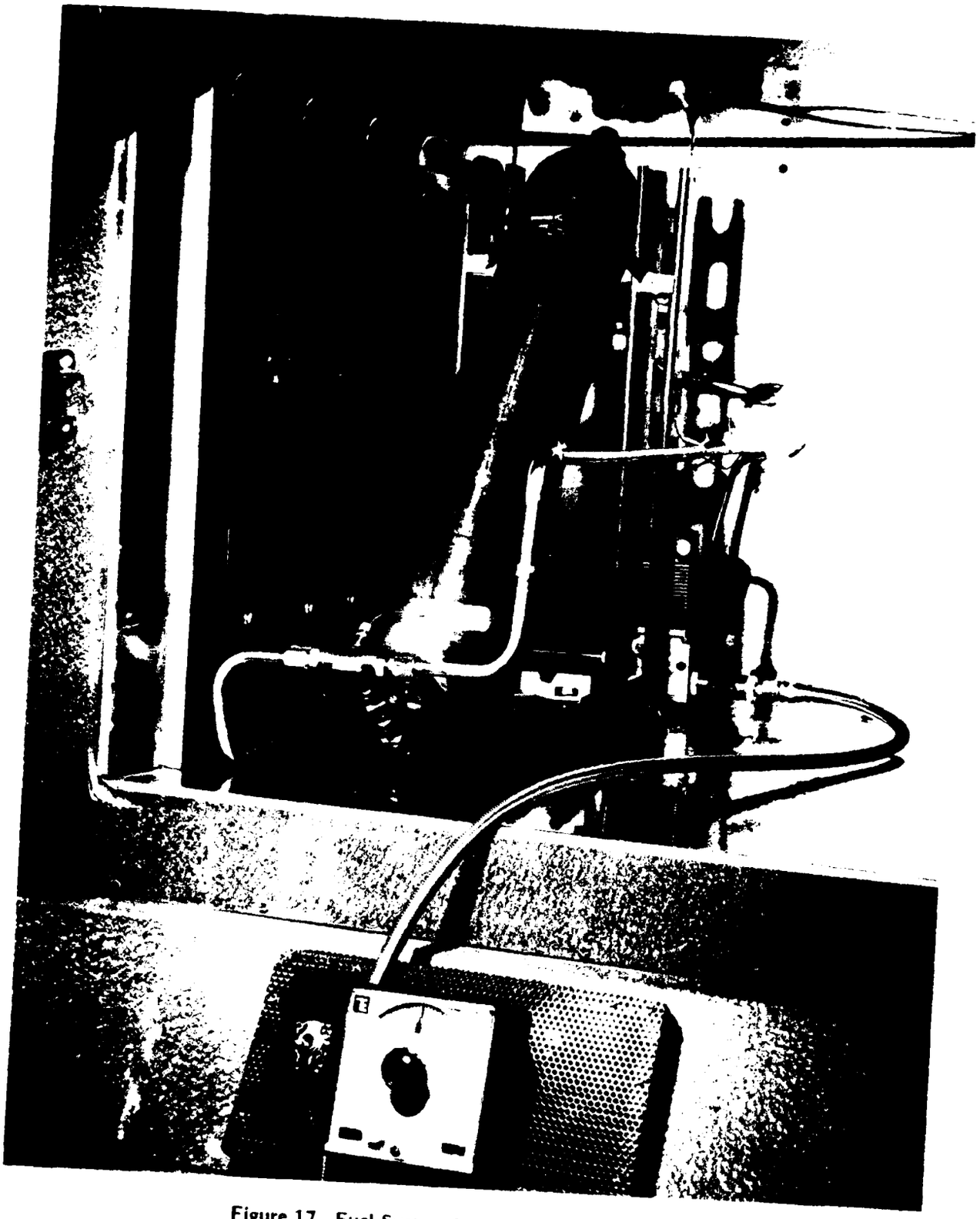

Figure 17. Fuel System Installation in Conditioning Oven

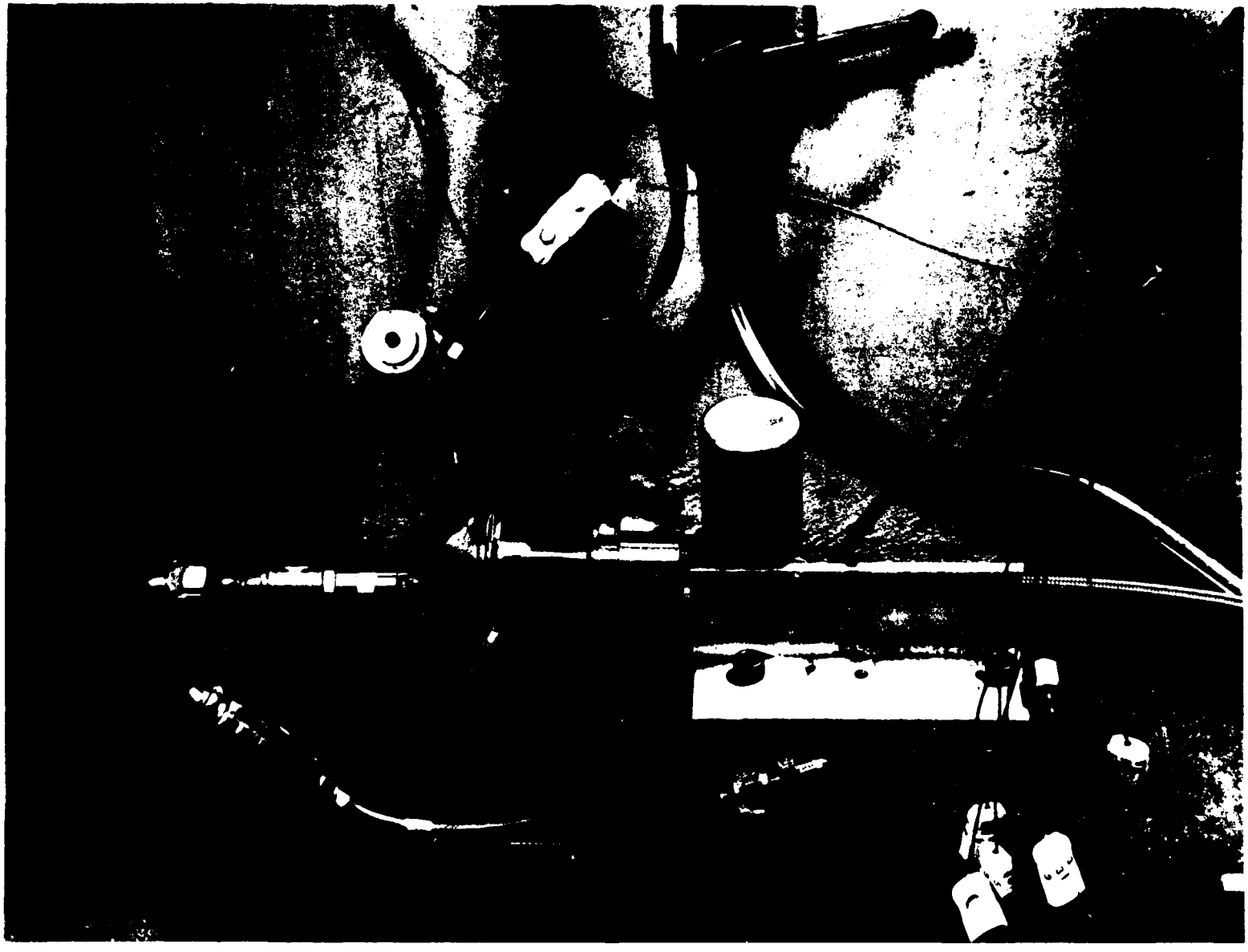

Figure 18. Workhorse Gas Generator

Tests H-1 and H-2 -- These tests consisted of checkout firings with the gas generator to calibrate fuel system pressures. This was necessary to assure that the motor would not be over-pressurized in initial test.

Test H-3 -- The plan was to accelerate the starter to an intermediate speed (1,000 to 2,000 rpm) with a low inlet pressure. The vane motor did not spin initially, and an attempt was made to increase the inlet pressure as the time progressed, with no spin occurring. The starter was disassembled, and it was noted that the rotor had contacted and galled the end plates.

Test H-4 -- The inlet pressure was raised and a second attempt was made to accelerate to 1,000 to 2,000 rpm. Starter rotation initiated, but the starter stopped by itself at a rotation speed of 750 rpm. Teardown inspection indicated that axial rotor growth had once again caused dragging at the end plates.

Test H-5 -- Prior to conducting the third test, the clearance between the ends of the rotor and the end plates was increased by shimming the end plates out to increase end clearance by 0.010 inch. The starter accelerated to 570 rpm and stopped abruptly. Again, rotor-to-end plate contact was observed.

Test H-6 -- The sharp corners at both ends of the rotor were beveled to try to provide more clearance at the areas that appeared to be contacting the end plates and the 0.010 shims were reinstalled as in run H-5. The starter accelerated this time to 1,050 rpm and stopped.

Test H-7 -- The starter was reassembled with 0.020-inch shims between the stator and the end plates. The starter stopped at 570 rpm during the fifth run attempt. The starter was disassembled, and an extensive dimensional check was conducted. The problems appeared to be related to deformations that had occurred in the stator casting. The stator end-plate mounting surfaces were no longer flat. The stator itself was deformed, allowing the end plates to cock relative to the bore of the stator. The stator from the second vane motor (which had never been tested) was dimensionally checked and found to be in tolerance. The blades had not changed appearance during the five initial hot tests; however, they had not yet been exposed to a full speed test.

Test H-8 -- Testing was resumed after the stator had been machined to re-establish rotor/stator concentricity and careful assembly to assure adequate clearance between the rotor and the body components. The starter accelerated to 70 rpm and stopped. Teardown revealed that the rotor had again contacted the output end plate. Additional extensive inspection revealed that the stator had once again deformed.

Test H-9 -- Prior to conducting this test, the original stator was removed and the new stator that had not been used was installed. The starter was then tested and accelerated up to a shaft speed of 3,430 rpm. The test was terminated when it was noted that the rate of change of rotor speed was approaching zero.

A review of the test data from this run indicated that the hot gas inlet pressure to the vane motor was low, 570 psig, as opposed to the 1,000- to 1,100-psig target.

Test H-10 -- The vane motor was allowed to cool to local ambient temperature after the run, and the subsequent test was then conducted at a higher gas generator fuel system pressure to increase the starter hot gas inlet pressure. The starter accelerated to 3,400 rpm at a faster rate than that noted during the H-9 hot gas test, but the test was terminated when the rotor acceleration rate again approached zero.

After run H-10 was completed and the test area was cleared for entry, an attempt was made to rotate the starter by hand (while hot). The starter could not be turned by hand.

Teardown inspection of the vane motor revealed that the rotor had contacted both the output end plate and the stator. Rotor contact had resulted in heavy metal deposition on the end plate and minor metal deposition at one place on the stator at the circumferential location where the rotor-to-stator clearance is minimal.

Samples of the metallic depositions were removed from the rotor, stator and the output end plates. These samples were then examined by photomicrograph and scanning electron microscope techniques. The investigations revealed that the depositions were Waspalloy, and it was concluded that the depositions were the result of inertia welding due to the loss of clearance between the rotor and the stator body.

Test H-11 -- The starter was repaired and re-assembled after Test H-10. The starter was then operated with the same increased rotor-to-endplate clearances that had been used for the previous hot run, using cold gas to power the starter, to assess the effects of increasing the clearance values.

Starter acceleration was noted to be substandard, and the test was terminatd at a rotor speed of 2,400 rpm. Teardown inspection revealed two things:

a. All of the blades were extensively damaged at the stator interface.

b. Four of the blades had been accidently installed backwards, with the vent slots positioned toward the low pressure of the rotor slot instead of the high pressure side.

Test H-12 -- The motor was rebuilt with the five best blades from the previous run and three new blades. A cold gas run with a 200/1,200 psig pressure ramp was conducted resulting in very slow acceleration to 1,000 rpm at which point the test was terminated.

Consideration was given to the possibility that deflection of the stator under maximum pressure was allowing gas to leak past the blade tips resulting in excessive gas consumption.

Theoretically, (with zero leakage) the gas consumption rate would be a linear function of rotor speed starting at zero (with zero rotor speed) and increasing to a maximum value at a rotor speed of 5,000 rpm. The actual gas consumption characteristics noted during previous cold gas tests was essentially constant and independent of speed.

This can be considered to be the result of parallel flow through two or more orifices. Leakage flow can be considered as a fixed orifice. The motor volumetric flow rate in parallel with it represents, in effect, an orifice which increases in equivalent area with time. Thus, as speed increases, more of the flow goes through, rather than around, the motor.

The excessive gas flow was tolerable during cold gas tests. In hot gas firings, the additional energy input resulted in loss of clearances and ultimate galling of motor surfaces. Increasing the end clearances resulted in higher leakage flow and greater thermal expansion, a self-defeating approach. It became necessary to address leakage flow at this point if hot gas performance was to be improved.

3. SPECIAL TESTS WITH NEW STATOR

The distortion problems observed with the cast stator led to a series of special tests with a heavy wall stator machined from a solid bar of Hastelloy C.

The inlet port size and location was identical with the cast stator. Problems observed with blade wear in prior runs appeared to be related to the localized position of the outlet port in the center of the stator. For the new stator, a pattern of holes was staggered across the full length of the stator to distribute wear evenly over the blades.

A special pressure tap was added through the end plate to measure pressure near the cam boss (equivalent to an average pressure felt at the base of the blades). The test was set up using carbon composite blades in the vented configuration (vents on the back), the cam ring, and no end seals. Performance data for Runs R-1 through R-7 are shown in Table 5.

Run No. R-1 -- For the first test, conducted with nitrogen gas, a baseline test was run for comparison with tests using the cast stator. As in previous tests, no end seals were installed. Initial angular acceleration was 79.2 rad/sec^2, however the rate decayed to 36.7 rad/sec^2 as the final speed of 2,164 rpm was approached. Inlet pressure ranged from 1,095 to 1,110 psig over the run. Gas pressure in the end cavity peaked at 240 psig at low speed,

TABLE 5
PERFORMANCE DATA — COLD GAS TESTS WITH HEAVYWEIGHT STATOR

Seq.	Configuration	Orifice Inlet Pressure (psig)	Motor Inlet Pressure (psig)	Orifice Pressure Drop (psid)	End Cavity Pressure (psig)	Gas Temp. (°R)	Max Speed, RPM (Ramp Time, sec)	Gas Flow Rate (lbm/sec)
R-1	• Carbon composite blades with vents on back side • Heavyweight stator • Cam ring • No end seals	1,143	1,095	60	250 (S) 190 (E)	511	2,190 (6.0)	1.516
R-2	Same as R-1	NO MOTOR SPIN						
R-3	Same as R-1 except pinned end seals installed	1,146	1,089	57	248 (S) 190 (E)	508	2,160 (9.0)	1.483
R-4	Same as R-3	NO MOTOR SPIN						
R-5	Same as R-3 except bearing vents plugged	1,130	1,092	54	275 (S) 260 (E)	509	640 (1.6)	1.433
R-6	Same as R-5	1,130	1,100	56.8	279 (S) 212 (E)	505	2,280 (8.75)	1.475
R-7	• New blades • Same as R-6 except inlet port moved 20° in direction of rotation	1,128 (S) 930 (E)	1,038 (S) 848 (E)	125 (S) 114 (E)	330 (S) 191 (E)	515 (S) 512 (E)	2,200 (7.0)	2.2 (S)(I) 1.9 (E)(I)

NOTES:
(S) START OF RAMP
(E) END OF RAMP
(I) ΔP TRANSDUCER FITTING LEAKING, DATA NOT VALID

and dropped to 190 psig at the end of the run. This pressure drives leakage flow out through the shaft-to-end plate clearance and overboard through the bearing vents.

The total gas flow rate was decreased from previous typical values of 2.17 lbm/sec. (Reference: Average of Runs 34 and 35 shown in Table 4 which bracket the inlet pressure for this run) to 1.516 lb/sec, a reduction of 28 percent.

This reduction in flow rate is accompanied by an increase in ramp time. The comparative runs 34 and 35 had ramp times of 5.8 and 6.3 seconds respectively to 5,000 rpm while this run achieved only 2,190 rpm in 5.7 seconds.

A correlating factor between the reduced acceleration rate and lower gas flow rate tended to confirm the theory of stator deflection. Bowing of the cast stator at the center on the high-pressure side of the motor permits gas leakage past the blade tips, since the straight blade does not seal on the bowed surface. This leakage produces higher pressures in the downstream cavities than would normally occur. The pressure, in turn, acts on the larger exposed blade area to produce increased torque. Thus, reduction in internal leakage should result in reduced torque and slower acceleration, as observed in this test.

Run No. R-2 -- A second test was attempted but the motor would not turn.

Run No. R-3 -- For the third test, the end seals were installed and pinned at the center such that their edges could not rub on the blades and prevent free motion in the blade slots. The acceleration rate after the ramp to maximum pressure peaked at 39 rad/sec^2 and decayed to 16.5 rad/sec^2 as the final speed of 2,150 rpm was approached.

The effect of the end seals was apparently only to increase drag. The seals had no measurable effect on the end cavity pressure, and total gas flow was essentially unchanged from the previous run (approximately 2 percent lower).

Run No. R-4 -- A repeat run was attempted but again the motor would not start.

Run No. R-5 -- The next tests in this series were conducted with the external leak path through the bearings blocked and the end seals removed. The first attempt was unsuccessful with the motor stopping at 700 rpm. Teardown revealed a locknut on the output bearing had loosened and rubbed on the bearing end plate. A lockwire was installed to prevent recurrence of this problem.

Run No. R-6 -- During this test, the maximum acceleration rate at startup was 38.7 rad/sec^2, consistent with the previous test, while the final rate was 21.8 rad/sec^2. For this run, as expected, end cavity pressure increased above that measured in the previous two tests to a maximum at startup of 280 psig and an end-of-run value of 212 psig versus 280 and 190 psig for Run R-1. The relatively small percentage change in flow rate (5.5 percent reduction) compared to Run R-1 indicates that the majority of the leakage is not

overboard through the bearing vents, but rather bypasses the motor internally. Leakage occurs via two major routes. The first is the gas flow path from a high pressure source at the rotor surface to the bottom of a blade via the vent slots in the blade. The gas travels in the rotor slot parallel to the rotor centerline and exits in the area of the cam boss. Leakage also occurs from high-pressure cavities along the surface of the rotor out into the end cavity. The leak flows combine in the end cavity and then flow back into a low-pressure cavity on the opposite side of the motor where they exit through the exhaust port without doing useful work. In fact, if the exhaust back pressure is raised in any significant amount a retarding torque is developed.

Run No. R-7 -- The inlet porting on the bar stock stator was modified and one additional cold gas test was conducted. The original inlet port was plugged, and a new port was machined 20° down stream to a point 55° from the minimum clearance position of the rotor to the stator. This modification was done to evaluate the effect of placing the inlet port such that two blades would always be located between the inlet port and the exhaust port, to evaluate the possibility that a portion of the inlet flow was reverse flowing past the first blade and directly out of the exhaust port.

The test results shown in Table 5 indicate that this phenomenon does not occur. Starter acceleration was similar to that obtained in previous testing. The gas flow rate increased in this test as also reflected in increases of the maximum and end-of-run cavity pressures to 330 and 260 psig, respectively. This effect may be explained by the fact that the new inlet port flows into a motor cavity of larger cross section increasing motor volumetric consumption per revolution. This leads, in turn, to an easier path for the high pressure gas flow into the end cavity, raising the cavity pressure.

4. STARTER REDESIGN -- PUSH-ROD ACTUATION

To achieve a more positive blade-to-stator contact and thereby reduce internal leakage, a redesign was accomplished wherein pairs of pushrods were installed between opposing pairs of blades. These replaced the cam actuation system and the cam bosses were removed from the end plates. To accommodate the geometrical length change of approximately 0.030 inch (the difference between the stator diameter and the chord across the stator through the rotor center at $\theta = 90^{\circ}$) the pushrods had to be designed to be spring loaded. For initial testing with cold gas, a pair of O-rings stacked in the center section between the movable halves of each pushrod, as shown in Figure 19, provided the necessary spring force.

Tests were conducted with phenolic blades without vent slots. Performance data for Runs R-8A through R-13 are shown in Table 6.

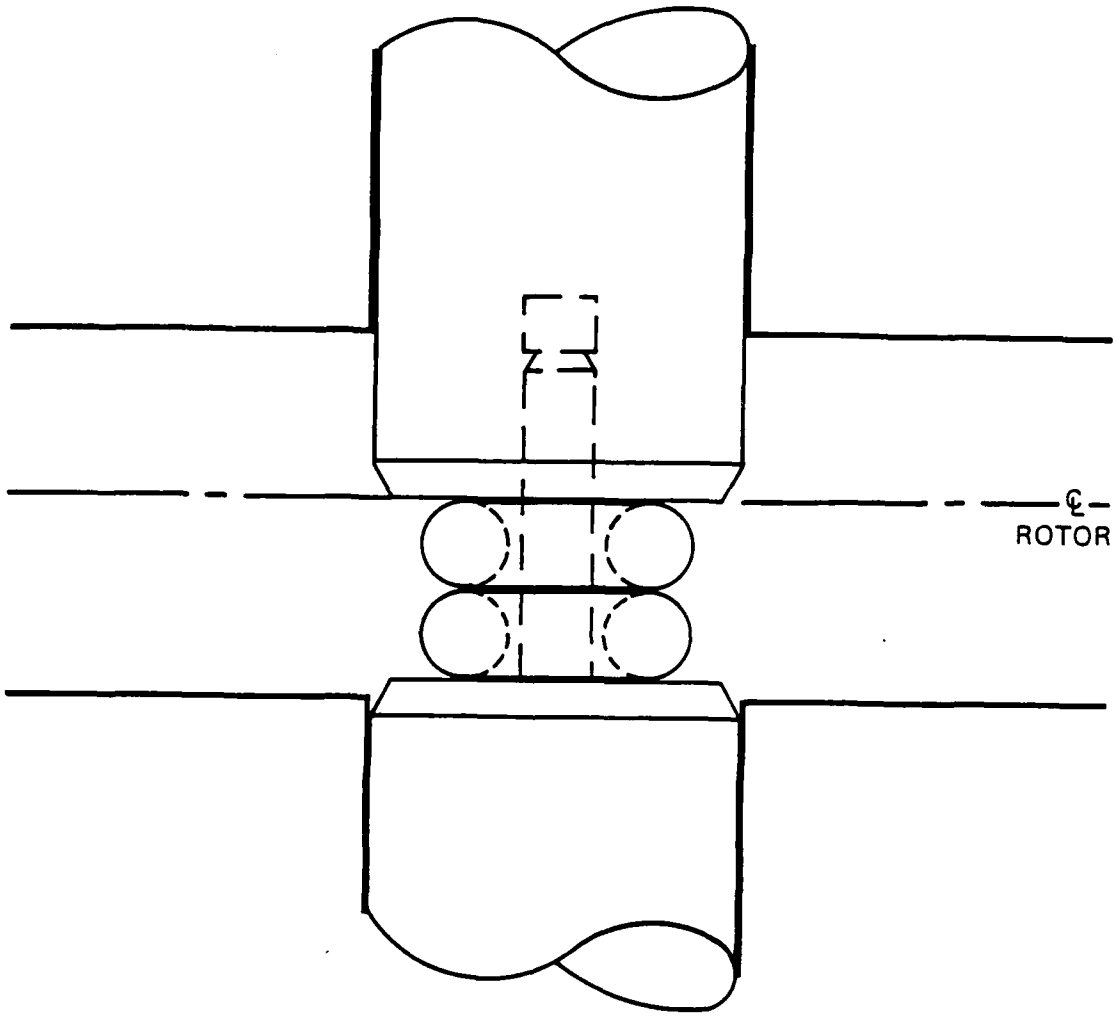

Figure 19. Length—Compensated Pushrods Using O-Rings

TABLE 6
PERFORMANCE DATA WITH PUSHRODS
(RUNS R-8A THROUGH R-13)

Seq.	Configuration	Orifice Inlet Pressure (psig)	Motor Inlet Pressure (psig)	Orifice Pressure Drop (psid)	End Cavity Pressure (psig)	Gas Temp. (°R)	Max Speed, RPM (Ramp Time, sec)	Gas Flow Rate (lbm/sec)	% Theoretical Flow
R-8A	● No end seals ● Phenolic blades ● No vent slots ● Pushrods (O-ring loaded) ● Heavy weight stator ● 235° inlet	1,152	1,063	127	318 (S) 255 (E)	516	2,000 (2.0)	2.203	96.2
R-8B	Same as R-8A	1,122	1,040	127	305 (S) 250 (E)	515	2,000 (2.0)	2.177	96.9
R-8C	Same as R-8A except 215° inlet	1,143	1,100	74	250 (S) 190 (E)	514	2,000 (2.8)	1.678	113.5
R-9	Same as R-8C	1,167	1,100	71.6	261 (S) 147 (E)	509	5,000 (7.8)	1.676	112.3
R-10	Same as R-8C except pinned end seals installed	1,140	1,080	74.6	228 (S) 160 (E)	507	5,000 (8.35)	1.695	115.2
R-11	Same as R-8C except carbon composite "zip weave" blades	1,152	1,110	78.6	—	521	370 (0.6)	1.725	117.3
R-12	Same as R-11	1,125	1,062	98	249 (S)	514	286 (0.56)	1.916	134.2
R-13	Same as R-11 except metal blades with carbon inserts	1,128	1,073	81	—	521	3,500 (4.95)	1.733	121.8

NOTES: (S) START OF RAMP; (E) END OF RAMP.

Runs R-8A and R-8B -- Two runs were conducted with the downstream inlet port location (235° position). Inlet pressure range was 1,115 to 1,020 psig on the first run and 1,140 to 1,065 psig on the second run. Both tests achieved 2,000 rpm in 2 seconds.

Run R-8C -- A test conducted with gas supplied at the original inlet position (215° inlet) and 1,130 to 1,080 psig inlet pressure reached a speed of 2,000 rpm in 2.8 seconds. Gas flow rate was calculated as 1.68 lbm/sec. The increased time and decreased flow rate were consistent with the previous tests of port locations.

Run R-9 -- A full-duration test was conducted using the 215° inlet port, achieving a speed of 5,000 rpm in 7.8 seconds. This represented a significant improvement over the best previous time (9.3 seconds, Ref. Run 20B per Table 2) achieved with phenolic blades. The gas flow rate was 1.68 lbm/second. This result was also achieved with lower inlet pressure (1,100 psig versus an average of 1,308 psig for Run 20B).

Run R-10 -- A final test with phenolic blades was conducted with the end seals re-installed and pinned in place. With an inlet pressure of 1,080 psig, the time to reach 5,000 rpm was 8.4 seconds slightly worse than without the seals. Calculated gas flow rate was 1.70 lbm/sec, again indicating the lack of effectiveness of these seals.

Runs R-11 and R-12 -- Two tests were conducted with a new design of carbon-composite blade incorporating a three-dimensional weave in an attempt to eliminate minor chipping and delamination at the tips which had occurred in previous tests. In both of these tests, conducted without end seals, the motor accelerated to approximately 300 rpm and stopped. Teardown revealed in each case that these blades had broken.

Run R-13 -- In an attempt to solve the problem of inadequate blade strength, a multi-part blade was designed. The assembly consisted of three layers of stainless steel spot welded together. Cutouts in each of the outer layers were provided for graphite inserts to provide low friction contact surfaces on the sides and at the tip of the blade. A test conducted with the metallic blade configuration was unsuccessful, with blade failure occurring at a speed of 3,500 rpm. Teardown inspection indicated that the failure was due to delamination of the blades. This failure released the carbon-rubbing blocks which then jammed the motor.

5. MOTOR MODIFICATION FOR IMPROVED END SEALS

The results of the cold and hot gas tests conducted up to this point in the program were reviewed in detail. In particular, the blade breakage, binding noted in hot gas runs, and bypass leakage of gas were of major concern. These concerns suggested three areas for improvement of the motor design. These were:

a. Improvement of the end seals to reduce bypass leakage

b. A means of increasing end clearance without simultaneously increasing overboard leakage

c. Stronger blades and/or reduced blade forces.

Items a and b were accomplished simultaneously by the motor redesign shown in Figure 20. The face seals were removed. To incorporate the new seals, the existing rotor and stator were each shortened by 0.50 inch, with half removed from each end. Rotor end plates, each 0.25-inch thick were bolted to each end of the rotor. Spacer plates having the same thickness as the rotor end plates were installed on each end of the stator. These are machined eccentrically with regard to the stator but are concentric to the rotor.

Three-piece spring-loaded carbon seals were installed in the rotor end plates contacting the inside diameter of the spacer plates to form the end seals. The benefits expected from this design modification were:

a. Reduction of leakage into the end cavity with corresponding reduction of overboard leakage and thermal distortion effects.

b. Leakage into the end cavity is independent of the end clearance. The clearance may be increased to any amount necessary to accommodate axial thermal expansion.

c. Leakage occurring around the end clearance of the blades does not bypass the motor and can thus perform some useful work.

In addition, the spring-loaded pushrod was redesigned to incorporate a series-parallel stack of small Belleville springs to replace the O-rings previously used. These were 0.187 inch O.D. by 0.093 inch I.D., and 0.010 inches thick with a height of 0.015 inches and maximum deflection of 0.005 inches each. This new combination provided a possibility of operation under hot gas conditions. Capability to vary the spring rate was provided by spacers of various lengths which could be added to the push rod, replacing a number of the springs.

The modified motor was assembled with phenolic blades and subjected to cold gas testing to characterize performance of the new configuration. Performance results with several versions of this configuration are summarized in Table 7 for test sequences 1 through 26.

Sequences 1 - 3 -- Initial tests using unvented blades produced similar results. The motor would start to spin at low pressure and then stop at about 10 rpm as the ramp pressure was applied. It was noted that the motor would restart at low pressure as system inlet pressure bled down, indicating that the pressure loads on the tips of the blades were

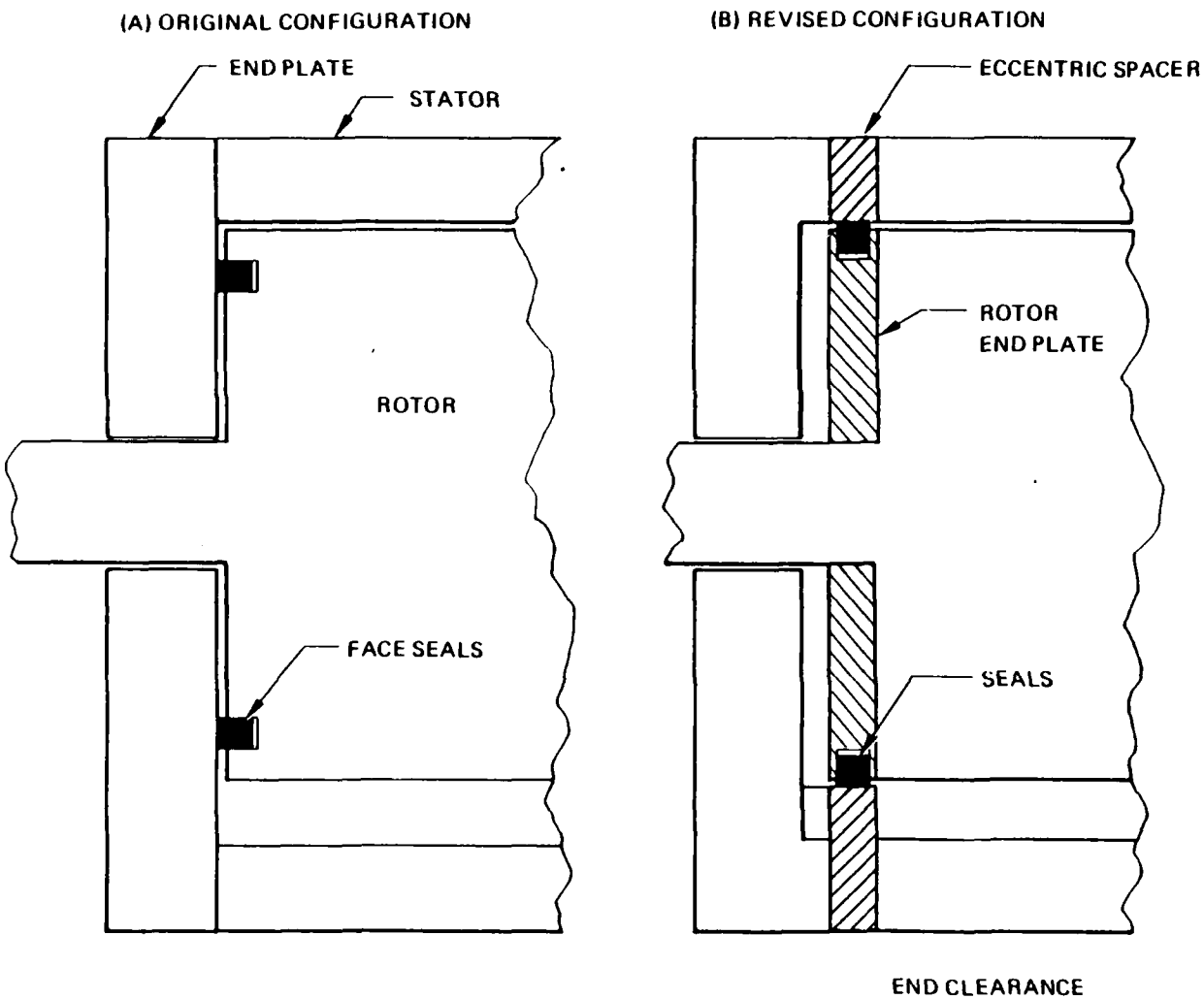

Figure 20. Comparison of Vane Motor Configurations

TABLE 7
PERFORMANCE DATA FOR REVISED MOTOR CONFIGURATION
(COLD GAS TEST SEQUENCES 1 THROUGH 26)

Seq.	Configuration	Orifice Inlet Pressure (psig)	Motor Inlet Pressure (psig)	Orifice Pressure Drop (psid)	End Cavity Pressure (psig)	Gas Temp. (°R)	Max Speed, RPM (Ramp Time, sec)	Gas Flow Rate (lbm/sec)	% Theoretical Flow
-1	• Phenolic blades • Short stator • New end seals • Spring-loaded pushrods • No vent slots • Heavyweight stator	693	678	20	< 10	501	—	0.691	—
-2	Same as -1	DATA NOT REDUCED, MOTOR DID NOT SPIN							
-3	Same as -1	1,074	1,035	73	372	517	—	1.612	—
-4	• Same as -1 except end seals removed • Blades vented on back side	1,071	1,026	77.6	350 (S) 170 (E)	499	5,000 (6.6)	1.689	104.0
-5	Same as -4 except end seal seals installed	1,047	1,001	74.2	60 max 140 on restart	499	5,000 (6.0) restarted to 1,575 RPM	1.633	103.3
-6	Same as -5 except end seal spring stiffer	1,040	990	73.2	18 max. 30 max on restart	500	5,000 (5.3)	1.607	102.7
-7	• Same as -6 except fixed shim under end seal	1,085	1,035	79	20 (S) 2 (E)	499	5,000 (4.95)	1.715	104.7
	• Restart	1,076	1,031	75	20 (S) —	495	—	—	—

NOTES: (S) START OF RAMP; (E) END OF RAMP

TABLE 7 (Continued)

PERFORMANCE DATA FOR REVISED MOTOR CONFIGURATION
(COLD GAS TEST SEQUENCES 1 THROUGH 26)

Seq.	Configuration	Orifice Inlet Pressure (psig)	Motor Inlet Pressure (psig)	Orifice Pressure Drop (psid)	End Cavity Pressure (psig)	Gas Temp. (°R)	Max Speed, RPM (Ramp Time, sec)	Gas Flow Rate (lbm/sec)	% Theoretical Flow
-8	Same as -6 except silicon carbide infiltrated carbon composite blades	1,125	1,089	76 (58.6 at 1 sec)	15	508	1,170 (1.6)	1.695	100.2
-9	Same as -8	1,098	1,058	74	18	506	770 (3.9)	1.658	100.5
-10	Same as -8	1,095 (S) 885 (E)	1050 (S) 840 (E)	74	14	518	3,360 (5.5)	1.637	127.4
-11	Same as -8 except phenolic blades	1,078 (S) 1,035 (E)	1,035 (S) 990 (E)	80 (S) 73 (E)	20 (S) 10 (E)	518	5,000 (5.5)	1.689	111.9
-12A	Same as -6 except lubricant-coated Inconel 600 blades	1,080	1,029	78	25	498	1,700 (2.1)	1.702	104.3
-12B	Same as -12A	1,110	1,052	79	20 (S) 10 (E)	498	3,680 (9.6)	1.736	104.1
-12C	Same as -12A	1,458 (S) 1,005 (E)	1,397 (S) 954 (E)	111 (S) 70 (E)	50 (S) 25 (E)	499 (S) 497 (E)	3,928 (10.3)	2.353 (S) 1.558 (E)	— 102.7 (E)
-13	Same as -6 except solid pushrods	1,155 (S) 1,088 (E)	1,098	74	280 (S) 265 (E)	505	5,000 (9.4)	1.702	— 99.2 (E)
-14	Same as -13 except blade vents on forward side	1,154	1,110	70.6	270 (S) 154 (E)	500	5,000 (8.1)	1.669	108.1

NOTES: (S) START OF RAMP; (E) END OF RAMP.

TABLE 7 (Continued)

PERFORMANCE DATA FOR REVISED MOTOR CONFIGURATION (COLD GAS TEST SEQUENCES 1 THROUGH 26)

Seq.	Configuration	Orifice Inlet Pressure (psig)	Motor Inlet Pressure (psig)	Orifice Pressure Drop (psid)	End Cavity Pressure (psig)	Gas Temp. (°R)	Max Speed, RPM (Ramp Time, sec)	Gas Flow Rate (lbm/sec)	% Theoretical Flow
-15A	Same as -14 except vent slot area increased 50%	1,164 (S) 987 (E)	1,110 (S) 945 (E)	72	90 (S) 40 (E)	505	5,000 (8.6)	1.685	123.0
-15B	Same as -15A	1,143	1,094	72	90 (S) 50 (E)	497	5,000 (8.6)	1.684	104.7
-16	Same as -12A except opposite blades linked with solid rods	1,139 (S) 915 (E)	1,097 (S) 1,028 (E)	75	20 (S) 10 (E)	508	3,360 (14.5)	1.696	160.1
-17	Same as -12A except blade weight reduced and slots forward	1,140	1,097	86 (S) 60 (E)	50 (S) 170 (E)	500	4,870 (6.3)	1.832 (S) 1.53 (E)	120.0 (S) 100.2 (E)
-18	Same as -16 except oval stator	1,163	1,106	69	138 peak	500	5,000 (9.7)	1.657	95.0
-19	Same as -17 except solid pushrods	1,172	1,098	72	100 (S) 10 (E)	500	4,871 (8.7)	1.699	111.2
-20	Same as -6 except coated alum. blades with slots forward	1,154	1,080	—	110 peak 10 (E)	500	3,357 (7.9)	—	—
-21	Same as -20 except powder metal blades	1,212	1,185	80 (S) 70 (E)	48 peak 20 (E)	500	4,530 (7.9)	1.822 1.704	110.6 (S) 103.5 (E)

NOTES: (S) START OF RAMP; (E) END OF RAMP.

TABLE 7 (Concluded)
PERFORMANCE DATA FOR REVISED MOTOR CONFIGURATION
(COLD GAS TEST SEQUENCES 1 THROUGH 26)

Seq.	Configuration	Orifice Inlet Pressure (psig)	Motor Inlet Pressure (psig)	Orifice Pressure Drop (psid)	End Cavity Pressure (psig)	Gas Temp. (°R)	Max Speed, RPM (Ramp Time, sec)	Gas Flow Rate (lbm/sec)	% Theoretical Flow
-22	Same as -20 except cast iron blades	1,170	1,104	78 (S) 74 (E)	30 max	532	3,514 (4.3)	1.713 (S) 1.669 (E)	118.7 (S) 115.6 (E)
-23	• Oval stator • Carbon composite blades • Slots forward • Notched solid pushrods	743	707	50	22 (S) 8 (E)	500	2,070 (6.4)	1.131	110.4
-24	Same as -23 except phenolic blades	1,224	1,128	92	10 (S) 35 (E)	504	5,000 (9.1)	1.955	125.6
-25	Same as -24 except additional slots on back of blades	1,244	1,147	92.8	10 (S) 260 (E)	504	5,000 (6.85)	1.979	100.9
-26	• Same as -25 except carbon composite blades • Large flywheel installed	1,244 (est. from -25)	1,146	92	—	510	2,300 (4.9)	1.959 (est.)	98.4

NOTES: (S) START OF RAMP; (E) END OF RAMP

overcoming the pushrod spring loads as inlet pressure increased. There was also concern that the new carbon end seals might be causing excessive friction by means of an unbalanced pressure load.

The results of these runs led to a test which simulated previous configurations as closely as was possible with the new design, specifically, the end seals were removed and the blades were vented on the trailing side as in Runs 31 through 39B shown previously in Table 4.

Sequence 4 was run in the above described configuration and achieved 4,970 rpm in 6.6 seconds from the start of the pressure ramp. This result proved that the end plates are performing a useful function in keeping leakage past the blades within the motor, since the time is comparable to the best previous runs with 15 percent less blade length and 19 percent less flow rate than comparable Run 35. Upon teardown, some galling was noted between the OD of the new end plates and offset spacers. The clearance was increased in this area.

Sequence 5 was a repeat run with the end seals re-installed. This run achieved 5,000 rpm in 6.0 seconds. After shutdown and braking of the flywheel, a successful restart was attempted with the motor allowed to spin only to 1,575 rpm prior to shutdown to minimize wear on the phenolic blades.

Sequence 6 repeated the previous run, except that the wave springs under the end seals were reformed to produce more spring force. This configuration reached 5,000 rpm in 5.3 seconds, the best results to date.

The effect of the end seals can be seen in two measured parameters:

a. Orifice pressure drop (a partial measure of gas flow rate).

b. End cavity pressure (a measure of leakage).

Figure 21 shows the effect of the addition of end seals on the gas flow orifice pressure drop. Total flow is reduced, leakage is reduced, and run time to 5,000 rpm decreases, all leading to reduced total gas consumption.

Overboard leakage, as monitored by the end cavity pressure tap, was substantially reduced by addition of the end seals, as shown in Figure 22. The Sequence 4 results are similar to previous cold gas runs with the old motor configuration, having the same maximum pressure and typical profile during the run. Addition of the end seals resulted in an order of magnitude reduction in the cavity pressure and thus of overboard leakage.

As a result of the galling problems experienced in Sequence 4, it was known that the radius of the end seals was no longer a good match with the I.D. of the off-set spacers, since their diameters had been increased to prevent metal-to-metal contact. The

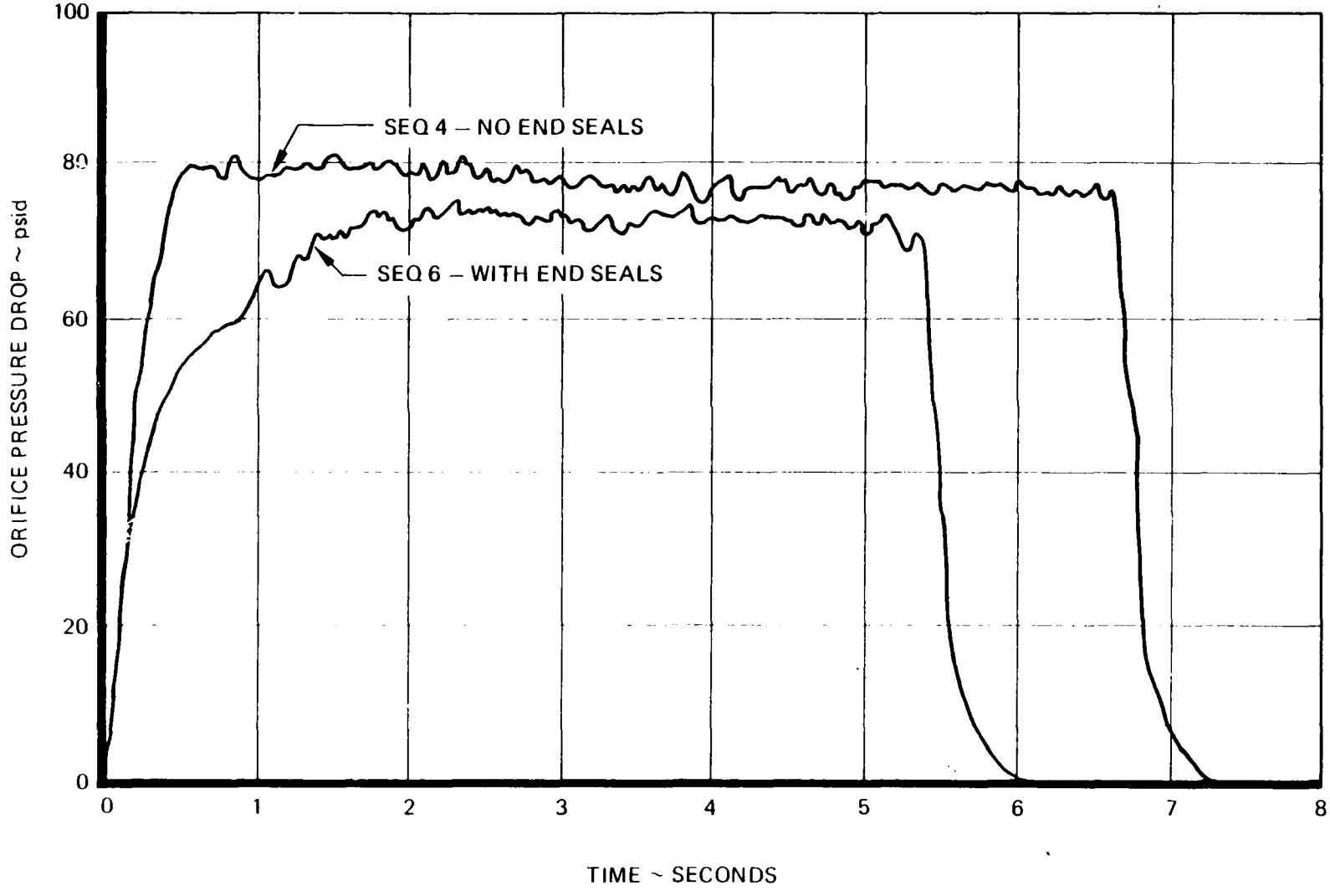

Figure 21. Effect of End Seals on Orifice ΔP and Run Time

Effect of Seals on Leakage-Produced End Cavity Pressure

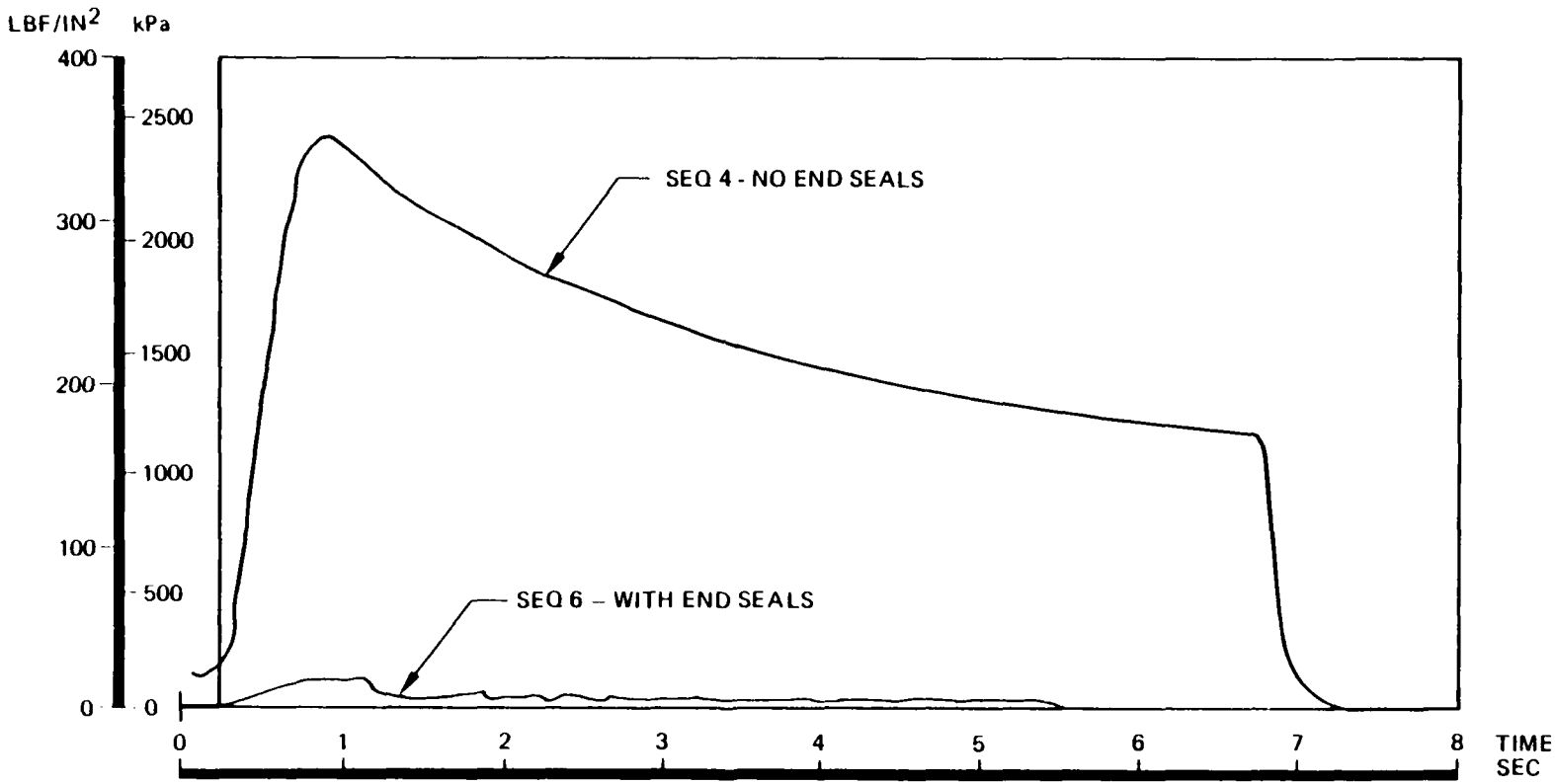

Figure 22. Effect of Seals on Leakage-Produced End Cavity Pressure

individual segments of the three-piece carbon end seals are somewhat flexible, therefore another run was planned having a further increase in the wave-spring force to see if leakage could be further reduced.

Sequence 7 -- For the final test of this series the spring load on the end seals was again increased by incorporation of a fixed shim beneath the wave spring. Minor modifications to the end plates were accomplished to prevent pushrod interference and allow a common blade configuration for all positions. With these modifications, a start and partial restart were conducted. The full duration start achieved a time just slightly better than the 5.3 seconds of Sequence 6, with similar results in the end cavity pressure measurement.

6. ALTERNATE BLADE MATERIAL EVALUATION

As a result of problems experienced with blade breakage and wear, materials with higher strength characteristics were examined to find suitable candidates for test. Materials selected for test consisted of:

a. Carbon-carbon composite infiltrated with silicon carbide to improve strength and hardness

b. Inconel 600 flame sprayed with a high-temperature lubricant coating

c. A sintered powder metal blade of chrome/nickel post-impregnated with a high-temperature lubricant material

d. A high aluminum content cast iron having reduced density and high hardness

e. Aluminum treated with a proprietary "Banadize" process to produce an extremely hard surface coating.

The results of tests conducted with these materials are presented in the following paragraphs.

7. SILICON CARBIDE INFILTRATED CARBON-COMPOSITE BLADES

Samples of the previous blade materials (carbon composite and phenolic) were sent to Refractory Composites, Inc., Pacoima, California (the supplier of the silicon-carbide blades) for relative strength testing. Results indicated that the silicon-carbide blades could be expected to be several times stronger than the carbon-composite material, but not as strong as the phenolic. Sample sets of blades were fabricated for testing.

Three tests were conducted with the silicon carbide-infiltrated blades.

Sequence 8 -- During the first test, the motor accelerated to 1,170 rpm and stopped abruptly. Teardown inspection revealed apparent delamination and chipping on the contact edge of approximately half of the blades, with several blades showing no apparent

damage. On the assumption that this might be only a quality problem with some of the blades and that some of the blades had inherently better construction than others of the lot, they were reused for the next run together with new blades.

The blades are abrasive, as might be expected from the silicon carbide infiltration, and produced some polishing of the mating bore.

Sequence 9 -- In this run, the motor speed reached only 770 rpm before stopping. Teardown again showed delamination and a chipping-type failure of the blade edges.

It was not clear whether the blade failures were all caused by the same mechanism or whether an initial failure introduced particles which then caused failure of other blades.

To determine if friction was the cause of initial failures, a set of blades was lubricated with molybdenum disulfide (as used in tests with the phenolic blades) to evaluate the effect. The object was to determine if a lubricant such as the type being used in the powder metal blades could be used to infiltrate these blades if lubrication was the only problem.

Sequence 10 -- This run achieved a speed of 3,360 rpm prior to blade failure. In this case, fairly large chunks were removed from one side of each blade corresponding to a raised groove of 0.002- to 0.004-inch height about 0.5-inch wide in the stator, probably caused by a piece from the first failed blade. This was the most damage that had occurred to the stator as a result of any blade failure, and was most likely due to the hardness and abrasive nature of the material. These results indicate that there is a basic structural problem with these blades, independent of the lubrication effects.

With the possibility of severe damage to the stator if further runs were attempted, no further tests were planned with these blades until the other candidates had been evaluated. The supplier indicated that further improvements in the blade strength could be accomplished by a change to the processing. New parts were therefore started into the manufacturing cycle to be used if further tests were desired with this material at a later date.

8. LUBRICANT-COATED INCONEL 600 BLADES

The next material to be evaluated was Inconel 600. Friction coefficients for most metals are excessive, therefore a survey of high-temperature lubricant coatings was conducted. The use of plasma-sprayed metal-glass and metal-glass-fluoride coatings for bearing lubrication up to 1,650°F is discussed in Reference (2). Friction coefficients range from 0.4 at ambient temperature to 0.2 at 1,650°F. Addition of silver to the mixture was

shown (Reference (3)) to reduce the ambient temperature friction coefficient to 0.25, such that over the range of temperature the coefficient varied between 0.25 and 0.2.

Inconel 600 blades were fabricated approximately 0.020-inch undersize in all dimensions to allow for the final coating thickness. The blades were coated with SURF-KOTE C-800, the trade name for a metal-glass-fluoride high-temperature lubricant applied per NASA Specification PS-101 by Hohman Plating and Manufacturing, Inc., Dayton, Ohio. The coating, applied by plasma spraying, consists of 30 percent nichrome, 30 percent silver, 25 percent calcium fluoride, and 15 percent glass by weight. The composition of the glass is 58 percent SiO_2, 21 percent BaO, 8 percent CaO, and 13 percent K_2O.

The coated blades must be machined dry at very low surface speed to avoid smearing the metal constituent over the lubricating material. Following completion of machining, the blades are heat treated in air for four hours at 1,600°F. The stated purpose of the heat treatment (Reference (2)) is to produce a solid-state migration of fluorides along the surface and also to mildly pre-oxidize the exposed metal. The surface is thus entirely covered with a combined fluoride-oxide film to prevent direct metal-to-metal adhesive contacts during sliding.

Sequence 11 -- Prior to testing with the coated Inconel 600 blades a checkout test, Sequence 11, was conducted with phenolic blades and spring-loaded pushrods to verify motor performance after cleanup of the stator bore to remove effects of the damage resulting from the failure of the silicon carbide composite blades. This test resulted in a time of 5.5 seconds to reach 5,000 rpm, consistent with the previous test results.

Sequence 12A -- The coated Inconel blades were installed in the motor with the spring-loaded pushrods for cold gas testing. Low-speed rotation of the motor installed in a lathe resulted in a squealing sound typical of unlubricated parts. The motor was qualitatively more difficult to turn by hand than with previous blades tested.

When pressurized at low pressure, the motor started to turn readily. An initial run was started, and terminated at 1,700 rpm to review the data prior to proceeding.

Sequence 12B -- A second start was conducted attempting to reach 5,000 rpm. The acceleration on the second start was somewhat reduced, e.g., during the first run, the acceleration between 714 rpm and 1,428 rpm was 74.8 rad/sec^2 (45-degree slope on the strip chart), while for the second run, the acceleration was only 55.3 rad/sec^2. (Comparable acceleration with phenolic blades was 138.4 rad/sec^2.) The motor reached 3,680 rpm in 9.6 seconds, and was still accelerating slowly when the run was terminated.

Sequence 12C -- A final start was conducted with higher inlet pressure, 1,450 psig vs. the normal 1,100 psig. The initial acceleration rate improved to 93.5 rad/sec^2, but then decreased due to an inadequate gas supply which decayed in pressure over the run to about 1,000 psig at the end of the run. The motor reached 3,928 rpm, at which point it was accelerating very slowly. The run was terminated at 10.3 seconds. Disassembly revealed significant wear at the blade tips although coating material was still present. The material appeared to smear over the edge of the blade somewhat. This is due possibly to the fact that the material is better suited to application to a concave surface as in a bearing bore. Further, there was evidence of high forces in the direction of the rotor slots since the pushrods had deformed the edges of the blade slightly. One blade, possibly due to this swaging action, was quite tight in the slot and could be felt when the motor was rotated by hand as a "cogging" effect as the pushrod/spring combination went solid, forcing the blade to move.

The results, while not totally as desired, were encouraging from the standpoint that the blades, while being greater than 6 times the weight, did not apparently generate 6 times the frictional torque. In an attempt to determine the ratio of the frictional torques, the motor deceleration curves after flow cutoff for the phenolic blades and metal blades were analyzed. The effect of the added blade mass on the rotor inertia was calculated to increase the deceleration time by 23 percent for the metal blade run. Actually, this run decelerated in 68.6 percent of the phenolic blade time between 4,000 and 3,000 rpm. Thus, the drag torque ratio is approximated by:

$$\frac{\text{Drag Torque Metal}}{\text{Drag Torque Phenolic}} = \frac{1.23}{0.686} = 1.79$$

The testing with metal blades emphasized the effects of the blade weight/frictional drag on the motor operation. To be successful, the blade weight would have to be reduced (which would reduce strength) or counterbalanced. Three configuration options were considered for improving the performance of metal blades, these were:

a. Lighter blades with spring-loaded pushrods

b. Linked blades with the stator bore shape modified (on the power side) to allow constant length blades with minimum clearance. Linking the blades effectively eliminates the blade centrifugal force loading and frictional effects, since the opposing blades balance each other except for the small contribution as the center of mass of the pair moves eccentrically relative to the rotor center.

c. Linked blades with spring-loaded insert tips to provide length compensation. These would require a wider slot at the top of the rotor to accommodate the tip insert.

9. MOTOR FRICTION ANALYSIS

To better understand the effects of friction coefficient and blade weight on motor performance, and to aid in interpretation of test results, additional analytical studies were conducted by Prof. C. H. Wolgemuth.

The model previously developed was modified to account for pushrods between the blades. A simplified approach was taken which ignores the spring force (negligible with respect to other forces) but allows transfer of force between pairs of blades. The vane-free body diagram is shown in Figure 23. The model includes normal forces due to $\omega^2 r$ and d^2r/dt^2 components, tangential forces resulting from $d\omega/dt$ and coriolis components (the latter arising from the vane motion in a rotating reference system), pressure forces in the normal and tangential directions, and gravitational forces. In the axial direction friction force (identified as F_{end} in Figure 23, is developed only on the portion of the blade exposed above the rotor as it contacts the eccentric spacer, consistent with the revised motor design.

To minimize the effects of blade weight, a concept was conceived whereby opposite pairs of blades would be linked together to counterbalance the weight. A simplified model of this concept was also analyzed as shown in Figure 24, considering the same dynamic forces as the pushrod model.

Pressure in the control volume behind the blade (lagging control volume) was computed from the leakage model for the desired absolute inlet pressure of 1,115 lbf/in.^{2}, as shown in Figure 25, where the centerline of the inlet port occurs at θ = 215 degrees. Forces, available gas power, and friction power losses versus angle were computed for various combinations of friction coefficient, inlet pressure, rotational speed and vane porting. Results of these calculations are summarized in Table 8, which also shows the maximum normal tip force near θ = 0 degrees (the location of full vane extension where breakage typically occurs) and the angle at which it occurs. Figures 26 (pushrod model) and 27 (linked-rigid model) present tip and end forces, F_3 and F_{end} versus rotation angle for identical friction coefficient, blade mass, speed, and blade venting. The latter figure also incorporates the tangential reaction force FRT_1 (Ref. Figure 24) between the blade and stator. Linking the blades has the effect of reducing the peak normal force from 740 lbf for the pushrod case to 492 lbf. Referring to the underlined cases in Table 8 for venting to the lagging control volume, it is noted that both configurations produce 10.51 hp/vane; however, the friction power for the linked vanes is 8.07 hp/vane versus 13.36

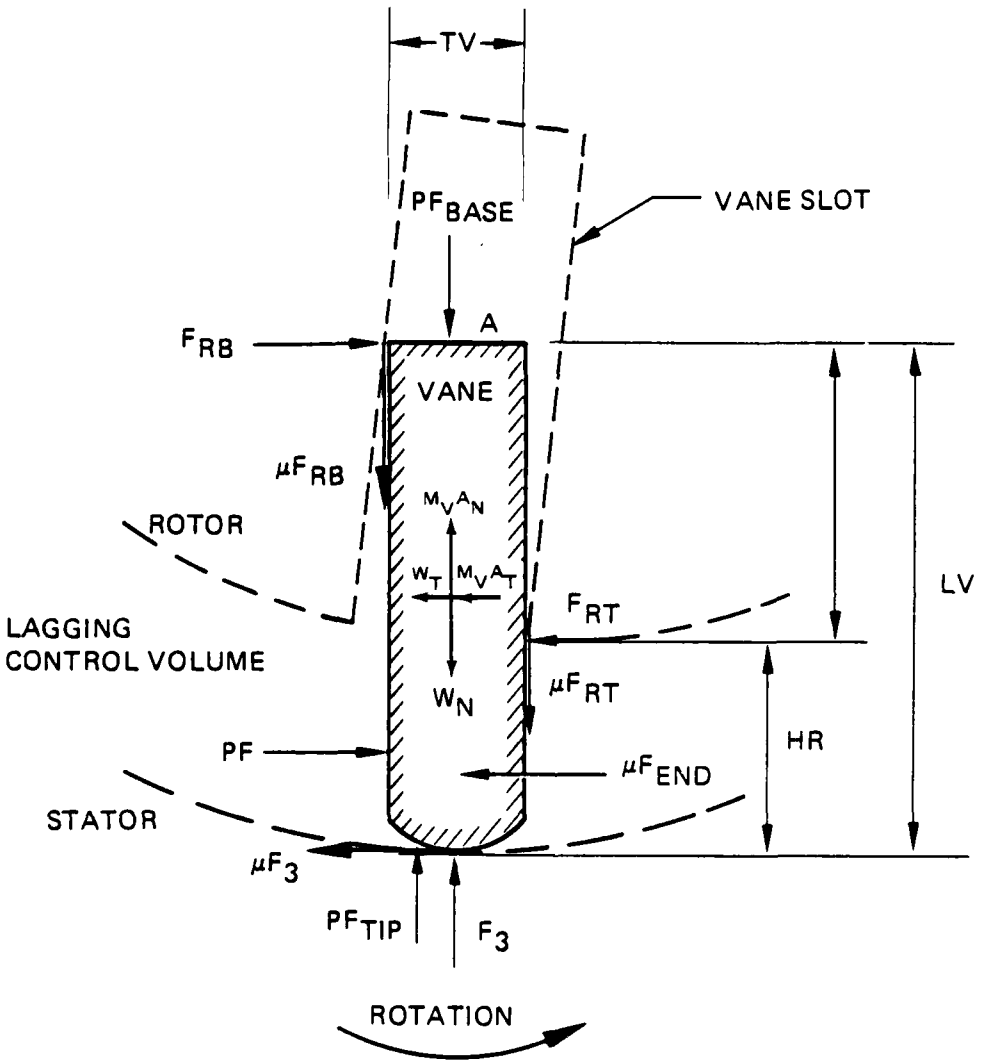

Figure 23. Free Body Diagram of Single Vane

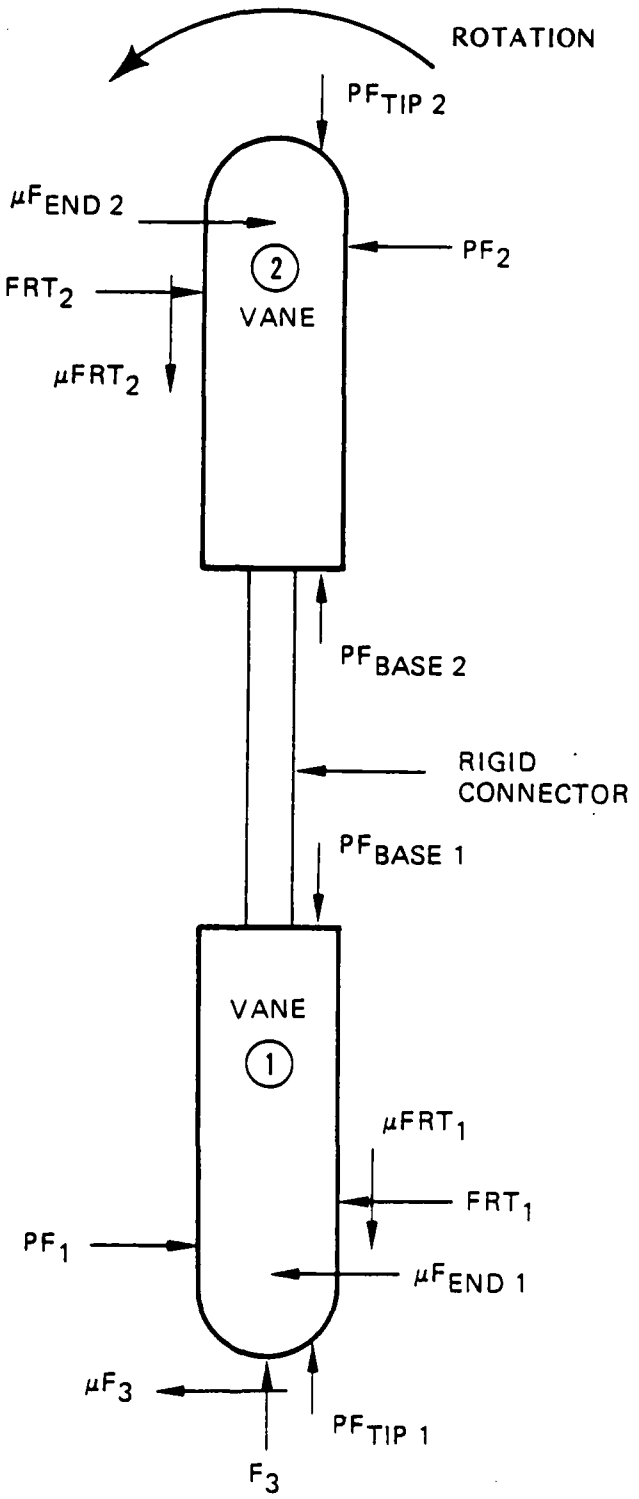

Figure 24. Model of Linked-Rigid Vanes

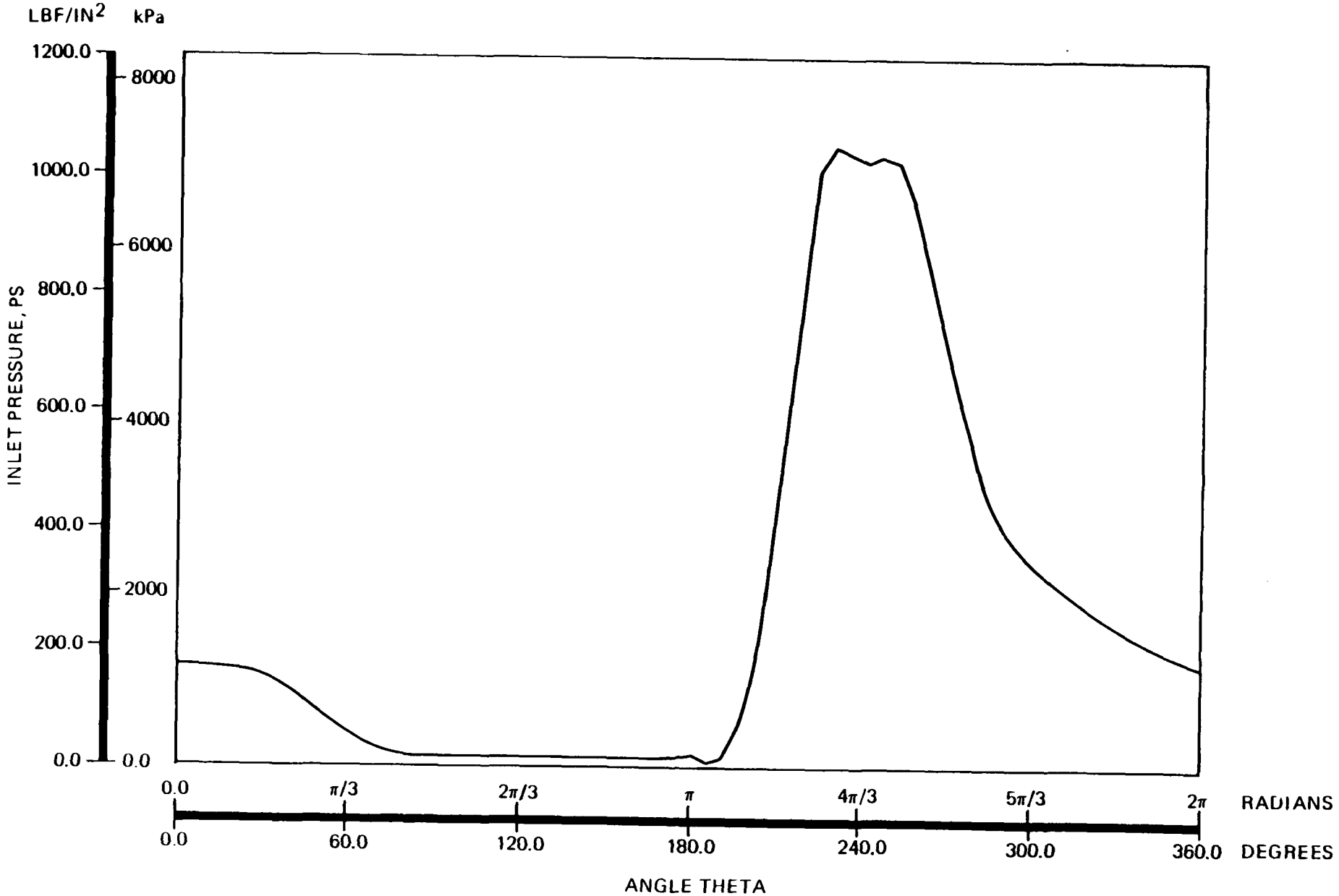

Figure 25. Pressure in Lagging Control Volume as a Function of Vane Angle

TABLE 8

FRICTION POWER AND FUEL POWER PER VANE FOR VARIOUS CONDITIONS

Linked-Rigid Vane Model

Coeff. of Friction	Vane Weight (lbf)	Speed RPM	Pressure lbf/in.^{2}	Ported to Control Volume	Fluid Power/Vane (hp)	Friction Power/Vane (hp)	F_3 (θ)* lbf (°)	F_3 (θ)* N (rad)
0.2	0.18	4,000	700	lagging	6.49	2.82	308 (11)	1,370 (0.19)
0.4	0.18	4,000	700	lagging	6.49	5.51	341 (6)	1,520 (0.10)
0.2	0.18	4,000	1,115	lagging	10.51	4.17	451 (17)	2,010 (0.30)
0.4	0.18	4,000	1,115	lagging	10.51	8.07	492 (6)	2,190 (0.10)
0.2	0.18	4,000	1,500	lagging	14.22	5.42	584 (17)	2,600 (0.30)
0.4	0.18	4,000	1,500	lagging	14.22	10.43	637 (11)	2,830 (0.20)
0.2	0.18	2,500	1,115	lagging	6.57	2.41	404 (17)	1,800 (0.30)
0.2	0.18	6,000	1,115	lagging	15.76	7.29	548 (17)	2,440 (0.30)
0.2	0.06	4,000	1,115	lagging	10.51	3.83	399 (17)	1,770 (0.30)
0.4	0.06	4,000	1,115	lagging	10.51	7.31	431 (11)	1,920 (0.20)
0.2	0.06	2,500	1,115	lagging	6.57	2.32	304 (17)	1,710 (0.30)
0.2	0.06	6,000	1,115	lagging	15.76	6.06	432 (17)	1,920 (0.30)
0.2	0.06	4,000	1,115	leading	10.51	2.23	29 (17)	130 (0.30)
0.4	0.06	4,000	1,115	leading	10.51	5.34	69 (17)	310 (0.30)
0.2	0.18	4,000	1,115	leading	10.51	2.38	80 (17)	360 (0.30)
0.4	0.18	4,000	1,115	leading	10.51	5.88	0	0 (0)
0.2	0.18	2,500	1,115	leading	6.57	1.40	33 (17)	150 (0.30)
0.2	0.18	6,000	1,115	leading	15.76	4.42	177 (17)	790 (0.30)
				Pushrod Model				
0.2	0.18	4,000	1,115	lagging	10.51	6.45	533 (6)	2,370 (0.10)
0.4	0.18	4,000	1,115	lagging	10.51	13.36	740 (6)	3,290 (0.10)
0.2	0.06	4,000	1,115	lagging	10.51	4.74	477 (6)	2,120 (0.10)
0.4	0.06	4,000	1,115	lagging	10.51	9.33	658 (6)	2,930 (0.10)
0.2	0.18	4,000	1,115	leading	10.51	5.65	216 (22)	960 (0.38)
0.4	0.18	4,000	1,115	leading	10.51	11.53	178 (6)	790 (0.10)

*Peak value of F_3 and the angle ( ) at which it occurs in the vicinity of a fully extended vane ($\theta = 0$).

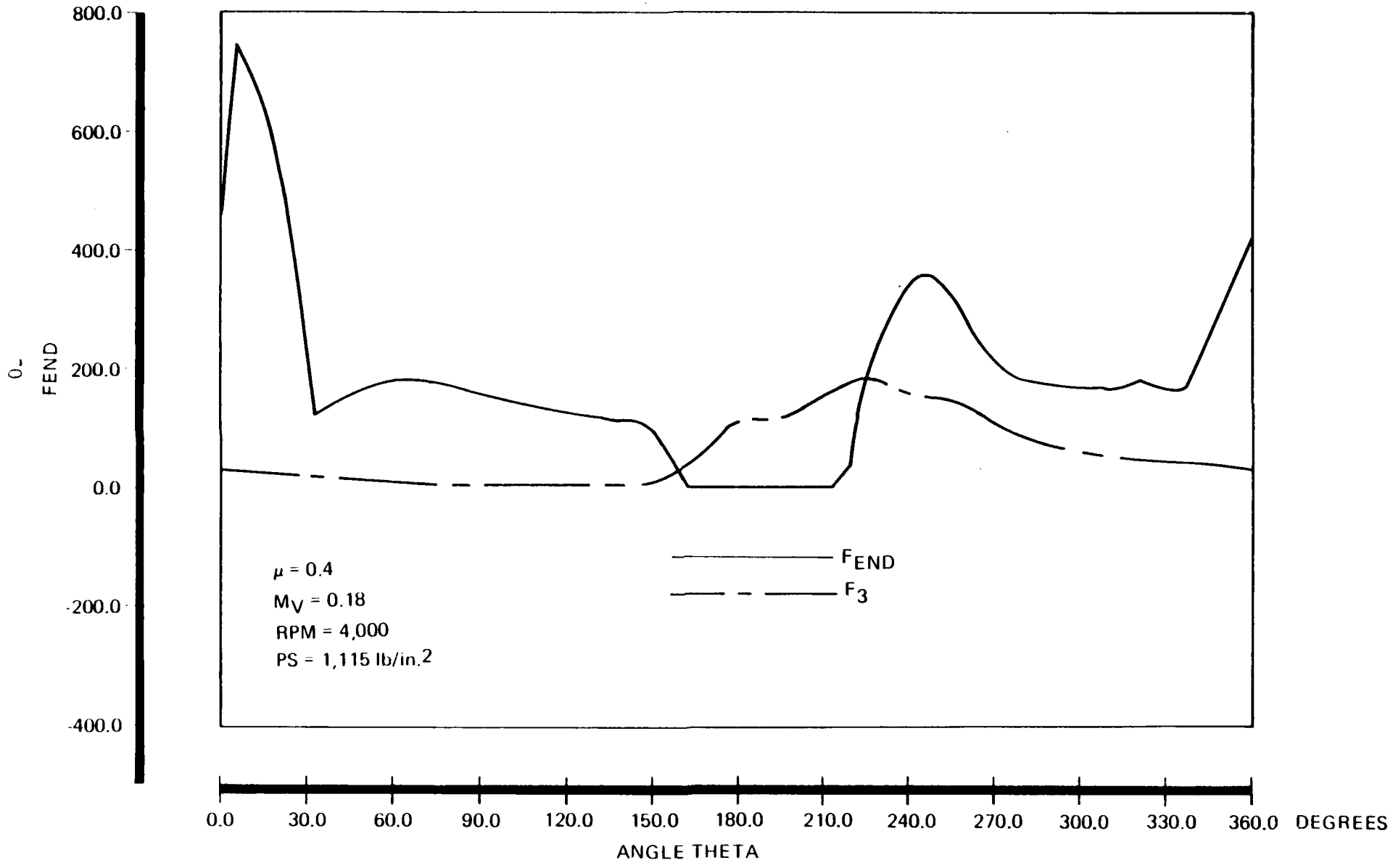

Figure 26. Tip and End Forces Versus Rotation Angle Pushrod Model Vented to Lagging Control Volume

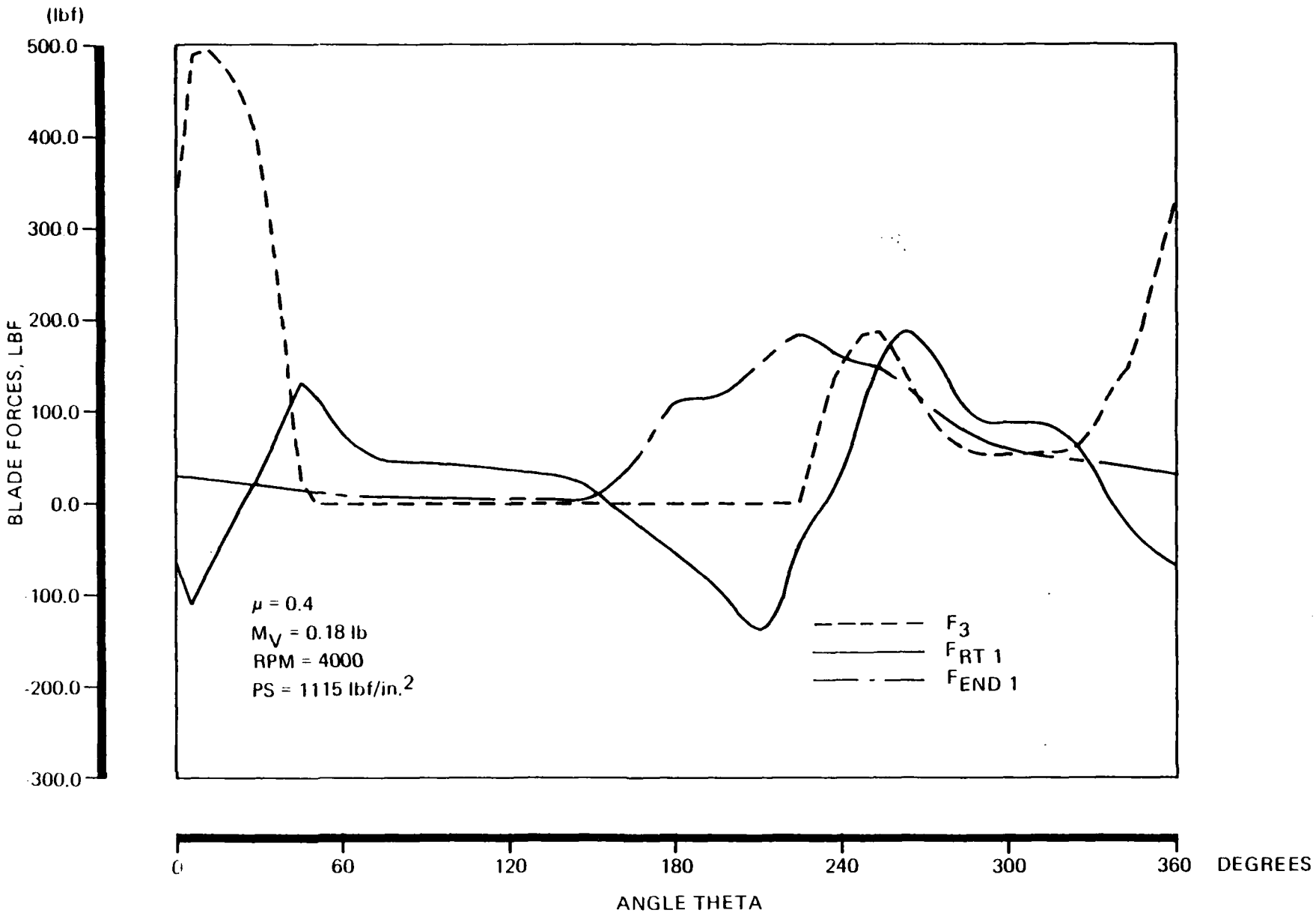

Figure 27. Vane Contact Forces Versus Rotation Angle Linked Rigid Model Vented to Lagging Control Volume

hp/vane for the pushrod case, a 40% reduction (of course this latter case, having a friction loss greater than its fluid input power would never have reached the speed at which the calculation was performed). Venting the leading edge of the blade with the linked blade model resulted in forces as shown in Figure 28. Of major significance to the blade breakage problem is the fact that the tip force, F_3, is zero at maximum blade extension (θ = 0) and achieves a low peak of approximately 250 lbf, nearly 75 degrees later when blade extension is substantially reduced. Friction power is further reduced to 5.88 hp/vane for leading edge venting, a 27 percent reduction from the case with trailing edge venting.

Figure 29 presents friction power per vane versus coefficient of friction for all cases run at 4,000 rpm, showing the effects of blade mass, venting location, and linking of the blades. The case for the pushrod weight of 0.18 lbf approximates the test case with lubricant coated Inconel 600 blades (test sequence 12C of Table 7). Since the motor acceleration was essentially zero at 4,000 rpm, the crossover point of the plot with the theoretical gas power defines the approximate overall coefficient of friction which is seen to be 0.314. This is consistent with the coating wear on the blade tip, where significant uncoated metal was observed at the end of the run, increasing the friction coefficient above the 0.2 value typical of the coating.

It should be noted that the above analysis does not account for changes in leakage in the various models. For example, zero values of tip force F_3, as occur in Figure 28 from θ = 210 to 360° imply that the blade is forced off the stator, thus allowing leakage to occur. Therefore, maximum motor efficiency does not necessarily occur for the minimum friction configuration, but as a tradeoff between leakage and friction.

As a preliminary to possible linked-blade tests and to provide additional information regarding blade pressure balance, a series of tests were conducted with phenolic blades and solid pushrods. The configurations tested and results obtained are summarized below.

Sequence 13 -- Solid pushrods were assembled with a set of phenolic blades, sized to produce minimum blade clearance of approximately 0.003 inch at closest approach. This configuration rotated very readily by hand with minimum drag. Time to speed was 9.4 seconds, significantly slower than the 5.0 to 5.5 seconds normally achieved with the spring-loaded pushrods. The difference was felt to be due in part to the fact that blade pressure balancing slots are on the trailing edge side of the blade, thus, blades approaching the inlet from the exhaust port are forced open by the unbalanced effect of inlet pressure, allowing leakage flow to produce reverse torque.

Sequence 14 -- This run was a repeat of Sequence 13, except that the blades were reversed in the slots to put the pressure vents on the leading edge. The attempt was to

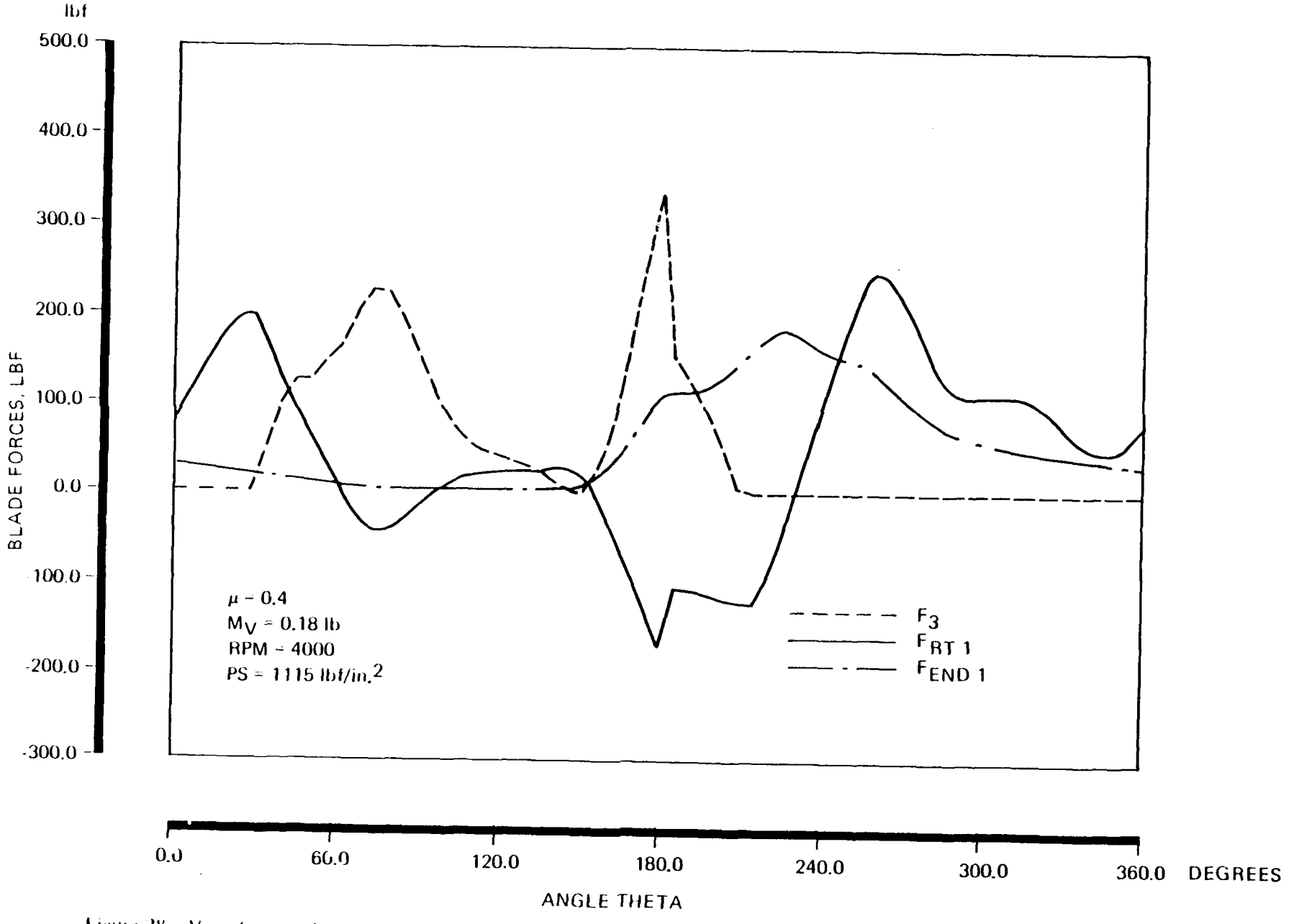

Figure 28. Vane Contact Forces Versus Rotation Angle for Linked-Rigid Model Vented to Leading Control Volume

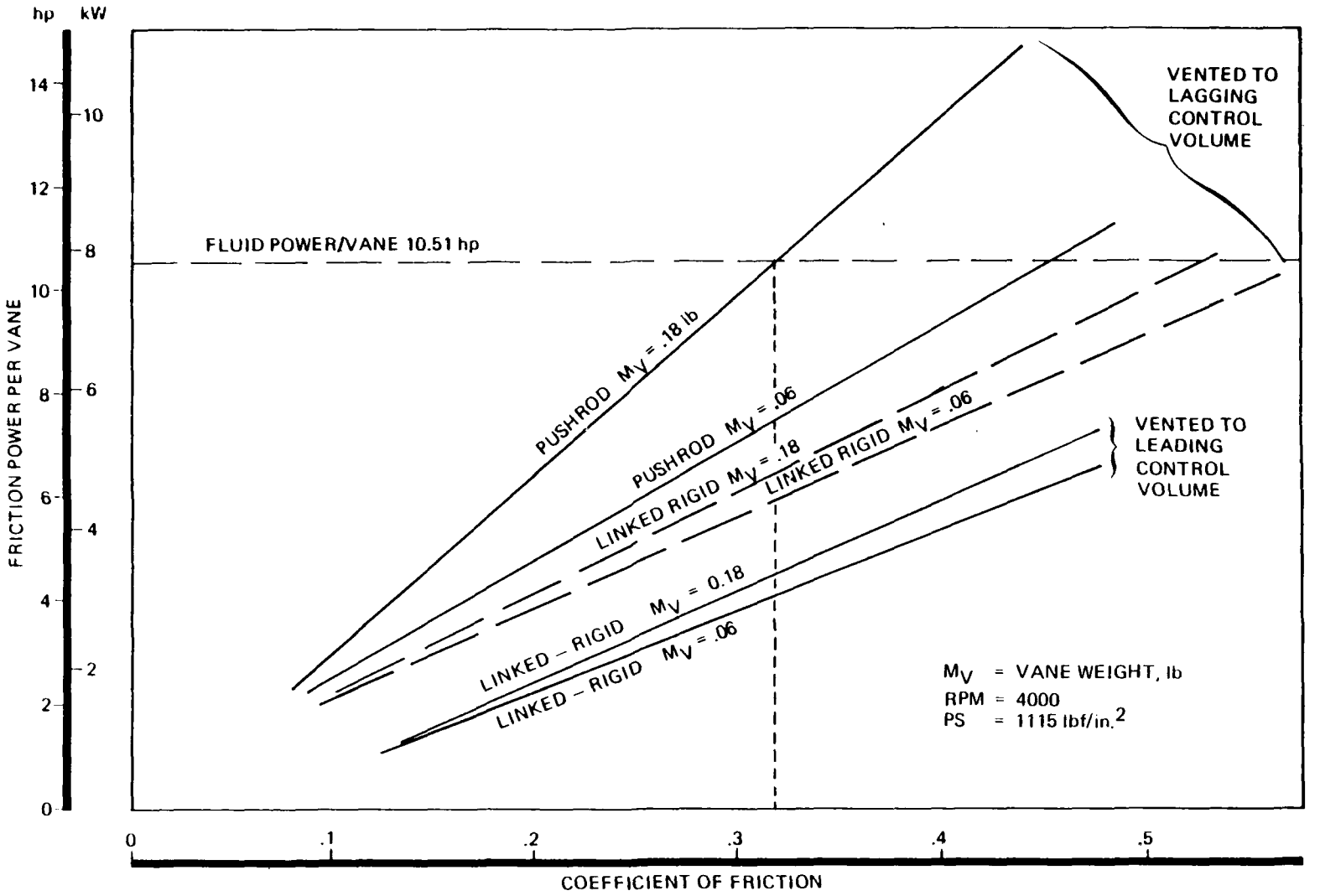

Figure 29. Friction Power per Vane Versus Coefficient of Friction

better pressure balance the blades, reducing reverse torque to improve overall performance. Time to speed with this configuration was 8.1 seconds, an improvement of 1.3 seconds or 13.8 percent.

Sequence 15A and 15B -- In order to determine whether the existing pressure balancing slot sizes were sufficient, Sequence 14 was repeated, except the slot area on the blades was doubled. Time-to-speed was 8.6 seconds in both Sequence 15A and 15B, possibly indicating that the added slot area was contributing to additional leakage through the motor by providing less flow resistance to leak paths that occur from underneath the blade, e.g. through the pushrod clearances.

10. MODEL CONFIRMATION TESTS

To investigate the improvements suggested by the analytical study, several tests were conducted as described in the following paragraphs.

Sequence 16 -- This test was the first conducted with a set of linked blades. The mechanism for tying pairs of blades together is shown in Figure 30. To assemble the blades into the rotor, the tie rods are first installed into one blade, and the hollow pushrods assembled over the tie rods. This subassembly is then installed on the rotor, leaving the threaded tie rods extending into the opposite blade slot. The opposite blade is then installed over the tie rods and inserted into the slot until the end of the tie rod appears at the cut-out in the blade. The nuts are then installed. As they are tightened, the blade is drawn into the slot, bottoming on the pushrod. In this position, the nuts are approximately half buried in the slot, and thus cannot fall out in operation. This configuration, running in a fixed diameter bore, has leakage clearances ranging from the setup minimum of approximately 0.003 inch at 90 degrees of rotation to 0.030 inch at 180 degrees rotation, resulting in major internal leakage.

Peak speed with this configuration was 3,000 rpm, occurring 15.5 seconds after initiation. These results were very encouraging considering the leakage situation, and indicated that reducing leakage via a constant length configuration stator should substantially improve the performance while maintaining friction at reduced levels.

Sequence 17 -- This test was conducted with lightweight Inconel 600 coated metal blades (0.107 lbm vs. the 0.188 lbm of the solid blades) to confirm the analytical study results. The weight reduction was accomplished by electric discharge machining internal square holes from the base of the blade nearly to the tip, leaving small webs between adjacent holes. This produced a honeycomb-like configuration having higher bending strength than if material had to be removed from the exterior surface. Based on previous tests with phenolic blades, the blade slots were faced forward for optimum performance.

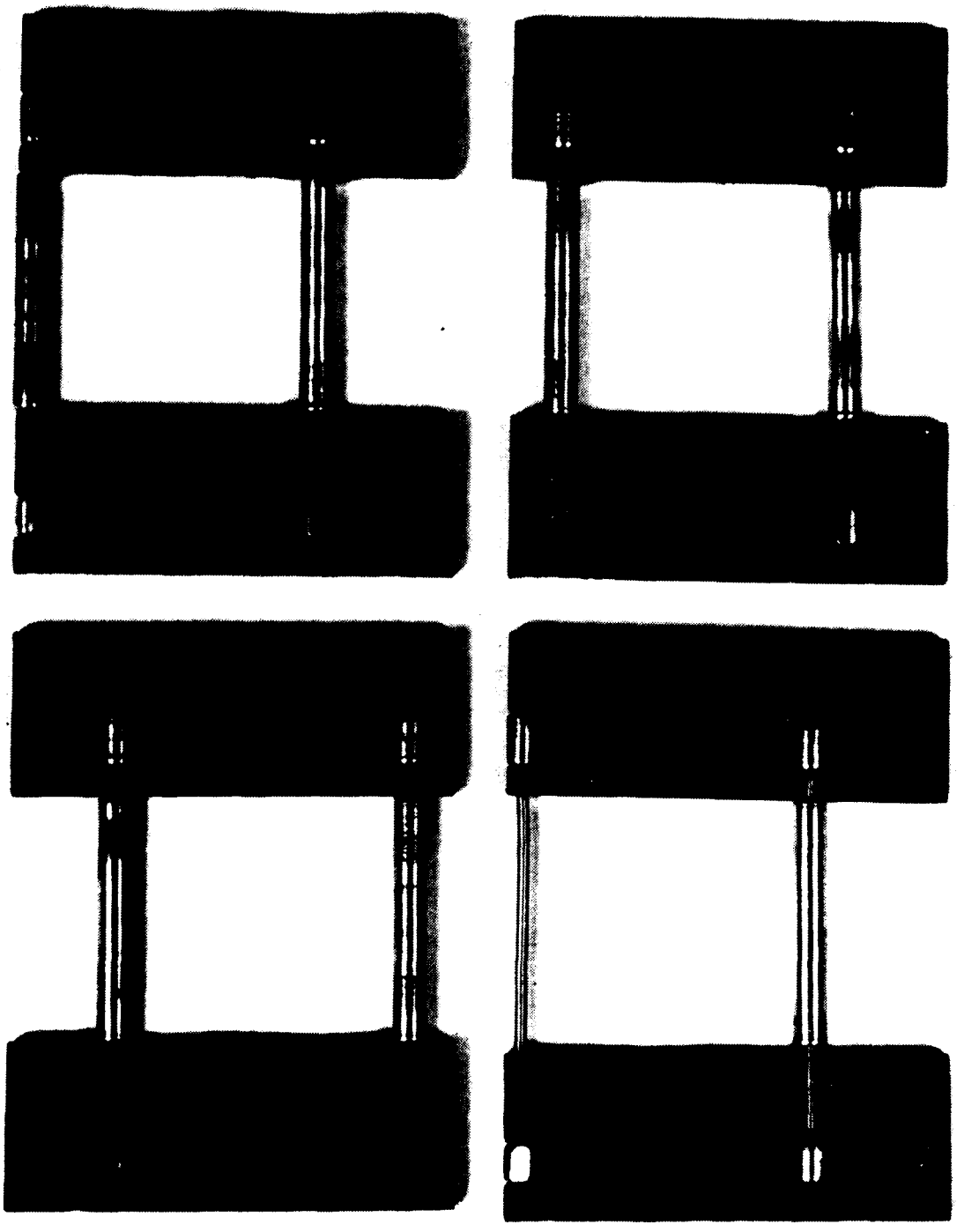

Figure 30. Linked Blade Assemblies

Spring loaded pushrods were installed. This test was very successful, resulting in a 6.3 second run time to reach 4,870 rpm at which point the run was terminated although still accelerating. Extrapolation of the curve indicates that an additional 0.5 seconds would have been required to reach 5,000 rpm had the run been continued. Post-test teardown indicated that a major portion of the lubricant coating was gone from the tip surface.

Sequence 18 -- Results with the linked blades in Sequence 16 indicated the possibility of improved performance if clearances could be minimized over the total cycle. As a first approximation to a constant length geometry a second circular bore, offset from the first in the direction of the inlet, was considered since it would be relatively simple to incorporate into the existing design. A computer program was established to assist in optimizing the location and size of the second bore prior to fabrication. The results indicated that an offset of the stator nominal centerline of 0.039 inches horizontally and 0.003 inches vertically (in the direction of the inlet) should be combined with a radius equal to 0.013 inches less than the existing bore. This produced a worst-case clearance of 0.0018 inches near the inlet and 0.0015 inches 90 degrees further in rotation. This configuration was incorporated into a new stator of the heavyweight design.

The linked metal blades were run in the new offset stator with slots facing rear. While analytical study results indicated this was not optimum for performance, it was the same as in the previous run in the round stator. Also, slight mismatches of the pushrod locations prevented reversing this configuration. Upon installation, the clearances were found to be slightly higher than expected (0.004 vs. 0.002 inch) probably due to the fact that the simplified analysis to optimize the offset geometry does not account for the shifting of the contact point on the blade as it rotates in the bore. This is still a substantial improvement over the 0.030 inch worst-case clearance that existed in the round stator. In the test run, the motor accelerated smoothly to 5,000 rpm in 9.7 seconds, a marked improvement over the previous test which achieved only 3,000 rpm in 15.5 seconds.

Teardown inspection indicated that the coating was completely gone from the tip and some increase in clearance to 0.008 - 0.010 had occurred as a result of wear.

Sequence 19 -- This test duplicated Sequence 17 except that solid pushrods were used instead of the spring-loaded ones. A speed of 4,870 rpm was the maximum that could be achieved with this configuration and was reached in 8.6 seconds. The run was continued for an additional second at constant speed prior to shutdown. Teardown inspection

revealed total loss of coating at the blade tip and evidence of some scuffing and metal deposition on the stator.

Sequence 20 -- 7075 aluminum blades were fabricated and subjected to the proprietary Banadize coating by Lovatt Technology Corporation, Santa Fe Springs, California. The blades, as received, did not have as thick a coating as expected resulting in an increase in clearance in the slot. The manufacturer indicated that the thickness varies with the type of aluminum and that the thickness applied was maximum for this material. The surface coating was very hard and also extremely smooth.

The blades were installed, slots forward, in the round stator with spring-loaded pushrods. A speed of 3,360 rpm was achieved in 6.7 seconds at which point the acceleration rate went to zero. Disassembly revealed total loss of the tip coating with smearing of the base metal. Heavy pushrod indications occurred in the base of the blade. It was apparent that despite the hard surface coating the parent material did not have sufficient strength to withstand the high unit loads imposed on the blades.

Sequence 21 -- This test duplicated Sequence 20 except the lubricant-impregnated chrome/nickel powder metal blades were employed. These blades were fabricated by Astro Met Associates, Inc. Cincinnati, Ohio.

The composition of the alloy powder for the parts was:

Component	Weight, %
Nickel	72.8
Chromium	15.00
Iron	7.00
Carbon	0.05
Silicon	0.40
Aluminum	0.75
Manganese	0.50
Copper	0.05
Niobium	0.90
Titanium	2.50
Sulfur	0.007

The sintered part is approximately 67 percent of solid metal density. The matrix is impregnated with a mixture (by weight) of 62 percent BaF_2 and 38 percent CaF_2. Bearing tests with this material, reported in Reference (4), also show low friction coefficient with the advantage that surface wear continuously exposes new lubricant material.

Considering that a linked configuration of these blades might be used in a later test, the slot location was changed to the center of the blade with a single slot instead of two to avoid interference of the linking mechanism with the slots as had previously occurred (Ref. Figure 30). This change reduced total slot area by 25 percent. With this configuration, a speed of 4,530 rpm was reached in 7.9 seconds at which point the speed curve went flat. Teardown inspection revealed two opposed blades broken along the edge of the slot. A relatively sharp corner at the base of the slot appeared to act as a stress-riser. Pushrod indentations were evident on the base of the blade. Tip wear was smooth on the blade although some indication existed of a swaging action tending to bulge and thicken the blade at the tip.

Sequence 22 -- This test was conducted with cast iron blades having a high aluminum content. The blade blanks were cast by Battelle, Columbus, Ohio to have the following composition.

Component	Weight, %
Carbon	1.5
Silicon	3.65
Manganese	0.7
Aluminum	21.5
Iron	Balance

The cast blanks were approximately 3.5-inch by 1.5-inch by 0.25-inch in size as received. The blanks were ground to finish thickness and then machined to the final blade dimensions. These blades were again fabricated with a single vent slot in the center. Installation was the same as the previous test.

This test achieved a speed of 3,514 rpm in 4.3 seconds and stopped abruptly. Three blades were found to be broken (each in the upper left hand corner). The most significant result of this test was that tip wear was very low with no smearing of the metal since it is very hard.

11. RESUMPTION OF HOT FIRE TESTING

To investigate the effects of the changes to the motor design on the thermal expansion problems previously experienced, hot gas testing was resumed. Performance data for hot gas runs RH-1 through RH-27B are summarized in Table 9.

Sequence RH-1 -- This initial test was conducted with phenolic blades since a final blade selection had not yet been made. It was recognized that the blades would not survive more than one run but it was anticipated that they would survive long enough to provide useful information regarding any remaining end clearance problems.

TABLE 9
HOT FIRE TEST DATA, SEQUENCES RH-1 THROUGH RH-27B

Seq.	Configuration	Fuel Inlet Pressure (psig)	Gas Inlet Pressure to Motor (psig)	End Cavity Pressure (psig)	Max. Speed (RPM)	Ramp Time (sec)	Fuel Temp. (°F)	Gas Temp. (°F)	Flow Rate (lbm/sec)	Comment
RH-1	• Circular stator • Phenolic blades • Spring-loaded pushrods	DATA NOT REDUCED			1,200	1.5	—	—	—	Blades failed at 1,200 RPM
-2	• Gas generator only	DATA NOT REDUCED								Checkout firing
-3	• Lightweight Inconel blades with coating	DATA NOT REDUCED								Motor did not spin
-4	• Oval stator • Fixed length pushrods • Carbon composite blades	1,425	687 max	—	1,071	4.0	—	—	—	
-5	• Same as -4	1,382	510	—	1,286	6.0	63	1,507	—	Motor jammed
-6	• Same as -4 except rotor notched 1.0" wide x 0.010 deep	1,335	615	< 10	1,250	5.5	59	1,547	—	Motor jammed
-7	• Same as -4 except rotor machined 0.010 across entire length	1,287	660	< 10	5,000	15.2	72	1,645 max	—	First hot run to 5,000 RPM
-8	• Same as -7	1,407	738 max 674 end of run	< 10	5,000	13.1	60	1,703 max	—	
-9	• Same as -7	1,035	930	60 peak 40 final	5,000	7.5	68	1,722	—	Higher flow capacity gas generator used

TABLE 9 (Continued)

HOT FIRE TEST DATA, SEQUENCES RH-1 THROUGH RH-27B

Seq.	Configuration	Fuel Inlet Pressure (psig)	Gas Inlet Pressure to Motor (psig)	End Cavity Pressure (psig)	Max. Speed (RPM)	Ramp Time (sec)	Fuel Temp. (°F)	Gas Temp. (°F)	Flow Rate (lbm/sec)	Comment
RH-10	• Same as -7	1,148	1,062	80 peak (<65 final)	5,000	6.1	66	1,681 peak (1,416 final)	—	
-11	• Same as -7 except silicon carbide blades			DATA NOT REDUCED						Motor stalled at 300 RPM
-12A	• Same as -11			DATA NOT REDUCED						No motor rotation
-12B	• Same as -11			DATA NOT REDUCED						No motor rotation
-13	• Same as -11	1,125	1,050	15 initial (60 final)	4,100	5.1	—	1,740 peak (714 final)		• Bearing replaced • Tachometer data lost-run terminated • T_{gas} dropped at end of run
-14	• Same as -11	1,185	1,080	8 initial (105 final)	4,070	11.0	66	1,726 peak (565 final)		Gas temp. dropped at end of run
-15	• Gas generator	1,122	1,027.5	N/A	N/A	N/A	55	1,758 peak (1,658 final)		Gas generator checkout
-16	• Same as -16	1,125 peak (563 final)	888 peak (188 final)	N/A	N/A	N/A	-53 initial -43 final	—		Gas generator checkout
-17	• Dual-gas generator	968	708	N/A	N/A	N/A	-47 initial -62 in 0.5 sec	1,538		Low temp. checkout firing of dual gas generator

TABLE 9 (Continued)

HOT FIRE TEST DATA, SEQUENCES RH-1 THROUGH RH-27B

Seq.	Configuration	Fuel Inlet Pressure (psig)	Gas Inlet Pressure to Motor (psig)	End Cavity Pressure (psig)	Max. Speed (RPM)	Ramp Time (sec)	Fuel Temp. (°F)	Gas Temp. (°F)	Flow Rate (lbm/sec)	Comment
		LARGE FLYWHEEL FOR BALANCE OF TESTS								
RH-18	• Same as -7 except secondary vent slots added	—	308	—	—	—		1,338	—	• -75 °F start • No motor rotation • Test with large flywheel
-19		DATA NOT REDUCED								• -60 °F start • No motor rotation • Pressure spike damaged gas gen.
-20	• Same as -18	1,260	transducer plugged	slow rise to 60	5,000	11.5	81	1,690	—	• -20 °F start • Ambient gas generator
-21	• Same as -20	1,272	1,050	95 final	1,710	—	56	1,609	0.553	• First hot restart attempt • Would not restart due to drag of loose end plate screws
-22	• Same as -20 except used Krytox 240A bearing grease	1,260	1,080	20 max	5,000	10.4	—	1,627	0.500	• First -65 °F start

TABLE 9 (Concluded)
HOT FIRE TEST DATA, SEQUENCES RH-1 THROUGH RH-27B

Seq.	Configuration	Fuel Inlet Pressure (psig)	Gas Inlet Pressure to Motor (psig)	End Cavity Pressure (psig)	Max. Speed (RPM)	Ramp Time (sec)	Fuel Temp. (°F)	Gas Temp. (°F)	Flow Rate (lbm/sec)	Comment
RH-23A	• Same as -22	1,287	960	14	2,770	5.8	50	1,580	—	
-23B	• Same as -22	1,280	966	6	2,286	4.7	50	1,59[illegible]	—	• First successful hot restart
-24A	• Same as -22	1,269	1,020	—	3,000	6.2	51	1,592	0.513	• Increased duration hot restart
-24B	• Same as -22	1,278	1,035	—	4,360	9.3	51	1,600	0.504	
-25A	• Same as -22	1,290	1,035	10	5,000	11.1	52	1,600	0.514	• Worst case duration hot restart
-25B	• Same as -22	—	1,050	12	5,000	11.2	15	1,610	0.516	
-26A	• Same as -22	1,365	927	27	643	1.7	53	1,525	0.509	• Motor conditioned accidently to -85 °F • Slow start • Restart O.K.
-26B	• Same as -22	1,259	990	15	5,000	12.6	54	1,591	0.481	
-27A	• Same as -22 except new carbon composite blades using Polycarbon, Inc. material	1,275	1,013	50 initial	5,000	12.3	64	1,580	0.479	• Checkout test of Polycarbon blade material
-27B		1,278	1,013	-	5,000	10.5	64	1,580	0.487	

This proved to be incorrect. Blade failure occurred at 1,200 rpm after about 1.5 seconds of operation therefore any potential galling problems were not experienced.

The acceleration rate was slower than normal due to a low inlet pressure of 750 psig versus the normal cold gas inlet pressure of 1,100 psig. The gas generator was apparently incapable of keeping up with the required motor flow rate.

Sequence RH-2 -- This run was a checkout firing of the gas generator without the motor. With inlet pressure of 1,500 psig and a chamber pressure of 1,070 psig, the flow rate from the generator was 0.28 lbm/sec., initially assumed adequate for the motor but unacceptable with the higher leakage rates currently being experienced.

To overcome this problem, a different gas generator was employed for future high pressure tests. This unit is capable of operation at higher flow rate and operating pressure to produce the required inlet pressure to the motor.

Sequence RH-3 -- A test was set up with the lightweight coated Inconel blades to investigate performance under hot conditions. This test was relatively unsuccessful since the motor turned slowly then jammed. The problem appeared to be that the higher coefficient of thermal expansion of the metal blades requires more clearance (both in blade length and thickness) if metal blades are ultimately to be used in the motor since they expand significantly more than the carbon composite blades.

Sequence RH-4 -- Since significant modifications to the design had been accomplished subsequent to the last use of carbon composite blades it was decided to re-test them in the new motor configuration. The oval stator was used which allows fixed length pushrods. The pushrods are notched at both ends to surround the blade, thereby partially sealing a leak path around the blade which occurs because the pushrods are larger in diameter than the blade thickness.

The first test was a low pressure cold gas checkout run (Run 23 as reported in Table 7). Acceptable performance was obtained and the configuration was committed to hot testing.

Sequence RH-5 -- This test achieved a speed of 1,250 rpm with pressure and speed versus time as shown in Figure 31 at which point rotation stopped. While hot, the rotor could not be turned by hand but did rotate after cooldown. Teardown revealed rotor/stator rubbing under the inlet due to thermal expansion of the rotor.

Sequence RH-6 -- The run above was repeated after the rotor had been machined to produce a circumferential groove 1-inch wide and 0.010-inch deep under the inlet to increase clearance in the area of maximum heat flux. The results essentially duplicated the previous run as shown in Figure 32. Teardown inspection showed the rubbing to occur

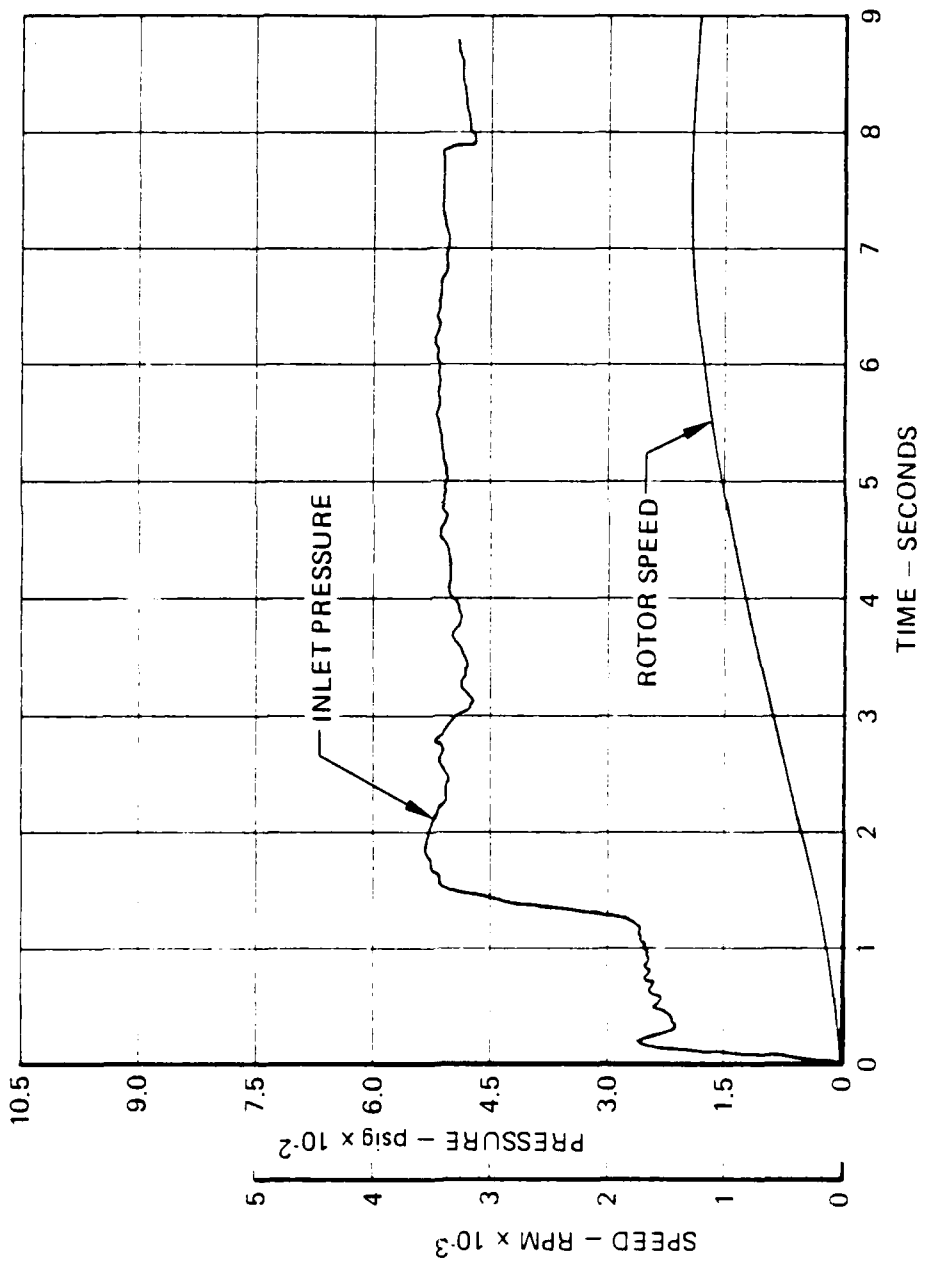

Figure 31. Inlet Pressure and Speed vs. Time – Test Sequence RH-5.

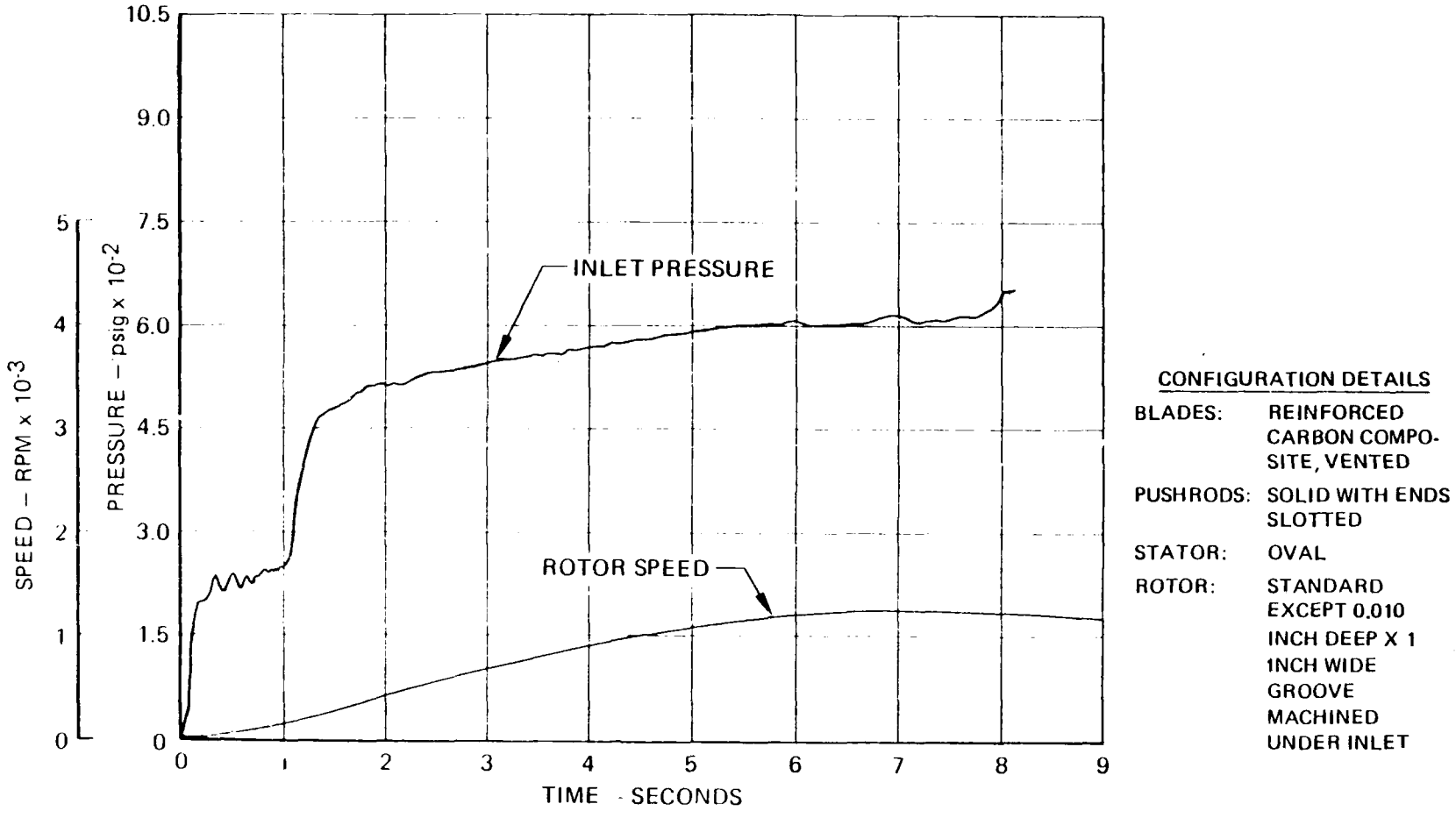

Figure 32. Inlet Pressure and Speed vs. Time – Test Sequence RH-6.

AD-A131 575 HYDRAZINE APU STARTER DEVELOPMENT(U) ROCKET RESEARCH 2/2
CORP REDMOND WASH D A PAHL JUN 83 RRC-83-R-905
AFWAL-TR-83-2039 F33615-78-C-2003

UNCLASSIFIED F/G 21/5 NL

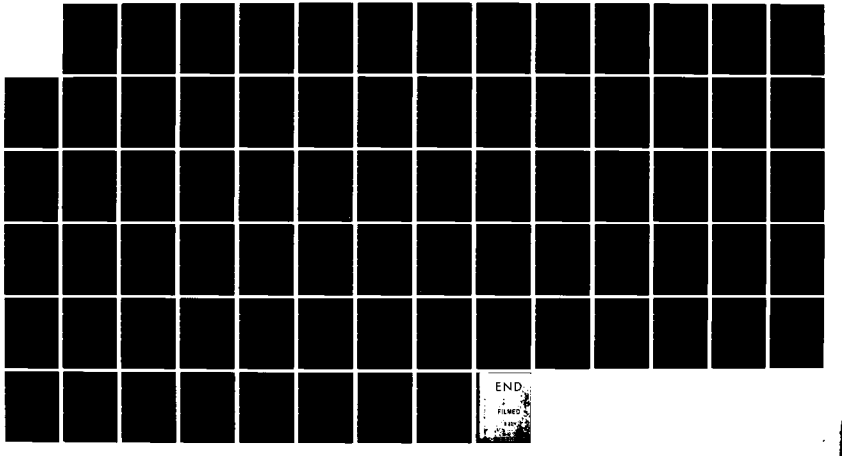

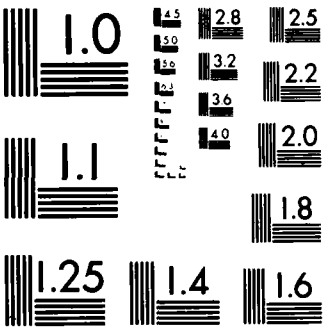

at the edges of the previously machined groove. The corner of the groove now had become the higher heat flux area.

Sequence RH-7 -- The rotor clearance was machined to the 0.010-inch depth across its entire length and the rotor was re-installed for test. This run, shown in Figure 33, achieved 5,000 rpm for the first time in a hot-fire test. As noted in the figure, the acceleration was smooth and nearly constant over the whole speed range.

Sequence RH-8 -- This run was a repeat of Sequence RH-7 and duplicated the previous results. Ramp times were 15.2 seconds for Sequence RH-7 and 13.8 seconds for Sequence RH-8. The limiting factor on speed was the flow output of the gas generator which produced a maximum output pressure in the range of 675 psig. A higher flow capacity gas generator was obtained and adapted to the motor inlet for further testing.

Sequence RH-9 -- For this test, the feed pressure to the new gas generator was set to achieve an estimated pressure mid-way between the 675 psig achieved in Sequence RH-7 and RH-8 and the 1,100 psig typically used in cold gas testing. For the actual run, a peak inlet pressure of 915 psig was achieved. Substantial improvement in operation was observed with ramp time reduced to 7.5 seconds as shown in Figure 34.

Sequence RH-10 -- The gas generator inlet pressure was raised again for this run resulting in a peak chamber pressure of 1,062 psig and a ramp time of 6.1 seconds with total run time on the order of 8.0 seconds. These results are plotted in Figure 35.

Since the angular acceleration is seen to be virtually constant over the ramp time, this run was used to calculate the actual motor torque output. The mean angular acceleration over the ramp is:

$$\frac{d^2\theta}{dt^2} = \frac{\dot{\theta}_2 - \dot{\theta}_1}{T_2 - T_1} = \left(\frac{5{,}000 - 286}{6.1}\right)\frac{2\pi}{60}$$

$$= 80.9 \text{ rad/sec}^2$$

For the flywheel inertia of 27.7 lbf-ft^2 the net torque was found to be 69.7 ft-lbf, well within the limiting value of 120 ft-lbf allowed.

Time to achieve 5,000 RPM versus motor inlet peak pressure at the end of the run for Sequences RH-7 through RH-10 is plotted in Figure 36.

12. RE-TEST OF SILICON CARBIDE INFILTRATED COMPOSITE BLADES

The success with the carbon composite blades led to consideration of re-evaluation of the silicon carbide configuration since blade wear could be significantly reduced with these harder blades.

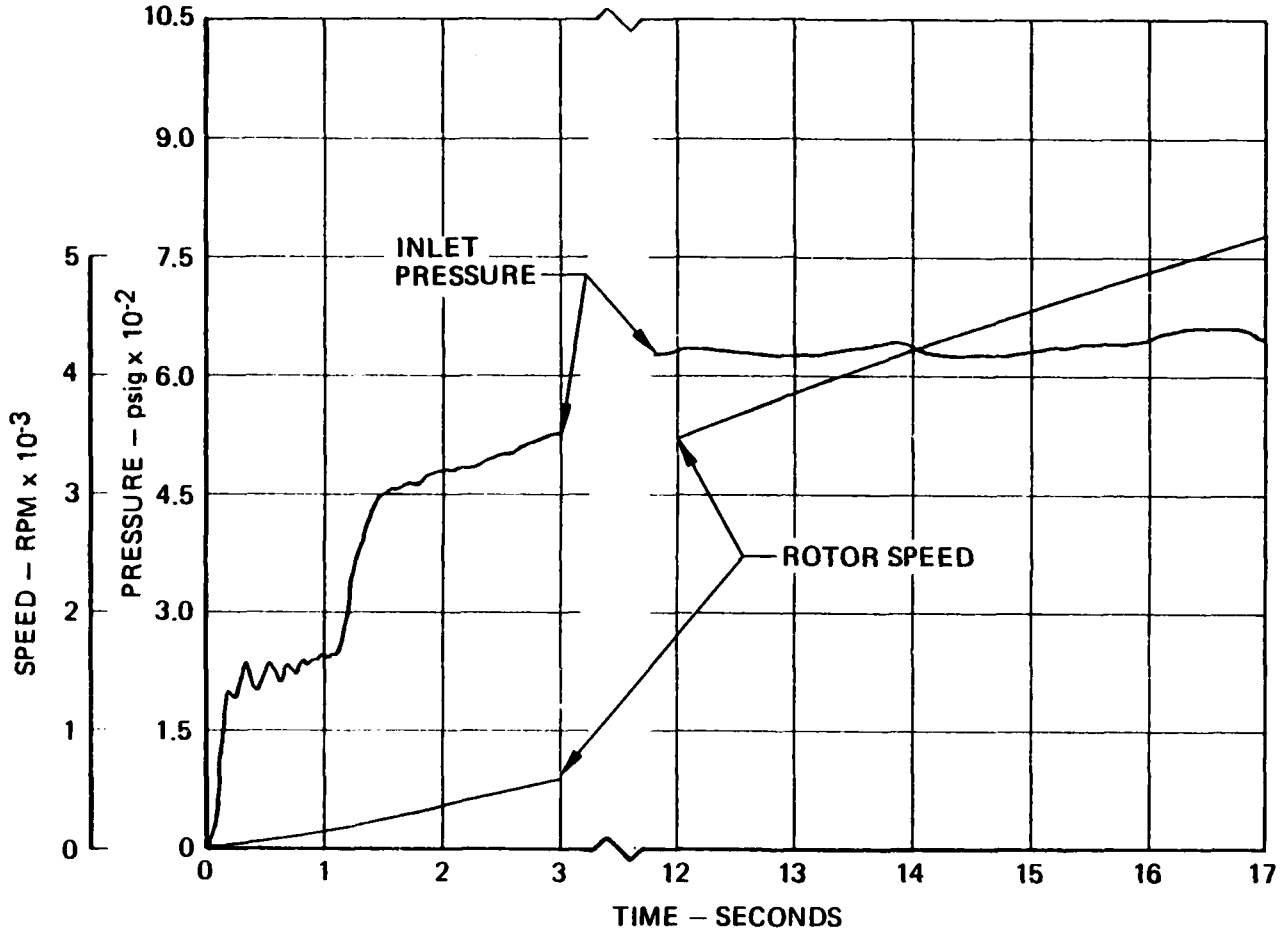

CONFIGURATION DETAILS

BLADES:	REINFORCED CARBON COMPOSITE, VENTED
PUSHRODS:	SOLID WITH ENDS SLOTTED
STATOR:	OVAL
ROTOR:	CLEARANCE INCREASED BY 0.010 INCH ACROSS FULL ROTOR WIDTH

Figure 33. Inlet Pressure and Speed vs. Time – Test Sequence RH-7.

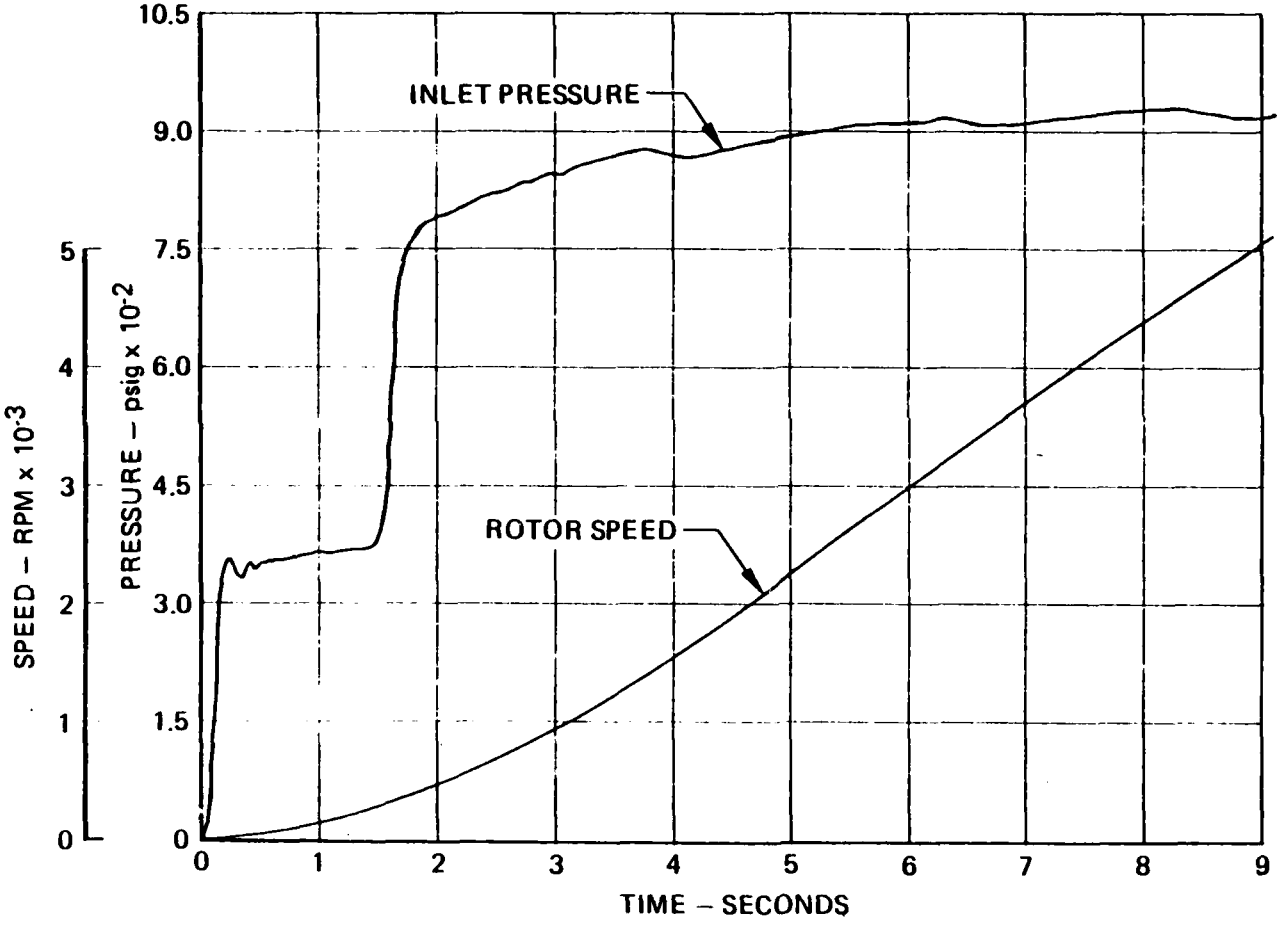

Figure 34. Inlet Pressure and Speed vs. Time – Test Sequence RH-9.

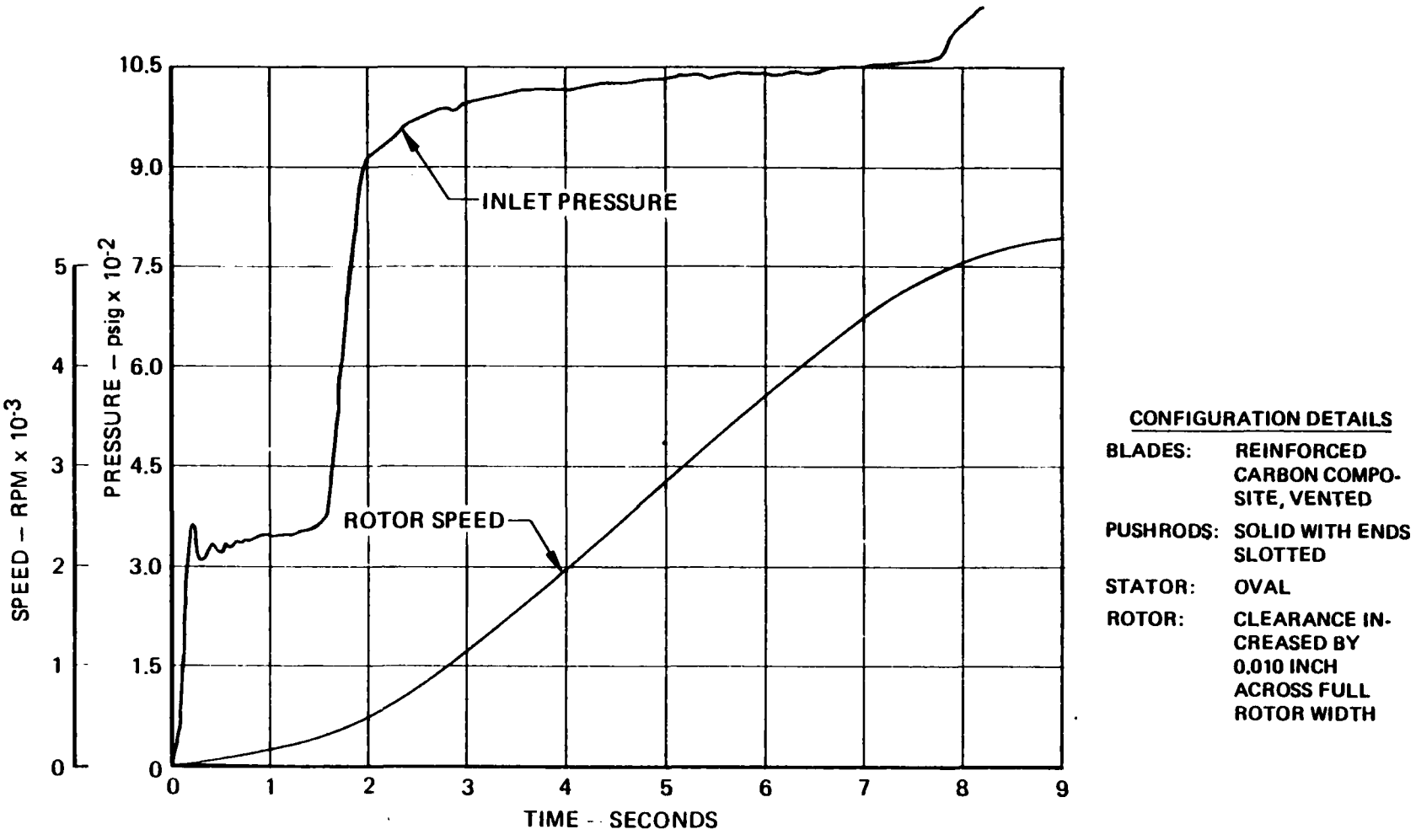

Figure 35. Inlet Pressure and Speed vs. Time – Test Sequence RH-10.

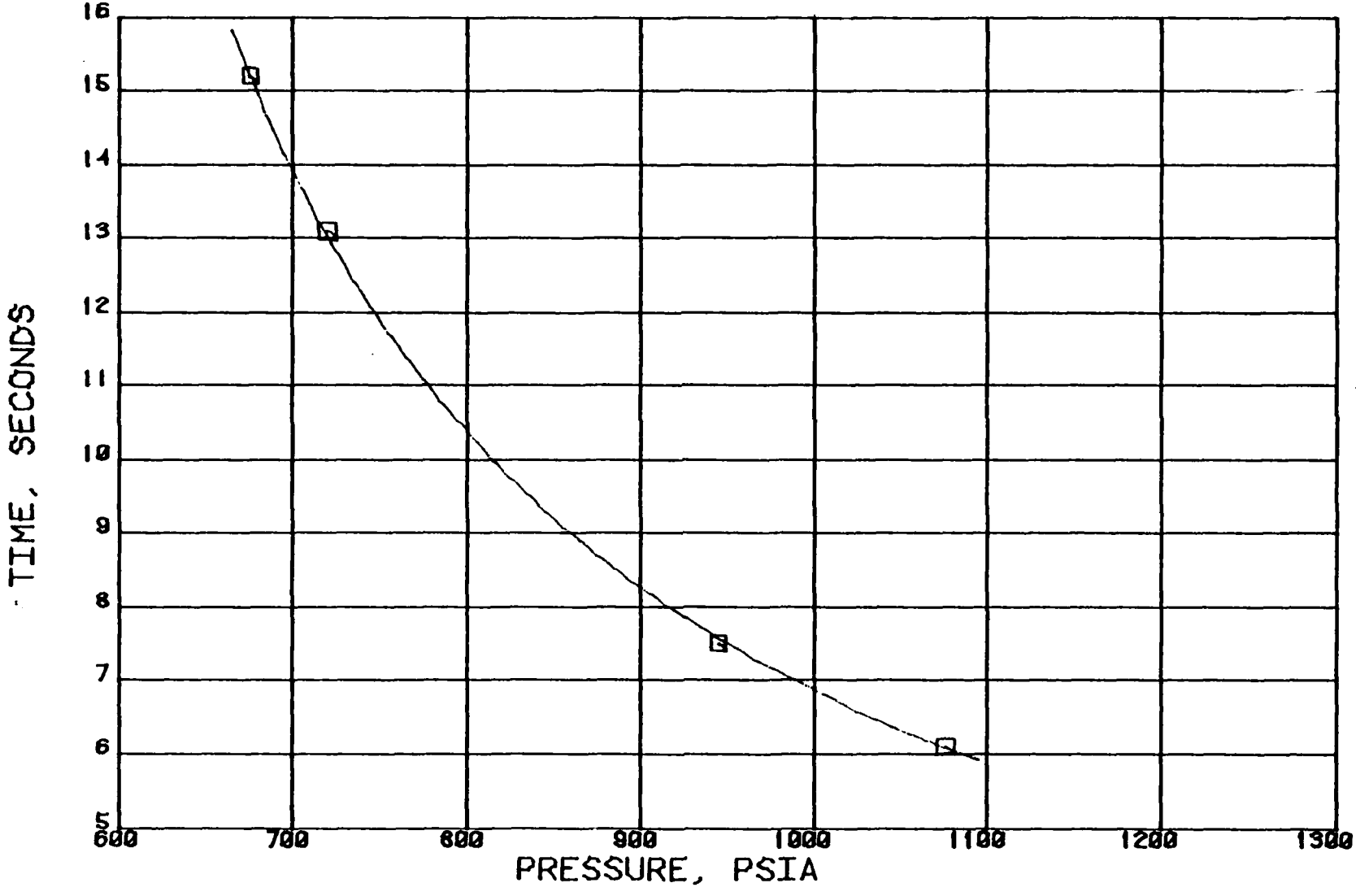

Figure 36. Time to 5,000 rpm Versus Inlet Pressure (Sequences RH-7 through RH-10)

Sequence RH-11 -- The motor accelerated to approximately 300 rpm at low pressure and stalled out upon application of the ramp pressure. After venting the system pressure, the motor could be rotated by hand. Teardown revealed no broken blades or obvious problems. The motor was re-assembled for test.

Sequence RH-12 -- The motor refused to turn upon application of the low pressure portion of the ramp. After tank venting, the motor was found to be free and capable of rotation. A second start was attemped with identical results. During teardown, it was observed that one of the bearings was quite rough. It could be rotated by hand but had obvious damage. It was concluded that the probable cause of the problems noted above was lockup of the bearing under the high side load resulting from the applied pressure. The bearing was replaced.

Sequence RH-13 -- This run started and appeared to accelerate normally. The tachometer readout was lost during the run and shutdown was commanded to avoid possible overspeed. Post-test review of the backup optical sensor data from the oscillograph revealed a speed of 4,100 rpm with an estimated ramp time of 5.1 seconds from 490 rpm to 4,100 rpm.

Sequence RH-14 -- The motor was inspected and found to be in good condition except that the mild steel rotor end plates were beginning to bow outward at the outer diameters due to operation at the high temperature with the applied pressure load acting behind them since there is not seal between the plates and rotor.

New end plates were fabricated of Hastelloy C material to reduce this bowing tendency in future hot runs; however, for this test, the old end plates were straightened to facilitate operations while new plates were fabricated.

Motor startup and ramping were smooth, however, the ramp time from 360 rpm to 4,070 rpm required 11 seconds at which point shutdown was commanded.

The previous runs with carbon/carbon composite blades were compared to the silicon carbide blade runs for possible differences to explain the almost 2 to 1 variation in ramp time observed.

A greater indication of wear on the stator with the silicon carbide blades indicated higher friction which would reduce performance. Also, the vent slot locations were found to be different. The carbon/carbon blades were cut down from existing blades previously tested with the cam positioning system. Since the older blades had notches at the base at each end to accommodate the cam operation system, they were cut back to the new stator length from either or both ends depending on the slot in which they were to be installed. This was done to assure that the full blade width was available in the pushrod

location (which varies for each pair of slots to avoid interference). The result was that the vent slots always fell between a pair of pushrods. With the silicon carbide blades (which were designed for the shorter rotor) the slots already exist and, in some blade locations, the slots overlap a pushrod. The effect of this difference is that the carbon/carbon blades have only 60 percent of their base area vented to the leading cavity (as opposed to the 100 percent expected) due to the partial sealing between under-blade cavities in the axial direction afforded by the pushrods.

Hand calculations were performed for several rotational positions of the blades indicating reduced tip force in some areas and increases in others with an apparent net favorable effect. Professor Wolgemuth re-analyzed the computer runs on the last two cases of his report (previously shown in Table 8) using a base area of two-thirds the previous value. The resulting friction power (per vane) for friction coefficients of 0.2 and 0.4 were 4.17 and 9.07 hp, reductions of 26.2 and 21.3 percent, respectively, from their previous values.

Pursuing these results further it was estimated that venting part of the under-blade area to the low pressure side and part to the high pressure would result in near-perfect pressure balance of the blade throughout a complete revolution, minimizing friction and also potentially reducing leakage by forcing the blades into contact with the stator on the power portion of the cycle.

To investigate this effect a set of cold gas runs were conducted with phenolic blades as summarized in previous Table 7.

Sequence C-24 -- Phenolic blades were machined to locate the vent slots between the pushrods as was the case with the carbon composite blades exhibiting the best performance in hot fire tests. These blades were installed with the vents on the leading edge of the blade (with solid pushrods) into the oval stator. With a nitrogen inlet pressure of 1,128 psig, the ramp time to 5,000 rpm was 9.1 seconds.

Sequence C-25 -- The phenolic blades from the previous run were reworked to provide small vent slots on the opposite (trailing edge) side of the blade. This vents the under-blade cavities outside the pushrods to the high pressure side of the blade. When this configuration was tested with an inlet pressure of 1,148 psig the ramp time was reduced to 6.85 seconds, an improvement of 24.7 percent. If inlet pressure had been reduced for this run such that the same ramp time was obtained as in the prior run, a reduction in gas consumption would have been achieved.

These results, although based on limited testing, were considered sufficiently conclusive such that the double venting approach was incorporated in subsequent testing.

13. LOW TEMPERATURE TESTING

Sequence RH-15 -- In preparation for the -65°F start testing, the gas generator was repacked with additional catalyst and subjected to a checkout firing at ambient temperature to establish a start sequence since the hardware being employed had not been designed or optimized for a low temperature start environment.

Sequence RH-16 -- During the first low temperature start a problem was encountered in actuating the propellant valve at -65°F and the actual start, consisting of a 200 ms pulse followed by the normal low feed pressure steady-state and ramp to high feed pressure occurred at -55°F. Satisfactory ignition was obtained; however, during the high feed pressure operation the outlet gas temperature dropped off indicating unstable operation of the catalyst bed with the cold propellant.

Since this hardware could not be readily modified to solve this problem, a second gas generator of the type originally employed was obtained. This was manifolded in parallel with the original gas generator to assure adequate flow rate capability.

Sequence RH-17 -- A checkout firing was accomplished with the dual gas generator at -65°F conditions. The previous fuel control valve opening problem at low temperature was resolved by incorporation of a 40-volt power supply to the valve.

Initial propellant entering the gas generator was at -47°F since some heatup occurred in the line while the system was being calibrated prior to firing. After approximately 0.5 seconds of operation, incoming propellant was -62°F. Operation of the gas generator pair was smooth with rising but stable gas temperature throughout the run.

Sequence RH-18 -- Based on the results of the C-24 and C-25 tests with phenolic blades, the secondary vent slots were machined into the carbon composite blades for these tests. To simulate the low temperature torque requirement of the APU, the second flywheel was installed on the test stand raising the total inertia to 41.2 lbf-ft^2. The dual gas generator was also installed. Because of the time required to install the motor after removal from the conditioning chamber, the unit was conditioned below -65°F to assure it would not be above the desired temperature at startup. Since the motor is conditioned in the same chamber as the propellant, this resulted in the propellant being subcooled also such that ignition took place with propellant near -75°F. As might be expected, a long ignition delay occurred on the initial pulse. Ignition was achieved and subsequent startup was normal.

No rotation of the motor occurred and the test was terminated. It was concluded that the initial pressure was not high enough to overcome the bearing drag due to the effect of the subcooled temperature on the bearing grease, and that subsequent tests should be run at higher pressure.

Sequence C-26 -- Prior to attempting another hot gas test, a checkout of the motor was made at ambient temperature with cold gas. Normal startup was achieved and the run was terminated at 2,300 rpm. Starting pressure was 188 psig and peak ramp pressure was 1,146 psig. Ramp time of 4.9 seconds to the noted speed indicated good performance with the higher inertia of the heavy flywheel.

Sequence RH-19 -- For this run, fuel temperature at startup was -60°F. A long ignition delay (on the order of 1.3 seconds) occurred on the initial pulse followed by a pressure spike to 1,383 psig. Upon subsequent steady-state startup, fuel flowrate dropped to a very low value, below the range at which the flowmeter would turn. Chamber pressure was erratic and gas temperature was very low. No rotation of the motor was observed.

Subsequent teardown of the motor revealed the cause of the problem. The excessive pressure spike had broken the catalyst retention bedplate in one gas generator, spilling catalyst into the motor inlet and tightly packing it such that the motor could not turn. The most probable cause of this failure was the parallel gas generator flow arrangement. Since ignition delay is not precisely repeatable at low temperature one generator ignited before the other. The initial pressure spike was fed back through the fuel manifold forcing flow at a high rate into the other gas generator inducing bed pressure drop significantly in excess of design values precipitating failure of the bed plate.

Sequence RH-20 -- A special test was conducted to evaluate the drag contribution of the bearing grease under low temperature conditions. A special fluorinated grease, Krytox 240AC, was being used in the bearings having a stated useful temperature range of -30°F to +550°F with short term service to 600°F. The manufacturer, Dupont, states that use at "much lower" temperature (unspecified) has been reported. Under these conditions it is believed that the thickener acts as a solid lubricant. This grease was the apparent source of the problem. The motor was pre-conditioned to -65°F and an attempt was made to rotate the motor shaft by hand. It could not be moved indicating that the bearings were the source of the low temperature problem. As a check on these assumptions, the motor was conditioned to -20°F for test. This is within the specified fluid range of the Krytox 240AC grease used in the bearings.

To avoid potential problems with the dual gas generator, this and subsequent tests were conducted with ambient temperature propellant.

The motor started readily and achieved a ramp time of approximately 11.5 seconds with fuel inlet pressure of 1,260 psig to the gas generator. A faulty chamber pressure transducer prevented an accurate reading of inlet pressure to the motor.

Sequence RH-21 -- This test was the first planned for the motor without refurbishment and inspection after the previous firing. It also was to be a cautious first simulation of a hot restart. The test was conducted at ambient temperature. The motor started normally and was ramped to 1,710 rpm at which point the initial ramp was terminated. The flywheel was then braked to a stop and the pressures re-set for the second start attempt. The motor would not turn upon the second application of pressure. This was initially assumed to be a thermal problem until it was determined, after motor cooldown to ambient temperature, that the motor still would not rotate.

Teardown revealed that the cap screws holding the end plates to the rotor had loosened and several were dragging on the end plate, preventing rotation. Initially, the end plates had to be removable to allow installation of two of the pushrods. When the original end plates were replaced with higher strength material, a rework was accomplished which permits installation and removal of the pushrods with end plates installed, thus, there was no reason not to make them a semi-permanent installation. This was accomplished by spot-brazing each bolt head after installation.

Sequence RH-22 -- This test was another attempt at -65°F operation. To determine if the bearing grease was the problem a substitute grease, Krytox 240AZ, was used which is specified for operation to -65°F. Upon installation in the stand after the cold soak the motor could be turned by rotating the flywheel by hand. Upon application of pressure, normal operation was observed together with a ramp time of 10.4 seconds. This was accomplished with a peak fuel inlet pressure of 1,259 psig and peak chamber pressure (equivalent to motor inlet pressure) of 1,080 psig at the end of the run and 975 psig at the start of the ramp.

14. LIMITED LIFE DEMONSTRATION

A series of tests encompassing 8 individual starts, were conducted without teardown of the motor between firings as a preliminary limited life demonstration.

Demonstrations were accomplished with the motor conditioned to -65°F as well as a series of increasing duration hot-restart tests culminating in a pair of full duration starts with the large flywheel.

Sequence RH-23A and -23B -- This test was the first attempt at a hot restart after having brazed the end plate cap screws in place. The first start had a ramp time of 5.8 seconds (equivalent in time to a full-speed ambient temperature motor start) and achieved 2,770 rpm with the large flywheel. Acceleration rate was 51.6 rad/sec^2.

The flywheel was stopped and pressures re-cycled for a second start. For the run, ramp duration was 4.7 seconds achieving a speed of 2,286 rpm. Acceleration rate was 54.6

rad/sec^2, slightly above the initial rate. Peak gas generator pressures for the runs were 960 and 966 psig respectively, with corresponding maximum gas temperatures of 1,580 and 1,591^{o}F.

Sequence RH-24A and -24B -- This test repeated the hot restart profile with slightly longer run times. The first run ramped to 3,000 rpm in 6.2 seconds while the restart ramped for 9.3 seconds and achieved 4,360 rpm. Peak chamber pressure for the runs were 1,020 psig and 1,035 psig with corresponding peak gas temperatures of 1,590 and 1,600^{o}F.

Sequence RH-25A and -25B -- This run consisted of t starts to 5,000 rpm. The first start had a ramp time of 11.1 seconds, a peak inlet ssure of 1,035 psig and a maximum gas temperature of 1,600^{o}F. For the second start p time was 11.2 seconds with inlet pressure of 1,050 psig and gas temperature of 10^{o}F. This latter test is considered an overstress test from the standpoint that for tual APU the required torque-speed curve for the restart would be reduced compared to the initial -65^{o}F start attempt. Thus the run duration and motor heating experienced in a real case would be less than has been demonstrated in this restart test.

Sequence RH-26A and -26B -- For this test, the motor was again conditioned to -65^{o}F prior to installation on the stand. The motor did not initially accelerate upon application of low pressure. As ramp pressure increased, the motor started to turn. The run was terminated by the technician due to excessive flame around the stand visible on the TV monitor. Upon inspection after shutdown, it was found that the exhaust gas collector manifold was slightly mislocated allowing part of the exhaust holes to vent externally. It was also noted that the motor was difficult to turn by hand. It was decided to continue with a hot restart. Upon application of low pressure the motor rotated normally and ramped to 5,000 rpm in 12.6 seconds. This slower speed was partly attributed to a lower than normal inlet pressure of 990 psig. Maximum gas temperature was 1,591^{o}F during the restart.

Teardown of the motor after this run revealed contamination of the fixed-end bearing lubricant including a number of small metal chips. The opposite bearing showed no damage and lubricant was apparent on the bearing. This condition confirms the need for a secondary seal in the motor shaft-to-bearing area to minimize gas flow in this direction.

Subsequent to this investigation an additional cause for the slow start was determined. A new conditioning chamber with digital controls (which does not have a continuous analog strip chart recording) was used in preconditioning the motor for this test. The chamber is very accurately controlled to the set temperature, however, the controller supplied with the unit was calibrated for centigrade rather than the fahrenheit

calibration that was ordered. Thus the motor was actually conditioned to -85°F prior to the start, contributing to the slow startup that was observed.

Sequence RH-27A and -27B -- The life and wear that had been accumulated on the carbon composite blades in previous tests was of concern if they were to be used in the life testing. The long lead time for fabrication of this material precluded obtaining any additional blades in time to support the test. As an alternate, a block of existing material was obtained from Polycarbon, Inc., North Hollywood, California and blades were machined from the block.

A start and hot restart were accomplished with this material achieving ramp times of 12.3 and 10.5 seconds respectively.

The blades were inspected after the test and found to be in good condition. As a result of these tests, the new material was selected for the initial Phase IV life testing.

These tests concluded work on the Phase III effort. The initial scope of Phase III had been planned as 35 hot fire tests including 10 full-duration starts at each of the three temperatures (-65°F, ambient, +130°F). The actual testing was increased significantly due to problems in achieving a satisfactory motor configuration and blade material for hot operation. In all, 74 individual motor starts were accomplished, 41 with cold gas and 33 with hot gas. Of the 33 hot tests, 4 were low temperature start attempts and 5 were hot restarts at temperatures above the design ambient upper limit of 130°F thereby verifying capability in this area.

SECTION V
LIFE TESTING

Program Phase IV was designed to obtain motor life information at preconditioning temperatures of -65, ambient, and +130°F. The goal was to accomplish 100 starts without maintenance as a means of evaluating potential life capability up to 1,000 starts.

To accomplish the maximum number of motor starts within the limited remaining contract funds, restructuring of the program test plan was necessary. Previous demonstrations of hot restart capability had shown that the motor could operate successfully with motor start temperatures above 130°F, therefore, tests at this specific ambient preconditioning temperature were eliminated.

Tests at -65°F require use of the heavy flywheel, a time consuming operation to remove and re-install. Three possible choices were available.

a. Conduct all tests with the large flywheel. Since -65°F tests represent a small fraction of the total tests, conducting all tests to a full 5,000 rpm represents a thermal overstress for tests at ambient or hot restart conditions which would normally have a shorter run time due to operation with the small flywheel.

b. Same as 1 except limit the run time in ambient and hot restarts to simulate correct thermal input. With this approach the majority of the runs would not go to 5,000 rpm and thus would not experience the full blade loads.

c. Conduct all tests with the small flywheel. This approach was adopted for the life testing since all runs experience full blade loads and only a minority of runs (the -65°F starts) experience a less-than-normal thermal input.

Results of the last tests of Phase III revealed that the maximum number of individual motor starts could be accomplished in a given time period by incorporation of a hot restart after each ambient or low temperature start. Thus the life test sequence was structured as follows:

Test No.	Initial Start Temp.	Hot Restart	Cumulative Starts
4-1	-65°F	Yes	2
4-2	Ambient	Yes	4
4-3	Ambient	Yes	6
4-4	Ambient	Yes	8
4-5	Ambient	Yes	10

This five-step sequence was to be repeated until the desired number of starts was accumulated or motor breakdown occurred.

To assist in evaluation of the motor operation additional instrumentation was added. Surface thermocouples were installed adjacent to the inlet (identified as TW-1 in subsequent tables) and 120° away (TW-2) in the direction of rotation. Location of a surface thermocouple in the third symmetrical location was not possible due to the exhaust duct. This thermocouple, TW-3, was therefore of the immersion type and was installed into a hole drilled lengthwise in the stator approximately 0.5 inches below the surface. A fourth thermocouple, TW-4, was located on the outer support of the fixed-end bearing in an attempt to monitor the bearing temperature both during the run and under soakback conditions after a hot restart.

In a similar manner a port was drilled to intersect the first of the multiple exhaust holes in the stator. Both pressure (PE) and exhaust temperature (TE) measurements were made through this port. To obtain the best estimate of the static pressure in the motor the exhaust port was plugged leaving only a small orifice to assure that the gas would not stagnate in the port and prevent a good temperature measurement.

Intermittent operation of these thermocouples was a continuing problem in the life tests as hot gas leakage from the bearing vents and around the exhaust duct damaged leadwires and detached the thermocouples.

Run No. 4.1A and 4.1B -- The motor was assembled with a set of newly fabricated blades, pushrods, seals, and bearings. The blades were machined from the large block of carbon composite material obtained from Polycarbon, Inc. The motor was conditioned to -65°F and installed for test. Results of the initial start and hot restart are summarized in Table 10. As a result of the time required to install the instrumentation prior to test, the motor external temperature averaged -11.7°F at the start (although internal temperature would be significantly lower) and 193°F at initiation of the hot restart. Time to speed was 9.7 and 9.0 seconds respectively for the cold start and hot restart. Propellant consumption for each run was calculated by two methods. As listed in the tables, Method A employs pre-and-post test readings of a calibrated sight glass while Method B uses average flowmeter readings over the initial low pressure start, ramp, and acceleration portions of the run. Problems exist with each method. For hot restarts, the propellant tank must be re-filled rapidly for minimum down-time. This can result in bubbles in the sight glass which distort the readings. The flowmeter method has problems due to the transient nature of the flow, however, the acceleration phase is the longest and can be measured accurately so that the discrepancies in the startup phases do not contribute major error.

TABLE 10

VANE MOTOR HOT GAS TEST DATA

RUN NUMBER: 4.1 TEST DATE: 1-24-83

PARAMETER	SEQUENCE A, START TEMP, F: -11.7 LOW PRESSURE	SEQUENCE A END OF RAMP	SEQUENCE A END OF RUN	SEQUENCE B, START TEMP, F: 193.3 LOW PRESSURE	SEQUENCE B END OF RAMP	SEQUENCE B END OF RUN
PR, PSIA	624.5	1451.0	1454.5	642.5	1466.5	1472.5
PIN, PSIA	546.0	1320.5	1338.5	561.0	1341.5	1350.5
PC, PSIA	377.7	908.7	1022.7	389.7	962.7	1024.7
PE,MAX PSIA	124.2	303.6	167.7	149.5	312.7	187.6
PE,MIN PSIA	22.8	46.1	91.7	25.8	44.1	115.1
PCC, PSIA	21.9	56.4	22.1	29.9	55.8	31.9
N2, RPM	129	387	4986	146	488	5017
W, LBM/SEC	0.2347	0.5498	0.4948	0.2476	0.5365	0.5229
TI, DEG F	70.0	79.6	76.0	66.3	66.3	68.3
TC, DEG F	950.0	1350.0	1595.0	1000.0	1400.0	1605.0
TE, DEG F	-15.0	350.0	625.0	215.0	560.0	1010.0
TW-1, DEG F	-5.0	10.0	105.0	215.0	210.0	425.0
TW-2, DEG F	-15.0	20.0	370.0	130.0	160.0	520.0
TW-3, DEG F	-15.0	-15.0	-15.0	235.0	235.0	240.0
TW-4, DEG F	-15.0	32.0	515.0	75.0	75.0	75.0
TIME TO SPEED, SEC		9.7			9.0	
FUEL CONSUMPTION, LBM						
METHOD A		4.968			5.067	
METHOD B		4.596			4.513	

NOTE 1: START TEMP = (TW-1 + TW-2 + TW-3) / 3

NOTE 2: ENTRIES FOR TW-1, TW-2, TW-3, & TW-4 FOR THE LOW PRESSURE DATA ARE AT TIME = 1.0 SECONDS

Two values of exhaust pressure are shown representing the maximum and minimum pressures in the cavity as the blade just crosses the first exhaust opening and the subsequent pressure after 45 degrees of rotation. Substantial thermal drift occurred with this instrumentation, thus the pressures recorded at the end of the ramp are most representative.

Run No. 4.2A and 4.2B -- The second set of runs, shown in Table 11 were initiated at average motor temperatures of 63°F and 255°F each having a ramp time of 10.8 seconds.

Run No. 4.3 -- An attempt at a third series of runs was unsuccessful as the motor would not turn. The problem was determined to be primarily of the form of surface delamination of the blades. This is most likely due to having machined the blades from a thick block with the result that part of the thickness of the outer layer of material was machined away.

Run No. 5.1A and 5.1B -- The motor was reassembled with the old carbon composite blades used through most of the Phase III runs, a new set of pushrods and new bearings. The first run, shown in Table 12, was again a start at low temperature. The temperature data shown in the table is in error for Sequence A due to incorrect calibration set-up. Run times of 11.3 and 9.9 seconds were recorded, the slower times being a result of reduced inlet pressure as pressure drop built up in the gas generators due to accumulated firing life at high flow rate.

Run No. 5.2A and 5.2B -- These tests, shown in Table 13, again consisted of an ambient start and hot restart with ramp times of 10.6 and 9.6 seconds.

Run No. 5.3A and 5.3B -- Test Run 5.3 is presented in Table 14. For these runs ramp times of 16.5 and 19.7 seconds occurred, the result of further reduction in gas generator output pressure. At the end of the second run, the motor was obviously experiencing difficulty and then stopped abruptly. Teardown inspection indicated that a contributor to the slow ramping was damage to (or loss of) parts of one or more blades leading to excessive leakage. The motor is generally able to tolerate this since small pieces of the blade material can exit the exhaust ports or get crushed between rotor and stator. The ultimate cause of the motor stopping suddenly was the fact that a pushrod left its slot and the end became trapped and deformed into the rotor/stator clearance totally jamming the parts.

Run No. 6.1 -- Both gas generators were repacked to allow testing to continue. The motor was re-built with new blades fabricated of the Polycarbon material, and also new pushrods and bearings.

For Run No. 6.1 shown in Table 15, the motor was preconditioned overnight to -100°F to allow time for setup. External stator temperatures in the range of -50 to -55°F

TABLE 11

VANE MOTOR HOT GAS TEST DATA

RUN NUMBER: 4.2 TEST DATE: 1-25-85

PARAMETER	SEQUENCE A, START TEMP, F: 63.0 LOW PRESSURE	SEQUENCE A END OF RAMP	SEQUENCE A END OF RUN	SEQUENCE B, START TEMP, F: 250.0 LOW PRESSURE	SEQUENCE B END OF RAMP	SEQUENCE B END OF RUN
PR, PSIA	621.0	1446.0	1454.0	629.0	1464.0	1464.0
PIN, PSIA	551.0	1329.0	1347.0	552.0	1351.0	1353.0
PC, PSIA	311.0	833.0	971.0	348.0	891.0	956.0
PE,MAX PSIA	129.0	247.0	157.0	146.0	298.0	173.0
PE,MIN PSIA	24.0	59.0	47.0	33.0	61.0	96.0
PCC, PSIA	29.6	7.2	6.0	32.2	62.4	0.0
N2, RPM	89	316	5172	117	269	5172
W, LBM/SEC	0.2659	0.5459	0.4860	0.2304	0.5404	0.5078
TF, DEG F	67.0	68.0	69.0	64.0	64.0	65.0
TG, DEG F	920.0	1340.0	1595.0	930.0	1350.0	1630.0
TE, DEG F	67.0	87.0	220.0	81.0	129.0	239.0
TW-1, DEG F	63.0	63.0	261.0	268.0	262.0	320.0
TW-2, DEG F	63.0	66.0	540.0	192.0	210.0	640.0
TW-3, DEG F	63.0	63.0	66.0	305.0	305.0	309.0
TW-4, DEG F	63.0	64.0	80.0	303.0	304.0	315.0

	SEQUENCE A	SEQUENCE B
TIME TO SPEED, SEC	10.8	10.8
FUEL CONSUMPTION, LBM		
METHOD A	4.849	4.355
METHOD B	5.153	5.154

NOTE 1: START TEMP = (TW-1 + TW-2 + TW-3) / 3

NOTE 2: ENTRIES FOR TW-1, TW-2, TW-3, & TW-4 FOR THE LOW PRESSURE DATA ARE AT TIME = 0.0 SECONDS

TABLE 12

VANE MOTOR HOT GAS TEST DATA

RUN NUMBER: 5.1 TEST DATE: 2-1-83

PARAMETER	SEQUENCE A START TEMP, F 81.7 LOW PRESSURE	SEQUENCE A START TEMP, F 81.7 END OF RAMP	SEQUENCE A START TEMP, F 81.7 END OF RUN	SEQUENCE B START TEMP, F 199.7 LOW PRESSURE	SEQUENCE B START TEMP, F 199.7 END OF RAMP	SEQUENCE B START TEMP, F 199.7 END OF RUN
PR, PSIA	643.0	1469.0	1473.0	639.0	1463.0	1465.0
PIN, PSIA	577.0	1367.0	1371.0	581.0	1364.0	1370.0
PC, PSIA	297.0	795.0	927.0	303.0	771.1	861.0
PE,MAX PSIA	164.0	241.0	148.0	125.0	292.0	156.0
PE,MIN PSIA	21.0	34.0	72.0	35.0	55.0	79.0
PCC, PSIA	17.0	29.0	23.2	25.2	48.4	47.4
N2, RPM	98	377	4975	65	275	4954
W, LBM/SEC	0.2478	0.4856	0.4470	0.2628	0.4861	0.4567
TE, DEG F	65.0	65.0	66.0	61.0	61.0	61.0
TG, DEG F	756.0	1230.0	1585.0	1070.0	1270.0	1622.0
TC, DEG F	129.0	220.0	830.0	300.0	420.0	940.0
TW-1, DEG F	5.0	5.0	110.0	230.0	230.0	360.0
TW-2, DEG F	125.0	127.0	143.0	165.0	165.0	174.0
TW-3, DEG F	115.0	79.0	136.0	177.0	-19.0	51.0
TW-4, DEG F	0.0	5.0	179.0	240.0	240.0	275.0
TIME TO SPEED, SEC			11.3			8.4
FUEL CONSUMPTION, LBM						
METHOD A			0.306			4.120
METHOD B			4.944			4.366

NOTE 1: START TEMP = (TW-1 + TW-2 + TW-3) / 3

NOTE 2: ENTRIES FOR Tw-1, TW-2, TW-3, & Tw-4 FOR THE LOW PRESSURE DATA ARE AT TIME = 0.0 SECONDS

TABLE 13

VANE MOTOR HOT GAS TEST DATA

RUN NUMBER: 5.2 TEST DATE: 2-2-83

PARAMETER	SEQUENCE A, START TEMP, F = 55.0			SEQUENCE B, START TEMP, F = 240.0		
	LOW PRESSURE	END OF RAMP	END OF RUN	LOW PRESSURE	END OF RAMP	END OF RUN
PR, PSIA	630.0	1464.0	1467.0	649.0	1473.0	1474.0
PIN, PSIA	559.0	1357.0	1368.0	567.0	1359.0	1365.0
PC, PSIA	277.0	729.0	918.0	306.0	801.0	868.0
PE,MAX PSIA	91.0	239.0	0.0	83.0	275.0	0.0
PE,MIN PSIA	16.0	55.0	0.0	25.0	67.0	0.0
PPC, PSIA	16.2	21.8	26.0	20.0	35.2	42.0
N2, RPM	61	288	5172	80	308	4231
W, LBM/SEC	0.3178	0.4950	0.4585	0.2749	0.4808	0.4383
TF, DEG F	59.0	62.0	64.0	53.0	55.0	56.0
TG, DEG F	310.0	1220.0	1590.0	710.0	1250.0	1589.0
TF, DEG F	210.0	250.0	830.0	340.0	470.0	920.0
TW-1, DEG F	55.0	100.0	150.0	260.0	260.0	400.0
TW-2, DEG F	50.0	120.0	520.0	180.0	185.0	940.0
TW-3, DEG F	60.0	60.0	60.0	280.0	280.0	280.0
TW-4, DEG F	55.0	65.0	75.0	280.0	280.0	300.0
TIME TO SPEED, SEC			10.6			9.6
FUEL CONSUMPTION, LBM						
METHOD A			4.616			0.000
METHOD B			4.764			4.975

NOTE 1: START TEMP = (TW-1 + TW-2 + TW-3) / 3

NOTE 2: ENTRIES FOR TW-1, TW-2, TW-3, & TW-4 FOR THE LOW PRESSURE DATA ARE AT TIME = 0.0 SECONDS

TABLE 14
VANE MOTOR HOT GAS TEST DATA

RUN NUMBER: 5.3 TEST DATE: 2-2-83

PARAMETER	SEQUENCE A, START TEMP, F = 90.0			SEQUENCE B, START TEMP, F = 325.0		
	LOW PRESSURE	END OF RAMP	END OF RUN	LOW PRESSURE	END OF RAMP	END OF RUN
PR, PSIA	645.0	1434.0	1436.0	651.0	1502.0	1508.0
PIN, PSIA	534.0	1322.0	1350.0	556.0	1385.0	1443.0
PC, PSIA	255.0	681.0	804.0	243.0	722.0	813.0
PE,MAX PSIA	77.4	178.8	157.9	50.5	137.1	171.8
PE,MIN PSIA	16.7	57.5	64.4	16.9	65.4	96.3
PCC, PSIA	17.6	26.5	40.9	22.4	56.0	76.8
N2, RPM	53	149	4795	26	82	3790
W, LBM/SEC	0.3957	0.4195	0.4092	0.3892	0.4578	0.3985
TF, DEG F	60.0	60.0	62.0	58.0	58.0	58.0
TC, DEG F	310.0	1270.0	1575.0	760.0	1330.0	1580.0
TT, DEG F	130.0	220.0	900.0	360.0	440.0	1010.0
TW-1, DEG F	90.0	90.0	220.0	330.0	330.0	870.0
TW-2, DEG F	90.0	160.0	560.0	265.0	770.0	870.0
TW-3, DEG F	90.0	90.0	110.0	380.0	380.0	390.0
TW-4, DEG F	90.0	100.0	140.0	390.0	400.0	460.0
TIME TO SPEED, SEC			16.5			19.7
FUEL CONSUMPTION, LBM						
METHOD A			6.472			6.058
METHOD B			6.439			8.379

NOTE 1: START TEMP = (TW-1 + TW-2 + TW-3) / 3

NOTE 2: ENTRIES FOR TW-1, TW-2, TW-3, & TW-4 FOR THE LOW PRESSURE DATA ARE AT TIME = 0.0 SECONDS

TABLE 15

VANE MOTOR HOT GAS TEST DATA

RUN NUMBER: 6.1 TEST DATE: 02-16-83

PARAMETER	SEQUENCE A, START TEMP, F: -48.3 LOW PRESSURE	SEQUENCE A, START TEMP, F: -48.3 END OF RAMP	SEQUENCE A, START TEMP, F: -48.3 END OF RUN	SEQUENCE B, START TEMP, F: 0.0 LOW PRESSURE	SEQUENCE B, START TEMP, F: 0.0 END OF RAMP	SEQUENCE B, START TEMP, F: 0.0 END OF RUN
PR, PSIA	637.2	1450.2	1456.2	0.0	0.0	0.0
PIN, PSIA	521.7	1199.7	1237.2	0.0	0.0	0.0
PC, PSIA	431.7	931.2	1025.7	0.0	0.0	0.0
PE,MAX PSIA	135.7	284.7	160.7	0.0	0.0	0.0
PE,MIN PSIA	19.7	31.7	81.7	0.0	0.0	0.0
PCC, PSIA	14.7	14.7	14.7	0.0	0.0	0.0
N2, RPM	61	231	4615	0	0	0
W, LBM/SEC	0.3969	0.8139	0.7466	0.0000	0.0000	0.0000
TF, DEG F	67.0	68.0	69.0	0.0	0.0	0.0
TG, DEG F	330.0	1110.0	1580.0	0.0	0.0	0.0
TE, DEG F	110.0	170.0	850.0	0.0	0.0	0.0
TW-1, DEG F	-50.0	-45.0	130.0	0.0	0.0	0.0
TW-2, DEG F	-40.0	-20.0	285.0	0.0	0.0	0.0
TW-3, DEG F	-55.0	-54.0	-51.0	0.0	0.0	0.0
TW-4, DEG F	0.0	0.0	0.0	0.0	0.0	0.0
TIME TO SPEED, SEC			0.0			0.0
FUEL CONSUMPTION, LBM						
METHOD A			6.369			0.000
METHOD B			6.398			0.000

NOTE 1: START TEMP = (TW-1 + TW-2 + TW-3) / 3

NOTE 2: ENTRIES FOR TW-1, TW-2, TW-3, & TW-4 FOR THE LOW PRESSURE DATA ARE AT TIME = 0.0 SECONDS

were noted indicating that internal parts were at or below -65°F. Normal start and ramp operation was observed with a ramp time of 9.0 seconds to 4,615 rpm. During the run a leaking fitting at the gas generator inlet resulted in a minor fire therefore the run was terminated before reaching 5,000 rpm. No hot restart could be attempted.

Run No. 6.2A -- Test 6.2A shown in Table 16 was an ambient temperature start. Normal operation occurred with a ramp time of 10.4 seconds. In an attempt to determine if the hot restarts were affecting the blade life, they were not attempted for this series until Run 6.3B.

Run 6.3A and 6.3B -- Test No. 6.3A shown in Table 17 was another ambient start with a ramp time of 11.2 seconds. Normal operation occurred during the test.

Test 6.3B was a hot restart following the above test as also shown in Table 17. A normal start occurred but the motor stopped at a speed of 1,357 rpm. Teardown indicated no problems with the blades, pushrods, end seals or bearings. The problem was traced to loss of an alignment dowel pin during a previous firing. Periodic removal and replacement of the pins during Phase III and IV testing together with wear from a number of abrupt motor stops resulted in loosening of the pins. When one pin was lost it allowed the end plate to shift relative to the stator causing rotor/stator rubbing which stopped the rotation.

Depletion of contract funds at this point led to termination of testing although the hardware could have been re-assembled as-is for more life tests.

1. FLOW RATE ANALYSIS

The higher than expected flow rate of hot gas in these tests was of concern and an analysis was conducted to determine possible causes.

Summary flow rate data from cold gas and hot gas tests of various configurations were compiled and compared with theoretical flow rate in their appropriate tables. The theoretical flow rate is calculated based on charging the inlet volume with gas at the measured inlet pressure and temperature with gas of a known molecular weight. Inlet volume for each configuration is calculated as the cavity volume ahead of the blade which is just passing the downstream edge of the inlet port. This volume must include such items as the volumes of the vent slots and the underblade volume exposed by the vent, the latter depending on whether the leading or trailing edge of the blade is vented.

The results of these calculations are summarized in Table 18. In general, cold gas tests where the blades would be expected to have relatively good contact with the stator show average flow rates compared to theoretical in the range of 105 to 115 percent (Data Sets 2, 4, 5). The configuration for Data Set 1 had no vent slots, thus, the high inlet

TABLE 16

VANE MOTOR HOT GAS TEST DATA

RUN NUMBER: 6.2 TEST DATE: 02-17-83

PARAMETER	SEQUENCE A LOW PRESSURE	SEQUENCE A END OF RAMP	SEQUENCE A END OF RUN	SEQUENCE B LOW PRESSURE	SEQUENCE B END OF RAMP	SEQUENCE B END OF RUN
	START TEMP, F 59.3			START TEMP, F 0.0		
PR, PSIA	625.2	1454.7	1466.7	0.0	0.0	0.0
PIN, PSIA	539.7	1294.2	1346.7	0.0	0.0	0.0
PC, PSIA	415.7	974.7	1085.7	0.0	0.0	0.0
PE,MAX PSIA	125.7	282.7	132.7	0.0	0.0	0.0
PE,MIN PSIA	30.7	62.2	100.7	0.0	0.0	0.0
PCC, PSIA	70.7	106.3	14.7	0.0	0.0	0.0
N2, RPM	129	309	5085	0	0	0
W, LBM/SEC	0.3031	0.6367	0.5656	0.0000	0.0000	0.0000
TF, DEG F	53.0	53.0	55.0	0.0	0.0	0.0
TC, DEG F	0.0	0.0	0.0	0.0	0.0	0.0
TE, DEG F	210.0	270.0	970.0	0.0	0.0	0.0
TW-1, DEG F	60.0	66.0	112.0	0.0	0.0	0.0
TW-2, DEG F	58.0	64.0	420.0	0.0	0.0	0.0
TW-3, DEG F	60.0	60.0	63.0	0.0	0.0	0.0
TW-4, DEG F	60.0	60.0	70.0	0.0	0.0	0.0
TIME TO SPEED, SEC			10.4			0.0
FUEL CONSUMPTION, LBM						
METHOD A			6.143			0.000
METHOD B			5.812			0.000

NOTE 1: START TEMP = (TW-1 + TW-2 + TW-3) / 3

NOTE 2: ENTRIES FOR TW-1, TW-2, TW-3, & TW-4 FOR THE LOW PRESSURE DATA ARE AT TIME = 0.0 SECONDS

TABLE 17

VANE MOTOR HOT GAS TEST DATA

RUN NUMBER: 6.3 TEST DATE: 02-18-83

PARAMETER	SEQUENCE A, START TEMP, F = 63.0			SEQUENCE B, START TEMP, F = 276.0		
	LOW PRESSURE	END OF RAMP	END OF RUN	LOW PRESSURE	END OF RAMP	END OF RUN
PR, PSIA	628.0	1459.2	1465.2	631.2	1463.7	1468.2
PIN, PSIA	544.2	1351.7	1346.7	554.7	1306.7	1477.2
PC, PSIA	419.2	982.2	1072.2	448.2	1021.2	1100.7
PE,MAX PSIA	124.7	259.7	186.7	100.7	223.7	236.7
PE,MIN PSIA	38.7	80.7	131.7	43.7	84.7	80.0
PCC, PSIA	19.7	29.5	14.7	27.7	101.3	14.7
N2, RPM	95	205	5172	102	194	1357
W, LBM/SEC	0.3020	0.6340	0.5578	0.2802	0.6085	0.5774
TF, DEG F	68.0	69.0	70.0	61.0	61.0	63.0
TG, DEG F	832.0	893.0	1060.0	780.0	940.0	1040.0
TE, DEG F	220.0	270.0	990.0	390.0	465.0	690.0
TW-1, DEG F	65.0	190.0	170.0	280.0	370.0	570.0
TW-2, DEG F	60.0	127.0	414.0	216.0	330.0	480.0
TW-3, DEG F	64.0	64.0	64.0	332.0	332.0	335.0
TW-4, DEG F	62.0	64.0	64.0	310.0	320.0	430.0

	SEQUENCE A	SEQUENCE B
TIME TO SPEED, SEC	11.2	5.4
FUEL CONSUMPTION, LBM		
METHOD A	6.318	0.000
METHOD B	6.286	2.736

NOTE 1: START TEMP = (TW-1 + TW-2 + TW-3) / 3

NOTE 2: ENTRIES FOR TW-1, TW-2, TW-3, & TW-4 FOR THE LOW PRESSURE DATA ARE AT TIME = 0.0 SECONDS

TABLE 18
SUMMARY FLOW COMPARISON

Data Set	Configuration	Reference	Average % Theoretical Flow
1	• Cast stator • Phenolic blades • No vent slots • Cam slip ring • End Seals • Cold gas	Table 2	141.5
2	• Cast stator • Carbon-composite blades, vented backside • Cam slip ring • No end seals • Cold gas	Table 4	107.0
3	• Heavyweight stator • Carbon-composite blades, vented backside • Cam slip ring • With and without end seals • Cold gas	Table 5 (R-1 through R-6)	74.8
4	• Heavyweight stator • Phenolic blades • No vent slots • O-ring pushrods • Cold gas	Table 6 (8C through 11)	114.6
5	• Heavyweight stator • Short motor • New end seals • Rotor end plates • Phenolic blades vented backside • Spring-loaded pushrods • Cold gas	Table 7 (-4 through -13)	105.4
6	• Heavyweight stator • Short motor • Rotor end plates • New end seals • Carbon-composite blades • Vented front side • Solid pushrods • Hot gas	Table 9 (-22 through -27B)	235.7

pressure acting on the tip of the blade drives the blade away from the stator promoting internal leakage as reflected in the resulting flow rate being 141 percent of theoretical.

The results with the short motor (Data Set 5) are better than the original design (Data Sets 4 and 2) since the leak path to the end clearance at the base of the rotor is eliminated by the rotor end plates used in the short motor.

The reasons for the calculated below-theoretical flow rates of Data Set 3 were not initially understood. The configuration volumes were such that these runs should have had the same theoretical flow rate as those from Data Set 2. The facts remain, however, that the flow rate and torque for these latter runs with the heavyweight stator were both reduced compared to the prior runs with the cast stator.

The explanation lies in an alternate interpretation of the data. Assuming that the results from Data Set 3 are truly representative of a low leakage run, then the other runs actually exhibit significantly higher leakage than calculated in the table. The actual displacement flow rate will be lower than the calculated theoretical flow rate used in the table for the following reasons;

a. Flow limiting at the entrance to the vent slot will prevent the underblade volumes from being fully pressurized reducing average pressure.

b. Flow limiting at the inlet as the trailing blade gradually covers the inlet port while the volume is increasing at a rapid rate will prevent attainment of expected pressure.

c. Flow limiting in the annulus formed by the diameter of the inlet port and the gap to the surface of the rotor. This latter is a probable cause for Data Set 3 since an undercut in the stator at the inlet position, designed to assist flow into the rotor (and incorporated in the cast stator) was not machined into the heavyweight stator. This change reduced the effective inlet area to 71 percent of the inlet bore and is a major factor in reducing the cavity pressure.

d. The basic flow process requires a finite pressure differential thus assuring that the maximum cavity pressure will be lower than the inlet pressure used for the theoretical displacement flow rate calculation. High leakage flow requires more flow through the inlet increasing the pressure drop and thereby further reducing the actual cavity pressure.

When all of these flow limiting factors are considered, it is apparent that the true displacement flow rate is less than that used to compute the percentage of theoretical flow in Table 18 with the largest deviations occurring in runs with the heavyweight stator due to the restricted inlet.

These flow limiting effects are less pronounced for hot gas which produces a larger volumetric flow rate through a given size orifice than cold gas, as noted in a subsequent

paragraph. Also, the reduction in stator diameter for the hot runs partially removes the inlet restriction discussed above since more annulus flow area is available.

For the hot gas tests (Data Set 6), the flow rate averaged 236 percent of theoretical. The critical difference between hot and cold gas flows lies in the increased sensitivity of hot gas flow to leakage.

Considering first a comparison of displacement flow, the flow rate ratio of cold gas to hot gas is directly proportional to molecular weight and inversely proportional to absolute temperature, Thus, for displacement flow, the ratio, $\dot{W}_{GN_2}/\dot{W}_{N_2H_4}$, equals 7.54 using the appropriate gas tempertures and molecular weight.

By contrast, leakage flow is a function of the square root of temperature, molecular weight, and the ratio of specific heat of the gas such that, for this case, $\dot{W}_{GN_2}/\dot{W}_{N_2H_4}$ equals 2.84. Thus, leakage flow will represent a larger proportion of total flow for hot gas then for cold gas.

Leakage in the hot gas runs is most probably due to a combination of the effects of the forward blade venting and solid pushrods (which allows the blade to lose contact with the stator) and possible warping of the stator due to uneven heating from the localized inlet flow. On the assumption that the leakage flow area is roughly equivalent to that which produced the flow difference between Data Sets 2 and 3, an estimate of the expected hot gas flow rate can be made. The difference between average flow rates of Data Sets 2 and 3 is 0.633 lbm/sec, assumed to be all leakage. Using the leakage flow ratio results in expected hot gas leakage of 0.223 lbm/sec. The theoretical displacement flow rate is 0.229 lbm/sec at 5,000 rpm for a total flow of 0.452 lbm/sec. This is close to the observed total hot gas flow.

It would at first appear that the main solution to this problem would be to reverse the vent slots to assure contact of the blades with the stator to minimize leakage. It is correct that leakage flow would be reduced, however, displacement volume increases due to the change in venting exposing more underblade volume. Friction force also increases. Since the total flow rate is nearly constant and independent of motor speed, the optimum combination depends on minimizing the product of flow rate and ramp time, i.e., total flow. This is a different approach than for a constant speed device where minimum flow rate is the desired goal.

The current blade orientation and venting configuration was optimized with cold gas test runs. The results of the above analysis indicate that this approach can lead to

erroneous results due to the differences in sensitivity between hot gas and cold gas. Re-optimization of the motor with hot gas would be necessary to minimize the total fuel consumption per run.

SECTION VI
CONCLUSIONS AND RECOMMENDATIONS

Results obtained from this program demonstrate that a hot gas vane motor can be employed successfully in an APU starting application. Beginning with a baseline design that would not reach rated speed on cold gas without breaking blades, the design evolved to the point that multiple starts, including hot restarts were possible with 1,600°F gas.

The following specific achievements were accomplished:

a. Operation at temperature extremes -- The motor was successfully operated at conditioned temperatures down to -65°F. Hot restart tests verified capability to start at temperatures in excess of +130°F.

b. Operation with decomposition products of a hydrazine-based propellant blend -- The motor operated on the RRC fuel blend designated TSF-1 with inlet gas temperature typically in the range of 1,550 to 1,600°F.

c. Operation within the desired start time -- Simulated starts with a flywheel achieved ambient temperature starts in the range of 5 to 6 seconds. Starts at -65°F with a larger flywheel achieved 5,000 rpm in 10 to 12 seconds. These times are consistent with analytical predictions.

d. Operation in a hot restart mode -- Final tests in this mode consisted of two sequential starts to 5,000 rpm with the large flywheel (simulating -65°F starts). This is an overstress test from the thermal input standpoint since a hot restart would experience a lower drag torque from the APU and thus ramp for a significantly shorter time on the restart.

e. Operation within the maximum torque limit -- The motor produces approximately 70 ft-lbf of torque during operation, well within the required limit of 120 ft-lbf.

The only contract goal not achieved was operation through 100 starts without maintenance. Blade wear was excessive and needs to be addressed through reduction of blade tip force or, alternatively, with harder blades (for example, the silicon carbide infiltrated carbon composite blades) combined with a hard coating on the stator to limit its wear. Analysis during the program on blade forces indicates several means of reducing frictional loads.

Analysis of flow rate results with hot gas produced the following recommendations for consideration in future work:

a. Blade venting optimization must be accomplished with hot gas.

b. The criteria for motor performance should be total flow per start, not minimum flow rate. This new criteria automatically includes blade friction effects and the effect of leakage on torque in the overall performance.

In summary, a hot gas vane motor has been shown to be capable of meeting performance requirements for APU starting. Analysis of results provide design and testing guidelines for future motors of this type.

NOMENCLATURE

A	=	base area of vane
A_N	=	radial component of acceleration
A_T	=	tangential component of acceleration
F_3	=	tip force between vane and stator
F_{END}	=	contact force at end of vane
F_{RB}	=	reaction force at base of vane
F_{RT}	=	reaction force at tip of vane
H_R	=	height of vane exposed beyond rotor
LV	=	length of vane within rotor slot
M_V	=	vane mass
P	=	pressure
PF	=	force produced by pressure differential acting over exposed vane area
PF_{base}	=	vane base pressure
PF_{tip}	=	vane tip pressure
TV	=	vane thickness
V	=	volume
W_N	=	radial force due to acceleration acting on blade mass
W_T	=	tangential force due to acceleration acting on blade mass
XV	=	length of vane within rotor slot
μ	=	coefficient of friction

APPENDIX

ANALYSIS AND COMPUTER SIMULATION OF THE VANE FRICTION AND THE VANE FORCES IN A SLIDING VANE EXPANDER

A Report Submitted to

Rocket Research Company

by:

Carl H. Wolgemuth, PhD

May 16, 1982

Introduction

This report describes the work done on modeling the vane expander to determine the effect of certain design and operating parameters on the friction power and certain key forces. Results will be described for two models; the pushrod model which approximates the original design and a linked-rigid vane model which approximates a rigid coupling of opposite vanes (180° angle between the linked vanes).

There are a number of assumptions that apply to both models. The base of the vane is assumed to be vented to either the control volume adjacent to its leading edge (leading control volume) or the control volume adjacent to its trailing edge (lagging control volume). Furthermore the pressure at the base of the vane was assumed equal to the pressure in the control volume to which the base was vented. No pressure drop through the vent or leakage from the volume at the vane base was included. Since the vent passages were quite large this was believed to be a valid assumption. The pressure force at the tip of the vane was based on a tip shape given by Rocket Research with the fraction of the tip area exposed to each control volume shown in Table 1 in Appendix A.

The control volume pressure variation as a function of rotor position, $P = f(\theta)$, was taken from earlier work done here for Rocket Research. The data for a model, PORT-3, with ports leading to the base of the vane and standard clearances where leakage occurred, was modified slightly and used in the study. The modification was necessary since the intake port location in this design is different from the earlier model. This same pressure variation was used for all models at all conditions except for those few cases where the supply pressure was changed from 1115 psia to either 700 or 1500 psia. When the supply pressure was changed a similar pressure variation was used.

The actual pressure variation used is shown in Appendix A (Figure A1). The pressure variation is a function of many variables, speed, leakage and heat transfer, but in this study the pressure as a function of theta was not changed. While some realism may be lost (when changing speeds for example), holding this parameter constant permits a clearer view of the effect of changes in design or operating variables and makes it somewhat easier to assess these effects. In any case this pressure variation is most sensitive to leakage (which depends on operating clearances) which was not varied for these models, so maintaining a single variation can be justified.

The theta equal zero position of the vane is always taken at the position where the vane is fully extended and at the bottom of the expander. The gravitational forces on the vane were included in the model although they are so small that they are really negligible. On the other hand the forces due to both the normal and tangential accelerations are quite significant. There are two components of the normal acceleration, the $\omega^2 r$ and the $\frac{dV_r}{dt}$ components. The $\omega^2 r$ component is due to the rotation and the $\frac{dV_r}{dt}$ is due to the vane's motion in the r direction. The vane, in one revolution of the rotor moves in toward the center of rotation a distance of two times the eccentricity (the distance between the center of the rotor and the center of the stator) and out from the center of rotation this same distance. The tangential acceleration also has two components, the $\frac{d\omega}{dt}$ and the Coriolis component. The Coriolis component is due to the motion of the vane in a rotating reference frame and this term is much larger than the $\frac{d\omega}{dt}$ term. The Coriolis component also changes sign, while the $\frac{d\omega}{dt}$ does not.

The Pushrod Model

The pushrod model assumes that the vanes are essentially independent of each other. The one exception to this is that when a vane is forced away from the stator, it pushes on the opposite vane through the pushrod. This model is a close approximation to the original design; however no spring forces

are included. The spring forces are extremely small compared to the net reaction force at the tip. When the vane is fully extended ($\theta = 0$) the spring force is less than 2 pounds while the reaction force may be several hundred pounds. At the maximum spring force position ($\theta = 90^{\circ}$) the spring force is still less than 10 pounds. When the vane is forced away from the stator the spring force is not a factor since the model without the spring force also predicts the same reaction force.

Figure 1 shows a free body diagram of the vane. The weight and acceleration components are not necessarily shown in the correct direction in this diagram, they are computed in the program and given the correct sign. Only that part of the end of the vane extending beyond the rotor was assumed to rub on stator. An average pressure (average between leading and lagging control volumes) was assumed to act on the opposite end of the vane. The three reaction forces, F_3, F_{RB}, and F_{RT}, were calculated by summing forces in the radial direction, the tangential direction and by taking moments about point A in Figure 1.

The results for several simulations using the pushrod model are presented. Figures 2 through 6 show results for a coefficient of friction equal to 0.2 ($\mu = 0.2$), a supply pressure of 1115 psia, the vane base vented to the lagging control volume, a speed of 4000 RPM, and a vane mass of 0.18 lb_m ($M_v = 0.18$) . Figure 2 shows the tangential inertia force, the normal inertia force and the net pressure force (the pressure force is tangential) as a function of rotor position. The positive directions for these forces are radially outward, and tangentially in the direction of rotation. As the vane moves inward from 0 to 180° rotor position, it must be decelerated to continue at a constant angular velocity, thus a force must be exerted on the vane in the tangential direction opposite to the direction of rotation. From Figure 2 it is apparent that the normal inertial force is rather high, and the tangential is fairly low and due mostly to the Coriolis acceleration which reverses direction every 180°. The scale chosen for these forces is the same for all plots of force for

the pushrod model. The forces shown on Figure 2 are independent of the coefficient of friction and whether the vane base is vented to the leading or lagging control volume. The inertia forces do vary with speed and mass of the vanes.

Figure 3 shows F_{end} and F_3 for this same case. In the 160° to 210° range, where F_3 is zero, the vane is not contacting the stator; however the contact force on the tip of the vane 180° from this vane has been increased due to the force transmitted through the pushrod. It is clear from Figure 3 that the force is quite high in the 340° to 30° range.

The forces F_{RB} and F_{RT} are plotted versus θ in Figure 4. The force at the contact point between the vane and the outer edge of the rotor, F_{RT}, is of some concern particularly when the vane is fully extended near zero degrees. The positive direction for these forces is in the direction shown in Figure 1. Thus when F_{RT} is negative at 0° the "back" side of the vane is contacting the outer edge of the rotor.

Figure 5 shows the friction power per vane dissipated via each of the 4 rubbing forces. QFRIC1 is the power due to the force F_3, QFRIC2 is due to F_{RB}, QFRIC3 is due to F_{RT} and QFRIC4 is due to F_{end}. Figure 6 represents the friction work per vane produced by all 4 rubbing forces in 1/64 of a revolution of the rotor. It can be regarded as a friction torque, and when multiplied by .6468 (for 4000 RPM) it provides the friction horsepower for one vane. The small anomaly in the curve in the vicinity of 90° is not real; it is a result of an error which did not get removed from the plotting program.

Figures 7 through 10 present similar results for a case identical to the previous one except that the coefficient of friction has been increased to 0.4. In the critical area of 0°, F_3 is extremely large and F_{RT} is also very large negatively (over -350 lb_f). The power dissipated in friction is extremely high, appreciably higher than that produced by the gas, so that the expander would not run at 4000 RPM with the coefficient of friction this high. This point will be discussed in a later section of the report.

The mass of the vanes was reduced from 0.18 lb_m to 0.06 lb_m and curves similar to those in Figures 2 through 10 were plotted. Figures B1 through B9 in Appendix B show the results of this analysis. The inertia forces were reduced to one third of their previous values and somewhat lower reaction forces resulted. The friction power was reduced from 6.45 to 4.74 hp/vane for a coefficient of friction of 0.2 and from 13.36 to 9.33 hp/vane for a coefficient of friction of 0.4.

The Linked-rigid Vane Model

When the vanes opposite each other in the rotor are connected together a configuration similar to that shown in Figure 11 will result. If the connector is flexible, then each vane can tilt in the slot independently of the position of the other connected vane. Determining the position of the vanes with this type of flexible connector is fairly involved and requires a knowledge of the stiffness of the connector since it does transmit a moment as well as a force to the vane. A simpler approach is to assume the connector rigid so that only three equations are required to determine the three reaction forces F_3, F_{RT1}, and F_{RT2}. This was done and the model was labled the linked-rigid vane model. Results for this model are shown in Figures 12 through 18.

Figure 12 shows the inertia forces and the pressure force as a function of rotor angle. The pressure force is identical to that for the pushrod model in Figure 2. Here PF1 is plotted from 0 to 180° and PF2 is plotted from 180 to 360°. In this model the normal inertia force has a much smaller $\omega^2 r$ component since r for the center of mass of the two vanes is much smaller. In fact r is zero at 90° and 270° where the center of mass coincides with the center of rotation. The curve shows approximately zero normal inertia force at these locations, the difference from zero resulting from the small $\frac{dV_r}{dt}$ term. The

slight negative value for the $\frac{dV_r}{dt}$ at the 90 and 270° locations indicates that the force is radially outward accelerating the center of mass out from the center of rotation. Both the tangential and normal inertia forces are for a mass of 0.36 lb_m, since two vanes are rigidly connected.

The tangential inertia force has about the same maximum value as the normal inertia force in this case, and about twice the maximum value for the pushrod model in Figure 2. The factor of 2 is due to twice as much mass, the tangential acceleration does not change since ω and the velocity of the vane in the rotating coordinate system do not change from the previous model. In Figure 12 the negative of the tangential force is plotted. The data were stored in a matrix when calculations were made from 0 to 180° and then plotted from 0 to 360°. In the manipulation of the data for plotting the sign was reversed; the sign is correct in the analysis. The actual tangential acceleration is negative from 0 to 180° and positive from 180 to 360°.

Figure 13 shows the reaction forces for the linked-rigid model for a coefficient of friction of .4 and a vane mass of .18 lb_m. The tip force is seen to be quite high in the 0 to 30° range (when the vane is fully extended). Note that whenever F_3 has a positive value the value 180° away from that location will have a value of F_3 equal to zero. This means that only one of the pair of vanes is in contact with the stator at any one time. Note also the fairly large negative value of F_{RT1} when the vane is fully extended near zero degrees. The peak values of F_3 and F_{RT} are not nearly as high for this model as for the pushrod model under the same conditions (see Figures 7 and 8). Values of F_{RT2} can be read from the F_{RT1} curve by simply reading at $\theta + 180°$. A similar relationship exists for F_{END2} and F_{END1}.

The power dissipated by the frictional forces is plotted on Figure 14, where QFRIC1 is due to F_3, QFRIC2 is due to F_{RT1} and F_{RT2}, and QFRIC4 is due to F_{END1} and F_{END2}. Thus each curve represents the friction of two vanes, 180° apart. From 0 to 180° each represents the power dissipated by one vane in one revolution. Thus in the 180 to 360° range the curves are identical in the 0 to 180° interval.

The total friction power dissipated by two vanes, 180° apart, is given by the curve in Figure 15. Again the second half of the curve is a repeat of the first. This work plotted is the friction work in 1/64 of a revolution.

Figures 16, 17 and 18 present results for the same model for the same conditions, except that venting is to the leading instead of lagging c.v. The scales for the plots are identical for both values of the coefficient of friction. Summaries of these cases will be presented in a later section of this report.

Task B Results

The objective in Task B was to determine the effect of the coefficient of friction on friction power and to estimate a value for the coefficient based on some test results. The results for this study as well as other studies are summarized in Tabl 1. Figure 19 shows the friction power per vane versus coefficient of friction for a variety of conditions. The push-rod model indicates that for a vane mass of .18 lb. the coefficient of friction would be about .32 for the friction power to equal the fluid power at 4000 RPM when the base is vented to the lagging control volume. This condition approximates the results of a certain test run at Rocket Research and the value of .32 for the coefficient of friction predicted by the model for these conditions is not unreasonable although it may be somewhat high. If the coating did not wear off at the vane tip a coefficient of .2 would be reasonable; however if metal to metal contact occurred at the tip a value as high as .4 would certainly be reasonable.

TABLE 1
FRICTION POWER AND FLUID POWER PER VANE FOR A VARIETY OF CONDITIONS

				Linked-rigid Vane Model			
μ	M_v lb_m	RPM	PS psia	Ported to control volume	Fluid power hp/vane	Friction power hp/vane	$F_3(\theta)^*$ lb_f
.2	.18	4000	700	lagging	6.49	2.82	308(11)
.4	.18	4000	700	lag	6.49	5.51	341(6)
.2	.18	4000	1115	lag	10.51	4.17	451(17)
.4	.18	4000	1115	lag	10.51	8.07	492(6)
.2	.18	4000	1500	lag	14.22	5.42	584(17)
.4	.18	4000	1500	lag	14.22	10.43	637(11)
.2	.18	2500	1115	lag	6.57	2.41	404(17)
.2	.18	6000	1115	lag	15.76	7.29	548(17)
.2	.06	4000	1115	lag	10.51	3.83	399(17)
.4	.06	4000	1115	lag	10.51	7.31	431(11)
.2	.06	2500	1115	lag	6.57	2.32	384(17)
.2	.06	6000	1115	lag	15.76	6.06	432(17)
.2	.06	4000	1115	leading	10.51	2.23	29(17)
.4	.06	4000	1115	lead	10.51	5.34	69(17)
.2	.18	4000	1115	lead	10.51	2.38	80(17)
.4	.18	4000	1115	lead	10.51	5.68	0
.2	.18	2500	1115	lead	6.57	1.40	53(17)
.2	.18	6000	1115	lead	15.76	4.42	177(17)
				Pushrod Model			
.2	.18	4000	1115	lag	10.51	6.45	533(6)
.4	.18	4000	1115	lag	10.51	13.36	740(6)
.2	.06	4000	1115	lag	10.51	4.74	477(6)
.4	.06	4000	1115	lag	10.51	9.33	650(6)
.2	.18	4000	1115	lead	10.51	5.65	216(22)
.4	.18	4000	1115	lead	10.51	11.53	178(6)

*Peak value of F_3 and the angle at which it occurs in the vicinity of a fully extended vane ($\theta = 0$)

It is clear from this figure that the linked-rigid model predicts lower friction, the lower mass vanes have lower friction, and venting the vane base to the leading control volume also significantly reduces the friction power.

Task C Results

In the early work on the single independent vane model the pressure on the vane tip was assumed to be that of the lagging control volume, then it was assumed to be that of the leading control volume, then finally it was assumed to be a combination based on the area distribution given by Rocket Research (see Appendix A). For the vane base vented to the lagging control volume the friction power was highest for the tip completely exposed to the leading control volume pressure and lowest for the tip completely exposed to the lagging control volume pressure. The distribution given by Rocket Research produced values between the other two cases. The high values were about 15% higher and the low values were about 15% lower than the distribution case. These studies were not repeated for the other models since it is believed that the area distribution given by Rocket Research represents the most realistic assumption for the models and complete independent control over the pressure on the tip is not possible, it was decided that more time should be spent on other models and these cases were not repeated.

Task D Results

The linked-rigid vane model was developed to simulate the tying together of two opposite vanes. Originally it was planned to simply set the centrifugal forces equal to zero for this part of the study, but we realized this assumption is very unrealistic. Thus the linked-rigid vane model was developed. Fgiure 19 shows a direct comparison between the pushrod and linked-rigid vane models. About a 40% reduction in friction

power is achieved by coupling the vanes together. A more detailed comparison between the pushrod and linked-rigid models can be obtained by comparing Figures 2 and 7 - 10 with Figures 12 - 15.

Task E Results

Figure 19 shows the effect of vane mass for both models for a speed of 4000 RPM. Figure 20 indicates that at low speed there is very little effect produced by decreasing the vane mass; however at high speed (6000 RPM) there is about a 17% reduction in friction power when the vane mass is reduced from .18 to .06 lb.

Task F Results

The difference in friction power between venting the undervane volume to the lagging or leading control volume is presented in Figure 19 for 4000 RPM and is shown in Figure 20 as function of speed. Over the range of speeds it appears advantageous to vent the vane base to the leading control volume when the vanes are linked together.

Task G Results

Figure 21 shows the effect of supply pressure on the friction power for values of the coefficient of friction of .2 and .4. Table 1 contains this data as well as the fluid power developed for these conditions. Since the three points in each case seemed to fall on a straight line, I extrapolated both lines back to zero supply pressure. It is tempting to suggest that this power (at zero supply pressure) represents the power dissipated by inertia forces only, since no pressure forces would be present.

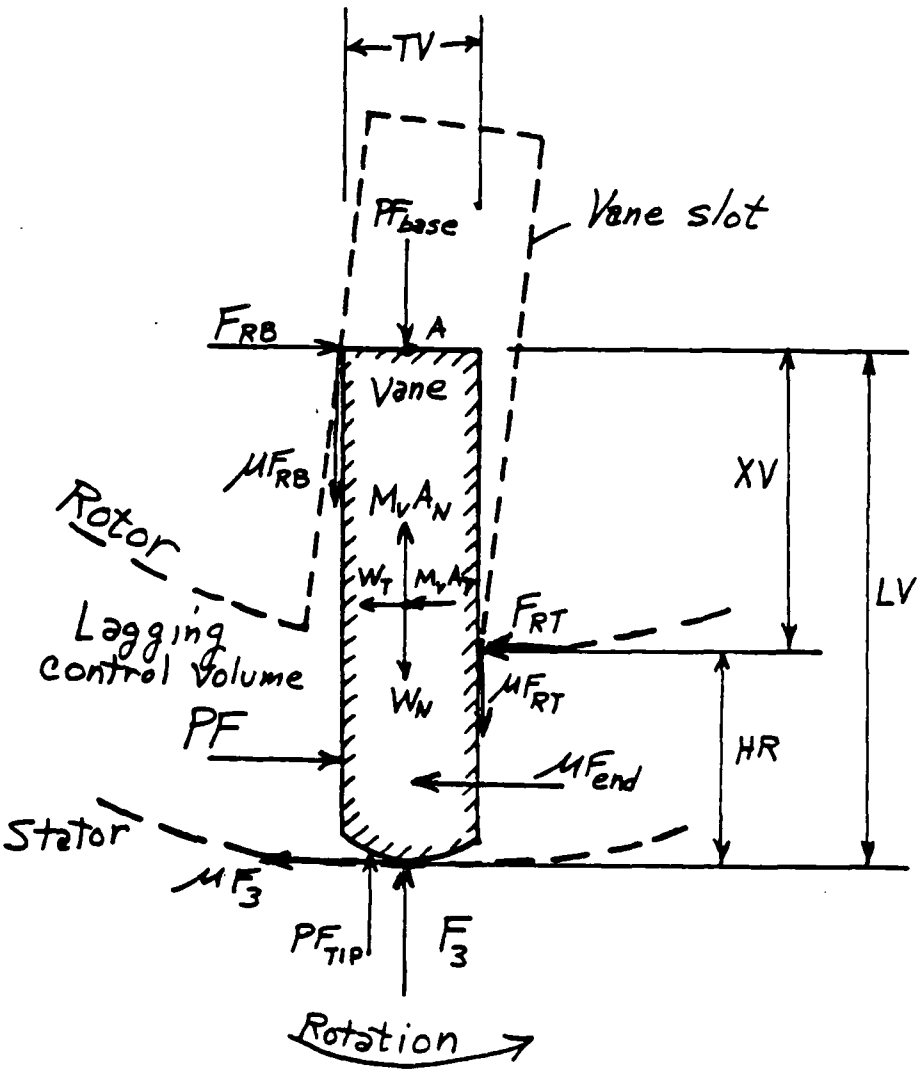

Figure 1 Free Body Diagram of Single Vane

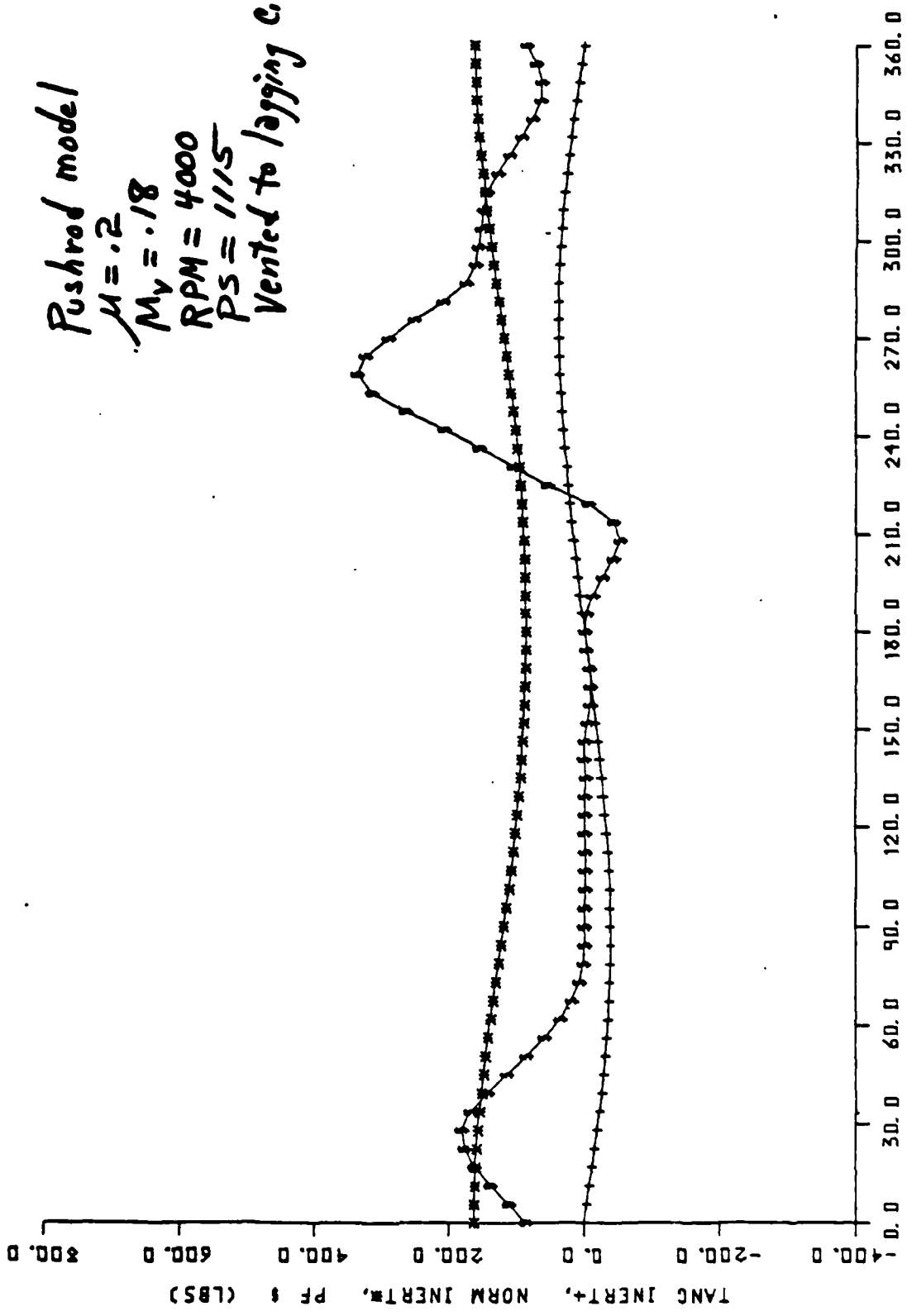

Figure 2 Inlet Pressure and Inertia Forces on a Vane

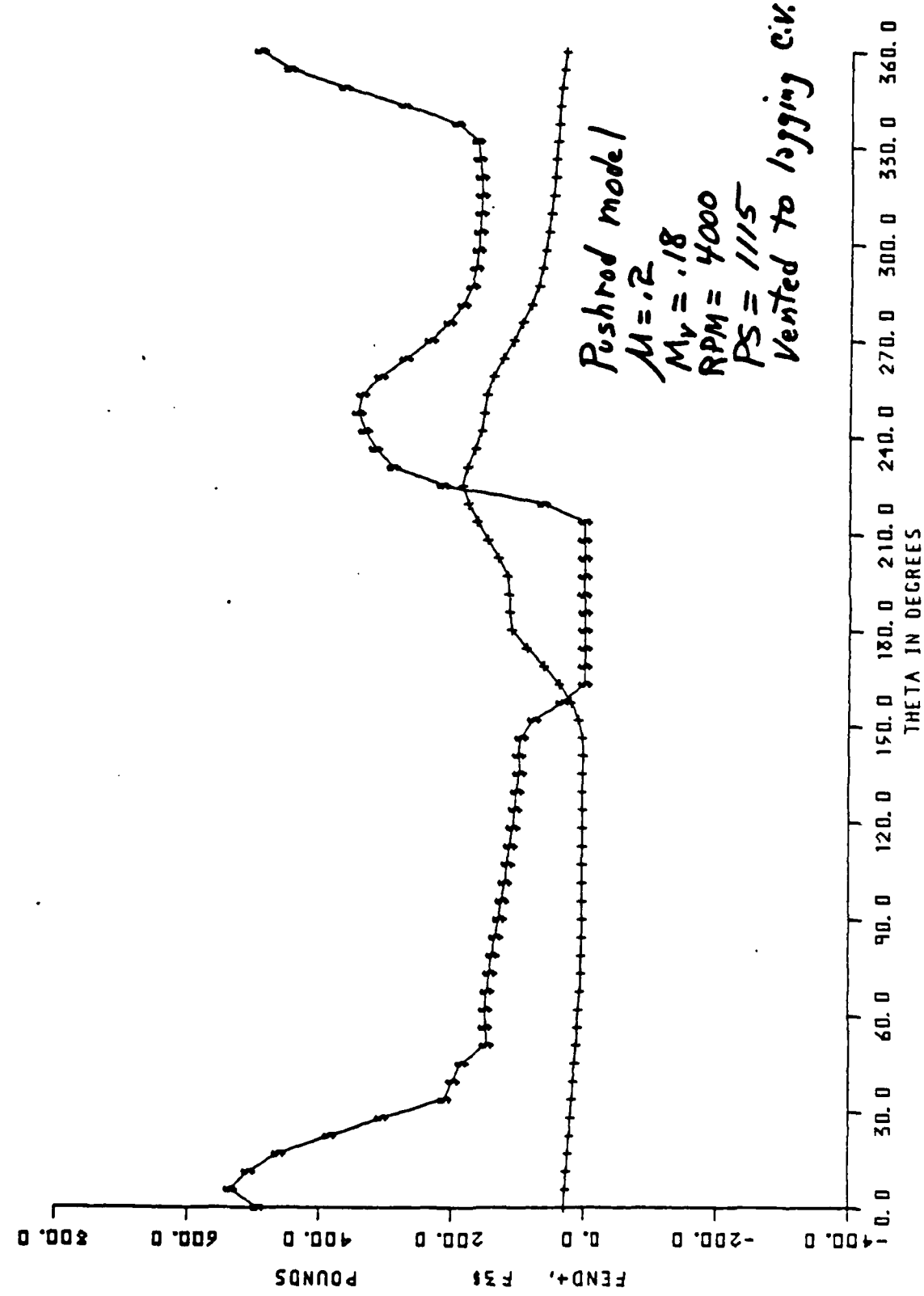

Figure 3 Tip and End Forces

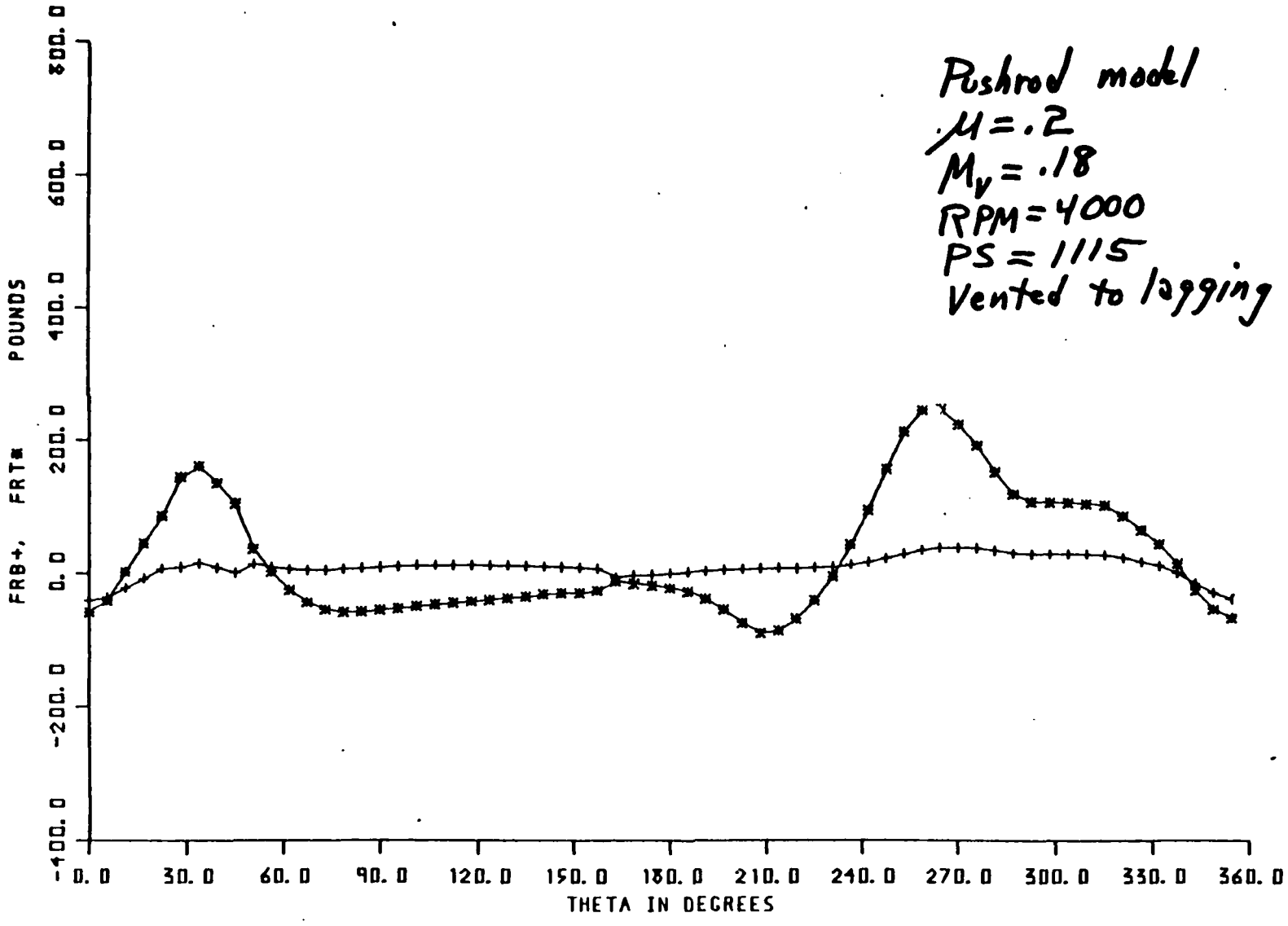

Figure 4 Reaction Forces on the Rotor Slot

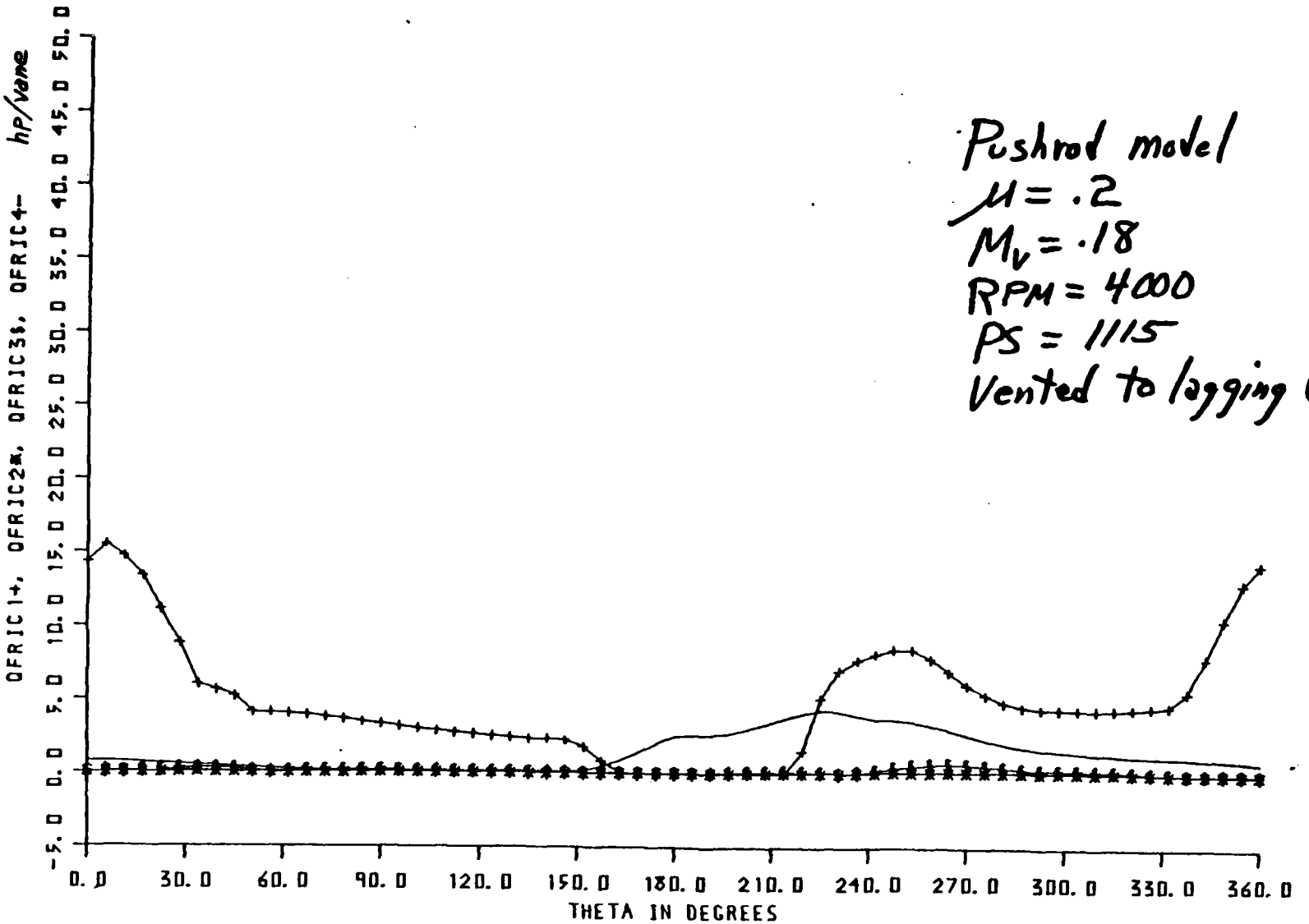

Pushrod model
$\mu = .2$
$M_v = .18$
RPM = 4000
PS = 1115
Vented to lagging C.V.

Figure 5 Power Dissipated by Each Rubbing Force

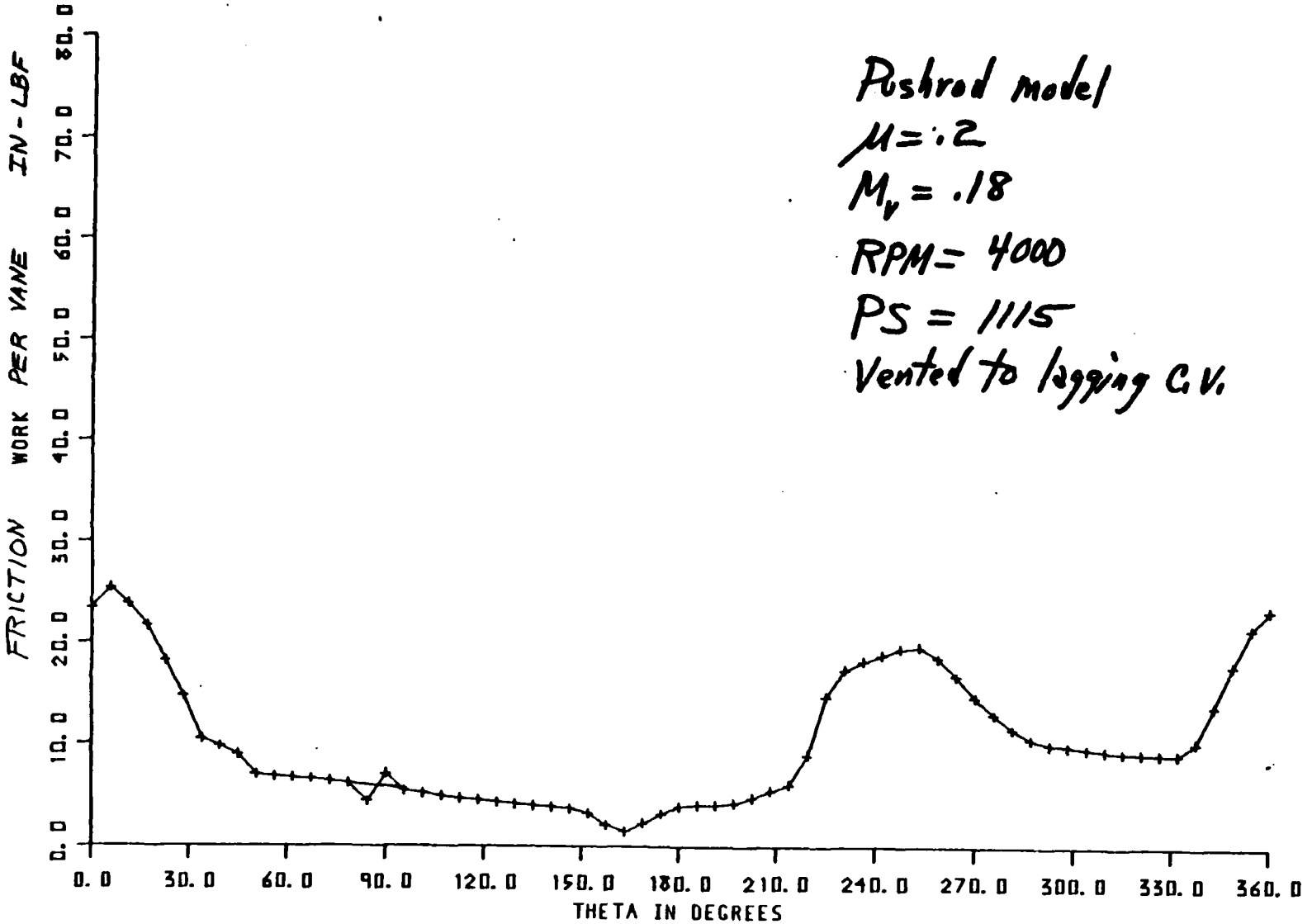

Figure 6 Friction Work per Vane.

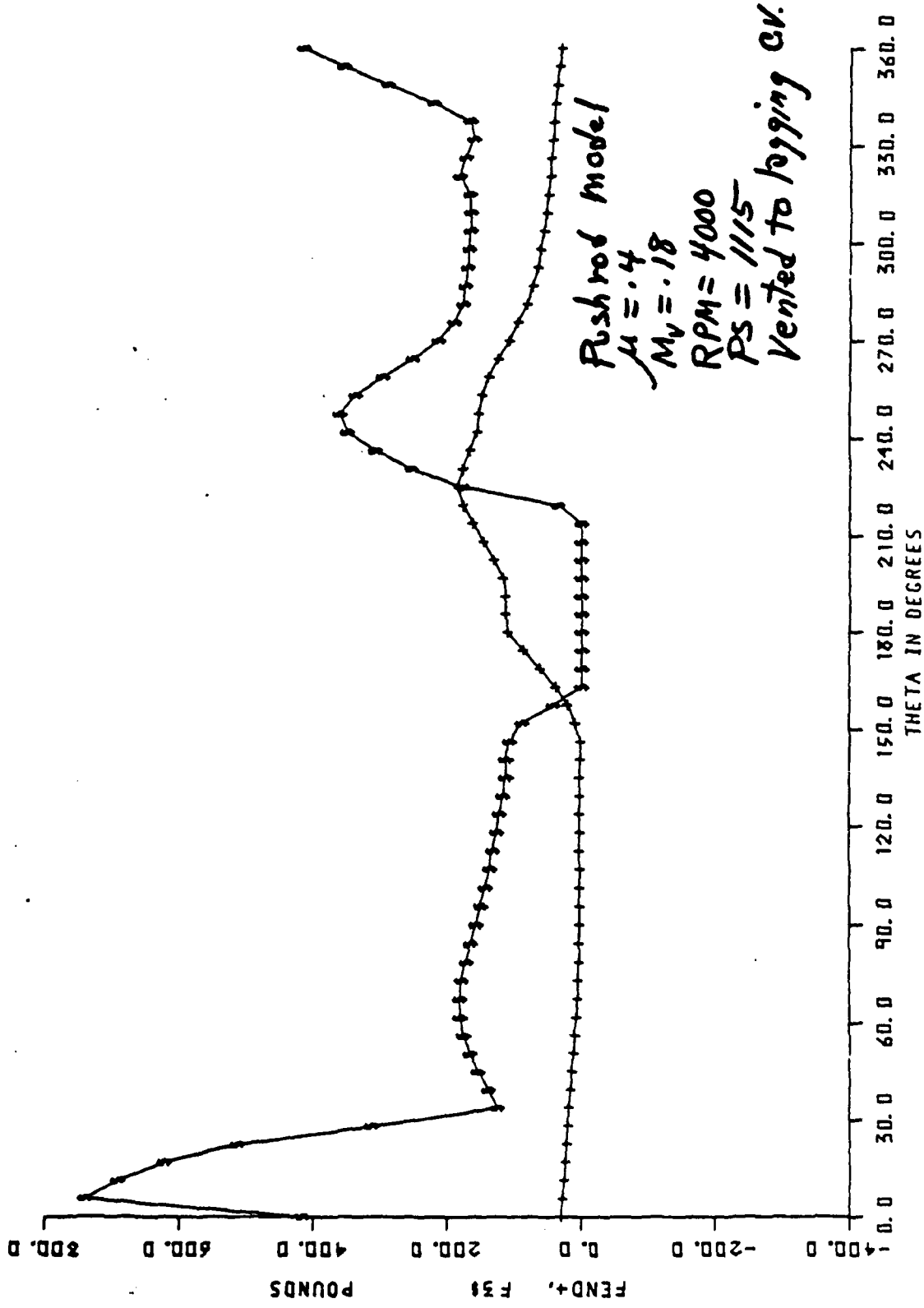

Figure 7 Tip and End Forces

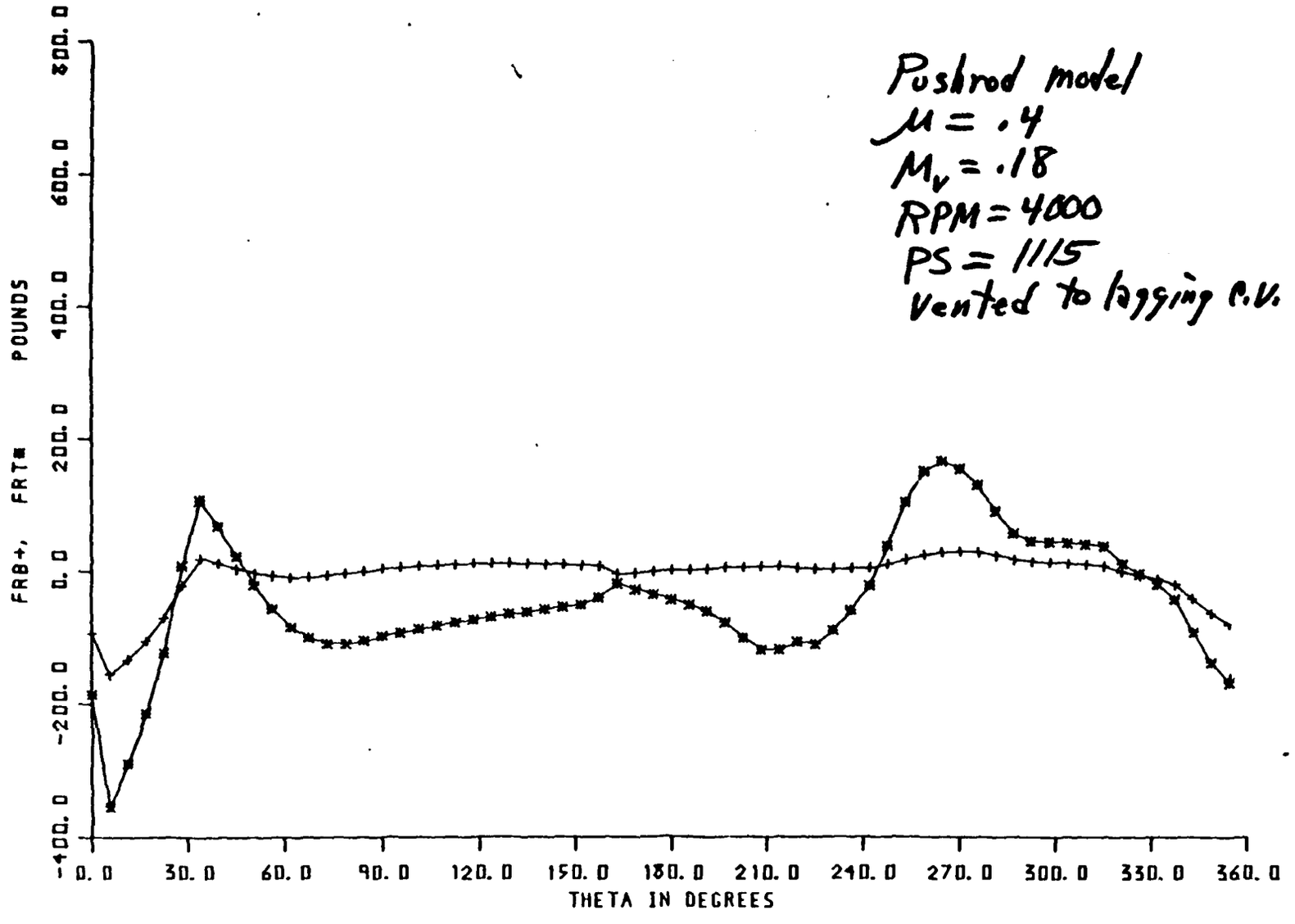

Figure 8 Reaction Forces on the Rotor Slot

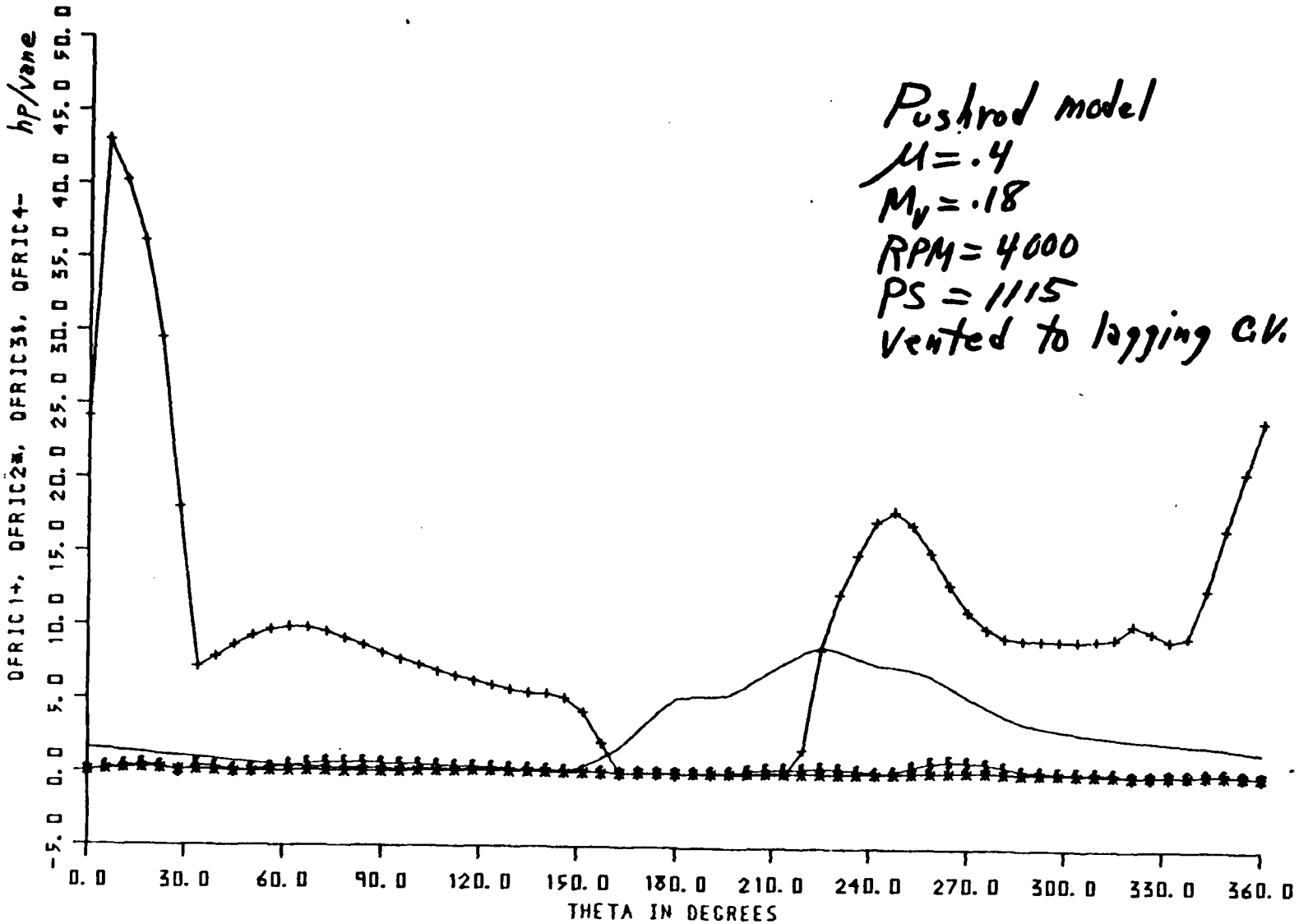

Figure 9 Power Dissipated by Each Rubbing Force

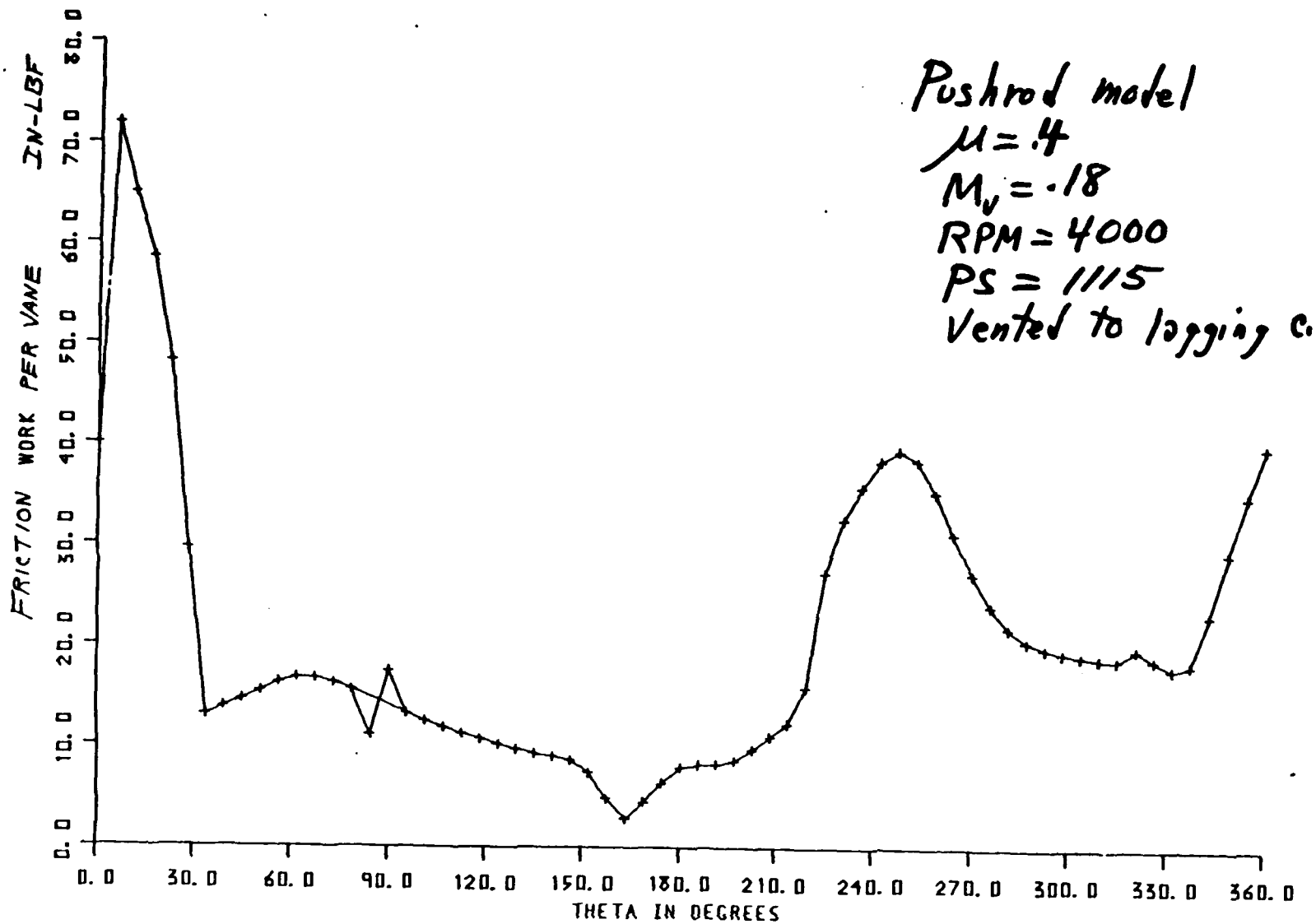

Figure 10 Friction Work per Vane

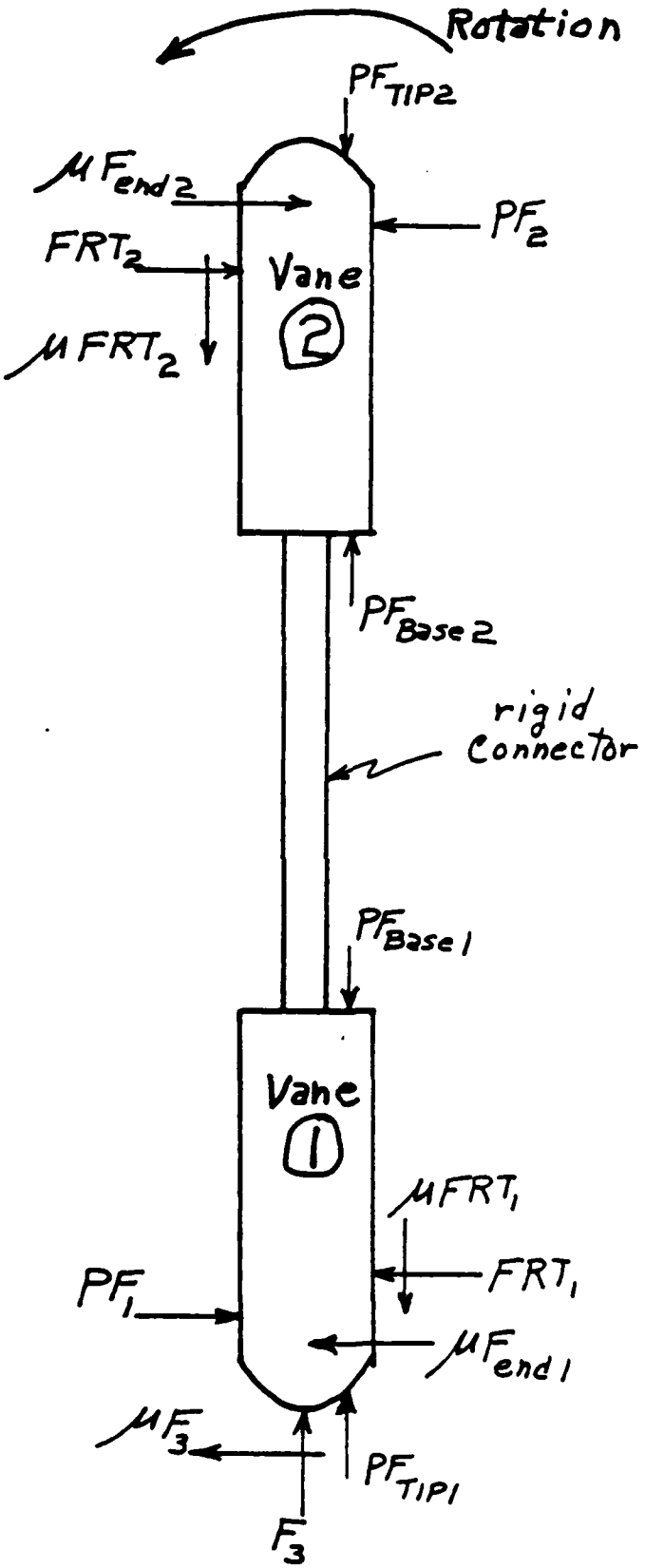

Figure 11 Model of Linked-Rigid Vanes

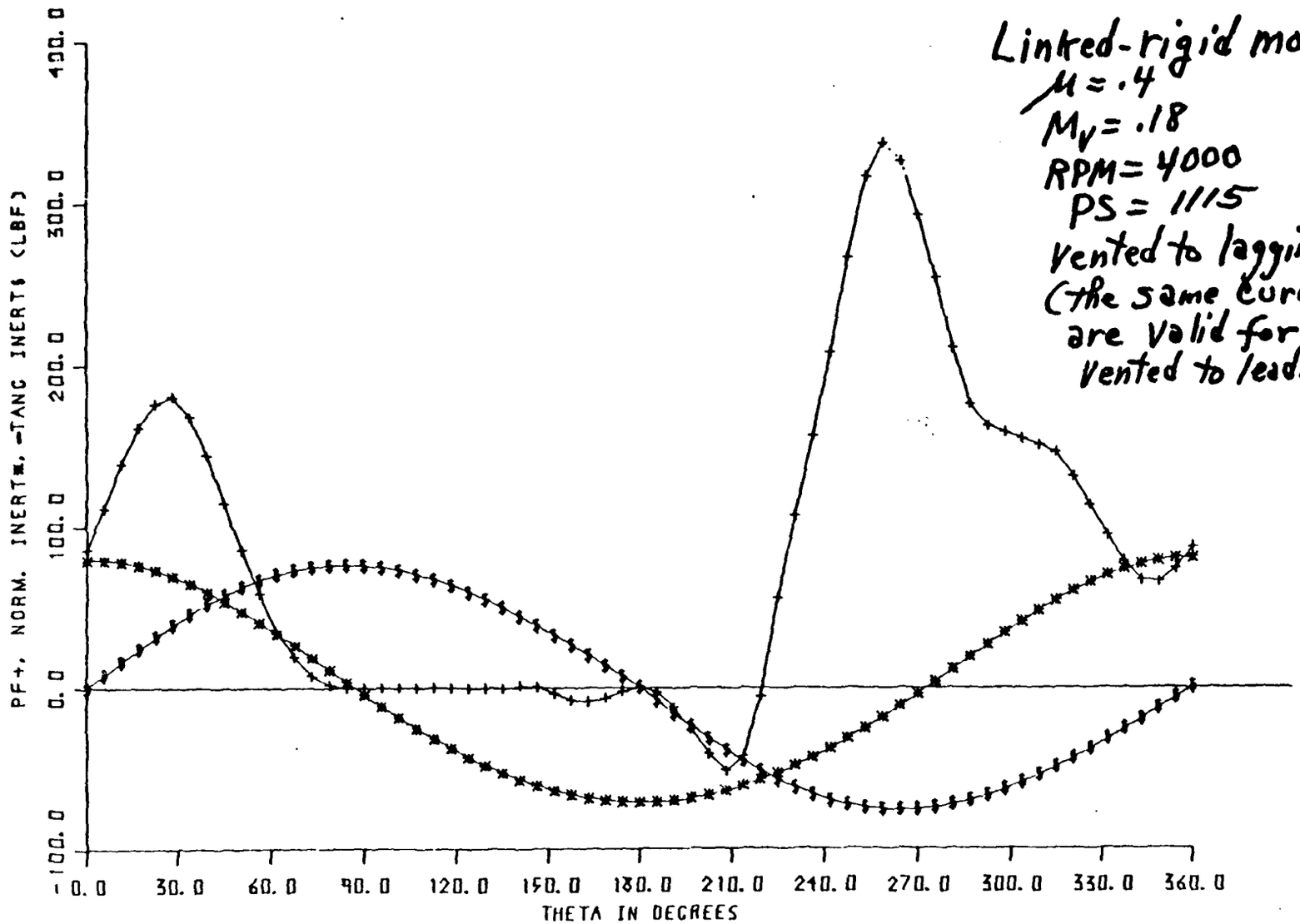

Linked-rigid model
$\mu = .4$
$M_V = .18$
RPM = 4000
PS = 1115
Vented to lagging C.V.
(The same curves are valid for vented to leading C.V.)

Figure 12 Net Pressure and Inertia Forces on the Vanes

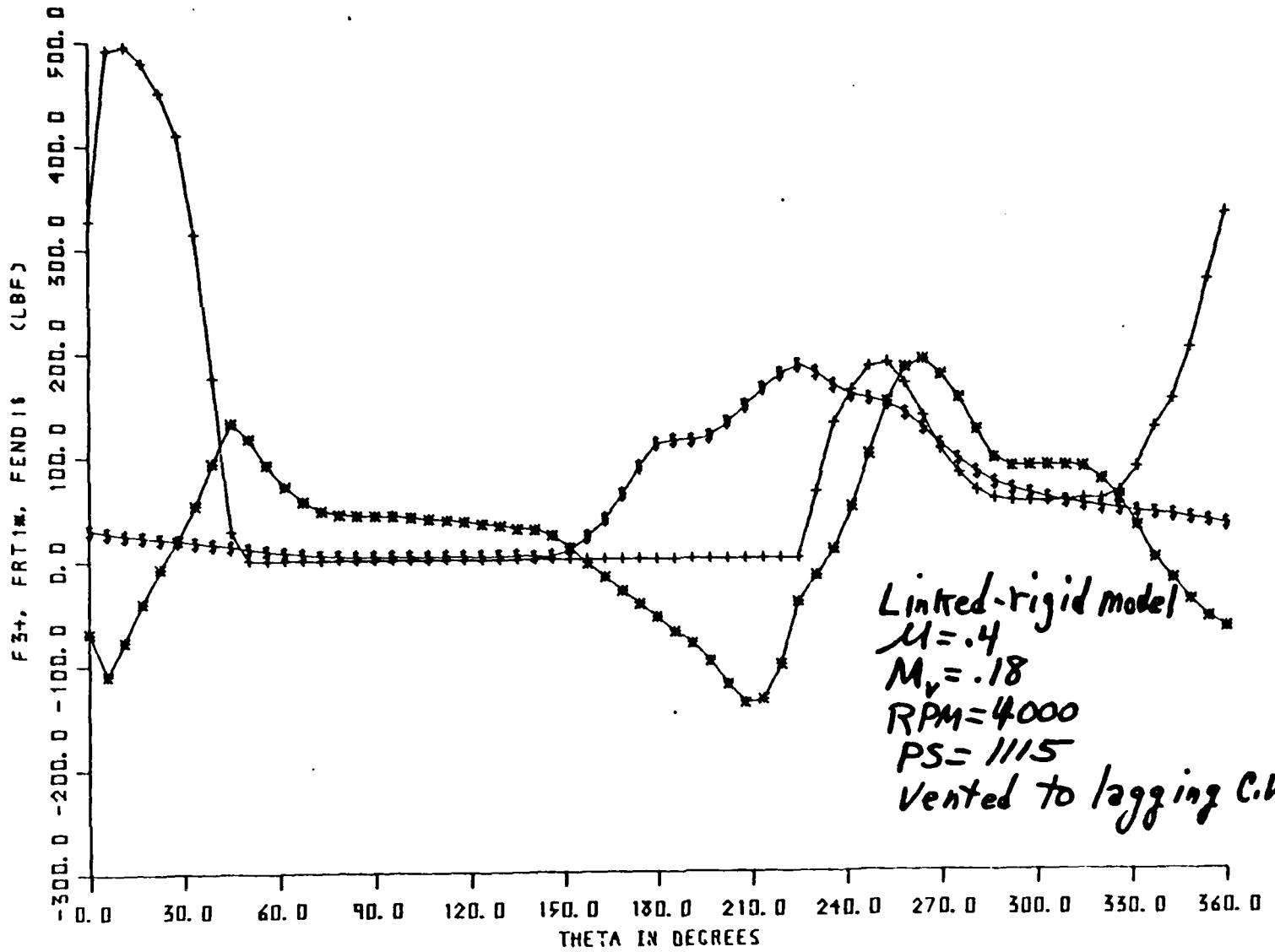

Figure 13 Vane Contact Forces

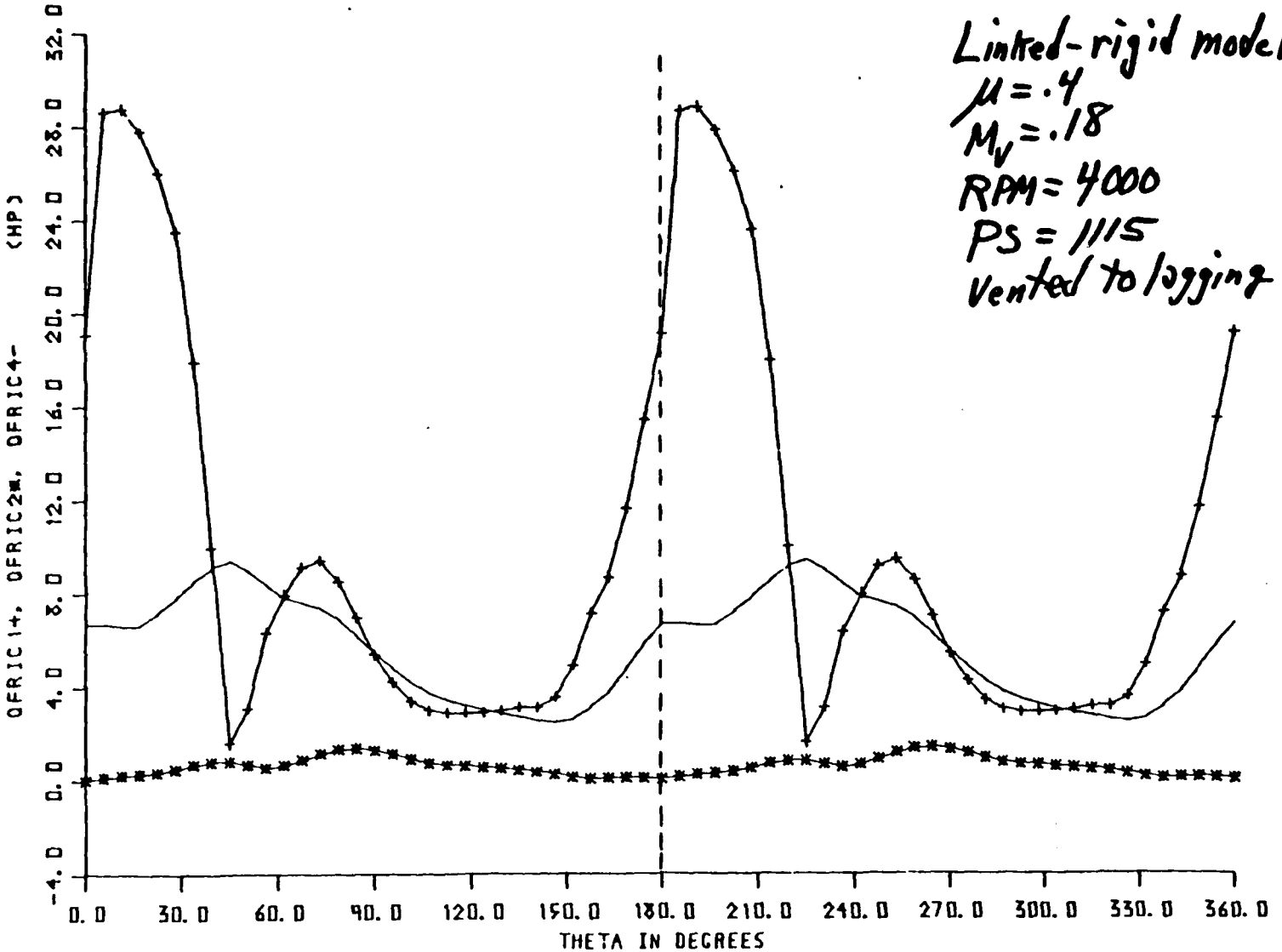

Figure 14 Power Dissipated by Rubbing Forces

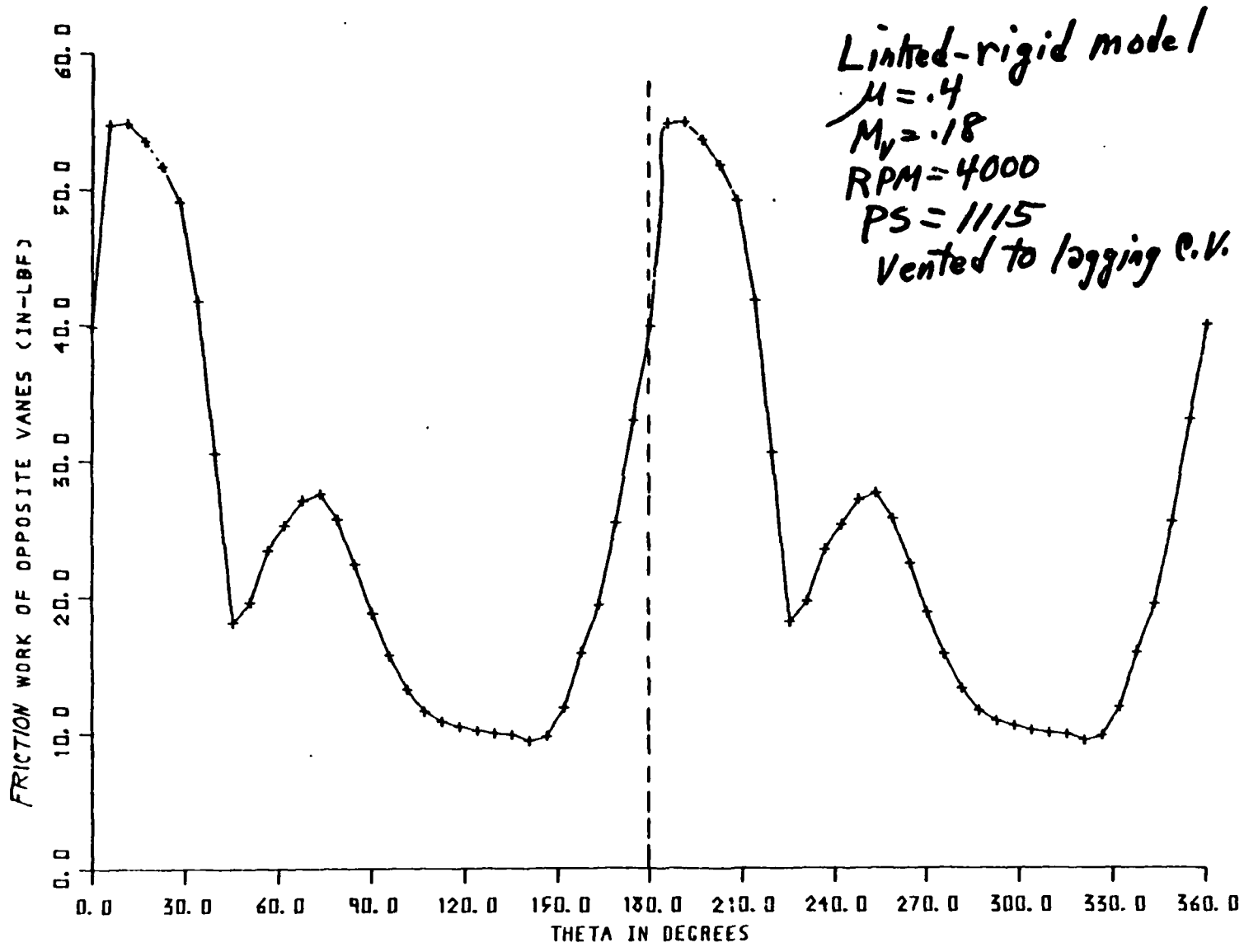

Figure 15 Friction Work for a Pair of Vanes

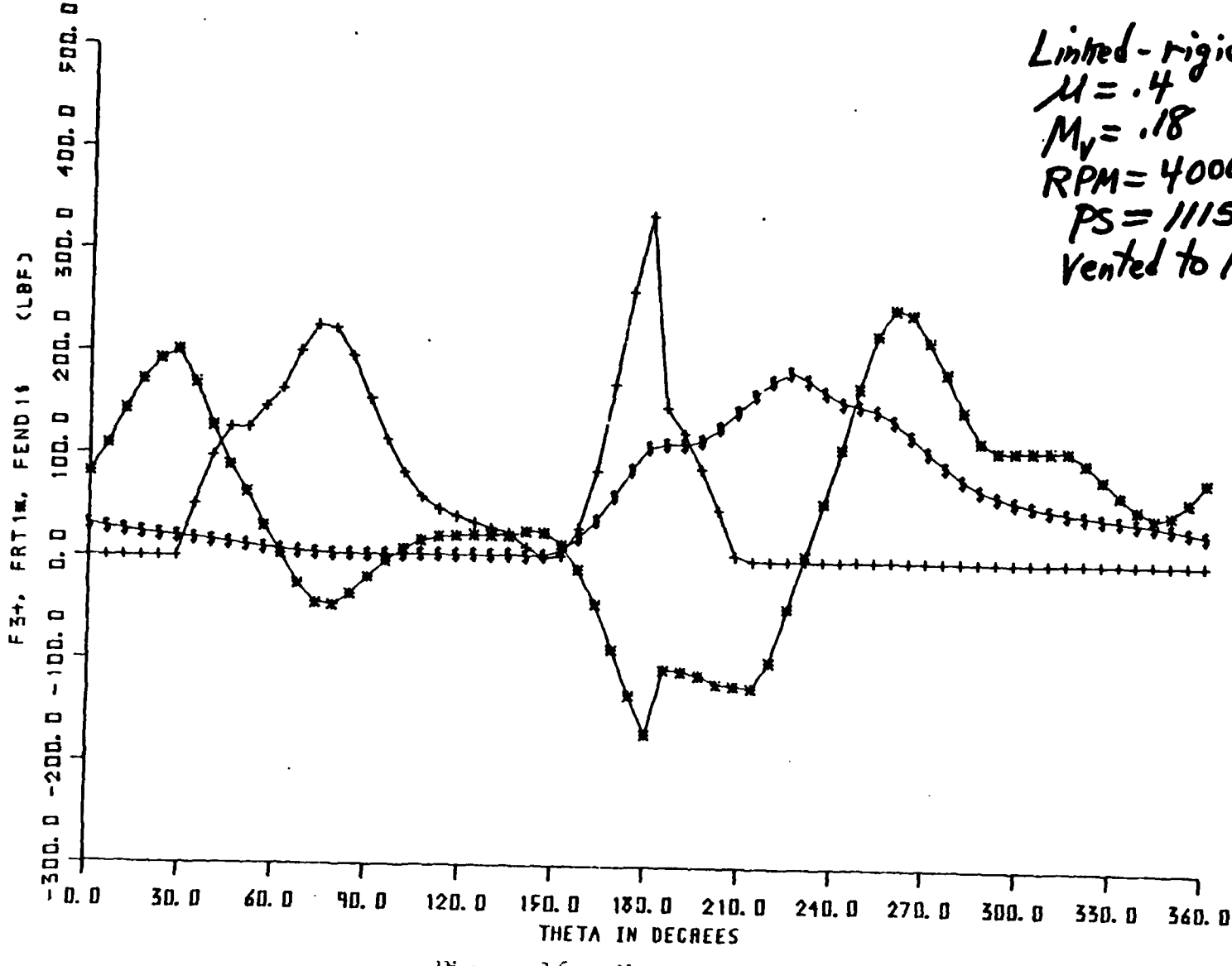

Figure 16 Vane Contact Forces

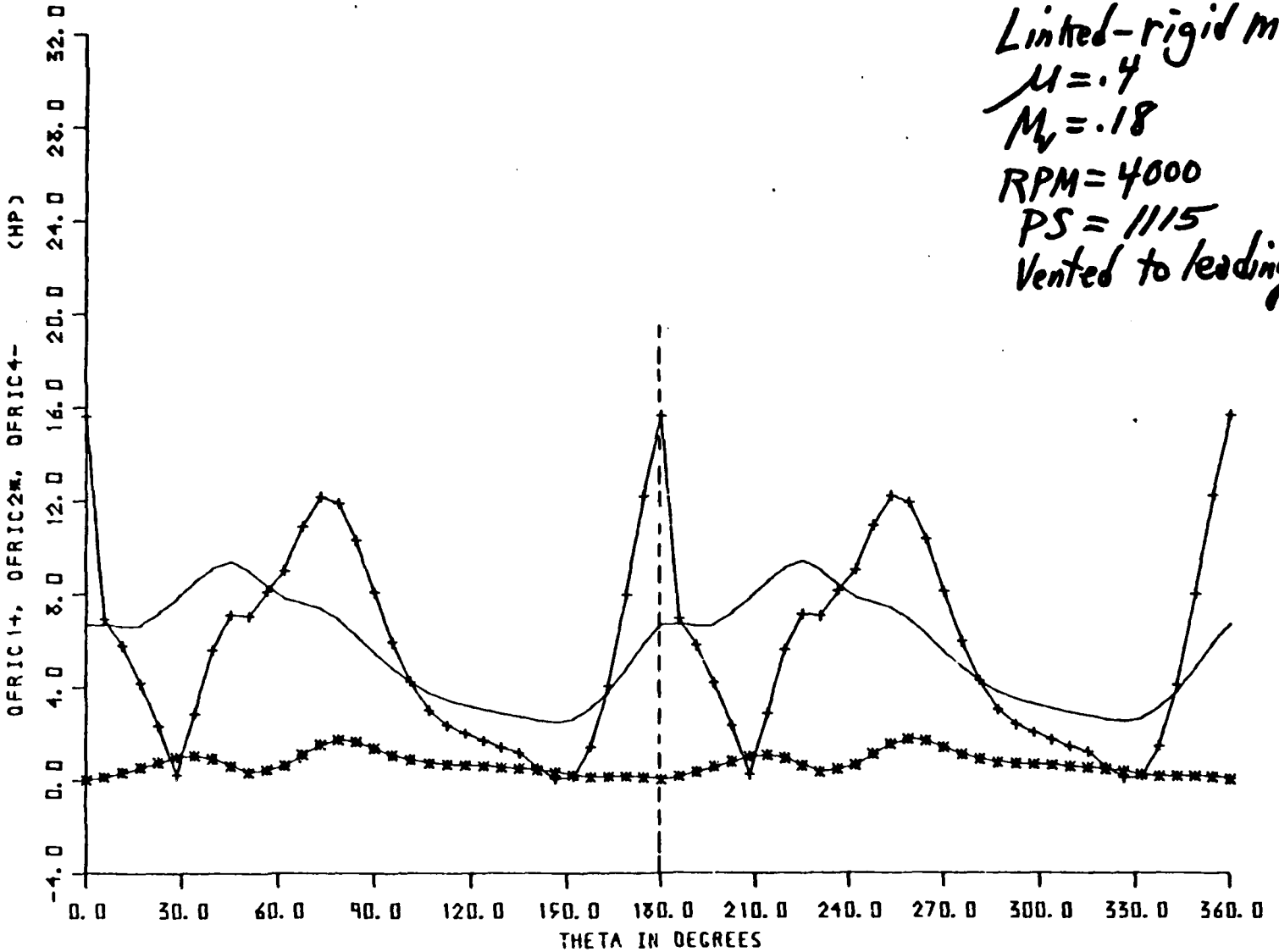

Figure 17 Power Dissipated by Rubbing Forces

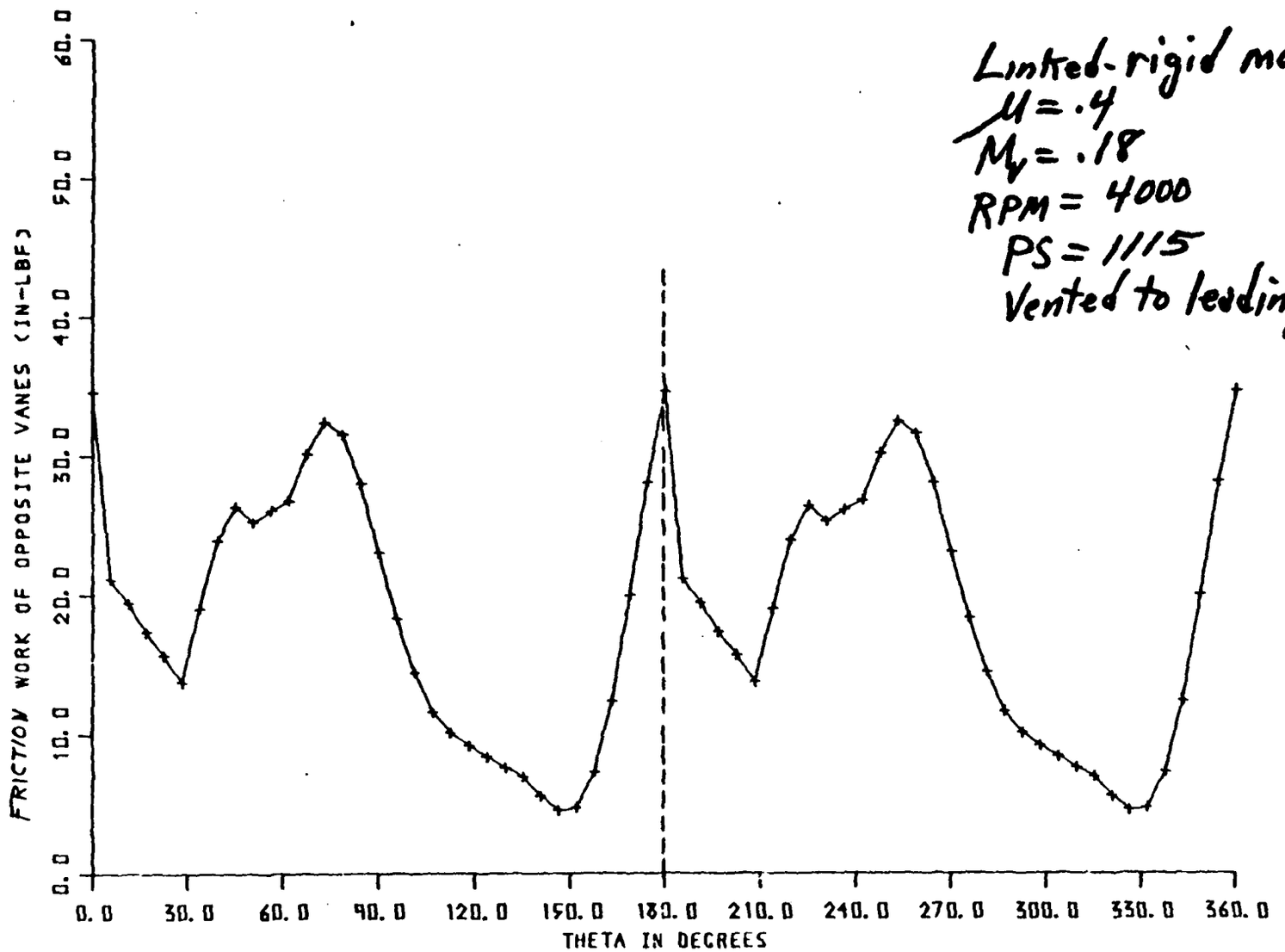

Figure 18 Friction Work for a Pair of Vanes

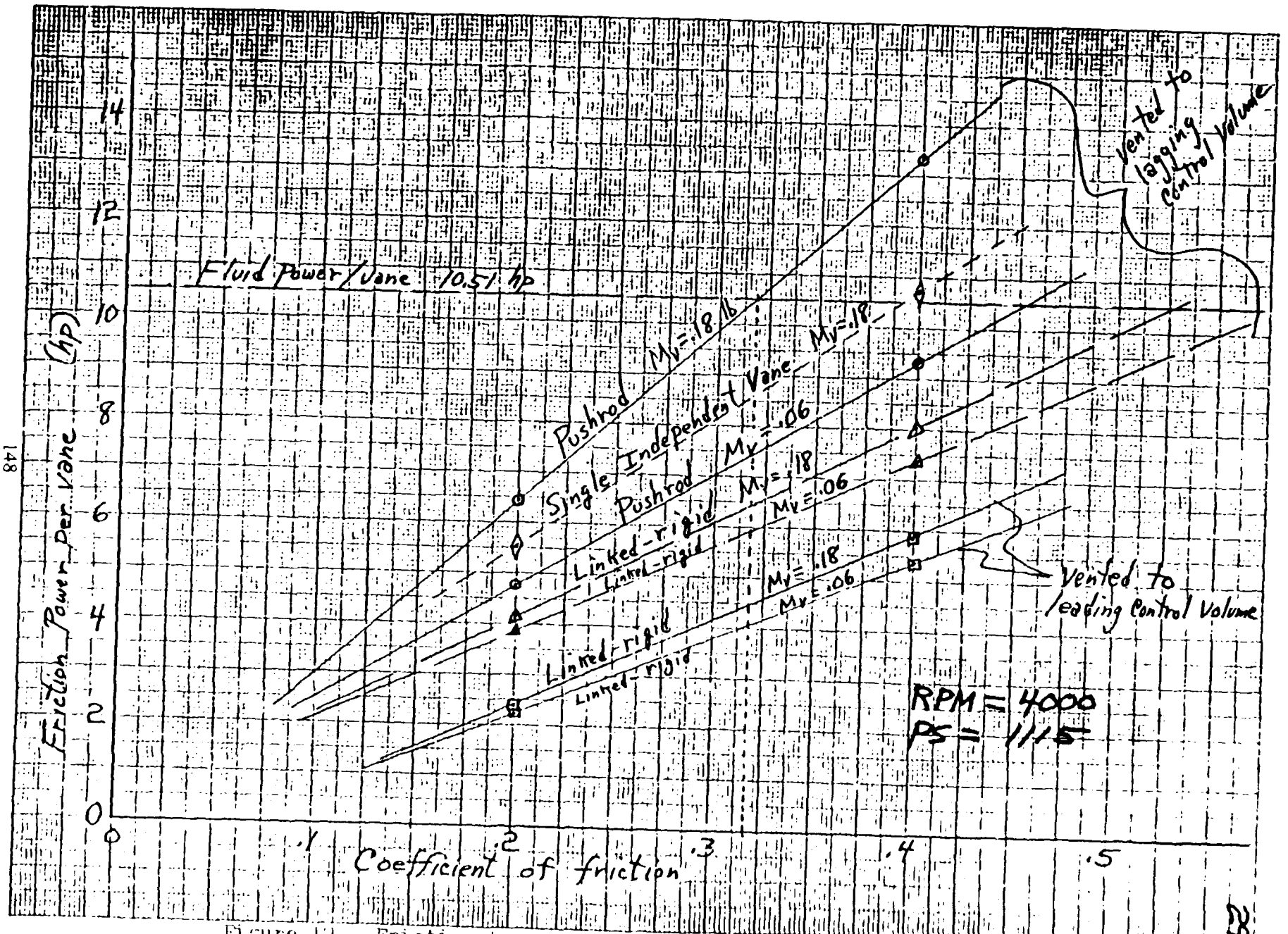

Figure 19 Friction Power per Vane versus Coefficient of Friction

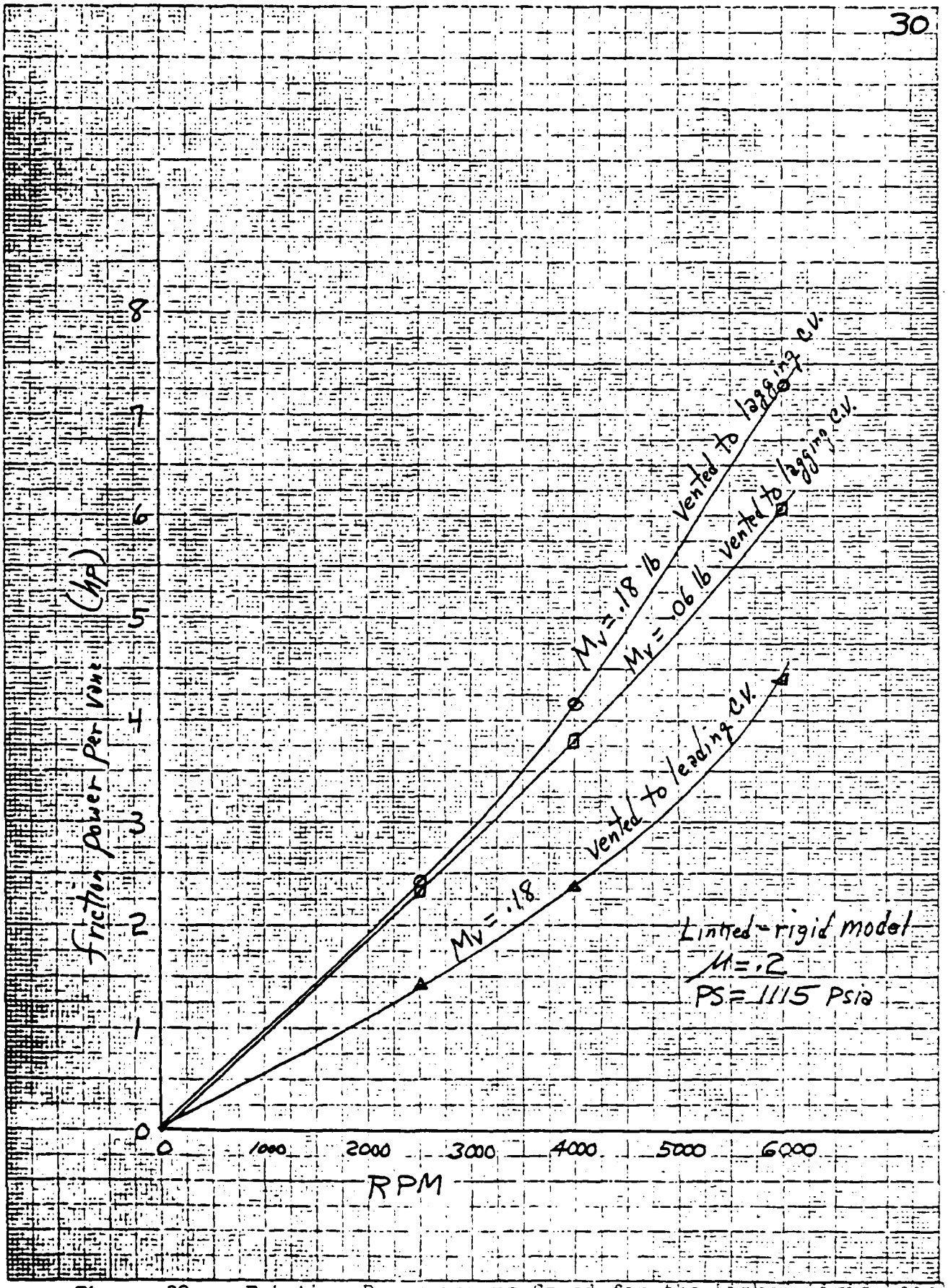

Figure 20 Friction Power versus Speed for the linked-rigid model

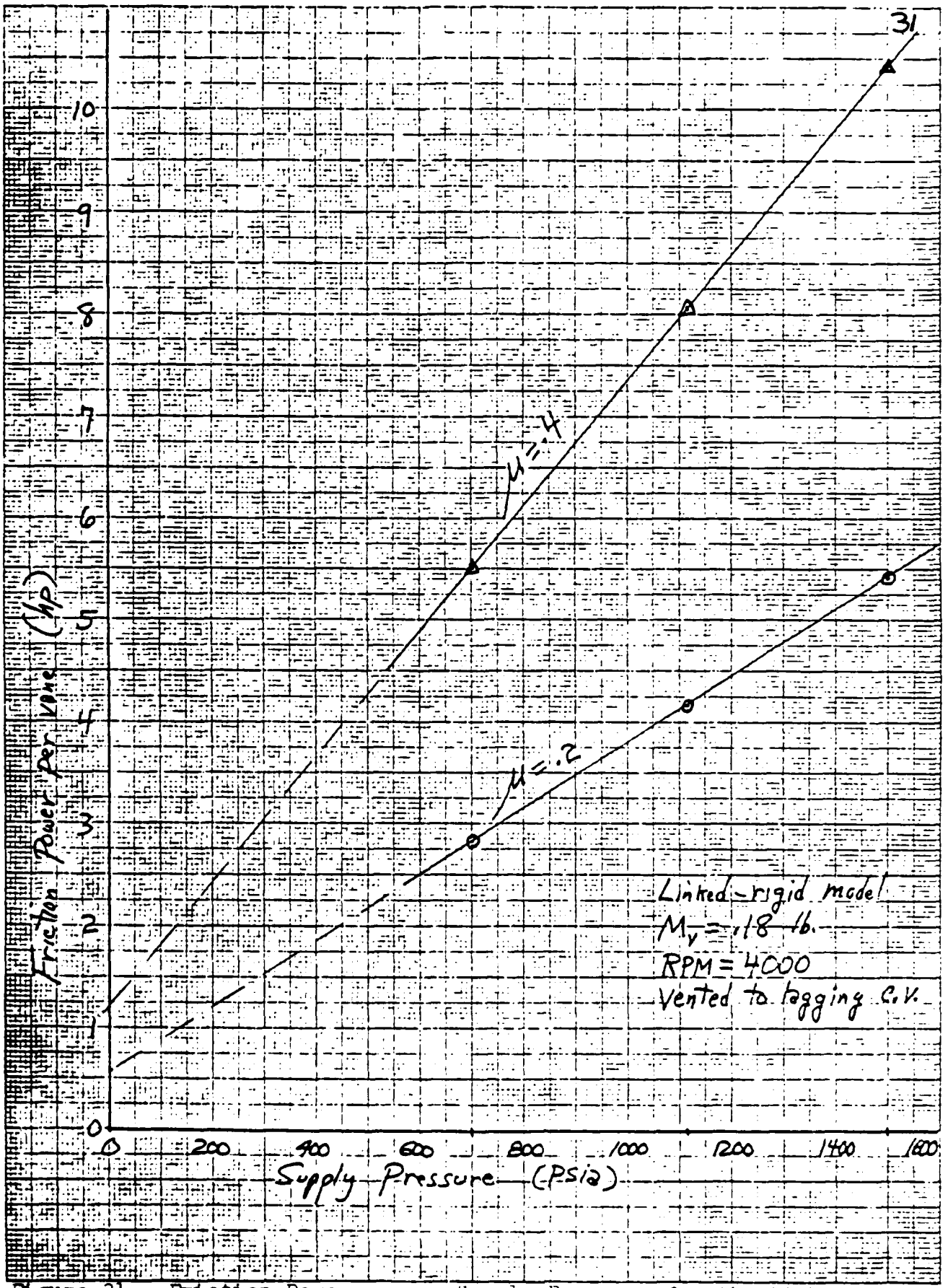

Figure 21 Friction Power versus Supply Pressure for the Linked-Rigid Model

APPENDIX A

Description of Vane Expander

Length of vane	3.105 in.
Thickness of vane	0.188 in.
Height of vane	1.135 in.
Radius of rotor	1.830 in.
Radius of stator	2.061 in.
Eccentricity	0.231 in.
Number of vanes	8
Angle between adjacent vanes	45°

TABLE A1
FRACTION OF VANE TIP AREA EXPOSED TO LAGGING CONTROL VOLUME VS. ROTOR ANGLE

Angle	Fraction	Angle	Fraction	Angle	Fraction
0.0	.500	129.0	.688	272.7	.258
4.4	.519	134.5	.673	277.6	.260
8.8	.537	140.1	.655	282.5	.264
13.2	.555	145.7	.637	287.3	.269
17.7	.574	151.3	.616	292.1	.276
22.1	.591	157.0	.595	296.9	.284
26.6	.608	162.7	.572	301.6	.294
31.0	.625	168.5	.548	306.2	.305
35.5	.641	174.2	.524	310.8	.317
40.1	.656	180.0	.500	315.4	.330
44.6	.670	185.8	.476	319.9	.344
49.2	.683	191.5	.452	324.5	.359
53.8	.695	197.3	.428	329.0	.375
58.4	.706	203.0	.405	333.4	.392
63.1	.716	208.7	.384	337.9	.409
67.9	.724	214.3	.363	342.3	.426
72.7	.731	219.9	.345	346.8	.445
77.5	.736	225.5	.327	351.2	.463
82.4	.740	231.0	.312	355.6	.481
87.3	.742	236.4	.298	360.0	.500
92.3	.742	241.8	.287		
97.4	.740	247.1	.277		
102.5	.736	252.5	.269		
107.7	.731	257.5	.264		
112.9	.723	262.6	.260		
118.2	.713	267.7	.258		
123.6	.702				

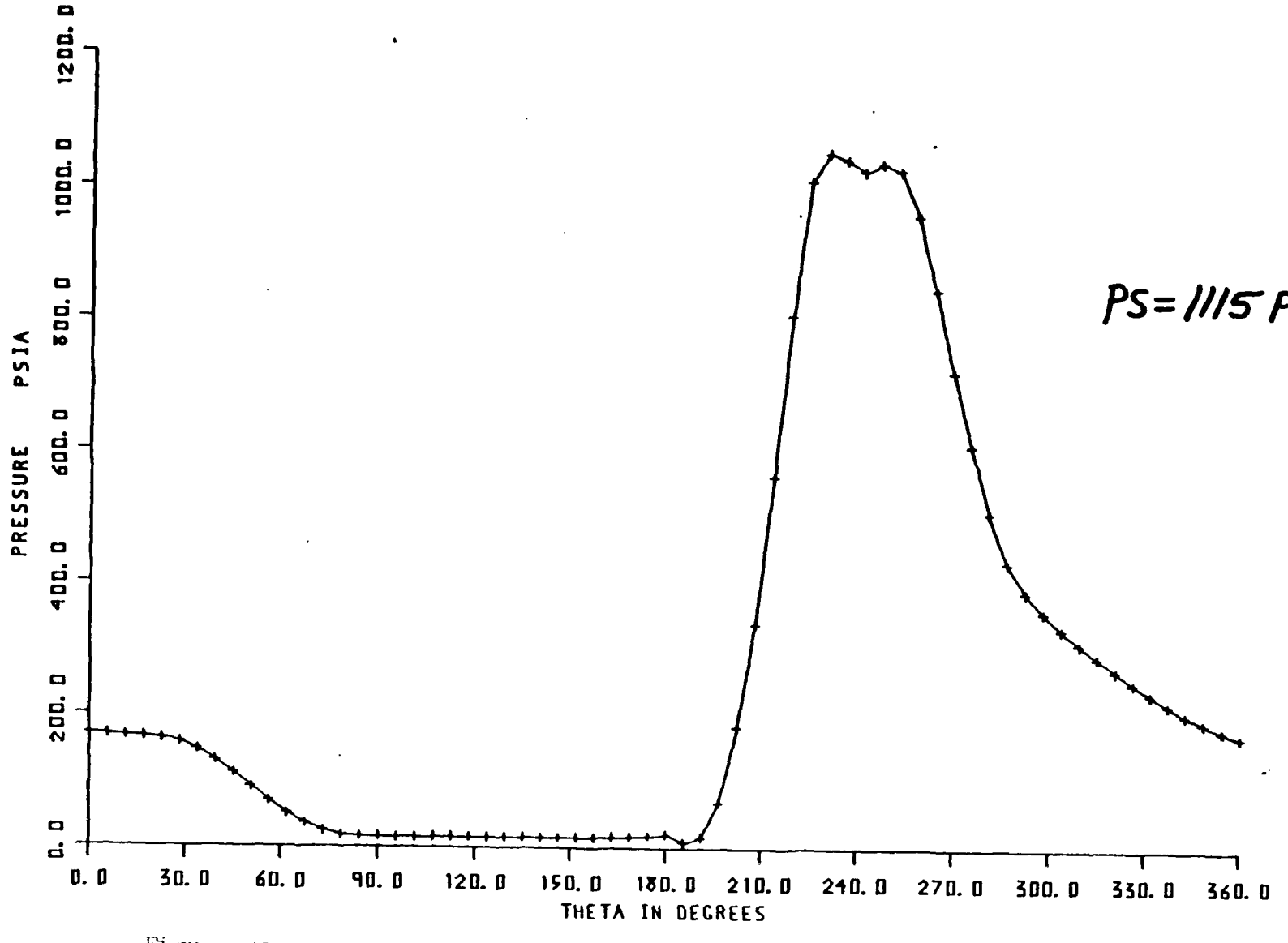

Figure A1 Pressure in Lagging Control Volume as a Function of Vane Angle

TABLE A2
ORIGINAL DATA FOR TABLE A1

LABEL: PRT007 -FORM XF/N:1 · COPIES 1

SPOOLED: 03/11/82 13:12
STARTED: 03/11/82 13:14, ON: MLC BY: PR2

	THETA	ALPHA	A/AT	
180	0.0	0.0	0.500	
	5.8	5.00	0.476	
	11.5	10.00	0.452	
	17.3	15.0	0.428	
	23.0	20.0	0.405	
	28.7	25.0	0.384	
	34.3	30.00	0.363	
	39.9	35.0	0.345	← INLET ℄
	45.5	40.0	0.327	
	51.0	45.0	0.312	
	56.4	50.0	0.298	
	61.8	55.0	0.287	
	67.1	60.0	0.277	
	72.3	65.0	0.269	
	77.5	70.0	0.264	
	82.6	75.0	0.260	
	87.7	80.0	0.258	
	92.7	85.0	0.258	
	97.6	90.0	0.260	
	102.5	95.0	0.264	
	107.3	100.0	0.269	
	112.1	105.0	0.276	
	116.9	110.0	0.284	
	121.6	115.0	0.294	
	126.2	120.0	0.305	
	130.8	125.0	0.317	
	135.4	130.0	0.330	
	139.9	135.0	0.344	
	144.5	140.0	0.359	
	149.0	145.0	0.373	
	153.4	150.0	0.392	
	157.9	155.0	0.409	
	162.3	160.0	0.426	
	166.8	165.0	0.445	
	171.2	170.0	0.468	
	175.6	175.0	0.481	
360-0	180.0	180.0	0.500	
	184.4	185.0	0.519	
	188.8	190.0	0.537	
	193.2	195.0	0.555	
	197.7	200.0	0.574	
	202.1	205.0	0.591	
	206.6	210.0	0.608	
	211.0	215.0	0.625	
	215.5	220.0	0.641	
	220.1	225.0	0.656	
	224.6	230.0	0.670	
	229.2	235.0	0.683	
	233.8	240.0	0.698	
	238.4	245.0	0.706	
	243.1	250.0	0.716	
	247.9	255.0	0.724	
	252.7	260.0	0.731	
	257.5	265.0	0.736	
	262.4	270.0	0.740	
	267.3	275.0	0.742	
	272.3	280.0	0.742	
	277.4	285.0	0.740	
	282.5	290.0	0.736	
	287.7	295.0	0.731	
	292.9	300.0	0.723	
	298.2	305.0	0.713	
	303.6	310.0	0.702	
	309.0	315.0	0.688	
	314.5	320.0	0.673	
	320.1	325.0	0.655	
	325.7	330.0	0.637	
	331.3	335.0	0.616	
	337.0	340.0	0.594	
	342.7	345.0	0.572	
	348.5	350.0	0.546	
	354.2	355.0	0.524	
180	360.0	360.0	0.500	

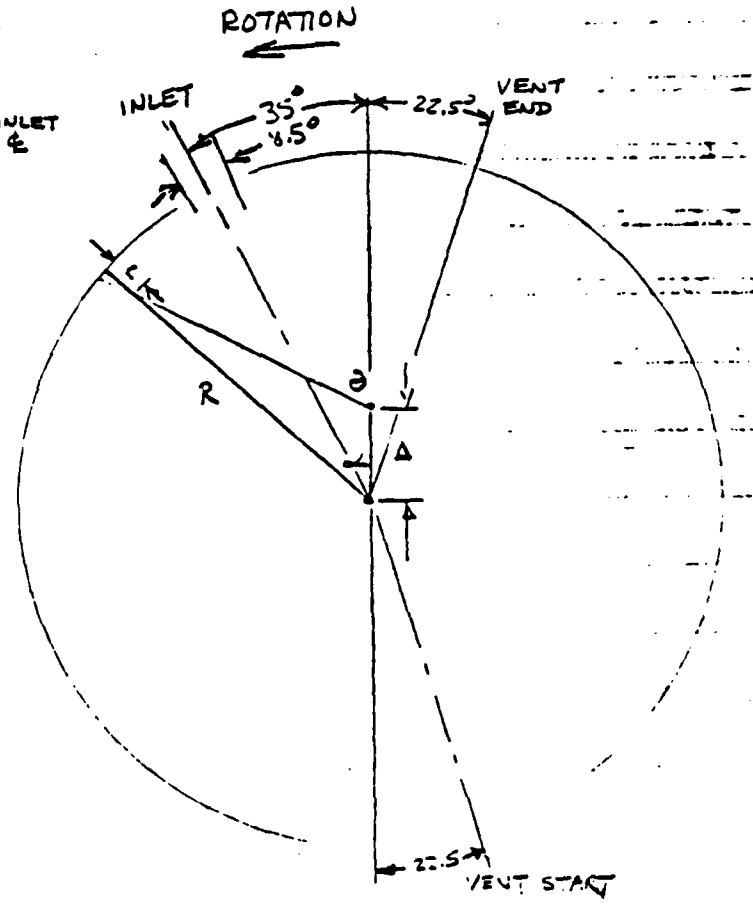

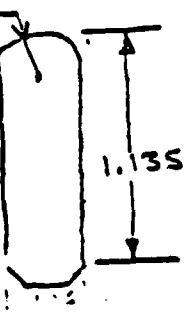

R = STATOR RADIUS = 2.061 IN

r = BLADE TIP RADIUS = 0.34 IN

Δ = ROTOR OFFSET = 0.2305 IN

α = POSITION ANGLE ABOUT CENTER OF STATOR

∂ = " " " " OF ROTOR

A/AT = FRACTION OF BLADE TIP EXPOSED TO TRANSIENT CHAMBER PRESSURE

BLADE THICKNESS = 0.133 IN

BLADE LENGTH = 3.105 IN = Z

BLADE WIDTH (TIP TO CORNER), W = 1.135

PINLET = 1100 psig

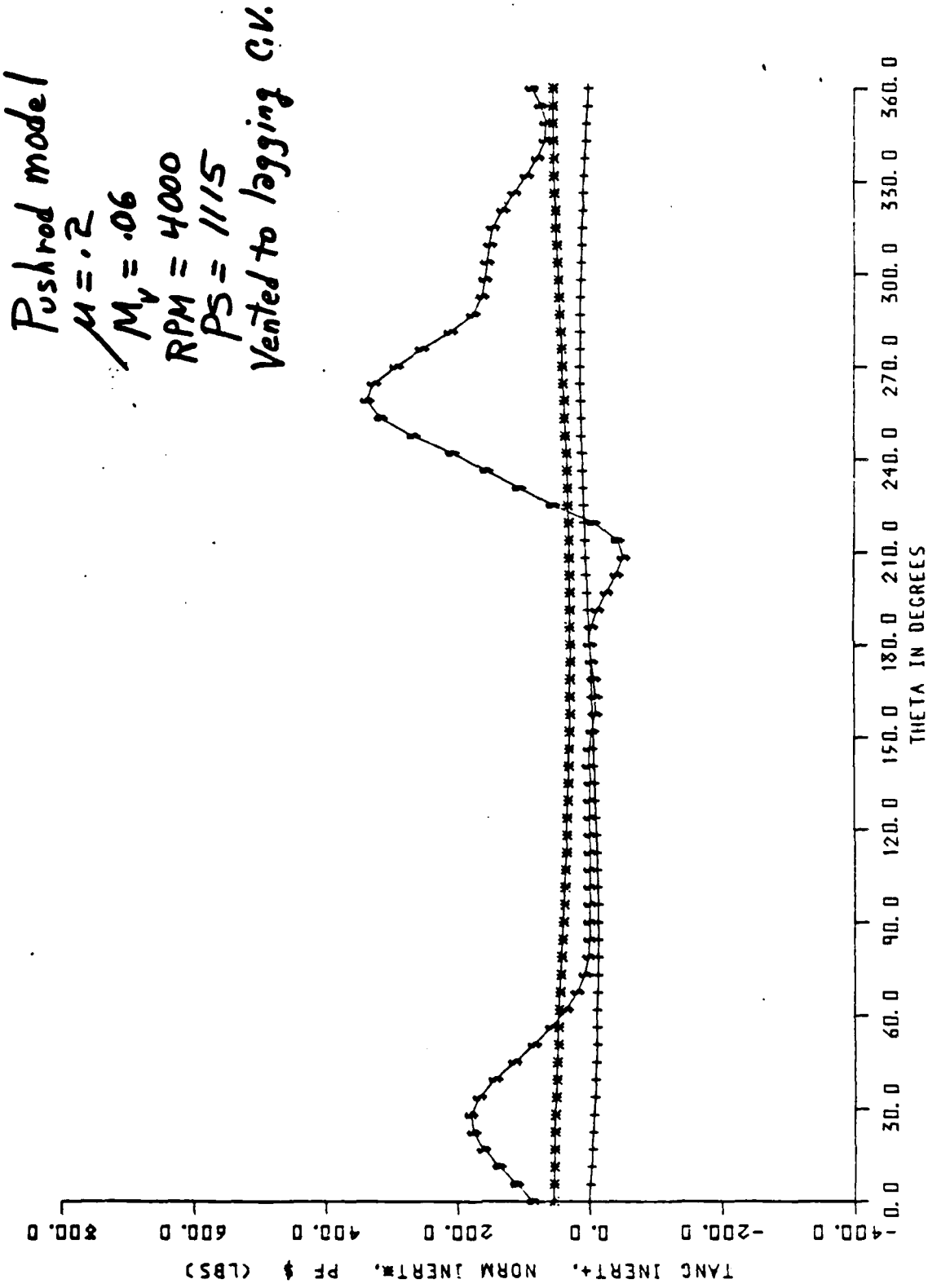

Figure B1 Pressure and Inertia Forces, M_v = .06

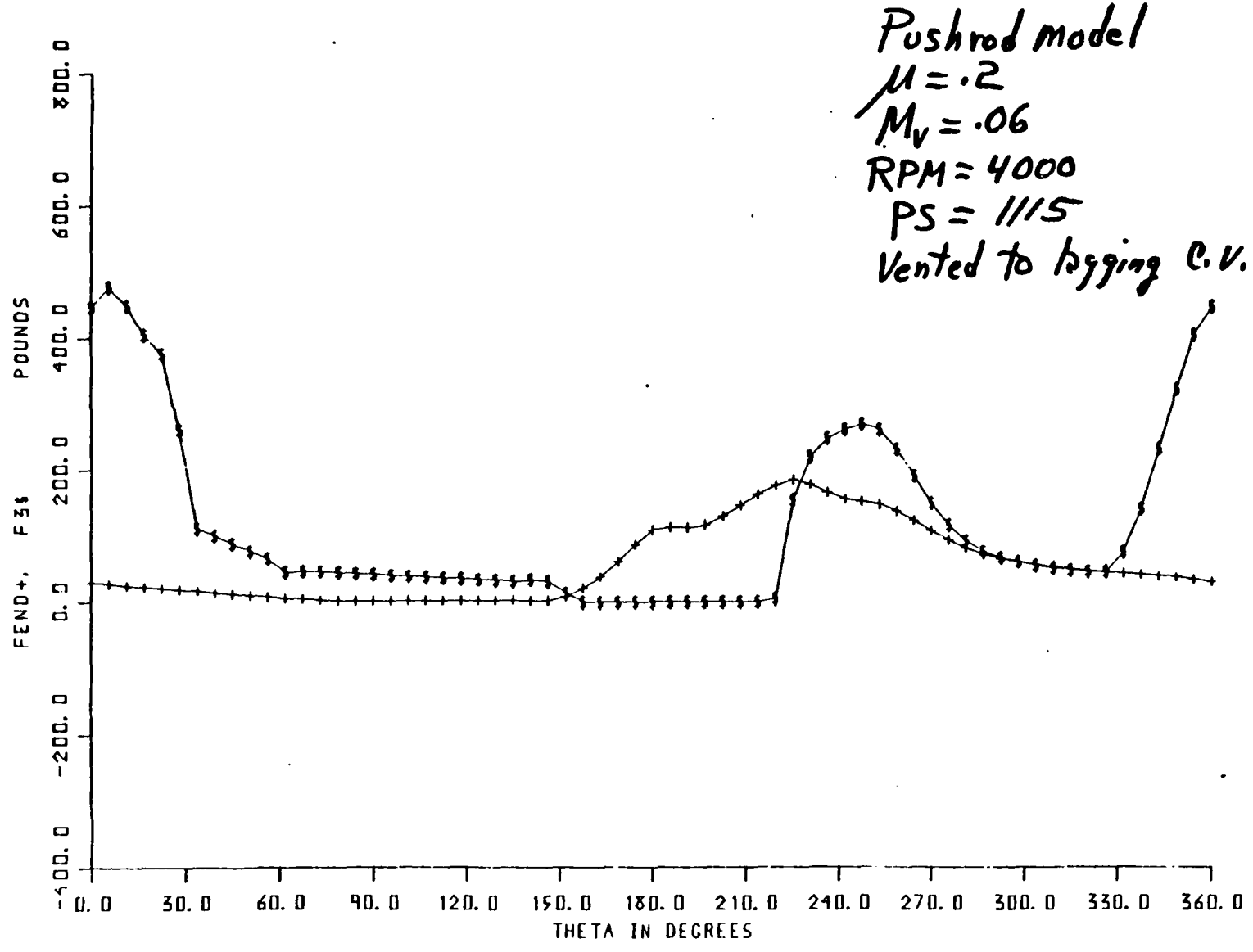

Figure B2 Tip and End Forces, M_V = .06, μ = .2

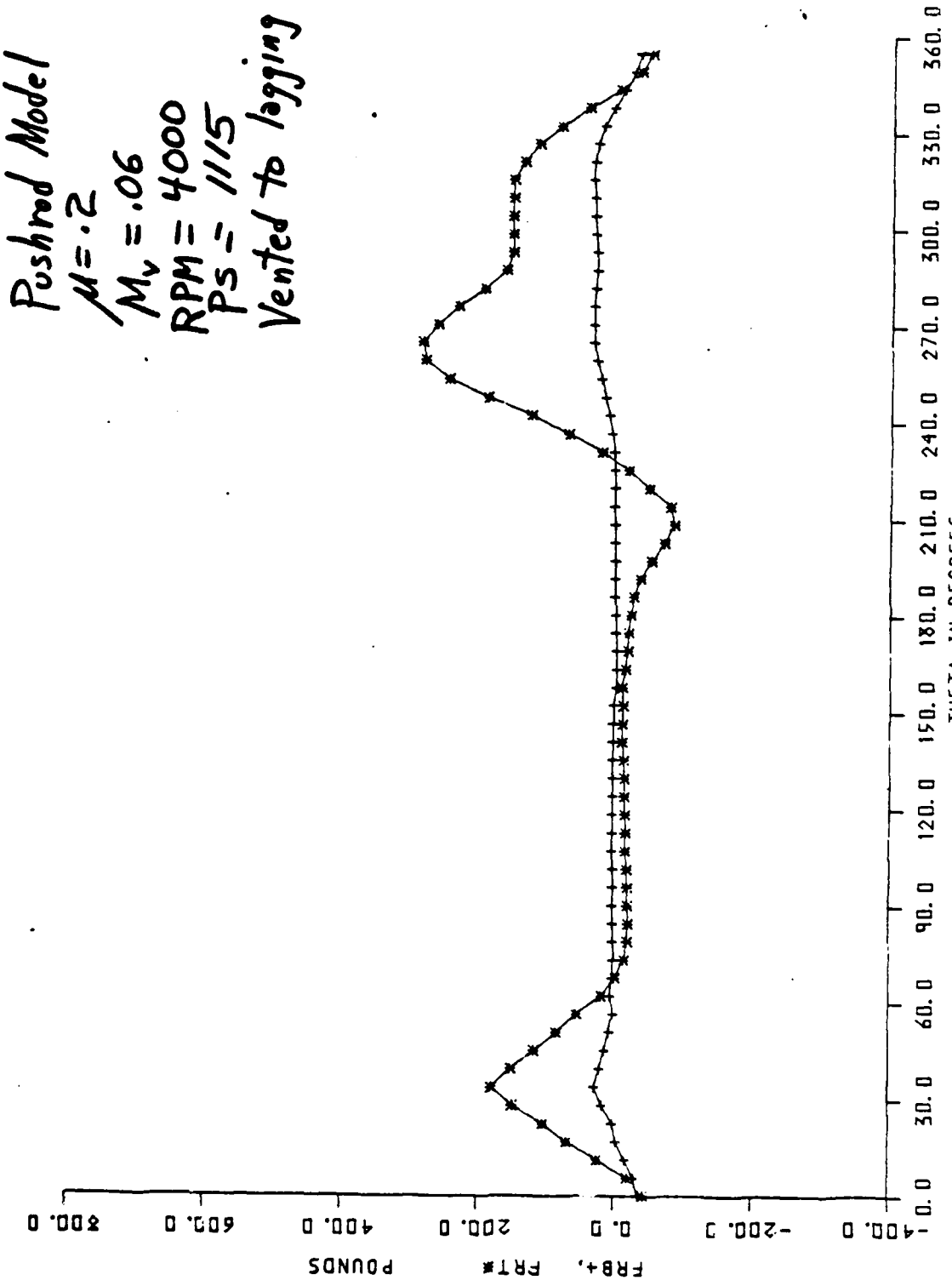

Figure B5 Reaction Forces on Rotor Slot, M_v = .06, μ = .2

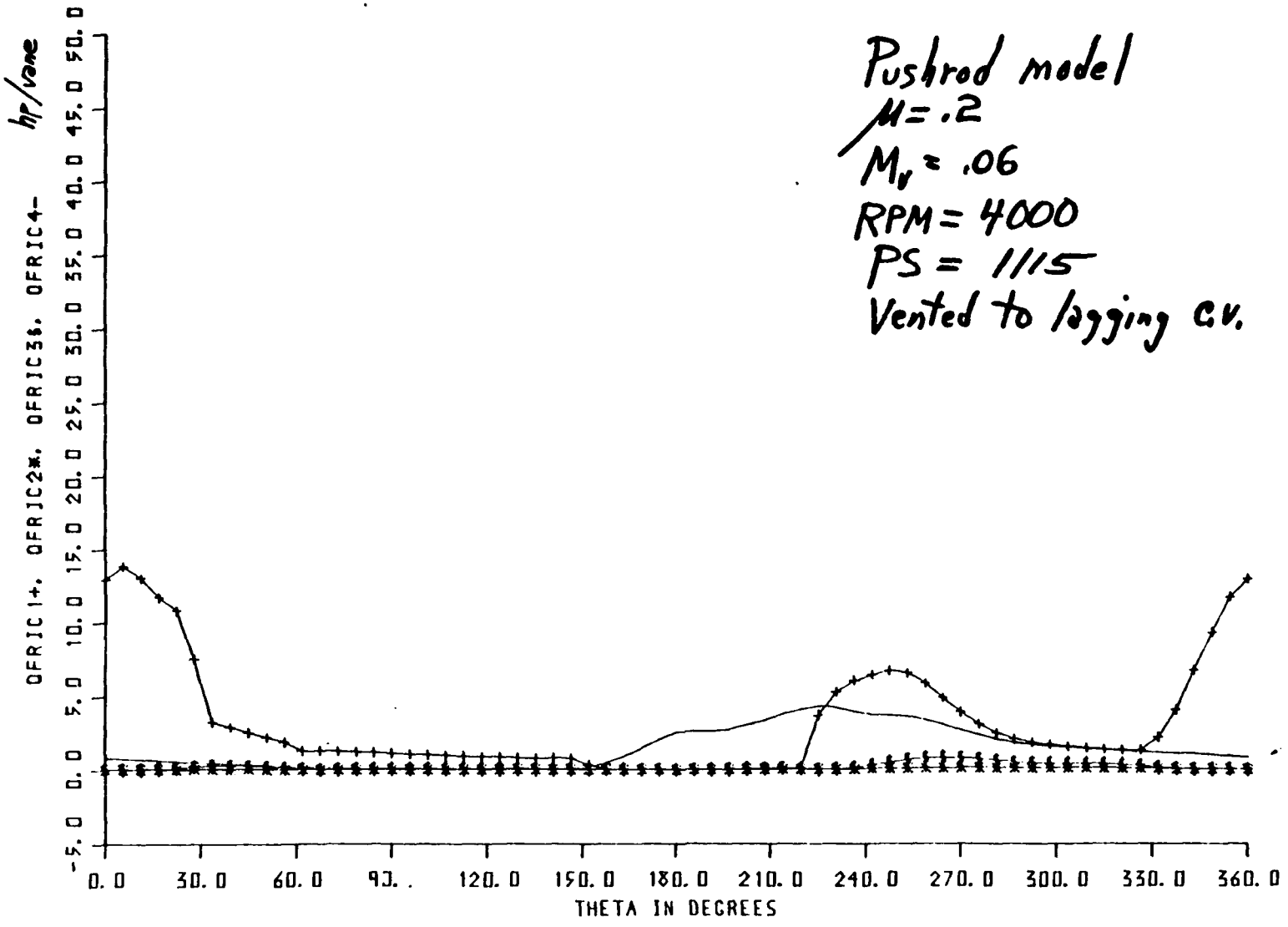

Figure B4 Power Dissipated by Each Rubbing Force, M_v = .06, μ = .2

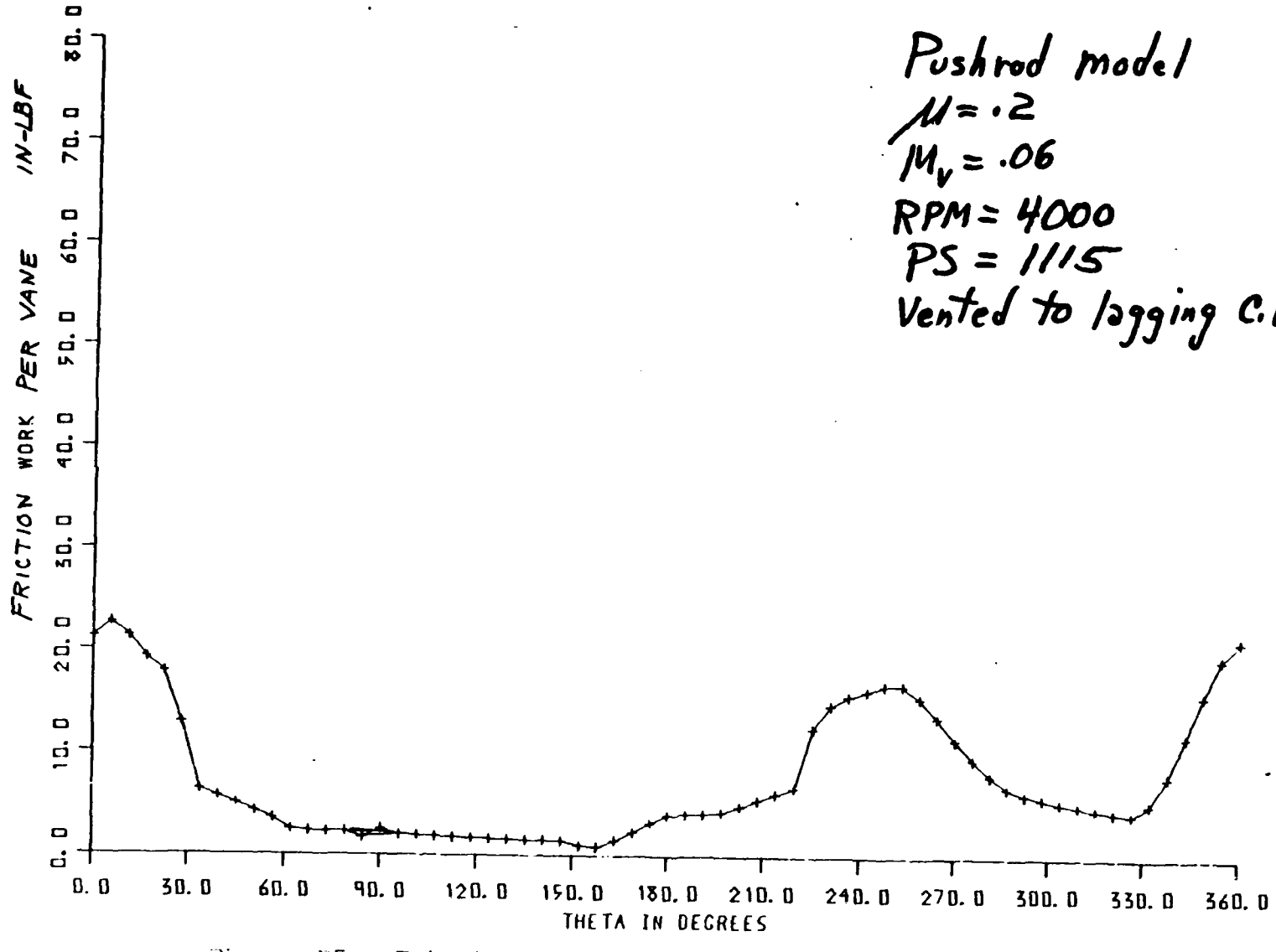

Pushrod model
$\mu = .2$
$M_v = .06$
RPM = 4000
PS = 1115
Vented to lagging C.V.

Figure B5 Friction Work per Vane, $M_v = .06$, $\mu = .2$

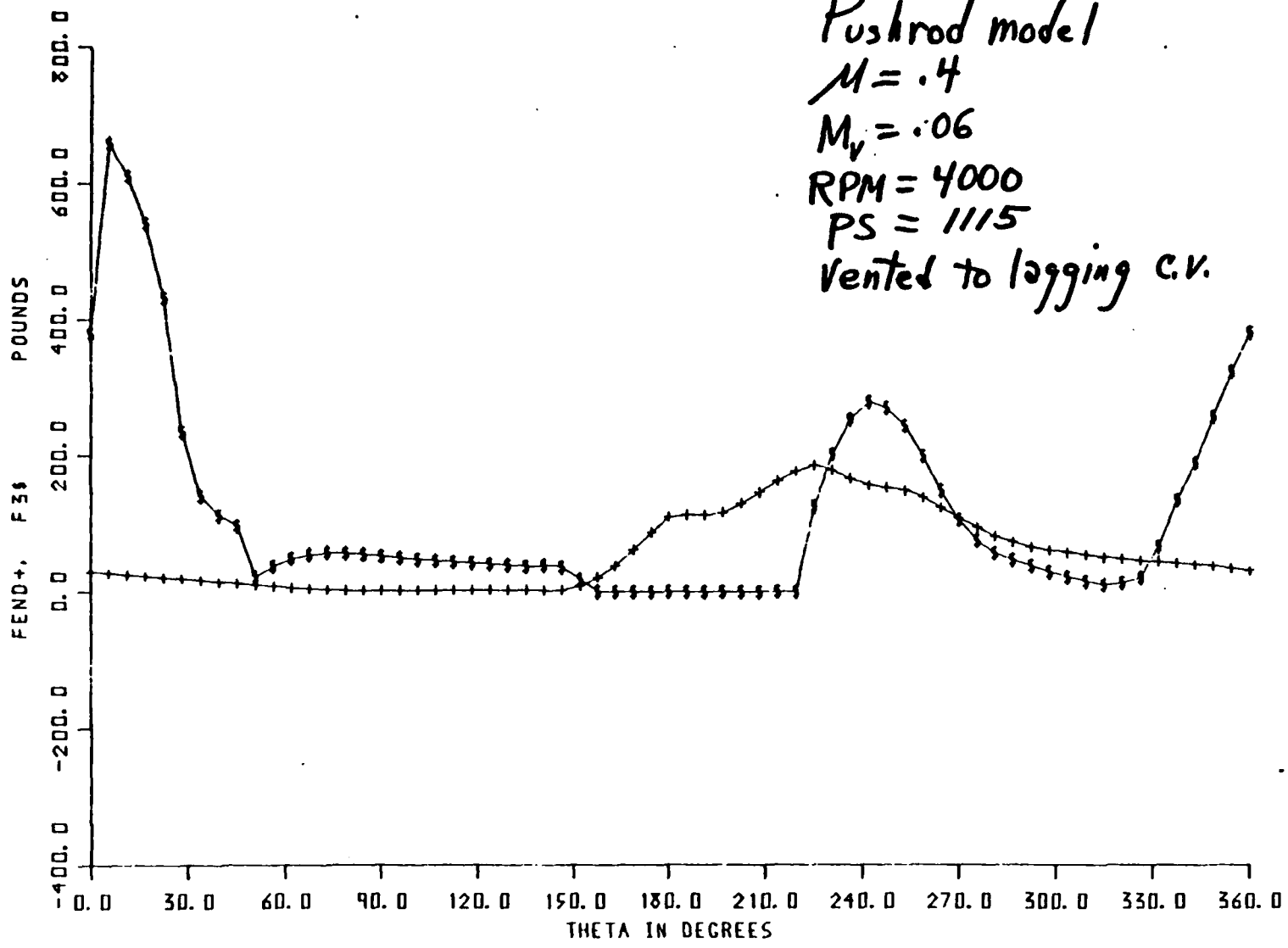

Figure B6 Tip and End Forces, M_v = .06, M = .4

41

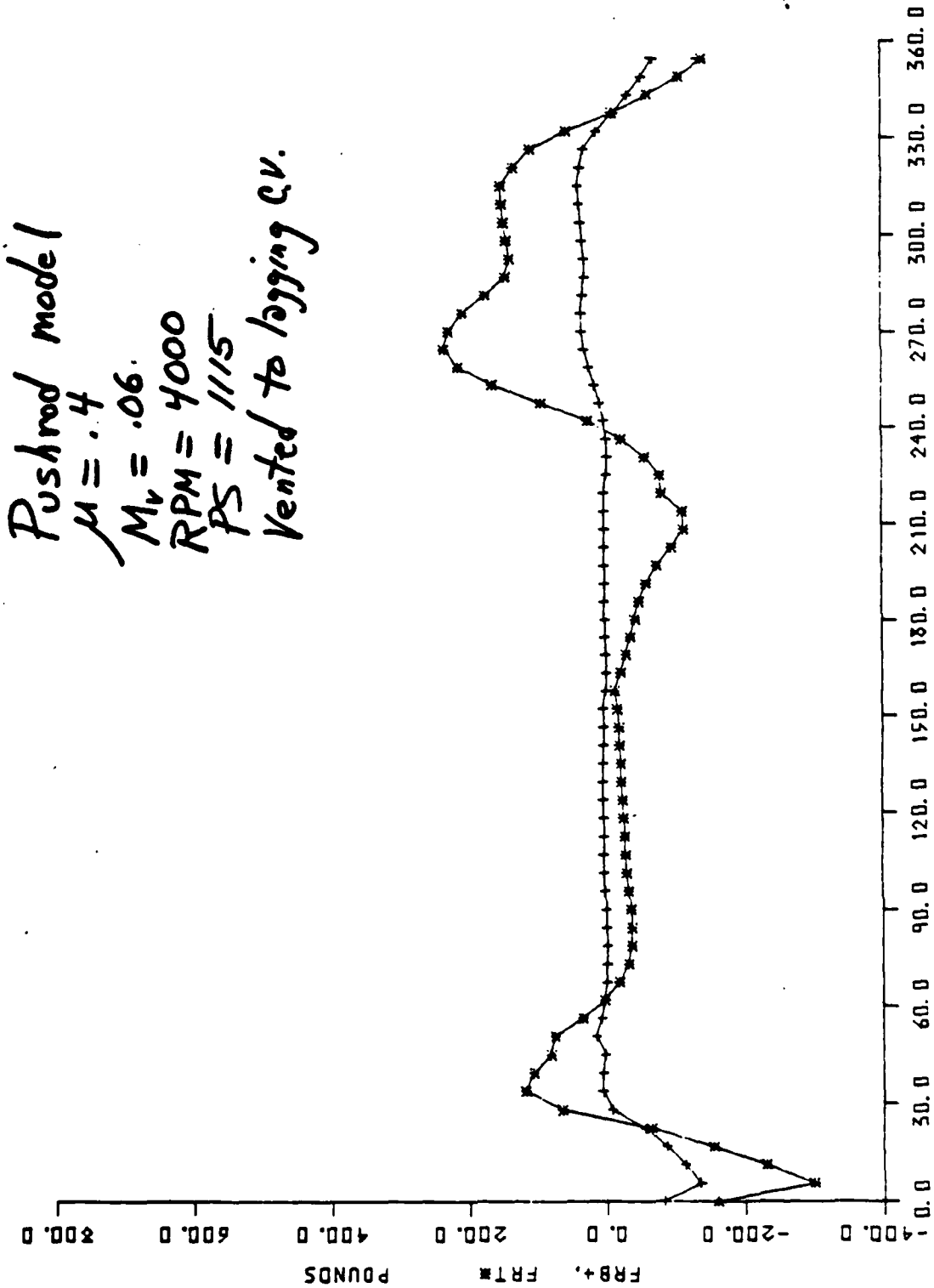

Figure 37 Reaction Forces on Rotor Blot, M_v = .06, μ = .4

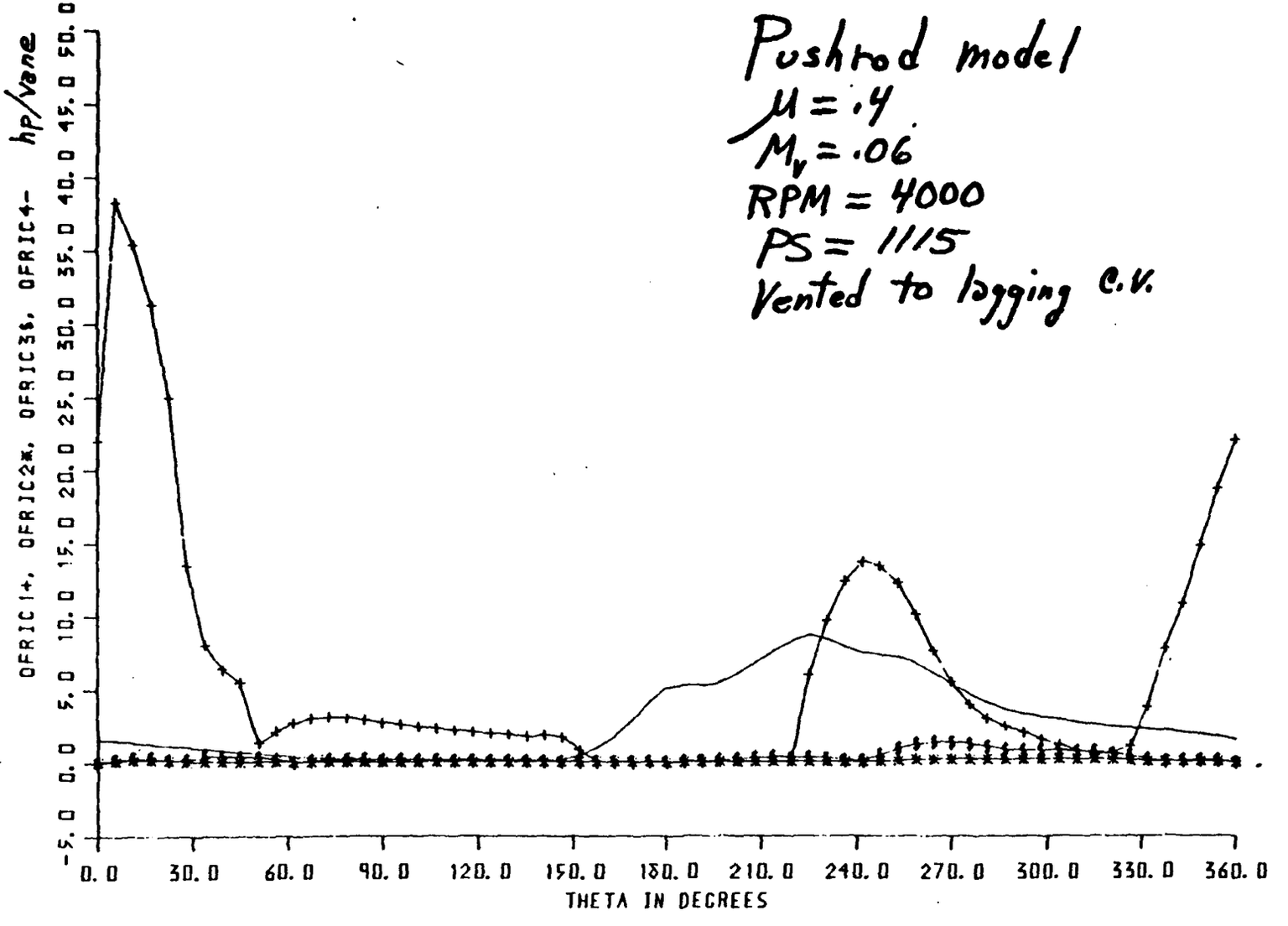

Figure B8 Power Dissipated by Each Rubbing Force, M_v = .06, μ = .4

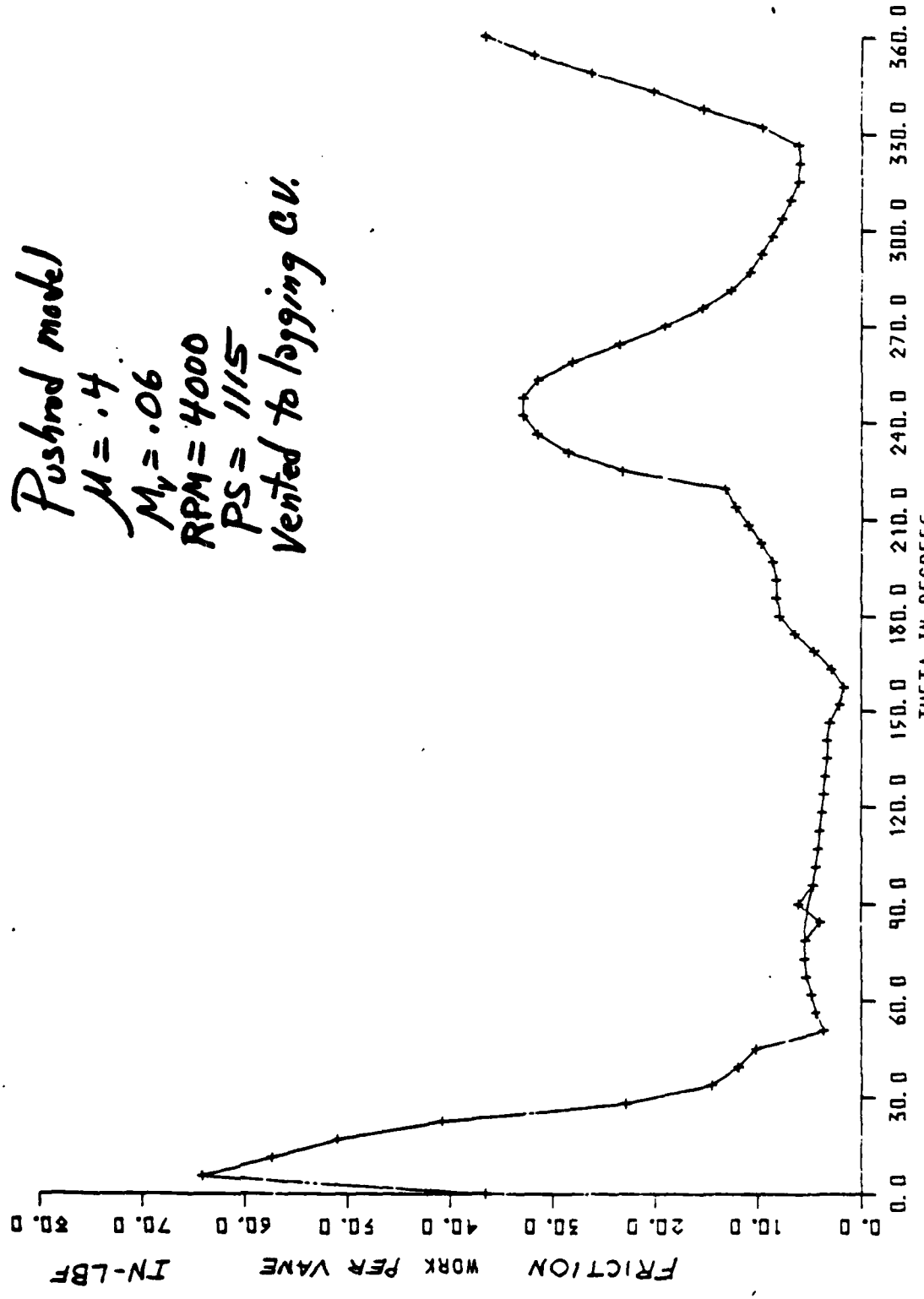

Figure B9 Friction Work per Vane, M_V = .06, M = .4

REFERENCES

1. C. H. Wolgemuth and D. R. Olson, "A Study of Breathing in Vane-Type Expanders," Intersociety Energy Conversion Engineering Conference, 1971.

2. H. E. Sliney, "Plasma-Sprayed Metal-Glass and Metal-Glass-Fluoride Coatings for Lubrication to 900°C," ASLE Transactions, 17(3) (1974) 182.

3. H. E. Sliney, "Wide Temperature Spectrum Self-Lubricating Coatings Prepared by Plasma Spraying," International Conference on Metallurgical Coating, San Diego, CA, April 1979.

4. H. E. Sliney, "Self Lubricating Composites of Porous Nickel and Nickel-Chromium Alloy Impregnated with Barium Fluoride-Calcium Fluoride Eutectic," ASLE Transactions, 9 (1966) 336.

*USGPO:1983-659-062-1040

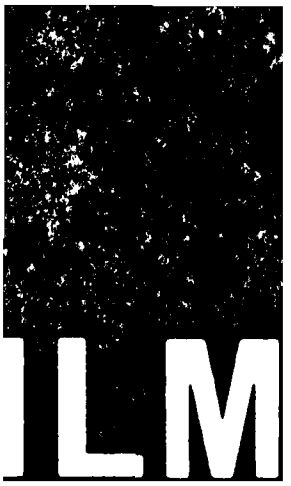
ILM